

# RADICAL FORMATION AND ELECTRON TRANSFER IN BIOLOGICAL MOLECULES

Thesis by

Jeremiah E. Miller

In Partial Fulfillment of the Requirements for the  
degree of

Doctor of Philosophy

CALIFORNIA INSTITUTE OF TECHNOLOGY

Pasadena, California

2003

(Defended June 3, 2003)

© 2003

Jeremiah E. Miller

All Rights Reserved

*This thesis is dedicated  
to my wife, Christine. I  
couldn't have done it  
without her.*

## ACKNOWLEDGEMENTS

*“Every passing hour brings the solar system forty-three thousand miles closer to Globular Cluster M13 in Hercules - and still there are some misfits who insist there is no such thing as progress.”*

*-Kurt Vonnegut, Sirens of Titan*

No human endeavor occurs in a vacuum. The work presented in this thesis could not have been done without the support and assistance of a large number of people. First and foremost, I must thank my wife, Christine. This thesis is dedicated to her for her enduring support and tolerance. She was there for me throughout the lows and the highs. Also, I have to thank my grandparents Tom and Leone Cory for providing me with a quiet sanctuary in the hills north of San Diego for the four years I have been at CalTech. When the rigors of graduate school got to be too much, I could always escape to their house for peace and quite, good food, and of course, cocktail hour (5 pm)! My parents also deserve special thanks for supporting me my whole life, and particularly during the rather difficult seven months I spent at CalTech before I joined the Gray group.

I have been lucky enough to learn from some of the best scientists around. My advisor, Harry Gray, is as good as they come. Harry knows something about all arenas of chemistry and was always willing to share his knowledge. Harry was supportive of me, encouraging me to do my best. In addition to strictly scientific input, Harry has helped me



to be a more “concise” writer and has shown me what it is to give a captivating lecture. And, of course, there are the trips to Europe. Thanks to Harry, I was able to attend both ICBIC 10 in Florence, Italy and EUROBIC 6 in Lund, Sweden and Copenhagen, Denmark. These two conferences stand out as highlights for my graduate career; allowing me to see parts of the world I had never thought of visiting. Last, but not least, I have to thank Harry for giving me a place to work at time when it seemed no one else would— needless to say, it made all the difference.

Professor Thomas Meade, now at Northwestern University, also deserves some special thanks. Tom advised me throughout my study of metal-modified DNA. He was a tireless supporter; he always had an encouraging perspective on my project. Tom introduced me to the interface between biology and chemistry; the time I spent working with him has undoubtedly helped shape my career.

Dr. Jay Winkler, director of the Beckman Institute Laser Resource Center, has also been essential to my success at CalTech. I worked for him as a graduate lab assistant in the BILRC for two years, and during that time I learned an enormous amount about kinetics, laser equipment and scientific rigor. Working in the laser lab also allowed me to develop an interest in laser spectroscopy, a technique which I had literally never even thought about before joining the Gray group. His help interpreting the data I collected in the BILRC was essential to my ability to formulate many of the hypotheses that drove my research.

Dr. Angelo Di Bilio taught me everything I know about EPR spectroscopy. He also deserves credit for helping me design the systems I worked with, since he was the first

researcher to label azurin with rhenium. Angelo's explanation of amino-acid radicals in protein environments was of great importance to my research, providing a context in which to view my results. Angelo also deserves thanks for helping me to understand the "big picture," placing my results in their proper context.

Then there are the postdoctoral researchers I have had the pleasure of working with in both the Gray group and the Meade group. Dr. Natia Frank got me started making metal-modified DNA and helped me do my very first laser experiments. Dr. Kristine Kilsa Jensen served a wonderful resource for fluorescence spectroscopy. She was also a patient teacher when it came to kinetic analyses. Also, she read both my research proposals and Chapter 4 of this thesis. Despite our disagreements of the nature of the hyphen, her input was essential to my refinement of this thesis and my proposals. Dr. Malin Abrahamsson has been a good coffee buddy, and a useful sounding board for various ideas I have had about photosystem II. Malin also graciously read Chapter 3 of this thesis. Dr. Pierre Kennepohl turned out to be a fine lab mate on the 3<sup>rd</sup> floor of Noyes (although he did monopolize my lab's phone extension!). Pierre was always willing to lend a hand, and helped me by reading Chapter 1 of this thesis. The recently arrived Dr. John Magyr is a welcome addition to the group- and of course he read Chapter 6 of my thesis.

My graduate student peers deserve many thanks as well. First, I must thank William Wehbi. Will was always ready with the coffee pot (and the chocolate) to entertain me, at least until someone better showed up! Will worked on a rhenium-labeled azurins and so we had many useful conversations about the results presented in Section II. Will taught me a

lot about EPR and Arabic linguistics, so I am indebted to him. I also must thank him for generously giving me parental DNA from which I made the mutants I worked with. This donation made it possible for me to obtain the desired proteins with only one or two rounds of PCR instead of five. Randy Villahermosa was an excellent co-worker during the time we overlapped in the Gray group. He taught me to use the BILRC to its fullest potential and how to present data accurately and clearly. Randy also preceded me as one-half the Gray group party committee– his advice in that area was invaluable. Elizabeth Mayo is a good friend and a perfect office mate. She knows how to have a good time (sometimes a little too good– see, for example, my bachelor party in Tijuana). During some of the rough patches here at CalTech, Libby has proven to be reliable friend and the perfect confidant. Wendy Belliston is a true friend. She read Chapter 5 for me and provided her own analysis of how to make my writing “concise.” Wendy and I have had many stimulating conversations about science, politics and Rod Stewart, Methuselah of Rock. Brian Leigh was a welcome colleague when he joined me as a graduate laboratory assistant in the BILRC. He will probably surpass me in his understanding of the electronics and equipment involved in the laser spectroscopy carried out in the BILRC. Also, Brian is ensuring that investigations into amino-acid radicals in azurin continue. Matt Allen was the first friend I made in graduate school; I actually first met him on a visit to MIT before I made the decision to come to CalTech. Matt was the best man at my wedding and an excellent friend. He is truly one of the most talented synthetic chemists I have ever known, never daunted by any reaction however challenging. Lily Ackermann also must be thanked here. Along with Matt, she was a great support during my rocky start to graduate school. Her company will be missed.

Then, there is Carlo Quinonez; a graduate student in the Division of Biology who worked for Tom Meade at the same time I did. Carlo is truly unique, and by far the most optimistic person I know. His cheerful demeanor often kept me going when my research was stalled. Carlo has been the source of countless entertaining hours, including more than one trip to his fathers bar in Tijuana, “El Palapas Del Tigre.”

Anne Katrine Museth (a researcher working for Professor Jack Richards) was an essential part of the small group of us (Will, Angelo and I being the other members) who worked on metal-labeled azurin. Her constant effort to improve the microbiological end of the project was essential. She also helped me personally by performing some of the PCR necessary for two of the azurin mutants I have investigated. Katrine also proved to have an interesting take on the world, leading to many informative discussions.

In addition to those thanked expressly above, I must thank the rest of the Gray group. Without them, graduate school would not have been the experience that it was for me. The environment in which any scientific work is done has a profound effect on that work, and so I have to thank the Gray group for keeping things challenging and interesting.

## ABSTRACT

Multi-step electron transfer is increasingly recognized as a means for moving charge in biological systems over long distances rapidly. Many postulated multi-step mechanisms rely on the formation of organic radicals (amino-acid radicals, nucleobase radicals) as intermediate electron or “hole” carriers. In this thesis, the multi-step mechanism for electron transfer in both proteins and DNA is investigated. These two systems form a natural complement; the role of electron transfer in DNA with regard to lesion repair is still unknown, as are the electron transfer events in the proteins that mediate the repair. Rhenium-labeled mutant *Pseudomonas aeruginosa* azurins serve as model systems for this phenomenon in proteins. The photo-active rhenium label in these azurins can be oxidized by a flash/quench reaction to provide a potent oxidant capable of generating a variety of radicals in the protein matrix. Three mutants (with one tryptophan residue each) were constructed to investigate the effect of tryptophan radicals on charge transfer in proteins. The properties of tryptophan radicals in three protein environments have been investigated; including a kinetically stable tryptophan radical that persists for more than 5 hrs at room temperature. The variation in these radicals plays a significant role in their effect on the oxidation of the remote copper center in azurin. The stable radical greatly reduces the rate of electron transfer from copper relative to the rhenium-labeled wild-type analogs, while another radical plays no role in copper oxidation. In order to examine multi-step electron transfer in DNA, a series of photo-active ruthenium and rhenium-thymine complexes were constructed. By attaching the metal complexes at the sugar of the deoxyribonucleic acid, they were incorporated into DNA strands by solid-state synthetic techniques. Two different

ruthenium-labeled DNA strands were produced in this way; one with a single guanine base and one with two side by side guanine bases. The strand containing a guanine-guanine sequence showed formation of a guanine radical by EPR under flash/quench conditions, while the strand containing a single guanine remained EPR silent. These strands represent an excellent template to examine a system which may or may not exhibit multi-step charge transfer.

## TABLE OF CONTENTS

|  |      |
|--|------|
| Acknowledgements .....   | iv   |
| Abstract .....   | ix   |
| Table of Contents .....  | xi   |
| List of Illustrations and/or Tables .....  | xiii |
| Abbreviations .....  | xix  |
| Section I. General Considerations .....  | 1    |
| Chapter 1. Thesis Summary and Theoretical Background .....   | 2    |
| 1.1. Thesis Summary .....  | 2    |
| 1.2. Semiclassical Electron Transfer Theory and the Multi-step Mechanism .....   | 6    |
| Chapter 2. Instrumentation and Experiment Design .....   | 13   |
| 2.1. Laser Experiments .....   | 13   |
| 2.1.1. The Flash/Quench Experiment .....   | 13   |
| 2.1.2. Atmosphere-Controlled Cuvettes .....  | 18   |
| 2.1.3. Sample Preparation .....  | 20   |
| 2.1.4. NS1 .....   | 21   |
| 2.1.5. NS2 .....   | 24   |
| 2.1.6. Data Analysis .....   | 26   |
| 2.2. EPR Spectroscopy .....  | 28   |
| 2.2.1 The Flash/Quench/Freeze Experiment .....   | 28   |
| 2.2.2. Atmosphere-Controlled EPR Tube .....  | 29   |
| 2.2.3. Sample Preparation .....  | 32   |
| 2.2.4. EPR Spectrometer .....  | 32   |
| 2.2.4. Miscellaneous Experimental Equipment .....  | 34   |
| References .....   | 35   |
| Section II: Tryptophan Radical Formation and Electron Transfer in<br>Rhenium-Modified <i>Pseudomonas aeruginosa</i> Azurin ..... | 38   |
| Chapter 3. Introduction .....  | 39   |
| 3.1. Natural Systems .....   | 39   |
| 3.2. <i>Pseudomonas aeruginosa</i> Azurin .....  | 45   |
| 3.2.1. Pulse Radiolysis Reduction of Cu(II) in Azurin .....  | 47   |
| 3.2.2. Cu(I) to Ru(III), Os(III) and Re(II) in Metal-Labeled Azurins .....   | 49   |
| Chapter 4. Synthesis and Characterization of Re-Modified Azurin .....  | 57   |
| 4.1. Synthesis and Characterization of the Rhenium Model Compound .....  | 57   |
| 4.2. Synthesis and Characterization of Metal-Modified Azurins .....  | 72   |
| 4.3. Experimental .....  | 84   |
| 4.3.1. Metal Complexes .....   | 84   |
| 4.3.2. Biological Buffers and Media .....  | 86   |
| 4.3.3. Site-directed Mutagenesis .....   | 88   |
| 4.3.4. Protein Expression .....  | 96   |

|   |     |
|---|-----|
| 4.3.5. Labeling Reaction.....                                 | 103 |
| 4.3.6. Purification of Labeled Azurins .....                  | 106 |
| 4.3.7. Measuring a Rate and Observing Radical Formation ..... | 111 |
| Chapter 5. Tryptophan Radicals.....                           | 115 |
| 5.1. Radical Formation in a Model System .....                | 115 |
| 5.2. Tryptophan Radicals in Azurin .....                      | 123 |
| 5.2.1. [Re(H83)WTAz] and [Re(H83)(W48)Az] .....               | 125 |
| 5.2.2. [Re(H107)(W108)Az] .....                               | 135 |
| 5.2.3. [Re(H107)(W110)Az] .....                               | 152 |
| 5.3. Comparison of Tryptophan Radicals .....                  | 161 |
| Chapter 6. Copper Oxidation in Re-Labeled Azurins .....       | 165 |
| 6.1. Copper Oxidation in [Re(H107)(W108)AzCu(I)].....         | 168 |
| 6.2. Copper Oxidation in [Re(H107)(W110)AzCu(I)].....         | 176 |
| 6.3. Summary.....   | 182 |
| Chapter 7. Conclusions .....                                  | 185 |
| References .....  | 188 |
| Appendix A.....   | 196 |

|  |     |
|--|-----|
| Section III: Guanine Radical Formation and Electron Transfer in Metal-   |     |
| Modified DNA .....   | 209 |
| Chapter 8. Introduction.....   | 210 |
| Chapter 9. Synthesis and Characterization of Metal-Modified              |     |
| Thymine Complexes and Metal-Modified DNA.....                            | 217 |
| 9.1. Metal-modified Thymine Complexes.....                               | 217 |
| 9.2. Metal-modified DNA .....  | 228 |
| 9.3. Experimental.....   | 238 |
| 9.3.1. Thymine Complexes .....   | 238 |
| 9.3.2. Metallated DNA .....  | 250 |
| Chapter 10. Generation of a Guanine Radical in Single Stranded DNA ..... | 254 |
| 10.1. Photophysics of <b>4</b> .....                                     | 254 |
| 10.2. Photophysics of Metallated DNA .....                               | 262 |
| Chapter 11. Conclusions .....  | 269 |
| References.....  | 271 |



## LIST OF FIGURES AND TABLES

## Section I. General Considerations

|   | <i>Page</i> |
|---|-------------|
| Chapter 1. Thesis Summary and Theoretical Background                            |             |
| Scheme 1.2-1: Representation of the multi-step mechanism .....                  | 12          |
| Chapter 2. Instrumentation and Experiment Design                                |             |
| Scheme 2.1.1-1: Simplified oxidative flash/quench reaction.....                 | 15          |
| Figure 2.1.2-1: Atmosphere-controlled cuvette .....                             | 19          |
| Figure 2.1.4-1: Simplified diagram of NS1 .....                                 | 22          |
| Figure 2.1.5-1: Simplified diagram of NS2 .....                                 | 25          |
| Figure 2.2.1-1: X-band EPR of [Re(H107)(W08)AzCu(II)] with Co(III) at 77 K..... | 30          |
| Figure 2.2.2-1: Atmosphere-controlled EPR tube .....                            | 31          |

Section II. Tryptophan Radical Formation and Electron Transfer in Rhenium-Modified *Pseudomonas aeruginosa* Azurin

|  | <i>Page</i> |
|--|-------------|
| Chapter 3. Introduction  |             |
| Figure 3.1-1: Crystal structure of the ET pathway in PSII.....                         | 41          |
| Scheme 3.1-1: Proposed mechanism for RNR .....   | 43          |
| Figure 3.2-1: Two views of azurin without a metal.....                                 | 46          |
| Figure 3.2.2-1: Absorption spectra of Re-labeled azurin .....                          | 52          |
| Figure 3.2.2-2: Electron tunneling timetable for Cu(I) to Ru(III) and “Re(II)” .....   | 54          |
| Scheme 3.2.2-1: Multi-step tunneling mechanism .....                                   | 55          |
| Figure 3.2.2-3: Structures of Re-labeled azurins .....                                 | 56          |
| Chapter 4. Synthesis and Characterization of Rhenium-Modified Azurin                   |             |
| Scheme 4.1-1: Synthesis of Re(I)(CO) <sub>3</sub> (phen)(imidazole) [ <b>3a</b> ]..... | 58          |
| Figure 4.1-1: Cyclic voltammetry of <b>3a</b> .....                                    | 59          |

|  |     |
|--|-----|
| Figure 4.1-2: Modified Latimer diagram for <b>3a</b> .....   | 60  |
| Figure 4.1-3: Optical characterization of <b>3a</b> .....  | 62  |
| Figure 4.1-4: Quenching of <b>3a*</b> by Ru(III)(NH <sub>3</sub> ) <sub>6</sub> .....              | 63  |
| Figure 4.1-5: MV <sup>•+</sup> spectra. ....   | 65  |
| Figure 4.1-6: X-band EPR of <b>3a</b> /Co(III) at 77K.....   | 67  |
| Figure 4.1-7: DFT calculations for <b>3a<sup>ox</sup></b> .....                                    | 69  |
| Figure 4.1-8: X-band EPR of <b>3a</b> /Co(III) at 77K, various pH's.....                           | 70  |
| Figure 4.2-1: Purification of W48F/H83Q/Y72F/Q107H/Y108W AzCu(II).....                             | 74  |
| Scheme 4.2-1: Labeling of azurin .....   | 76  |
| Figure 4.2-2: Overlay of azurin crystal structures .....   | 78  |
| Figure 4.2-3: Spectra of Re-labeled azurins .....  | 79  |
| Figure 4.2-4: Quenching of [Re(H107)(W110)AzCu(I)] by Ru(III)(NH <sub>3</sub> ) <sub>6</sub> ..... | 81  |
| Table 4.2-1: Properties of Re-labeled azurins.....   | 83  |
| Figure 4.3.3-1: Sequence for H83Q/W48F/Y72F/Q107H/Y108F .....                                      | 89  |
| Figure 4.3.3-2: Sequence for W48F/Y72F/Y108F .....   | 91  |
| Figure 4.3.3-3: DNA Gel.....   | 94  |
| Figure 4.3.3-4: Sequence for H83Q/W48F/Y72F/Q107H/Y108W .....                                      | 97  |
| Table 4.3.4-1: FPLC gradient for unlabeled protein purification by Mono-Q .....                    | 100 |
| Table 4.3.4-2: FPLC gradient for unlabeled protein purification by Mono-S .....                    | 101 |
| Table 4.3.4-3: Mass spectra for unlabeled azurin mutants .....                                     | 103 |
| Table 4.3.6-1: FPLC gradient for Re-labeled azurin purification by Mono-S.....                     | 107 |
| Table 4.3.6-2: Mass spectra for Re-labeled azurin mutants .....                                    | 108 |
| Table 4.3.6-3: FPLC gradient for separation of Zn(II) and Cu(II) azurin.....                       | 109 |
| Figure 4.3.6-1: FPLC separation of Zn(II) and Cu(II) azurin .....                                  | 110 |
| Figure 4.3.6-2: UV/Vis absorption of metal removal from [Re(H83)(W48)AzM].....                     | 112 |
| <b>Chapter 5. Tryptophan Radicals</b>  |     |
| Figure 5.1-1: Schematic of a one-electron oxidation of tryptophan .....                            | 116 |
| Figure 5.1-2: X-band EPR of W <sup>•</sup> in a dipeptide.....                                     | 119 |
| Figure 5.1-3: NS1 transient absorption spectra of W <sup>•</sup> in a dipeptide .....              | 121 |

|  |     |
|--|-----|
| Figure 5.1-4: NS2 spectra of W <sup>•</sup> .....  | 122 |
| Figure 5.2.1-1: Tryptophan fluorescence .....  | 127 |
| Figure 5.2.1-2: X-band EPR of [Re(H83)WTazZn(II)]/Co(III) at 100 K .....                               | 128 |
| Figure 5.2.1-3: NS2 spectrum, [Re(H83)WTazZn(II)]/Co(III) .....  | 129 |
| Figure 5.2.1-4: X-band EPR of [Re(H83)(W48)AzZn(II)] with Co(III) at 77 K .....                        | 130 |
| Figure 5.2.1-5: NS2 spectrum, [Re(H83)(W48)AzZn(II)] with Co(III) .....                                | 132 |
| Figure 5.2.1-6: NS2 comparison of radical spectra at 20 $\mu$ s after excitation .....                 | 133 |
| Figure 5.2.1-7: NS1 transient absorption, [Re(H83)WTazZn(II)]/Co(III) .....                            | 134 |
| Figure 5.2.1-8: NS1 transient absorption, [Re(H83)(W48)AzZn(II)]/Ru(III) .....                         | 136 |
| Figure 5.2.2-1: Two different tryptophan-108 environments .....  | 137 |
| Figure 5.2.2-2: Tryptophan fluorescence .....  | 139 |
| Figure 5.2.2-3: X-band EPR of [Re(H107)(W108)AzZn(II)]/Co(III) at 77K .....                            | 140 |
| Figure 5.2.2-4: X-band EPR of [Re(H107)(W108)AzZn(II)]/Co(III), aerated .....                          | 141 |
| Figure 5.2.2-5: EPR decay of W108 <sup>•</sup> at room temperature .....                               | 143 |
| Figure 5.2.2-6: NS2 spectrum of [Re(H107)(W108)AzZn(II)]/Co(III) .....                                 | 144 |
| Figure 5.2.2-7: NS2 spectrum of [Re(H107)(W108)AzZn(II)]/Co(III), various pH's .....                   | 145 |
| Figure 5.2.2-8: NS1 transient absorption, [Re(H107)(W108)AzZn(II)]/Co(III) .....                       | 146 |
| Figure 5.2.2-9: X-band EPR of [Re(H107)(W108)AzCu(II)]/Co(III) at 77 K .....                           | 148 |
| Figure 5.2.2-10: X-band EPR of [Re(H107)(W108)AzCu(II)]/Co(III)/Mo(IV) .....                           | 150 |
| Figure 5.2.3-1: Tryptophan fluorescence .....  | 153 |
| Figure 5.2.3-2: X-band EPR of [Re(H107)(W110)AzZn(II)]/Co(III) .....                                   | 154 |
| Figure 5.2.3-3: X-band EPR decay of [Re(H107)(W110)AzZn(II)]/Co(III) .....                             | 155 |
| Figure 5.2.3-4: NS2 spectrum, [Re(H107)(W110)AzZn(II)]/Co(III) .....                                   | 156 |
| Figure 5.2.3-5: NS2 spectra, [Re(H107)(W110)AzZn(II)]/Co(III), various pH's .....                      | 157 |
| Figure 5.2.3-6: NS1 transient absorption, [Re(H107)(W110)AzZn(II)]/Co(III) .....                       | 158 |
| Figure 5.2.3-7: NS1 transient absorption, [Re(H107)(W110)AzZn(II)]/Co(III) .....                       | 160 |
| Figure 5.3-1: NS2 spectra, W48 <sup>•</sup> , W108 <sup>•</sup> , W110 <sup>•</sup> , comparison ..... | 162 |
| Figure 5.3-2: Normalized fluorescence spectra .....  | 163 |

## Chapter 6. Copper Oxidation in Re-labeled Azurins

|  |     |
|--|-----|
| Figure 6-1: Relevant ET pathways .....   | 166 |
| Figure 6.1-1: NS1 transient absorption, [Re(H107)(W108)AzCu(I)]/Ru(III) .....      | 170 |
| Figure 6.1-2: NS1 emission spectra, [Re(H107)(W108)AzCu(I)]/Ru(III) .....          | 171 |
| Figure 6.1-3: NS1 spectra, [Re(H107)(W108)AzCu(I)], pH 9.8 .....                   | 172 |
| Scheme 6.1-1: Explanatory mechanism.....   | 173 |
| Figure 6.1-4: Reciprocal plot of concentration of W108 <sup>•</sup> vs. time ..... | 174 |
| Figure 6.2-1: NS1 transient absorption, [Re(H107)(W110)AzCu(I)]/Ru(III) .....      | 177 |
| Figure 6.2-2: Rate constants for Cu(I) oxidation in [Re(H107)(W110)AzCu(I)] .....  | 179 |
| Figure 6.2-3: NS1 transient absorption, [Re(H107)(W110)AzCu(I)]/Ru(III) .....      | 181 |
| Figure 6.3-1: Kinetics of Cu(I) oxidation by “Re(II)” .....                        | 183 |
| <b>Appendix A. Protein Mutation and Purification</b>                               |     |
| Table A-1: FPLC purification of unlabeled protein on a Mono-S column.....          | 196 |
| Table A-2: FPLC purification of labeled protein by IMAC column .....               | 197 |
| Table A-3: FPLC purification of labeled protein on a Mono-S column.....            | 197 |
| Figure A-1: Sequence data for H83Q/W48F/Y72F/Q107H/Y108W .....                     | 198 |
| Figure A-2: Sequence for Y72F/Y108F .....  | 199 |
| Figure A-3: FPLC purification of H83Q/W48F/Y72F/Q107H/Y108W, Mono-S.....           | 200 |
| Figure A-4: FPLC purification of [Re(H107)(W108)AzCu(II)], IMAC .....              | 201 |
| Figure A-5: FPLC purification of [Re(H107)(W108)AzCu(II)], Mono-S .....            | 202 |
| Figure A-6: FPLC purification of H83Q/W48F/Y72F/Q107H/Y108F/F110W .....            | 203 |
| Figure A-7: FPLC purification of [Re(H107)(W110)AzCu(II)], IMAC .....              | 204 |
| Figure A-8: FPLC purification of [Re(H107)(W110)AzCu(II)], Mono-S .....            | 205 |
| Figure A-9: FPLC purification of Y72F/Y108F, Mono-S .....                          | 206 |
| Figure A-10: FPLC purification of [Re(H83)(W48)AzCu(II)], IMAC .....               | 207 |
| Figure A-11: FPLC purification of [Re(H83)(W48)AzCu(II)], Mono-S .....             | 208 |

## Section III. Guanine Radical Formation and Electron Transfer in Metal-Modified DNA

### Page

## Chapter 9. Synthesis and Characterization of Metal-Modified Thymine Complexes and Metal-Modified DNA

|   |     |
|---|-----|
| Scheme 9.1-1: Synthesis of acceptor and donor ruthenium complexes.....                  | 218 |
| Scheme 9.1-2: Synthesis of a new ruthenium donor and new rhenium acceptors .....        | 219 |
| Table 9.1-1: Selected physical data for metal-labeled thymine complexes.....            | 220 |
| Figure 9.1-1: Crystal structure of compound <b>9</b> .....                              | 221 |
| Figure 9.1-2: Absorption spectra of <b>6</b> .....                                      | 223 |
| Figure 9.1-3: CV data for <b>6</b> in water.....  | 225 |
| Figure 9.1-4: Absorption spectra of <b>4</b> , <b>8</b> , <b>9</b> .....                | 227 |
| Scheme 9.2-1: Synthesis of single-stranded DNA incorporating complex <b>4</b> .....     | 229 |
| Figure 9.2-1: Non-metallated DNA strands.....   | 230 |
| Figure 9.2-2: Enzyme digestion HPLC traces .....  | 232 |
| Figure 9.2-3: CD spectra of the double stranded DNA <b>13/15</b> and <b>17/15</b> ..... | 234 |
| Figure 9.2-4: CD spectra of the double stranded DNA <b>12/14</b> and <b>16/14</b> ..... | 236 |
| Figure 9.2-5: CD spectra of the double stranded DNA <b>12/14</b> .....                  | 237 |

## Chapter 10. Generation of a Guanine Radical in Single Stranded DNA

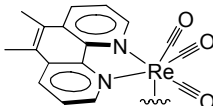
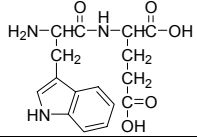
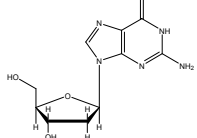
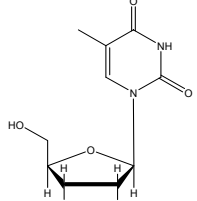
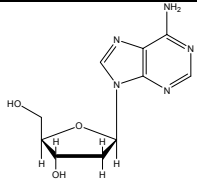
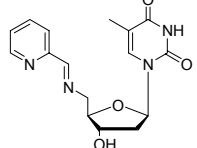
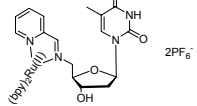
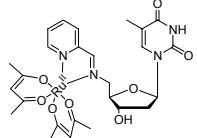
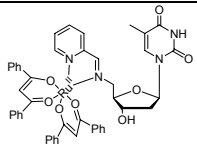
|  |     |
|--|-----|
| Figure 10.1-1: Schematic representation of the flash/quench .....        | 255 |
| Figure 10.1-2: NS1 emission spectra, <b>4</b> .....                      | 257 |
| Figure 10.1-3: NS1 transient absorption, <b>4</b> .....                  | 258 |
| Figure 10.1-4: Flash/quench/freeze X-band EPR of <b>4</b> .....          | 260 |
| Figure 10.1-5: Comparison of flash/quench/freeze X-band EPR spectra..... | 261 |
| Figure 10.2-1: NS1 emission spectra, <b>13</b> .....                     | 263 |
| Figure 10.2-2: NS1 transient absorption <b>13</b> .....                  | 264 |
| Figure 10.2-3: NS1 emission spectra, <b>13/15</b> .....                  | 265 |
| Figure 10.2-4: NS1 transient absorption, <b>13/15</b> .....              | 266 |

|   |     |
|---|-----|
| Figure 10.2-5: Comparison of X-band EPR spectra at 77K..... | 268 |
|---|-----|

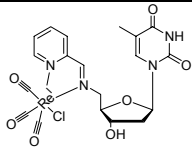
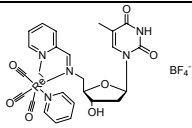
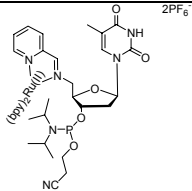
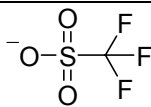

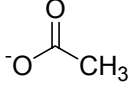
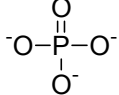
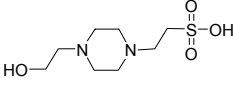
## ABBREVIATIONS

## Chemicals

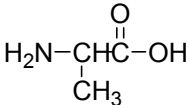
| Abbreviation   | Full Name   | Structure |
|--|---|-----------|
| $\text{Co(III)(NH}_3)_5\text{Cl} \bullet 2\text{Cl}$   | cobalt pentamine chloride, chloride salt                                  |           |
| $\text{Co(II)(H}_2\text{O)}_6$   | hexaquo cobalt(II)  |           |
| $\text{Ru(III)(NH}_3)_6 \bullet 3\text{Cl}$  | ruthenium hexamine, chloride salt   |           |
| $\text{MV}^{2+} \bullet 2\text{Cl}$  | methylviologen, (paraquat), N,N-dimethyl-4,4'-bipyridinium, chloride salt |           |
| $\text{MV}^{+\bullet}$   | methylviologen radical cation   |           |
| phen   | 1,10-phenanthroline   |           |
| dmphen   | 4,7-dimethyl-1,10-phenanthroline  |           |
| bpy  | 2,2'-bipyridine   |           |
| $\text{Ru(II)(bpy)}_3 \bullet 2\text{Cl}$  | ruthenium tris-(2,2'-bipyridine)  |           |
| $[\text{Re(I)(CO)}_3(\text{phen})(\text{imidazole})_2] \bullet 2\text{SO}_4$<br>(Section II, <b>3a</b> ) | rhenium tricarbonyl (dimethyl-1,10-phenanthroline) imidazole              |           |

|                                       |   |   |
|---------------------------------------|---|---|
| Re(I)(CO) <sub>3</sub> (dmphen)       | rhodium tricarbonyl (4,7-dimethyl-1,10-phenanthroline)  |    |
| Trp-Glu                               | Tryptophan-Glutamate  |    |
| Gu (G)                                | guanine   |    |
| Th (T)                                | thymine   |    |
| Ad (A)                                | Adenine   |   |
| T <sub>impy</sub><br>(Section III, 3) | 1-(4-hydroxy-5-[(pyridine-2ylmethylene)-amino]-methyl]-tetrahydrofuran-2-yl)-5-methyl-1H-pyrimidine-2,4-dione   |  |
| Section III, 4                        | bis (2,2'-bipyridine) ruthenium (1-(4-hydroxy-5-[(pyridine-2ylmethylene)-amino]-methyl]-tetrahydrofuran-2-yl)-5-methyl-1H-pyrimidine-2,4-dione) bis hexafluorophosphate |  |
| Section III, 6                        | bis (acetylacetonate) ruthenium (1-(4-hydroxy-5-[(pyridine-2ylmethylene)-amino]-methyl]-tetrahydrofuran-2-yl)-5-methyl-1H-pyrimidine-2,4-dione)                         |  |
| Section III, 8                        | bis (benzylbenzoate) ruthenium (1-(4-hydroxy-5-[(pyridine-2ylmethylene)-amino]-methyl]-tetrahydrofuran-2-yl)-5-methyl-1H-pyrimidine-2,4-dione)                          |  |



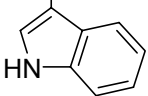
|                        |   |   |
|------------------------|---|---|
| Section III, <b>9</b>  | rhenum tricarbonyl (1-(4-hydroxy-5-[(pyridine-2ylmethylene)-amino]-methyl)-tetrahydrofuran-2-yl)-5-methyl-1H-pyrimidine-2,4-dione) chloride   |    |
| Section III, <b>10</b> | rhenum tricarbonyl pyridine (1-(4-hydroxy-5-[(pyridine-2ylmethylene)-amino]-methyl)-tetrahydrofuran-2-yl)-5-methyl-1H-pyrimidine-2,4-dione) tetrafluoro borate  |    |
| Section III, <b>13</b> | bis (2,2'-bipyridine) ruthenium (1-(4-hydroxy-5-[(pyridine-2ylmethylene)-amino]-methyl)-tetrahydrofuran-2-yl)-5-methyl-1H-pyrimidine-2,4-dione) diisopropyl-phosphoramidous acid 2-cyano-ethyl ester bis hexfluorophosphate |    |
| OTf <sup>-</sup>       | triflate (trifluoromethane sulfonate)   |   |
| THF                    | tetrahydrofuran   |  |
| OAc                    | acetate   |  |
| Pi                     | phosphate   |  |
| HEPES                  | 2-[4-(2-Hydroxy-ethyl)-piperazin-1-yl]-ethanesulfonic acid  |  |

## Amino-Acids

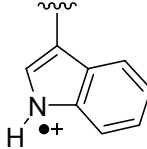
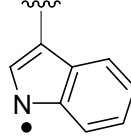
| Abbreviation 1 | Abbreviation 2 | Name    | Strucutre   |
|----------------|----------------|---------|---|
| A              | Ala            | Alanine |  |

|   |     |               |   |
|---|-----|---------------|---|
| C | Cys | Cysteine      | $  \begin{array}{c}  \text{O} \\  \parallel \\  \text{H}_2\text{N}-\text{CH}-\text{C}-\text{OH} \\    \\  \text{CH}_2 \\    \\  \text{SH}  \end{array}  $   |
| D | Asp | Aspartic Acid | $  \begin{array}{c}  \text{O} \\  \parallel \\  \text{H}_2\text{N}-\text{CH}-\text{C}-\text{OH} \\    \\  \text{CH}_2 \\    \\  \text{C}=\text{O} \\    \\  \text{OH}  \end{array}  $   |
| E | Glu | Glutamic Acid | $  \begin{array}{c}  \text{O} \\  \parallel \\  \text{H}_2\text{N}-\text{CH}-\text{C}-\text{OH} \\    \\  \text{CH}_2 \\    \\  \text{CH}_2 \\    \\  \text{C}=\text{O} \\    \\  \text{OH}  \end{array}  $                   |
| F | Phe | Phenylalanine | $  \begin{array}{c}  \text{O} \\  \parallel \\  \text{H}_2\text{N}-\text{CH}-\text{C}-\text{OH} \\    \\  \text{CH}_2 \\    \\  \text{C}_6\text{H}_5  \end{array}  $  |
| G | Gly | Glycine       | $  \begin{array}{c}  \text{O} \\  \parallel \\  \text{H}_2\text{N}-\text{CH}-\text{C}-\text{OH} \\    \\  \text{H}  \end{array}  $  |
| H | His | Histidine     | $  \begin{array}{c}  \text{O} \\  \parallel \\  \text{H}_2\text{N}-\text{CH}-\text{C}-\text{OH} \\    \\  \text{CH}_2 \\    \\  \text{C}_4\text{H}_3\text{N}_2  \end{array}  $  |
| I | Ile | Isoleucine    | $  \begin{array}{c}  \text{O} \\  \parallel \\  \text{H}_2\text{N}-\text{CH}-\text{C}-\text{OH} \\    \\  \text{CHCH}_3 \\    \\  \text{CH}_2 \\    \\  \text{CH}_3  \end{array}  $   |
| K | Lys | Lysine        | $  \begin{array}{c}  \text{O} \\  \parallel \\  \text{H}_2\text{N}-\text{CH}-\text{C}-\text{OH} \\    \\  \text{CH}_2 \\    \\  \text{CH}_2 \\    \\  \text{CH}_2 \\    \\  \text{CH}_2 \\    \\  \text{NH}_2  \end{array}  $ |

|   |     |            |  |
|---|-----|------------|--|
| L | Leu | Leucine    | $  \begin{array}{c}  \text{O} \\  \parallel \\  \text{H}_2\text{N}-\text{CH}-\text{C}-\text{OH} \\    \\  \text{CH}_2 \\    \\  \text{CHCH}_3 \\    \\  \text{CH}_3  \end{array}  $  |
| M | Met | Methionine | $  \begin{array}{c}  \text{O} \\  \parallel \\  \text{H}_2\text{N}-\text{CH}-\text{C}-\text{OH} \\    \\  \text{CH}_2 \\    \\  \text{CH}_2 \\    \\  \text{S} \\    \\  \text{CH}_3  \end{array}  $   |
| N | Asn | Asparagine | $  \begin{array}{c}  \text{O} \\  \parallel \\  \text{H}_2\text{N}-\text{CH}-\text{C}-\text{OH} \\    \\  \text{CH}_2 \\    \\  \text{C}=\text{O} \\    \\  \text{NH}_2  \end{array}  $  |
| P | Pro | Proline    | $  \begin{array}{c}  \text{O} \\  \parallel \\  \text{C}-\text{OH} \\    \\  \text{HN} \quad \text{Cyclopentane ring}  \end{array}  $  |
| Q | Gln | Glutamine  | $  \begin{array}{c}  \text{O} \\  \parallel \\  \text{H}_2\text{N}-\text{CH}-\text{C}-\text{OH} \\    \\  \text{CH}_2 \\    \\  \text{CH}_2 \\    \\  \text{C}=\text{O} \\    \\  \text{OH}  \end{array}  $  |
| R | Arg | Arginine   | $  \begin{array}{c}  \text{O} \\  \parallel \\  \text{H}_2\text{N}-\text{CH}-\text{C}-\text{OH} \\    \\  \text{CH}_2 \\    \\  \text{CH}_2 \\    \\  \text{CH}_2 \\    \\  \text{NH} \\    \\  \text{C}=\text{NH} \\    \\  \text{NH}_2  \end{array}  $ |
| S | Ser | Serine     | $  \begin{array}{c}  \text{O} \\  \parallel \\  \text{H}_2\text{N}-\text{CH}-\text{C}-\text{OH} \\    \\  \text{CH}_2 \\    \\  \text{OH}  \end{array}  $  |
| T | Thr | Threonine  | $  \begin{array}{c}  \text{O} \\  \parallel \\  \text{H}_2\text{N}-\text{CH}-\text{C}-\text{OH} \\    \\  \text{CHOH} \\    \\  \text{CH}_3  \end{array}  $  |

|   |     |            |   |
|---|-----|------------|---|
| V | Val | Valine     | $\begin{array}{c} \text{O} \\ \parallel \\ \text{H}_2\text{N}-\text{CH}-\text{C}-\text{OH} \\   \\ \text{CHCH}_3 \\   \\ \text{CH}_3 \end{array}$   |
| W | Trp | Tryptophan | $\begin{array}{c} \text{O} \\ \parallel \\ \text{H}_2\text{N}-\text{CH}-\text{C}-\text{OH} \\   \\ \text{CH}_2 \\   \\ \text{HN} \end{array}$  |
| Y | Tyr | Tyrosine   | $\begin{array}{c} \text{O} \\ \parallel \\ \text{H}_2\text{N}-\text{CH}-\text{C}-\text{OH} \\   \\ \text{CH}_2 \\   \\ \text{C}_6\text{H}_4 \\   \\ \text{OH} \end{array}$  |

### Tryptophan Radicals

| Abbreviation          | Name                      | Structure   |
|-----------------------|---------------------------|---|
| $\text{W}^{\bullet+}$ | tryptophan radical cation |  |
| $\text{W}^{\bullet}$  | tryptophan radical        |  |

### Protein Systems

| Abbreviation | Name                                  |
|--------------|---------------------------------------|
| Az           | <i>Pseudomonas aeruginosa</i> azurin. |
| RNR          | ribonucleotide reductase              |
| PS(II)       | photosystem II                        |

### Kinetic and Physical Parameters and Abbreviations

| Term                        | Explanation   |
|-----------------------------|---|
| $k \text{ (s}^{-1}\text{)}$ | Unimolecular rate constant for reactions $\text{A} \rightarrow$ |

|                               |   |
|-------------------------------|---|
|                               | products. From the rate equation $-\frac{d[A]}{dt} = k[A]$  |
| $k$ ( $M^{-1}s^{-1}$ )        | Bimolecular rate constant for reactions $A + B \rightarrow$ products. From the rate equation $-\frac{d[A]}{dt} = k[A][B]$   |
| $\tau$                        | Lifetime (half life) of a unimolecular reaction, $\frac{1}{k} = \tau$   |
| MLCT                          | Metal to Ligand Charge Transfer. Absorption feature due to promotion of an electron from a metal centered molecular orbital to a ligand centered molecular orbital. |
| $\beta$ ( $\text{\AA}^{-1}$ ) | Distance decay factor for ET at the non-adiabatic limit. See Chapter 1  |
| $g$                           | $g$ tensor for an unpaired electron. Value from the spin Hamiltonian describing the interaction of an unpaired electron with an external magnetic field.            |
| ET                            | Electron Transfer   |
| UB                            | Uniform barrier model for electron transfer. See Chapter 1  |
| TP                            | Tunneling pathway model for electron transfer. See Chapter 1.   |
| <b>A</b>                      | Electron acceptor in an ET reaction.  |
| <b>B</b>                      | Bridge between donor and acceptor in an ET reaction.  |
| <b>D</b>                      | Electron donor in an ET reaction.   |

## Experimental Techniques

| Abbreviation        | Name                                   | Description  |
|---------------------|--|--|
| flash/quench        | oxidative flash/quench                 | see Chapter 2  |
| flash/quench/freeze | oxidative flash/quench/freeze          | see Chapter 2  |
| EPR                 | Electron Paramagnetic Resonance        | Microwave absorption spectroscopy of unpaired electrons in a magnetic field.                   |
| ENDOR               | Electron-Nuclear Double Resonance      | EPR spectroscopy allowing resolution of the unpaired electron interactions with nearby nuclei. |
| ESEEM               | Electron Spin Echo Envelope Modulation | EPR technique to resolve hyperfine couplings to the  |

|           |  |   |
|-----------|--|---|
|           |  | unpaired electron.  |
| MALDI-TOF | Matrix Assisted Laser Desorption Ionization-Time-of-Flight mass spectroscopy | Samples are trapped in a matrix and then vaporized along with the matrix by a laser. The fragments of this process are identified by time-of-flight mass spectroscopy |
| ESI-MS    | Electro-Spray Ionization Mass Spectroscopy                                   | Molecules fragmented by passage through a high voltage field are analyzed by mass spectroscopy.   |

## Experimental Apparatus

| Abbreviation | Name         | Description  |
|--------------|--------------|--|
| NS1          | Nanosecond-1 | Single-wavelength time-resolved spectrometer. See Chapter 2. |
| NS2          | Nanosecond-2 | Broad-band time-resolved spectrometer. See Chapter 2.        |

## Mutation Notation

In Section II, mutations to the sequence of azurin are recorded in the following fashion: the single letter of the wild-type amino-acid is followed immediately by the single letter of the replacement amino-acid. So, H83Q is an abbreviation for replacement of histidine at position 83 with glutamine by site-directed mutagenesis.

Rhenium labeling of these mutants is described in detail in Chapter 4. The rhenium fragment labels at surface histidines on the azurin. With this in mind, the various mutants are described by the general formula  $[\text{Re}(\text{HX})(\text{N})\text{AzM}]$  where X is the position of the histidine, N is the relevant intervening amino-acid configuration, usually either a single

tryptophan (W) or tyrosine (Y) or the wild-type protein (WT). M is the metal coordinated to C112, usually either zinc (Zn) or copper (Cu); M is followed by the formal oxidation state, e.g., Cu(I) or Zn(II).

## **I. General Considerations**



## *Chapter 1*

### **THESIS SUMMARY AND THEORETICAL BACKGROUND**

#### **1.1. Thesis Summary**

This thesis encompasses work on metal-modified DNA and rhenium-labeled *Pseudomonas aeruginosa* azurin with the goal of understanding the nature and scope of long-range electron transfer (ET) in biological systems [1, 2]. This is a topic that has been probed extensively over the last several years leading to a number of explanations for long-range charge transfer in both DNA and proteins. Primarily, this event seems to be the product of transfer through a sigma bond network: the sugar backbone in DNA or the peptide backbone in proteins. This explanation fails to fully account for the observed distances traversed by electrons on short timescales in both natural and modified biological molecules. To address this issue, a modification of the existing model, multi-step electron transfer has been proposed. The multi-step mechanism in biological systems can be described as the transfer of electrons mediated by intermediate charge carriers, often a nucleobase or amino-acid centered radical [3, 4]. In the interest of more fully understanding the multi-step mechanism, organic radical formation in DNA and azurin as potential charge carriers has been investigated.

The studies of electron transfer in both metal-modified DNA proteins are intimately linked to one another by the many interfaces in nature between proteins and DNA. For one, the bio-synthesis of DNA relies on the action of ribonucleotide reductase, an enzyme which functions by production of a cysteine radical (perhaps through a multi-step ET reaction [5]) in the reduction of ribonucleotides to deoxyribonucleotides [6]. Another important interface of DNA and proteins is the various repair, and damage prevention mechanisms that may be operating on DNA. DNA lesions (often caused by free radicals [7]) are repaired by a large class of enzymes, some of which apparently employ radicals to transfer the necessary charge for repair of this damage [8].<sup>1</sup> In order to fully treat both elements of this research, this thesis is organized into three general sections.

Section I covers the fundamental framework in which these investigations were carried out. Chapter 1 is devoted to a discussion of the theoretical basis for ET in biological systems. The general theory to describe these reactions is semiclassical electron transfer theory. Of central importance is a modification of that theory referred to as the multi-step mechanism. These underlying precepts shape the rest of the investigations in this thesis. Chapter 2 covers the experimental apparatus and technique used to discover the properties of metal-modified biological molecules.

Section II is a thorough treatment of the formation of tryptophan radicals and their role (or lack thereof) in copper oxidation in rhenium-labeled azurins. Chapter 3 is intended to introduce the natural and unnatural protein systems that exhibit long-range electron transfer and radical formation in the course of their function. Chapter 4 covers the

---

<sup>1</sup> For a detailed discussion of these protein-DNA interactions, see Chapter 3 and Chapter 8.

construction and characterization of Re-labeled azurins and the basic photophysics of these molecules and related model compounds. Chapter 5 discusses the formation of tryptophan radicals in three separate Re-labeled azurin mutants. In this chapter, issues regarding the longevity of the photogenerated radicals are reviewed. Of particular interest is the unusually long lifetimes of the radicals generated in the folded polypeptide: the hydrophobically encapsulated tryptophan radical generated at position 48 apparently lasts on the order of 30 min at room temperature, while the more exposed radical at position 108 persists for more than 5 hrs at room temperature. These results are particularly interesting in light of the microsecond lifetime of tryptophan radicals generated in monomers in aqueous media [9]; showing nature's ability to control reactive intermediates by formation of the appropriate peptide environment. In addition to the persistence of these radicals, absorption features of the one-electron oxidized tryptophans are fully discussed. It appears that the absorption features (and therefore the electronic structure) of tryptophan radicals are strongly dependent on protein environment, showing a variation of  $\lambda_{\text{max}}$  for the absorption band of at least 50 nm. Chapter 6 covers the attempts to make these radicals participate in the oxidation of the remote copper center in azurin. The tryptophan radical at position 108 apparently shuts down ET from the Cu(I) to the oxidized tryptophan, due presumably to the massively inert nature of the radical. A radical generated at position 110, on the other hand, fails to participate at all in the oxidation of Cu(I). This reaction most likely proceeds by another radical mediated event (see the thesis of W. Wehbi [10]). The ultimate lesson learned here is that amino-acid radicals must be perfectly tuned by the

protein environment to participate meaningfully in charge transfer. Chapter 7 collects these results and puts them in the proper context.

Section III is a discussion of (i) the synthesis of metal-thymine complexes and ruthenium modified DNA strands and (ii) the production of guanine radicals in DNA strands. Chapter 8 covers the fertile field of electron transfer in DNA, along with the emerging consensus that a multi-step mechanism (mediated by guanine radicals) is the appropriate description of long-range ET in DNA. Chapter 9 details synthetic strategies employed in constructing thymine-ruthenium and rhenium complexes and their subsequent incorporation in strands of DNA. The properties of these modified DNA strands are covered in some detail, including higher order structure. Chapter 10 discusses the formation of a guanine radical in single stranded DNA and the implications that this event holds for using such constructs to understand ET in DNA. Of particular interest is the effect of radical formation on the photophysical properties of the constructs. Chapter 11 collects these results and demonstrates the foundation of a system in which multi-step and single step electron transfer could be studied in parallel.

## 1.2. *Semiclassical Electron Transfer Theory and the Multi-step Mechanism*

Electron transfer is a key component of a great variety of biological processes [1]; particularly in proteins (Chapter 3). These reactions are useful in biological systems only if they are (i) sufficiently controlled and (ii) sufficiently rapid. That is, to meet the demands of biological ET, charge transfer events must only occur between well-defined locations as a result of the appropriate stimulus and they need to happen rapidly enough to contribute to important biological reactions. These conditions are met in a number of systems: for example, photosystem II (PSII) exhibits ET as a result of light absorption over distances as far as 24 Å on a short ( $\mu$ s) timescale [11]. How biological molecules modulate ET over these long distances is an area of intense research [12]; in fact it is this question that underlies the research presented in this thesis. In order to fully understand the relevant issues involved in the study of ET in biological molecules, a brief review of the theoretical underpinnings for this event is necessary. To that end, a discussion of semiclassical ET theory and the perturbations introduced by a multi-step mechanism follows.

Efforts to explain electron transfer between a donor (**D**) and acceptor (**A**) have been underway for quite a period of time [13]. The central tenet of semiclassical ET theory (SETT) is that the rate of ET between **D** and **A** is dependent upon the temperature ( $T$ ) the reaction driving force ( $-\Delta G^\circ$ , roughly estimated from difference in redox potentials of **D/D**<sup>+</sup> and **A/A**<sup>-</sup>), the reorganization energy ( $\lambda$ , the energy associated with the change in both inner sphere (e.g., ligand) and outer sphere (e.g., solvent) orientation between reactants and product states), and the electronic coupling matrix element ( $H_{AB}$ , the coupling between the

electronic states of the reactants and the electronic states of the products) (Equation 1,  $h$  = Planck's Constant  $k_B$  = Boltzmann's Constant).

$$k_{ET} = \sqrt{\frac{4\pi^3}{h^2 \lambda k_B T}} H_{AB}^2 \exp\left\{-\frac{(\Delta G^0 + \lambda)^2}{4\lambda k_B T}\right\} \quad (1)$$

One of the first things to notice about the relationship in Equation 1 is that it is one-dimensional in vibrational space. That is, the vibrational states of the **D** and **A** are assumed to be relatively unchanged between the reactants and the products. From an examination of this equation, it is clear that the relationship between  $\lambda$  and  $-\Delta G^\circ$  dictates both the transition state parameters and the height of the barrier to ET. At the optimized driving force ( $-\Delta G^\circ = \lambda$ ), rates of ET are referred to as “activationless”; that is, the rate depends only on the electronic interaction of the **D** and **A**. This situation leads to the counterintuitive condition that the rate of reaction does not always increase with an increase in driving force. In fact, as  $-\Delta G^\circ$  increases beyond  $\lambda$  the rates fall off precipitously, leading to the so-called inverted effect (see reference [14] for a discussion).

This balance between  $\lambda$  and  $-\Delta G^\circ$  can be clearly seen from considering ET between Fe(III) and Fe(II) in H<sub>2</sub>O. The exchange reaction between Fe(II)(H<sub>2</sub>O)<sub>6</sub> and Fe(III)(H<sub>2</sub>O)<sub>6</sub> proceeds with  $\tau = 30$  ms even with the two species in direct contact. This is due to the large energy required to rearrange inner sphere ligands and repolarize outer sphere solvent: a 0.14 Å change in the Fe-O distance between Fe(III)/Fe(II) and a significant repolarization of solvent around the complexes contribute to a 2.7 eV  $\lambda$ . Using the contact distance

reorganization energy and extrapolating to separation between ferrous and ferric ions of 20 Å, the time required for the electron to move between the two sites is  $10^{17}$  years. Even if the void is filled with water, that time is still  $2 \times 10^3$  years, far too long to be useful in a biological system [12, 13]. Thus, the fact that ET takes place with comparable  $-\Delta G^\circ$  over  $> 20$  Å in biological systems suggests that nature is manipulating the ET parameters in some way.

One of the primary methods for this control of ET is alteration of  $\lambda$ . Resonance raman investigations of plastocyanin from parsley have shown very little energy ( $\sim 0.2$  eV) is required to reorganize the ligands around the metal center upon a change in redox state between Cu(II) and Cu(I) [15]. Compared with small molecule copper complexes (e.g., for Cu(II)(phen)<sub>2</sub>/Cu(I)(phen)<sub>2</sub>  $\lambda \sim 2$  eV [12, 16]) this energetic requirement is quite small. This has the effect of greatly enhancing electron transfer rates at biologically relevant driving force in the protein over the small molecules.

Along with changes in  $\lambda$ , proteins can increase the rates of ET over long distances by altering  $H_{AB}$ . When **D** and **A** are in direct contact, the coupling is often so strong that the products of the ET reaction (**D**<sup>+</sup> and **A**<sup>-</sup>) are formed every time the transition state is achieved. This is the adiabatic limit for ET, a situation where the charge transfer is independent of  $H_{AB}$ , depending instead on the frequency of motion along the reaction coordinate. On the other hand, when the reactants are well separated in space, **D** and **A** are often poorly coupled (as they are in biological systems) and so the reactants must form the transition state many times before they are converted to the products. With the **D** and **A** separated by a medium treated as a simple square barrier, the rate of electron transfer will

drop off with an exponential dependence on distance, often expressed as a distance decay factor,  $\beta$  (Equation 2). In a vacuum,  $\beta$  is predicted to be  $3.5 \text{ \AA}^{-1}$ , while in tunneling mediated by water  $\beta$  is on the order of  $1.7 \text{ \AA}^{-1}$  [12].

$$H_{AB} = H_{AB}^0 \exp\left\{\left(\frac{\beta}{2}\right) \times R\right\} \quad (2)$$

At the non-adiabatic limit, the direct overlap of the electronic states of the **D** and **A** is small, so the charge transfer reaction must be controlled by the intervening medium. When the **D** and **A** are linked to one another by a series of covalent and/or non-covalent bonds, the medium between the two is often described as a bridge (**B**). Early attempts to understand this electronic coupling treated the **B** as simply a square barrier, with no regard to its composition. From analysis of ET between a cytochrome and the photosynthetic reaction center, the rate of ET was estimated to depend exponentially on distance with  $\beta \sim 1.4 \text{ \AA}^{-1}$  [17]. One formulation of this model holds that the  $\beta$  of  $1.4 \text{ \AA}^{-1}$  is simply the weighted average of the  $\beta$  for ET through a vacuum ( $3.5 \text{ \AA}^{-1}$ ) and the  $\beta$  for ET through atoms ( $0.9 \text{ \AA}^{-1}$ ); with the weighting factor determined by average empty space and average atoms in between the **D** and **A** [18]. Also known as the uniform barrier model (UB), this formulation of ET in biological systems pays no attention to the nature of the individual bridge states beyond their physical dimensions.

Another way to describe ET through a bridge at the non-adiabatic limit is the so-called superexchange model. This model holds that the coupling between **D** and **B** and



between **B** and **A** is the defining factor in determining the nature of  $H_{AB}$ . That is, the total electronic coupling can be understood as the product of the coupling for each **B** site to other **B** sites and to both the **D** and **A**. With this description, ET between **D** and **A** is controlled by perturbations to their wavefunctions by mixing with the bridge wavefunction. The mixing results in a better effective electronic overlap of **D** and **A**, allowing the electron to tunnel through an otherwise substantial barrier. Given the complex networks that connect redox sites in proteins, superexchange had to be altered to treat the various types of bonds along potential pathways; a revision referred to as the tunneling pathway model (TP) [19]. Three kinds of interactions are considered important in this model: covalent bonds, hydrogen bonds and through space contacts; each with a different degree of coupling. Covalent bonds promote the strongest electronic coupling while hydrogen bonds and through space contacts contribute less to the total electronic coupling. Perhaps the central feature of TP is its prediction that the pathway for ET is vitally important. That is, in contrast to UB, this model predicts that the specific sequence of amino-acids (or nucleobases) has a large effect on the rate of electron transfer. Theoretical treatment of protein structure in the TP shows that the coupling through  $\beta$ -strand is more efficient ( $\beta \sim 1 \text{ \AA}^{-1}$ ) than along an  $\alpha$ -helix ( $\beta \sim 2 \text{ \AA}^{-1}$ ), provided that hydrogen bonding does not play a significant role in the charge transfer through the helix [20]. Substantial experimentation on metal-modified proteins support this model, suggesting that the ET pathway is indeed of penultimate importance [12].

In the context of these models, multi-step ET is an important modulator of ET in biological systems. This mechanism can be most easily understood as a series of single step

tunneling events between the **D** and intervening **B**, and then between **B** and **A** (Scheme 1.2-1). This differs from the superexchange mechanism in that the bridge does more than shape the wavefunctions of the **D** and **A**, it becomes an intermediate donor or acceptor. In proteins (and in artificially modified DNA) this typically translates into the formation of radicals in between the primary **D** and **A** (specific examples in both cases can be found in Chapter 3 and Chapter 8). Although some attempts have been made to explain this phenomenon with quantum mechanics [21], the problem is more easily understood in terms of simple kinetics. That is, each step obeys Equation 1, but since the individual steps are over short distances ( $< 14 \text{ \AA}$  for systems with  $\beta \sim 1 \text{ \AA}^{-1}$ ) the charge can move from **D** to **A** in a reasonable time frame, displaying an apparent distance dependence value much lower than the  $\beta$  of the individual steps. The other problem that multi-step ET can overcome is the reduction of rate due to a  $-\Delta G^\circ$  in the inverted region. If the redox difference between **D** and **A** is much larger than  $\lambda$ , then the time for charge transfer should be quite long. The protein can solve this problem by forming intermediate charged states. If the intermediate oxidized or reduced **B** state had a higher redox potential than **A**, the individual steps would be in a non-inverted region of the Marcus curve allowing the entire reaction to proceed at a reasonable rate.



**Scheme 1.2-1:** Representation of the multi-step mechanism. (**D**) electron donor (**B**) intervening bridge (**A**) electron acceptor.

## *Chapter 2*

# **INSTRUMENTATION AND EXPERIMENT DESIGN**

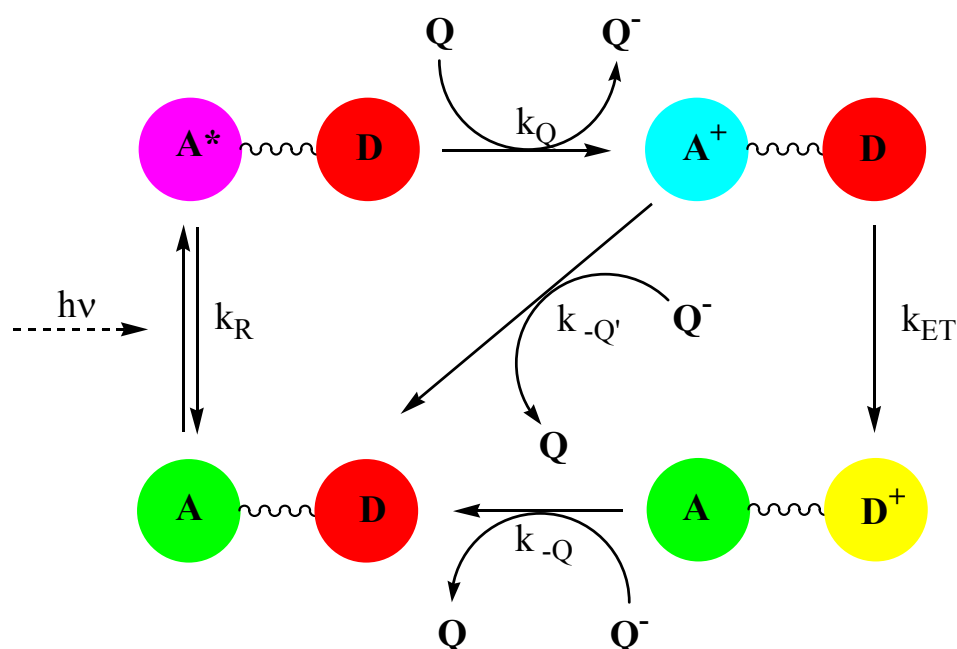
### **2.1. *Laser Experiments***

The primary method I have employed for observation of the kinetic processes involved in charge transfer and radical formation in biological molecules is time-resolved laser spectroscopy. All of the equipment used for these experiments came from the Beckman Institute Laser Resource Center (BILRC) directed by Dr. Jay Winkler. For purely kinetic measurements, a spectrometer designated as nanosecond 1 (NS1) was used. For broad-band absorption spectra at short timescales, a spectrometer designated as nanosecond 2 (NS2) was used. Detailed descriptions of the instruments, as well as the sample preparation and experiment design follow.

#### **2.1.1. *The Flash/Quench Experiment***

In order to study charge transfer in DNA and azurin, a method for inducing a change in the redox states is necessary. One of the most efficacious methods of quickly inducing a change in redox states is the so-called flash/quench technique [22]. This method employs

irradiation of a molecule to a reactive excited state. The excited state can then interact with an exogenous electron donor (reductive flash/quench) or an exogenous electron acceptor (oxidative flash/quench). Commonly, the exogenous electron donor or acceptor is referred to as a quencher, because it causes an observable decrease in the lifetime of the excited state of the putative donor or acceptor. In the systems at issue here, the oxidative flash/quench is used exclusively; hereafter referred to as simply the flash/quench. In this schema, the photo-oxidized molecule is conventionally referred to as the acceptor; that is, it will ultimately receive an electron for some kind of donor molecule. After the flash/quench, the acceptor can then either react with the reduced quencher or with another electron donor in the system. For both the metal-modified azurins (Section II) and metal-modified DNA (Section III), the acceptor is covalently attached to a bridge between it and a suitable electron partner (either a organic nucleobase/amino acid or a redox active metal center). A representation of this experiment can be found in Scheme 2.1.1-1. Several features of this kinetic scheme are important. First, the bimolecular quenching reaction must be able to out-compete relaxation of the excited state to the ground state. That is, the quencher must be able to oxidize the excited state before it can return to the relatively unreactive ground state by radiative and non-radiative decay pathways. In practice, this requires  $k_R < \sim 4 \times 10^7 \text{ s}^{-1}$ , or a lifetime greater than 25 ns. This requirement comes in large part because the biological systems at study here are often sensitive to the ionic strength of the solutions they are dissolved in. Thus, even given a near-diffusion controlled quenching rate of  $k_Q \sim 1 \times 10^{10} \text{ M}^{-1} \text{ s}^{-1}$ , effective quenching an excited state (which may comprise 1% of the possible acceptors) in a solution of 20  $\mu\text{M}$  acceptor would require 16 mM quencher (75%



**Scheme 2.1.1-1:** Simplified oxidative flash/quench reaction between a covalently linked donor [D] and acceptor [A] with an oxidative quencher [Q]. (●) ground state of A (●) ground state of D (●) excited state of A [ $A^*$ ] (●) one-electron oxidized A [ $A^+$ ] (●) one-electron oxidized D [ $D^+$ ]. Rate constants:  $k_R$ , relaxation of  $A^*$  to A;  $k_Q$  oxidation of  $A^*$  to  $A^+$  by quencher [Q];  $k_{-Q'}$  reduction of  $A^+$  by reduced quencher [ $Q^-$ ];  $k_{ET}$  oxidation of D by  $A^+$ ;  $k_{-Q}$  reduction of  $D^+$  by  $Q^-$ .

quenching), a potentially large contribution to the ionic strength of a solution. A second necessity is that the recombination between the reduced quencher and the oxidized acceptor needs to be slower than the oxidation of the donor by the acceptor. Given the small quantities of  $\mathbf{A}^+$  and  $\mathbf{Q}^-$  generated, this is typically not a problem (for an exception, see Chapter 6). To continue the example conditions above, assuming 75% of the excited molecules are quenched, there would be  $0.15\ \mu\text{M}$   $\mathbf{A}^+$  and  $\mathbf{Q}^-$  in solution. Assuming, once again, near diffusion controlled back reaction,  $k_{-Q} \sim 1 \times 10^{10}\ \text{M}^{-1}\text{s}^{-1}$ , the rate is on the order of  $200\ \mu\text{M/s}$ . Comparing this to a donor oxidation with  $k_{\text{ET}} \sim 1 \times 10^4\ \text{s}^{-1}$ , with the same concentration  $\mathbf{A}^+$ , the rate of donor oxidation is  $\sim 1.5\ \text{mM/s}$ , an order of magnitude faster than the recombination reaction. Finally, the reduction of  $\mathbf{D}^+$  only occurs when the quencher used can return the electron (this is also true of the other recombination pathway discussed). If the electron can be returned, the bimolecular reaction should occur with same kind of kinetics as discussed for reduction of  $\mathbf{A}^+$  by  $\mathbf{Q}^-$ . In both cases of bimolecular charge recombination, the kinetics could be slowed even further by a change in the driving force of the reaction, pushing recombination into the inverted region (see Chapter 1). As a simple example, consider the reaction of  $[\text{Re(I)(phen)(CO)}_3(\text{imidazole})]^+$  (compound **3a**, Section II) with  $\text{Ru(III)(NH}_3)_6$ . The excited state of **3a** is a  $\sim 0.5\ \text{V}$  reductant, while  $\text{Ru(III)(NH}_3)_6$  is a  $0.1\ \text{V}$  oxidant. Thus, the driving force for the oxidation of  $\text{Re(I)}^*$  by  $\text{Ru(III)}$  can be estimated to be  $\sim 0.4\ \text{eV}$ . The back reaction, on the other hand, is between the  $\text{Re(II)}$  form of **3a**, a  $1.85\ \text{V}$  oxidant, while  $\text{Ru(II)(NH}_3)_6$  is a  $0.1\ \text{V}$  reductant, suggesting a driving force of  $\sim 1.75\ \text{eV}$ , a change in driving force of  $1.3\ \text{eV}$ . Ultimately, since the reaction of interest is the oxidation of the donor by the acceptor, regeneration of  $\mathbf{D}$  is less important.

As suggested above, the type of quencher used will influence the properties of the flash/quench reaction. There are two major classes of quencher, reversible and irreversible. Reversible quenchers readily change redox state without decomposition, allowing for cycling of the reaction. That is, with a reversible quencher, the ground state of the donor and acceptor are regenerated on a short timescale without significant damage to the system. Two kinds of reversible oxidative quenchers are employed in the present study: ruthenium hexamine chloride  $[\text{Ru(III)(NH}_3)_6\bullet 3\text{Cl}]$  and N,N-Dimethyl-4,4'-bipyridinium chloride (methyl viologen,  $\text{MV}^{2+}$ ).  $\text{Ru(III)(NH}_3)_6\bullet 3\text{Cl}$  is by far the most heavily used reversible quencher in this report; the  $\text{Ru(III)/Ru(II)}$  couple is 0.10 V vs. NHE [23], well within the range of the excited states for the complexes investigated. An added benefit of this quencher is that it shows no substantial absorption in the visible region of the electromagnetic spectrum in either the  $\text{Ru(III)}$  or  $\text{Ru(II)}$  form, allowing for an uncomplicated analysis of signals with maxima between  $\sim 350$  nm and  $\sim 850$  nm.  $\text{MV}^{2+}$  was also used ( $\text{MV}^{2+}/\text{MV}^{+\bullet} = 0.45$  V vs. NHE [24]), primarily due to the well known spectrum of the one electron reduced radical cation,  $\text{MV}^{+\bullet}$  [24]. This allows for independent confirmation of oxidation of the acceptor by observing  $\text{MV}^{+\bullet}$  transients.

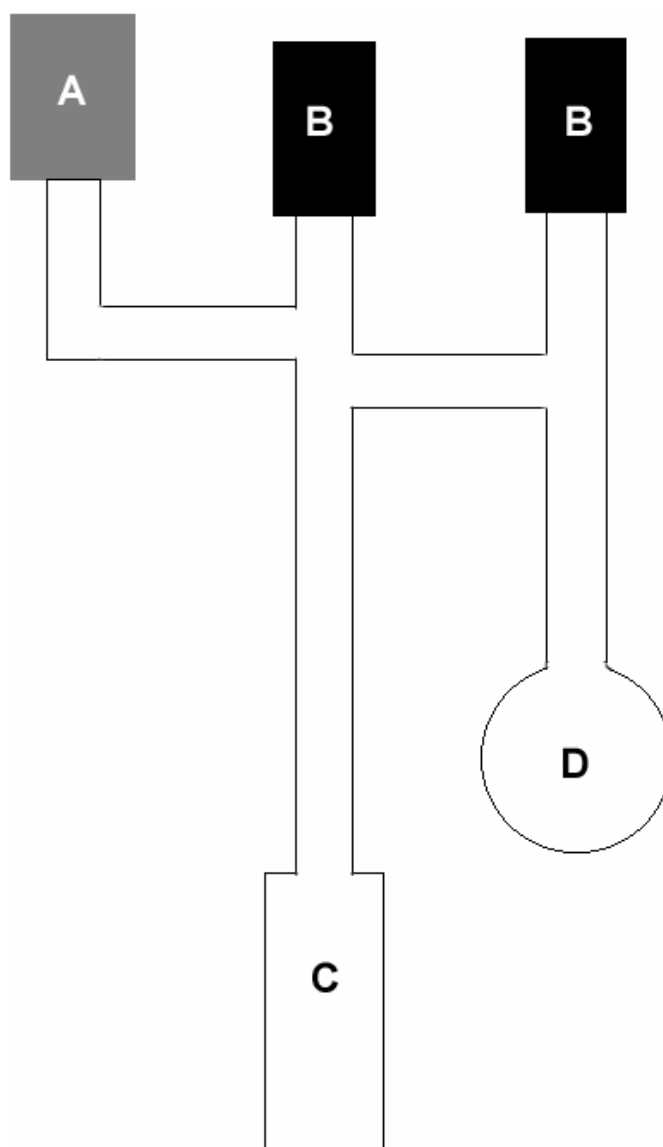
Irreversible quenchers decompose upon a change in oxidation state. Thus, the electron can never be returned to  $\text{D}^+$  by the reduced quencher. The primary consequence of this is that the oxidized species, if it is sufficiently “hot” will abstract an electron from somewhere else; often, in the biological molecules studied, this electron abstraction leads to decay of the system being studied. Therefore, irreversible quenchers are not generally used when one would like to signal average, since they often cause a change in concentration of



the species to be studied. For the work with radicals, particularly for absorption spectra and EPR, only one kind of irreversible quencher was employed, cobalt pentamine chloride (chloride salt)  $[\text{Co(III)(NH}_3)_5\text{Cl} \bullet 2\text{Cl}]$ . When this quencher is reduced, the ammonia ligands dissociate, leaving behind  $\text{Co(II)(H}_2\text{O)}_6$ . As such, the half-wave potential of the compound is unknown, but the anodic peak for  $\text{Co(III)(NH}_3)_5\text{Cl} \bullet 2\text{Cl}$  is at  $\sim 0.3$  V vs. NHE [25]. This presents a problem for investigating copper oxidation in azurin. Since the  $\text{Cu(II)/Cu(I)}$  potential in this protein is 0.31 V vs. NHE, the  $\text{Co(III)}$  may oxidize the  $\text{Cu(I)}$  in competition with the intramolecular ET reaction.

### **2.1.2. Atmosphere-Controlled Cuvettes**

It is well known that the excited states of both  $\text{Re(I)(phen)(CO)}_3\text{(X)}$  ( $\text{X} = \text{N donors}$  [26]) and  $\text{Ru(bpy)}_2\text{(LL)}$  ( $\text{LL} = \text{dimine ligands}$  [27]) complexes are quenched by the presence of oxygen. More disturbing, a product of this quenching is singlet  $\text{O}_2$ , a compound known to wreak havoc in biological systems [28, 29]. In order to avoid this complication in metal-labeled DNA and Re-labeled azurins, specially designed cuvettes were employed (Figure 2.1.2-1). The atmosphere-controlled cuvette is equipped with a ground glass joint (Figure 2.1.2-1, A) to allow easy connection of the cell to a schlenk line for degassing. These cuvettes are designed such that the sample may be placed in the cuvette (Figure 2.1.2-1, C) and isolated from the atmosphere by a Teflon stopper (Figure 2.1.2-1, B). The biological molecule to be studied can also be isolated from the quencher added to the round bottom flask portion (Figure 2.1.2-1, D) by another Teflon stopper. This arrangement



**Figure 2.1.2-1:** Atmosphere-controlled cuvette for laser experiments. (A) ground glass joint (B) Teflon stopper (C) far UV quartz cuvette, with quartz/glass junction (NSG) (D) 5 ml round bottom flask.

allows one to examine the photophysics of the biological molecule without quencher, add quencher and evaluate the results, all with only a single trip to the vacuum line. The idea is to run the control experiments on a solution in the cuvette portion without quencher, and then to simply open the stopper between the round bottom portion and the cuvette portion and tilt the entire apparatus, pouring the liquid into the round bottom. The contents can be mixed by swirling the cell and then returned to the cuvette (equipped with a stir bar) for measurement.

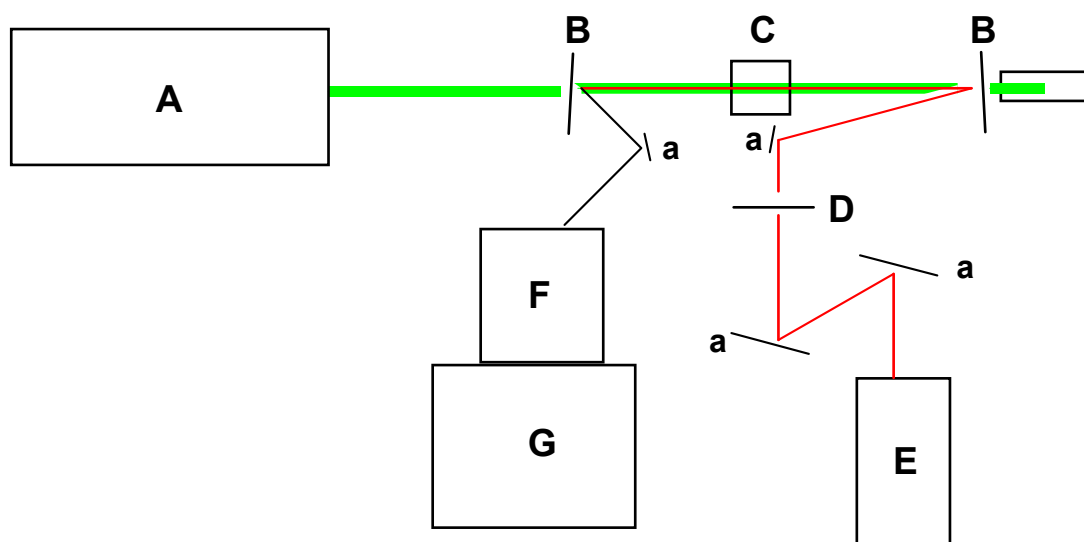
### **2.1.3. *Sample Preparation***

Sample preparation for the laser experiments on NS1 is essentially the same for both metal-modified DNA complexes and Re-labeled azurin. First, at least 1.2 ml of the solution was needed for a 3 ml cuvette to meet the necessary physical dimensions for the experimental apparatus (e.g., excitation beam height, sample holder configuration). To avoid the potential complication of a bimolecular reaction between two biological molecules, the concentration of either the DNA complexes or azurin was kept in the range of 15-45  $\mu\text{M}$  in buffer. Individual experimental concentrations are listed in figure captions or the text. The buffers were designed to (i) provide a relatively constant ionic strength for the solution before and after addition of quencher and (ii) to provide a stable pH in the presence of photoreleased acids or bases (e.g.,  $\text{NH}_3$  release from the reduction of  $\text{Co(III)(NH}_3)_5\text{Cl}\cdot 2\text{Cl}$  or proton release from the oxidation of tryptophan). Therefore, the buffers were prepared at an ionic strength of 50 mM or higher for most experiments.

Individual buffers pH and concentration are listed in figure captions or the text. The solutions of the DNA or azurin were placed in the cuvette portion of atmosphere-controlled cuvette, while the appropriate quencher was added as a solid to the round bottom portion. The entire cell was then attached to a vacuum line with an internal pressure of approximately 30 mtorr. The solution and solid were then subjected to repeated pump/purge: the cell would be opened to the vacuum until degassing of the buffer was evident, then the entire cell was re-filled with argon and allowed to stand for 1 min under a constant flow of argon. During this time, the solution in the cuvette was stirred by a magnetic stir bar. This cycle was repeated a minimum of 5 times to ensure the most complete removal of oxygen possible. It should be noted that this method undoubtedly leaves behind some amount of oxygen; but it is simply unavoidable since neither DNA nor azurin are particularly stable to large changes in temperature which would be necessitated by the more thorough freeze/pump/thaw technique.

#### **2.1.4. NSI**

NS1 is a versatile spectrometer, used heavily in the BILRC over the last several years (see, for example, [30-32]). A simplified schematic of the apparatus is shown in Figure 2.1.4-1. The essentials of this instrument have been described [22], so only a few points will be covered here. The pump source for NS1 (and, for that matter, for NS2) is a Spectra-Physics Nd:YAG laser coupled with MOPO. The Nd:YAG unit produces pulses at 1064 nm with a 10 ns duration. These pulses are tripled, to put out pulses at 355 nm of



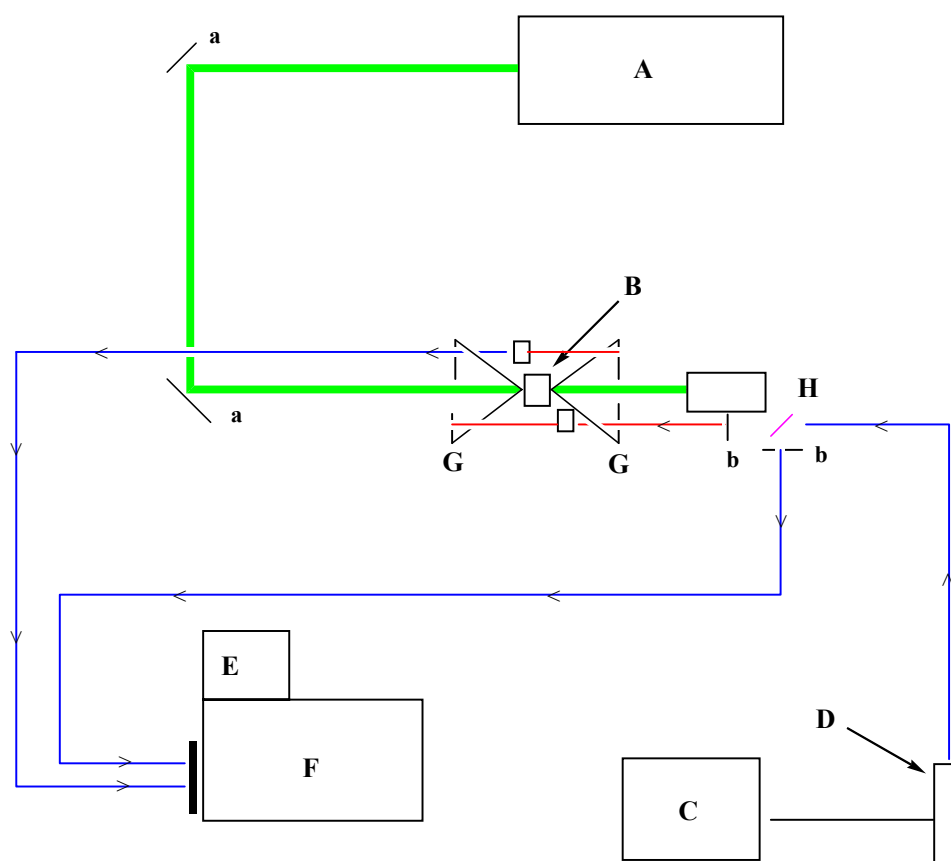
**Figure 2.1.4-1:** Simplified diagram of NS1. (A) Nd:YAG-MOPO laser source (B) concave collection mirror (C) sample (D) 1 mm pinhole (E) probe source, either Xe-arc lamp or HeNe laser (F) monochrometer, 1 nm resolution (G) 7 stage photomultiplier tube (a) turning mirror. (—) Laser pathway (—) probe path.

approximately 300 mJ/pulse. In the experiments performed on Re-labeled azurins (Section II), this output was reduced by 90% with a partial reflectance mirror and the power further modulated by a polarizer to give pulses at the sample of between 1 and 3 mJ/pulse. For the DNA section, the 355 nm coherent light was used to drive the MOPO and produce pulses at 470 nm of approximately 40 mJ/pulse. Once again the power of the laser was attenuated by a polarizer to a power at the sample of between 1 and 3 mJ/pulse. Emission induced in this instrument was measured by focusing of light collected in the concave mirrors (Figure 2.1.4-1, C) into the monochrometer attached to the PMT. Transient changes in the absorption were measured by one of two methods. For wavelengths well away from the emission of the metal complexes studied (for Re, <510 nm >700 nm; for Ru <600 nm >750nm) the sample was probed after the laser excitation by a Xe arc lamp. This lamp can be pulsed for a 500  $\mu$ s duration, allowing for a greater signal to noise ratio for timescales less than 500  $\mu$ s. The probe light was collected by the concave mirrors (Figure 2.1.4-1, C) and focused into the monochrometer attached to the PMT. The drawback of this method is that since the concave mirrors collect all the light produced after the pulse, emission from the sample was also collected. This means that transient absorption spectra at wavelengths with significant emission registered that emission as a bleach (e.g., loss of absorption). This was particularly problematic for observations of Cu(I) oxidation in Re-labeled azurins; Cu(II) absorbs strongly from  $\sim$  600 nm to  $\sim$ 650 nm, a range in which there is substantial Re(I)\* emission. To get around this problem, a second technique for probing changes in absorption was developed. Instead of a broad-band arc lamp, a HeNe laser was used. This device produces continuous coherent light at 632.8 nm. Given the narrow radius of this

light, it can be bounced off a very small section of the collection mirrors. This allows the remainder of the mirror to be covered (typically by an iris) thus reducing the amount of emitted light collected. In this way, the persistent bleach due to emission at 632.8 nm is minimized. The current collected from the PMT was converted to voltage, and amplified by a custom-made amplifier with a bandwidth of 200 MHz, setting the instrument limit for detection at 5 ns. For longer timescales, a more sensitive amplifier allowed resolution out to 100 ms. The digitized data, after processing, was referenced to the probe intensity in the absence of laser excitation (a blank) to give transient absorption traces of  $\Delta OD$  vs. time or an unreferenced luminescence decay trace of intensity vs. time.

### **2.1.5. NS2**

In order to obtain broad-band transient absorption spectra the following spectrometer was constructed (Figure 2.1.5-1). For excitation, the same laser described in 2.1.4 was used. In all experiments with NS2, 355 nm light was used, with the appropriate optical arrangement. The pulse intensities were modulated with a polarizer to give a power of 1.5 mJ/pulse at the sample. The samples are excited with this pulse, and probed with a microsecond flash lamp. The flash lamp exhibits a 4  $\mu$ s jitter, which means that the temporal resolution of the instrument has an error of 4  $\mu$ s. Based on the distance the light must travel and inherent delays in the electronics, the minimum time between a pulse from the laser and a probe from the flash lamp is 16  $\mu$ s. The delay between probe and pump is set by a Stanford Research Systems digital delay generator (model DG535). The probe



**Figure 2.1.5-1:** Simplified diagram of NS2. (A) Nd:YAG-MOPO laser source; (B) sample; (C) digital delay generator; (D)  $\mu\text{s}$  flash lamp; (E) dual strip photodiode array; (F) monochromator, 300 nm resolution; (G) concave collection mirror; (H) splitter; (a) turning mirror; (b) focusing lense. (—) Laser pathway (—) fiber optic cable (—) probe path. Arrows indicate direction of light.



light is collected and transferred by a fiber-optic line to a Spex 270M monochrometer. A grating with a 500 nm blaze and 300 grooves/mm in the monochrometer gives a dispersal of  $\sim 300$  nm. The light from the probe is split before the sample to provide a reference light source, allowing for a subtraction of the sample and a blank to give  $\Delta OD$  transient absorption spectra. Dispersed light from the probe and reference is sent to a cooled ( $\sim -30$  °C) Princeton Instruments 2-strip photodiode array (DPDA-1024) and the resulting information handled by a Princeton Instruments ST-116 controller. The data is processed by Lab View software, written by R. Villahermosa. In order to calibrate the spectra, band pass filters are placed in front of the monochrometer while the probe light is on. These filters allow only a narrow range of light to pass through, so by assigning the maximum of each filter to a pixel on the DPDA, the calibration curve for the monochrometer can be derived. Before each collection cycle, transient absorption spectra of  $MV^{+\bullet}$  (generated in a solution of  $Ru(II)(bpy)_3\bullet 3Cl$  with  $MV^{2+}$  in ethanol) is obtained to verify that the instrument is working correctly.

### 2.1.6. Data Analysis

Manipulation of the data acquired from NS1 and NS2 was relatively straightforward. For the NS1 data, rate constants were abstracted from a linear least squares regression fit of the luminescence or absorption data by Equation 3.

$$y(t) = C_0 + \sum C_n e^{-k_n t} \quad (3)$$

This equation is valid so long as the processes responsible for the signal are one or more first-order reactions, represented by the rate constant  $k_n$ . In general, the summation is not expressed for more than three exponentials, since this can result in artificially accurate fits.<sup>2</sup> As a measure of the goodness-of-fit, plots of the difference between the actual signal and calculated fit (residual plots,  $\Delta Y$ ) were examined. If the fit is accurate, the residual will show overall a slope of 0 with little variation in intensity. Fitting of the data was continued until changes in the  $\Delta\chi^2$  (another goodness-of-fit parameter) ceased. For NS2, the only change to the data was the application of a moving average with a period of 4 to the signal to minimize effects of electronic noise. This moving average results in a reduction of the resolution of the signal from 0.3 nm to 1.2 nm.

---

<sup>2</sup> That is, the more parameters used for a fit, the better the fit regardless of the physical correspondence of those parameters.

## 2.2. EPR Spectroscopy

The primary complement to the laser experiments described above was electron paramagnetic resonance (EPR). This technique is both very sensitive and offers a fair amount of insight into the nature of species with unpaired electrons such as paramagnetic metals or organic radicals. This technique is applied in this thesis to verify the existence of Ru(III) or Re(II) species after the flash/quench and to identify and characterize the radicals formed by these oxidants.

### 2.2.1 The Flash/Quench/Freeze Experiment

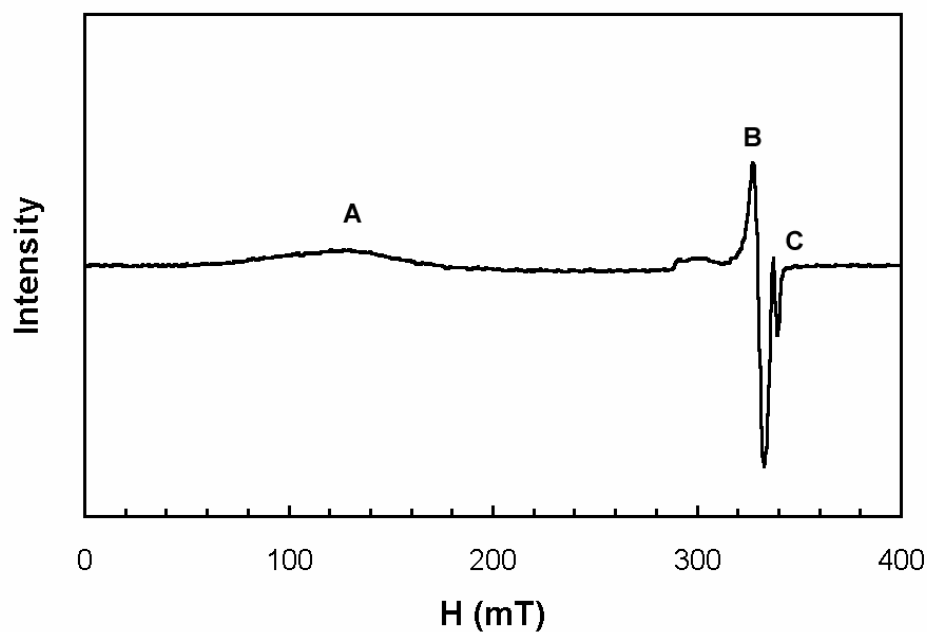
In analogy to the flash/quench experiment described above, the flash/quench/freeze experiment relies on photo-excitation of either Re(I) or Ru(II) and subsequent reaction of these excited states with an exogenous electron donor or acceptor. In the experiments described in Section I and Section II, an oxidative flash/quench with the irreversible oxidative quencher  $\text{Co(III)(NH}_3)_5\text{Cl}\bullet 2\text{Cl}$  formed the basis for this technique. The primary addition to the flash/quench experiment is that, coincident to photo-excitation of the sample, the bulk solution is frozen in liquid nitrogen. This allows for trapping of photogenerated intermediates in various electron transfer reactions. Since the freezing of the solution is never uniform, the delay between excitation of the sample and freezing varies. If the sample is excited while freezing, we estimate that the delay is seconds; however, in cases where the photogenerated species is slow to decay

([Re(H107)(W108)AzZn(II)] in Section II) the sample may be excited for 10 s before freezing to increase the yield of the radical.

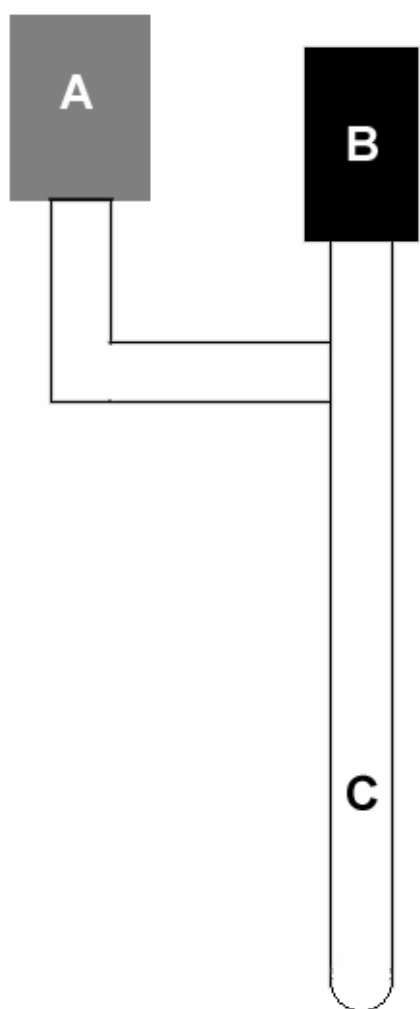
As an example of this technique, consider the photogeneration of a tryptophan radical in the Re-labeled azurin mutant [Re(H107)(W108)Az] (Section II). This mutant supports a surprisingly long lived tryptophan radical, and so was the subject of intense study by EPR. In Figure 2.2.1-1, a flash/quench/freeze EPR experiment of [Re(H107)(W108) AzCu(II)] in a solution saturated with  $\text{Co(III)(NH}_3)_5\text{Cl}\bullet 2\text{Cl}$  is shown at 20 K. All of the products of the flash/quench/freeze experiment are visible: the signal for Co(II) at  $g\ 3.84$  [33], the classic blue copper EPR ( $g_{\perp}\ 2.24\ g_{\parallel}\ 2.05$ ) and the photogenerated W108 radical at  $g\ 2.004$ .

### **2.2.2. Atmosphere-Controlled EPR Tube**

As noted above, oxygen often interacts unfavorably with both DNA and proteins after energy transfer from a photo-excited metal complex. Even if this process turns out to be unimportant, oxygen can react with radicals to give peroxy species (see Section II). In order to examine the initial radical products in the flash/quench/freeze experiment, oxygen must be excluded from the sample. To that end, atmosphere-controlled EPR tubes have been developed (Figure 2.2.2-1). As with the atmosphere-controlled cuvettes discussed above, the specialized EPR tube is equipped with a ground glass joint for connection to a vacuum line (Figure 2.2.2-1, A), and a Teflon stopper (Figure 2.2.2-1, B) to isolate the



**Figure 2.2.1-1:** X-band EPR of [Re(H107)(W08)AzCu(II)] with Co(III) at 77 K. 300  $\mu$ M [Re(H107)(W08)AzCu(II)] in 50 mM KPi pH 7.16 saturated with Co(III)(NH<sub>3</sub>)<sub>5</sub>Cl•2Cl at 20 K. Settings:  $\nu$  = 9.473711 GHz; modulation frequency = 100 kHz; modulation amplitude = 2.0 G; microwave power = 101.1 mW; time constant = 20.48 ms; conversion time = 80.92 ms; 20 scans. (A) Co(II) (B) Cu(II) (C) W108 radical, partially obscured by high microwave power.



**Figure 2.2.2-1:** Atmosphere-controlled EPR tube. (A) ground glass joint (B) Teflon stopper (C) quartz EPR tube.

sample from the atmosphere. The EPR tube itself (Figure 2.2.2-1, C) is high-quality quartz, used to avoid extraneous signals from boro-silicate glass.

### **2.2.3. *Sample Preparation***

Samples for a flash/quench/freeze EPR experiment are prepared in a straightforward manner. First, between 100  $\mu\text{l}$  and 200  $\mu\text{l}$  of a relatively concentrated solution of metal-modified DNA or Re-labeled azurin in the appropriate buffer is prepared. The same buffers used for the laser experiment samples were used for these EPR experiments for the reasons detailed in 2.1.3 above. These solutions were saturated with  $\text{Co(III)(NH}_3)_5\text{Cl}\bullet 2\text{Cl}$  by adding a small amount of solid to the solutions to be studied in the dark and allowed to incubate at room temperature for 5 min. The solutions were then removed by glass pipette and added to the atmosphere-controlled EPR tube. The tube was then degassed by pump purge as described in 2.1.3 above.

### **2.2.4. *EPR Spectrometer***

The spectrometer used for all of the EPR experiments was an X-band Bruker EMX with a standard  $\text{TE}_{102}$  cavity. To perform the flash/quench/freeze experiment, a photolysis apparatus was custom built by Dr. Angelo Di Bilio. A Xe arc lamp was used as the excitation source; the light was passed through an IR water filter and a 355 nm long pass filter to ensure that the sample was only excited in the visible region; in this way direct

excitation of the biological molecules themselves was avoided. The light was focused on a quartz cold finger filled with liquid nitrogen, allowing for irradiation of the sample concomitant with freezing. Then the sample was either transferred to a specially designed dewar with a protruding cold finger filled with liquid nitrogen to acquire spectra at 77K; or the tube was equipped with a vacuum collar and placed in a modified TE<sub>102</sub> cavity fit with a liquid He powered cryostat to obtain EPR at temperatures from 10 K to 250 K.



### **2.3. *Miscellaneous Experimental Equipment***

$^1\text{H}$ ,  $^{13}\text{C}$ , and  $^{31}\text{P}$  NMR were recorded on a Varian Mercury (300 MHz  $^1\text{H}$ , 123 MHz  $^{31}\text{P}$ , 75.5 MHz  $^{13}\text{C}$ ) or a Varian AMX (126 MHz  $^{13}\text{C}$ ) spectrometer. The chemical shifts are reported relative to TMS (0 ppm) for  $^1\text{H}$  and  $^{13}\text{C}$  NMR and 85% phosphoric acid (0 ppm) for  $^{31}\text{P}$  NMR. All mass spectra were acquired by the PPMAL at CalTech. Electrospray mass spectra (ESI-MS) were acquired on a Perkin Elmer/Sciex API 365 triple quadrupole/electrospray mass spectrometer and matrix assisted laser desorption ionization time-of-flight spectra (MALDI-TOF) were acquired on a PerSeptive Biosystems ELITE spectrometer. HPLC purification was performed on a Waters model 600E with a 715 ultra wisp autoinjector system and a 991-photodiode array detector. Infrared spectra were acquired on a BioRad Excalibur series spectrometer. Absorption spectra were recorded on a HP 8452A diode array spectrometer. Fluorescence emission spectra were recorded on a Shimadzu RF-5001 PC spectrometer equipped with a Hamamatsu R-928 photomultiplier tube. Circular dichroism spectra were recorded on an Aviv model 62A DS spectrometer. Kinetic analyses were performed by a nonlinear least squares regression using Marquardt's algorithm. Cyclic voltammetry experiments were conducted on either a CH Instruments 660 Electrochemical Workstation using a glassy carbon working electrode, Pt auxiliary electrode and Ag/AgCl reference electrode; or a Bioanalytic Systems 100W work station using a glassy carbon working electrode, Pt auxiliary electrode and a standard calomel reference electrode.

## REFERENCES

- [1] Gray, H. B.; Ellis, W. R. *Bioinorganic Chemistry*; University Science Books: Mill Valley, 1994 315-363.
- [2] Lewis, F. D. In *Electron Transfer in Chemistry*; Balzani, V., Ed.; Wiley-VCH: Weinheim, 2001; Vol. 3, pp 105-175.
- [3] Winkler, J. R. Electron Tunneling Pathways in Proteins *Curr. Op. Chem. Biol.* **2000**, *4*, 192-198. FIELD Reference Number:156 FIELD Journal Code:9811312 FIELD Call Number:.
- [4] Giese, B. Long-Distance Charge Transport in DNA: The Hopping Mechanism *Acc. Chem. Res.* **2000**, *33*, 631-636.
- [5] Yee, C. S.; Gie, J.; Chang, M. C. Y.; Nocera, D. G.; Stubbe, J. Radical Initiation by the Class I Ribonucleotide Reductases: Long-Range Proton-Coupled Electron Transfer?, *225th ACS National Meeting*, **2003**
- [6] Eklund, H.; Uhlin, U.; Farnegardh, M.; Logan, D. T.; Nordlund, P. Structure and Function of the Radical Enzyme Ribonucleotide Reductase *Prog. Biophys. Mol. Biol.* **2001**, *77*, 177-268.
- [7] Brash, D. E.; Rudolph, J. A.; Simon, J. A.; Lin, A.; McKenna, G. J.; Baden, H. P.; Halperin, A. J.; Ponten, J. A Role for Sunlight in Skin-Cancer - UV-Induced P53 Mutations in Squamous-Cell Carcinoma *Proc. Natl. Acad. Sci. U.S.A.* **1991**, *88*, 10124-10128.
- [8] Aubert, C.; Vos, M. H.; Mathis, P.; Eker, A. P. M.; Brettel, K. Intraprotein Radical Transfer during Photoactivation of DNA Photolyase *Nature* **2000**, *405*, 586-590.
- [9] Jovanovic, S. V.; Harriman, A.; Simic, M. G. Electron-Transfer Reactions of Tryptophan and Tyrosine Derivatives *J. Phys. Chem.* **1986**, *90*, 1935-1939.
- [10] Wehbi, W. A. Amino Acid Radicals in Rhenium-Modified Copper Proteins *California Institute of Technology*, **2003**.
- [11] Faller, P.; Debus, R. J.; Brettel, K.; Sugiura, M.; Rutherford, A. W.; Boussac, A. Rapid Formation of the Stable Tyrosyl Radical in Photosystem II *Proc. Natl. Acad. Sci. U.S.A.* **2001**, *98*, 14368-14373.

- [12] Gray, H. B.; Winkler, J. R. *Electron Transfer in Metalloproteins*; Verlag GmbH: Weinheim, 2001; Vol. 3 3-23.
- [13] Marcus, R. A.; Sutin, N. *Electron Transfers in Chemistry and Biology* *Biochim. Biophys. Act.* **1985**, *811*, 265-322.
- [14] Winkler, J. R.; Di Bilio, A. J.; Farrow, N. A.; Richards, J. H.; Gray, H. B. *Electron Tunneling in Biological Molecules* *Pur. Appl. Chem.* **1999**, *71*, 1753-1764.
- [15] Di Bilio, A. J.; Hill, M. G.; Bonander, N.; Karlsson, B. G.; Villahermosa, R. M.; Malmstroem, B. G.; Winkler, J. R.; Gray, H. B. *Reorganization Energy of Blue Copper: Effects of Temperature and Driving Force on the Rates of Electron Transfer in Ruthenium- and Osmium-Modified Azurins* **1997**, *119*, 9921-9922.
- [16] Augustin, M. A.; Yandell, J. K. *Oxidation of Heme-Proteins by Copper(II) Complexes - Rates and Mechanism of the Copper Catalyzed Autoxidation of Cytochrome-C, Myoglobin and Hemoglobin* *Inorg. Chim. Acta* **1979**, *37*, 11-18.
- [17] Hopfield, J. J. *Electron Transfer between Biological Molecules by Thermally Activated Tunneling* *Proc. Nat. Acad. Sci. U.S.A.* **1974**, *71*, 3640-3644.
- [18] Moser, C. C.; Page, C. C.; Dutton, P. L. *Photosynthesis: Bacterial Reaction Center*; Verlag GmbH: Weinheim, 2001; Vol. 3 24-38.
- [19] Beratan, D. N.; Onuchic, J. N.; Hopfield, J. J. *Electron-Tunneling through Covalent and Noncovalent Pathways in Proteins* *J. Chem. Phys.* **1987**, *86*, 4488-4498.
- [20] Beratan, D. N.; Betts, J. N.; Onuchic, J. N. *Protein Electron-Transfer Rates Set by the Bridging Secondary and Tertiary Structure* *Science* **1991**, *252*, 1285-1288.
- [21] Berlin, Y. A.; Burin, A. L.; Ratner, M. A. *Charge Hopping in DNA* *J. Am. Chem. Soc.* **2001**, *123*, 260-268.
- [22] Chang, I. J.; Gray, H. B.; Winkler, J. R. *High-Driving-Force Electron-Transfer in Metalloproteins – Intramolecular Oxidation of Ferrocycytochrome-C by Ru(2,2'-Bpy)<sub>2</sub>(Im)(His-33)<sup>3+</sup>* *J. Am. Chem. Soc.* **1991**, *113*, 7056-7057.
- [23] Bard, A. J.; Faulkner, L. R. *Electrochemical Methods: Fundamentals and Applications*; 2nd ed.; John Wiley & Sons: New York, 2001 809.
- [24] Villahermosa, R. M. *Electron Tunneling through Phenylene Bridges* PhD *California Institute of Technology*, **2002**, 242.

- [25] Gafney, H. D.; Adamson, A. W. Excited-State Ru(Bipyridyl)<sub>3</sub><sup>2+</sup> as an Electron-Transfer Reductant *J. Am. Chem. Soc.* **1972**, *94*, 8238-&.
- [26] Sacksteder, L. A.; Lee, M.; Demas, J. N.; Degraff, B. A. Long-Lived, Highly Luminescent Rhenium(I) Complexes as Molecular Probes - Intramolecular and Intermolecular Excited-State Interactions *J. Am. Chem. Soc.* **1993**, *115*, 8230-8238.
- [27] Zhang, X. Y.; Rodgers, M. A. J. Energy and Electron-Transfer Reactions of the Mlct State of Ruthenium Tris(Bipyridyl) with Molecular-Oxygen - a Laser Flash-Photolysis Study *J. Phys. Chem.* **1995**, *99*, 12797-12803.
- [28] Cadet, J.; Douki, T.; Pouget, J. P.; Ravanat, J. L. In *Singlet Oxygen, Uv-a, and Ozone*, 2000; Vol. 319, pp 143-153.
- [29] Piette, J. Mutagenic and Genotoxic Properties of Singlet Oxygen *J. Photochem. Photobiol. B-Biol.* **1990**, *4*, 335-339.
- [30] Rack, J. J.; Winkler, J. R.; Gray, H. B. Phototriggered Ru(II)-Dimethylsulfoxide Linkage Isomerization in Crystals and Films *J. Am. Chem. Soc.* **2001**, *123*, 2432-2433.
- [31] Kuciauskas, D.; Freund, M. S.; Gray, H. B.; Winkler, J. R.; Lewis, N. S. Electron Transfer Dynamics in Nanocrystalline Titanium Dioxide Solar Cells Sensitized with Ruthenium or Osmium Polypyridyl Complexes *J. Phys. Chem. B* **2001**, *105*, 392-403.
- [32] Tezcan, F. A.; Crane, B. R.; Winkler, J. R.; Gray, H. B. Electron Tunneling in Protein Crystals. *Proc. Nat. Acad. Sci., USA* **2001**, *98*, 5002-5006.
- [33] Bennet, B. EPR of Co(II) as a Structural and Mechanistic Probe of Metalloprotein Active Sites: Characterization of an Aminopeptidase *Curr. Top. Biophys.* **2002**, *26*, 49-57.

## **II. Tryptophan Radical Formation and Electron Transfer in Rhenium Modified *Pseudomonas aeruginosa* Azurin**

## *Chapter 3*

### **INTRODUCTION**

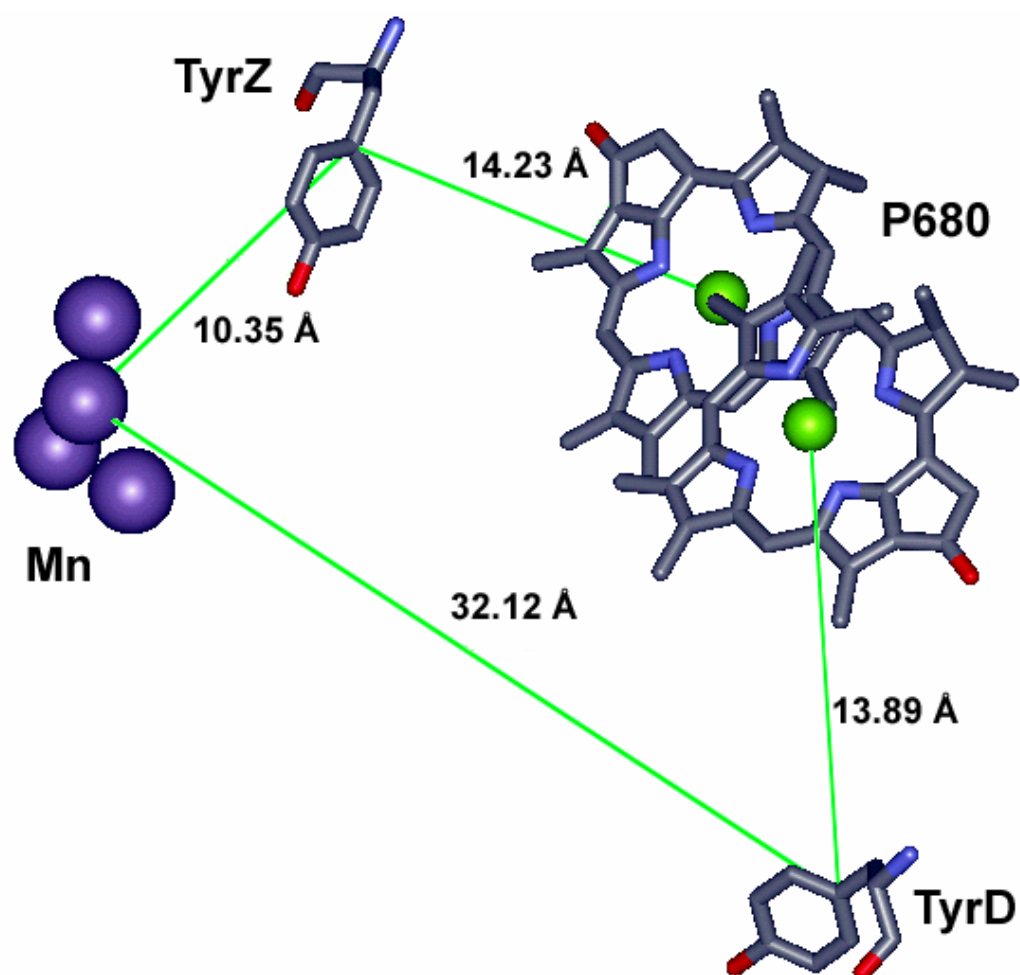
Many biological systems, especially those that operate during photosynthesis and respiration, move electrons and holes rapidly through proteins over very long molecular distances. According to the semiclassical model of ET, single-step  $\sigma$ -bond mediated tunneling cannot, in general, move charge more than 20 Å on the microsecond timescale (see Chapter 1, [1]), so it is suspected that multi-step tunneling occurs in cases where charge moves very rapidly over more than 20 Å. As a general introduction to multi-step electron transfer in proteins, it is most useful to consider some examples.

#### **3.1. *Natural Systems***

An informative example of a biological event that makes use of long-range ET is photosynthesis. In plants, this process of converting light into chemical energy (carbohydrates) by fixing CO<sub>2</sub> with H<sub>2</sub>O is carried out in chloroplasts. There are two protein conglomerations that mediate this conversion, photosystem I (PSI) and the extensively studied photosystem II (PSII). PSII is responsible for the absorption of light resulting in the transfer of electrons from water to a manganese cluster and concomitant evolution of O<sub>2</sub>. The net result of this reaction is the consumption by the manganese cluster

of two  $\text{H}_2\text{O}$  molecules generating four electrons, four protons and one molecule of  $\text{O}_2$ ; the electrons are destined to reduce  $\text{CO}_2$  as indicated above, and the  $\text{O}_2$  is just a happy accident that allows us to continue breathing [2]. PSII is comprised of more than 14 membrane spanning subunits, 3 hydrophilic peripheral subunits and more than 40 cofactors. The operative pathway in  $\text{O}_2$  evolution is bound up in subunit D1: A chlorophyll pair ( $\text{P}_{680}$ ) is photoexcited, transferring an electron to a nearby plastoquinone resulting in the one-electron oxidized  $\text{P}_{680}^+$ . This cation is quickly reduced by a nearby tyrosine residue, the so-called TyrZ. This tyrosine, in turn, oxidizes the manganese cluster at the heart of the D1 subunit, which is the ultimate electron abstractor from water [3]. The crystal structure of PSII has recently been solved, albeit at somewhat low resolution (3.7 Å) [4]. This structure suggests that from the closest approach of  $\text{P}_{680}$  to the manganese cluster is on the order of 24 Å (Figure 3.1-1).

Despite this relatively long distance, ET from the manganese cluster to  $\text{P}_{680}^+$  takes only between 30  $\mu\text{s}$  and 1 ms [5]. It is still disputed whether or not the deprotonation of the tyrosine radical also plays a role in liberation of  $\text{O}_2$  [5-8], but clearly the TyrZ radical is involved in the ET event; mutants that lack TyrZ were unable to function [9, 10]. Another interesting aspect of PSII is the presence of another tyrosine (TyrD), symmetrically located relative to  $\text{P}_{680}$  (each tyrosine is approximately 14 Å distant from  $\text{P}_{680}$ ); the primary difference between the two is that TyrD is in a different subunit (D2) than the redox active manganese cluster [4, 5]. TyrD is more easily oxidized than TyrZ by  $\sim 200$  mV [11], yet ET between  $\text{P}_{680}^+$  and TyrD is relatively slow [5]. Furthermore, mutations of the protein which remove TyrD show no effect on the rate of ET or efficiency of the enzyme [10]. This is a



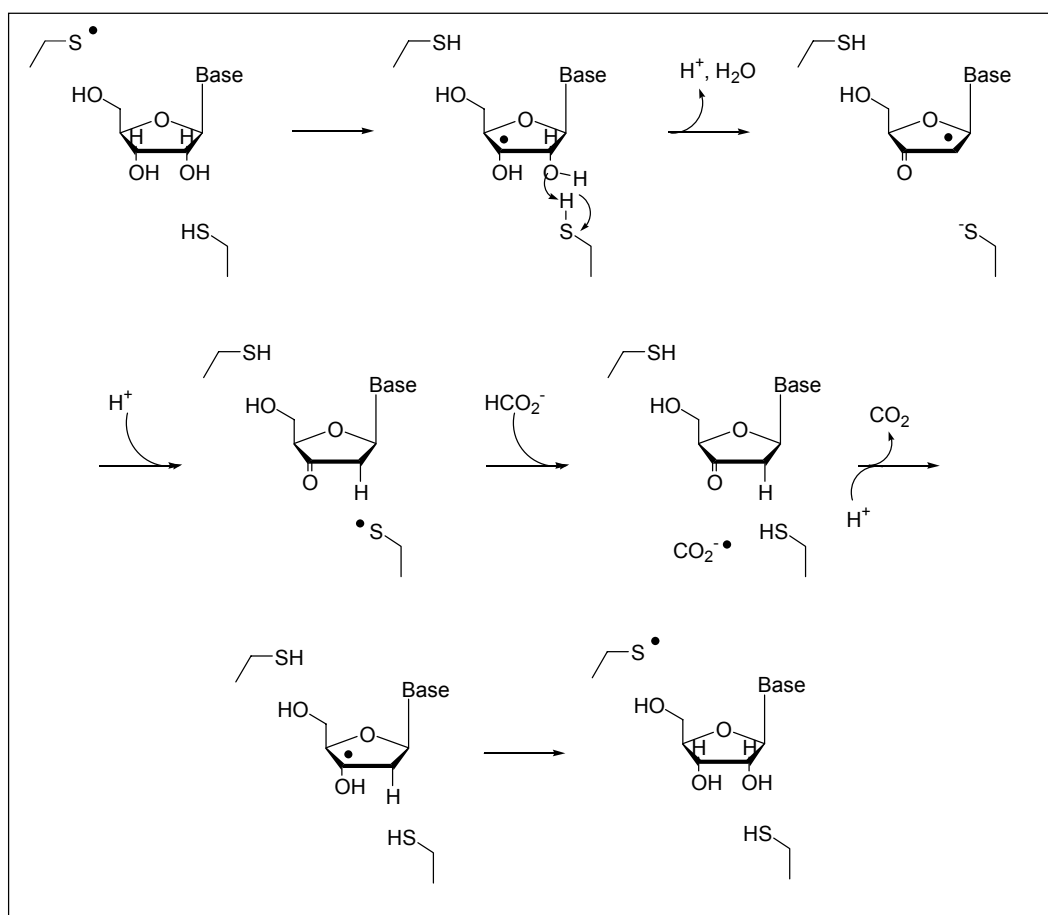
**Figure 3.1-1:** Crystal structure of the ET pathway in PSII at 3.7 Å resolution [4, 12].



perfect example of the fine-tuning of the protein by nature to select an ET pathway: even though the distances between the P<sub>680</sub> and each tyrosine are the same, only TyrZ is directly involved in O<sub>2</sub> production.

Another instructive example is ribonucleotide reductase (RNR). While ribonucleotides are readily synthesized from basic materials (amino acids, ammonium, etc.) deoxyribonucleotides, the building blocks of DNA, must be formed by a more complex mechanism (Scheme 3.1-1, [2, 13]). Hence, the existence of RNR, a biological machine composed (generally) of a radical stabilizing unit and a reductase unit. There are three major classes of RNR, each employing a thiyl radical synthesized in different ways to reduce the ribose: Class I RNR first generates a tyrosyl radical which then oxidizes a cysteine residue in the active site to give the operative thiyl radical, Class II RNR uses a radical on the cobalmin cofactor to develop the thiyl radical and Class III RNR employs a stable glycyl radical to produce the thiyl radical [14]. The thiyl radical is an essential part of the DNA formation mechanism: it participates in the crucial first step of hydrogen atom abstraction (see Scheme 3.1-1) [13]. Some more recent studies have pointed out that the mechanism of Class I RNR must hinge on a long-range ET event mediated by a radical. In order for this class of RNR to turn over as fast as it does, the tyrosyl radical must oxidize the distant [ $\sim 35$  Å] cysteine through a radical mediated (multi-step) pathway [15]. Thus, it is likely that without multi-step ET mediated by amino-acid radicals, DNA could not be synthesized and so life would not exist as we know it.

A number of other enzymes make use of amino-acid radicals to accomplish their functions, among them prostaglandin synthase 1 (tyrosyl radical) [16], galactose oxidase

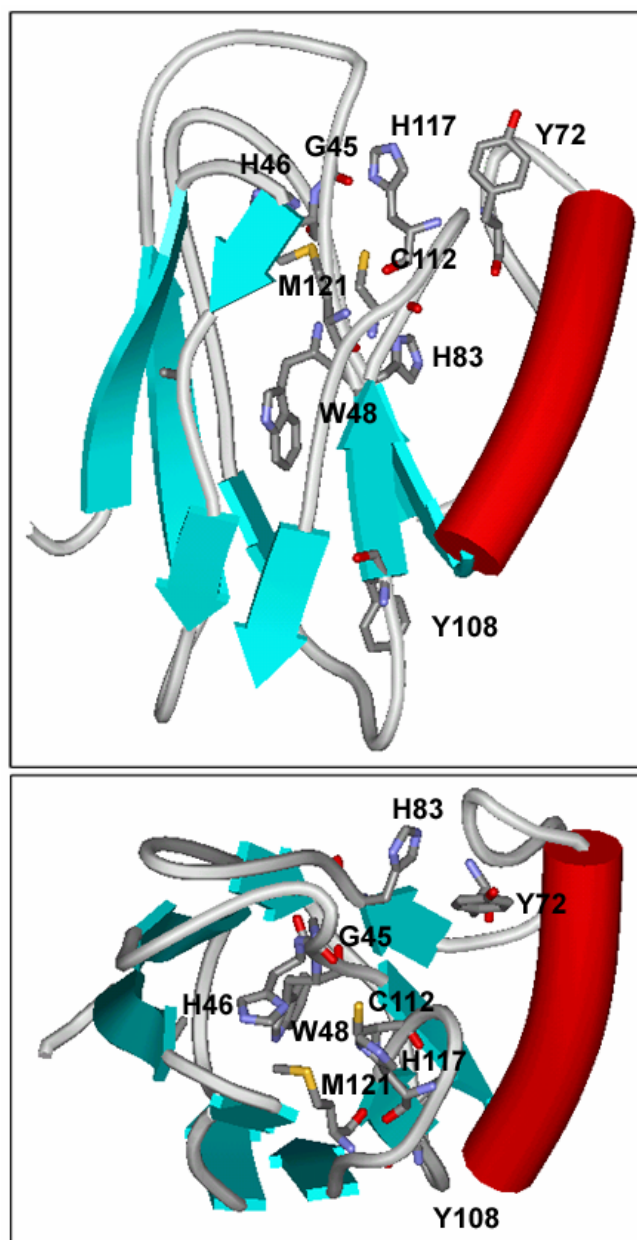


**Scheme 3.1-1:** Proposed mechanism for RNR [13].

(tyrosyl radical bound to copper) [17], pyruvate formate lyase (glycyl radical) [18] and cytochrome c oxidase (tryptophan radical) [19]. While these enzymes may not involve charge transfer mediated by amino-acid radicals, they certainly produce radicals of an unusual nature. It is often the case that organic radicals in biological systems are the source of much chaos; as in the postulated radicals involved in the formation of pyrimidine <6-4> pyrimidone dimers in DNA [20]. Yet the above enzymes manage to use these amino-acid radicals to effect positive change without degradation of the protein itself. How exactly these radicals are controlled is still a question to be answered: it must be a function of protein environment, but in what way?

### 3.2. *Pseudomonas aeruginosa* Azurin

In order to both examine the nature of multi-step ET in proteins and to understand how proteins deal with and control amino-acid radicals, this section of the thesis focuses on a series of rhenium modified *Pseudomonas aeruginosa* azurins. Azurin from *P. aeruginosa* (hereafter simply azurin) is a member of the cuproredoxin family and serves as an electron shuttle in the denitrifying process involving cytochrome  $c_{551}$  and nitrite reductase. This azurin is a small (128 residue) protein; the redox active metal in the wild-type protein is a type 1 copper center, ligated by two histidines (H46 and H117) and a cysteine (C112) giving a roughly trigonal planar structure. Two weakly interacting ligands lie above and below the plane: methionine (M121) and glycine (G45). In the natural form of the enzyme, the Cu(II)/Cu(I) potential has been measured to be 0.31 V vs. NHE [21]. This metal binding site can also ligate a series of other metals, such as cobalt [22, 23], nickel [23, 24] and zinc [25]. Wild-type azurin also contains two tyrosines (Y72, Y108), one tryptophan (W48) and a single surface histidine (H83) (Figure 3.2-1).  $\beta$ -strands extend from the metal binding ligands forming a  $\beta$  sheet. From detailed calculations, and interpretation of the characteristic absorption spectrum and EPR spectrum, it has been determined that the ligand most strongly coupled with the metal center in the copper form of the protein is the sulfur atom of C112; while H46 and H117 are only one-third as well coupled and the out-of-plane ligands (M121, G45) only one-tenth as well coupled [26, 27]. Although this arrangement certainly favors ET pathways that couple through C112; strong intrastrand hydrogen bonds likely ameliorate this effect by directing all charge transfer events through



**Figure 3.2-1:** Two views of azurin without a metal; from the crystal structure of apo-azurin, 1.85 Å resolution [12, 28]. The red barrel represents the  $\alpha$  helix portion, blue arrows represent  $\beta$ -strands.

the C112. This combination of properties makes azurin the perfect scaffold in which to examine the nature of ET through proteins. A number of methods have been developed to induce charge transfer through azurin; as a brief introduction I will focus on two major approaches.

### **3.2.1 *Pulse Radiolysis Reduction of Cu(II) in Azurin***

A good starting point for the discussion of ET in azurin is the work in which pulse radiolysis is used to generate a radical anion on the disulfide bond at C3-C26. The disulfide bond is approximately 27 Å distant from the copper, along a  $\beta$ -strand with two possible hydrogen bond networks leading to coupling with copper through C112. A number of mutants of azurin were constructed to examine the effect of the intervening sequence of amino acids. In particular, the effect of aromatic amino-acids on the rate of ET between the reduced disulfide bond and Cu(II) were examined. Mutations involving copper coordination and the related local protein environment were used to alter the Cu(II)/Cu(I) redox couple and hence the driving force of the reaction. By comparing the rates of ET for the various mutants, the researchers were able to deduce a number of thermodynamic parameters for the protein [29]. At least three important results came out of this and other experiments conducted on pulse radiolysis of azurin. First, the total reorganization energy of the system ( $\lambda$ ) was found to be largely insensitive to mutations unless they involved the immediate environment of the copper center [30]; suggesting that the primary player in the value of  $\lambda$  for these systems is the energy required to reorganize the ligands around copper

on going from Cu(II) to Cu(I) (see Chapter 1). Second, the distance dependence of the rate of ET in these systems was determined to be  $\beta \sim 1.0 \text{ \AA}^{-1}$ , a finding which is in line with the notion that the ET is mediated by a  $\beta$ -strand (assuming the TP model is accurate, Chapter 1). Third, there was some indication that the placement of aromatic residues in the electron transfer path accelerated the rates of ET in azurin. That is, the inclusion or removal of tryptophan residues at sites along the likely ET pathway significantly increased the rate of Cu(II) reduction [31].

It should be noted that the pulse radiolysis method employed here has some rather significant drawbacks; for one, the pulse radiolysis generated radicals interact with the protein in a non-specific fashion. While the decomposition of the irradiated water leads mostly to carbon dioxide radicals, some of the initial products (e.g., hydroxyl radicals) remained. These radicals are free to interact with any part of the protein they come in contact with, not just the disulfide bridge. Thus, at a minimum, reaction of these powerful reductants react with Cu(II) to give Cu(I) has to be accounted for. Another problem related to the promiscuity of the pulse radiolysis products is that the donor, in this case the reduced disulfide, was identified by single wavelength monitoring at 410 nm, a place other radicals, particularly tyrosine [32], might absorb. Finally, the system studied here had the drawback of having a fixed separation between the donor and acceptor of 27 Å. Since neither the disulfide bridge nor the copper center can be easily moved without significant structural perturbation, this distance is fixed.

### 3.2.2. *Cu(I) to Ru(III), Os(III) and Re(II) in Metal-Labeled Azurins*

A parallel approach to investigate charge transfer in azurin involving complexation of a photo-active metal complex to the surface of the protein has been developed. Recognizing that histidine could act as an ideal ligand for coordination compounds, the surface histidine, H83, on azurin was exploited. Initially, coordination of a  $\text{Ru(III)(NH}_3)_5$  fragment to H83 was used to effect electron transfer [33]. In this experiment,  $\text{Ru(II)(bpy)}_3$  in solution was irradiated by a laser pulse, generating an excited state that transferred an electron to the  $\text{Ru(III)}$  surface label. The resulting  $\text{Ru(II)(NH}_3)_5$  fragment was able to reduce the  $\text{Cu(II)}$  some distance away. This approach suffers from one of the drawbacks mentioned above, namely, the photo-excited  $\text{Ru(II)}^*$  complex is still somewhat promiscuous (although certainly less so than the radicals in the pulse radiolysis experiment above); it reduces the  $\text{Cu(II)}$  center by a bimolecular reaction. As a way of avoiding this problem, a series of photo-active  $\text{M(II)}$  fragments [ $\text{M(II)} = \text{Ru(II)}$  and  $\text{Os(II)}$ ] with  $\text{M(III)/M(II)}$  couples between 1.09 and 0.72 V vs. NHE were coordinated to H83 [34]. Two photoreactions are possible with these labels. First, if the label is close enough on to the copper center, the excited state can directly reduce the  $\text{Cu(II)}$ ; giving  $\text{M(III)}$  and  $\text{Cu(I)}$  as products. These products can then react to give the initial reactants back,  $\text{M(II)}$  and  $\text{Cu(II)}$ . This method is not the most desirable one, for a few reasons. To start with, the reaction is limited by the lifetime of the excited state; e.g., if the label is moved too far away to donate an electron to  $\text{Cu(II)}$  on the timescale of the excited state decay, then no ET is observed. The other problem with this so-called photo-induced ET process is that the ET is an excited

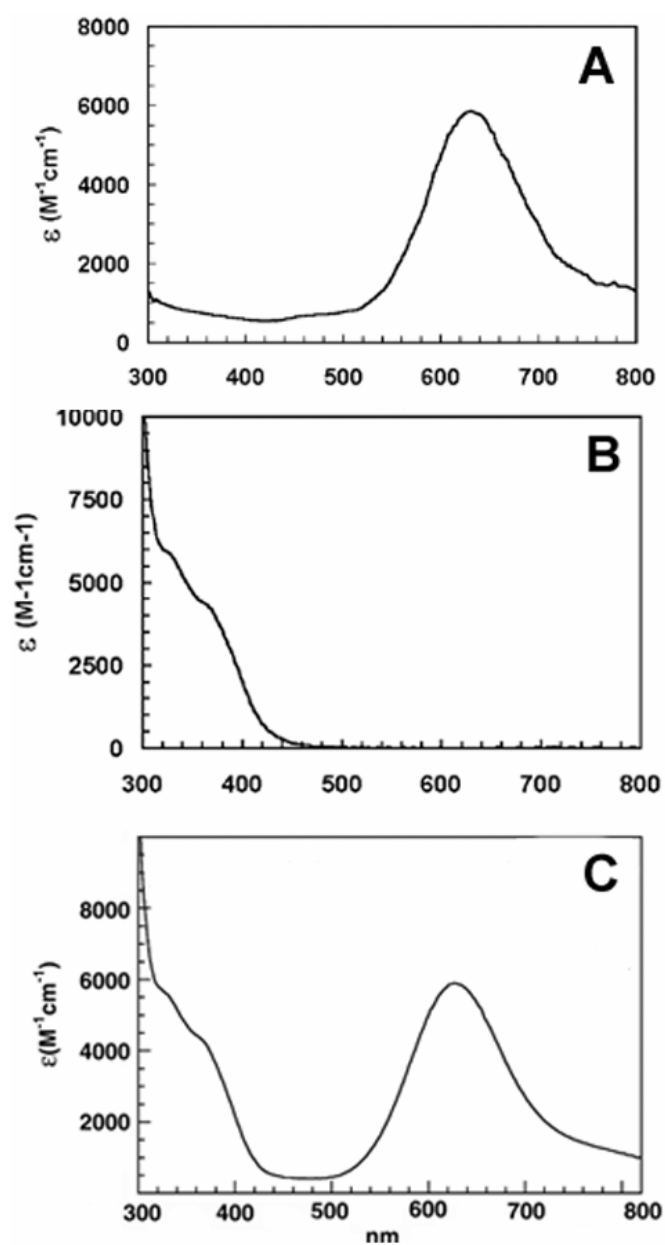


state process, not a ground state process which is often seen in natural systems. Fortunately, there is another way to study ET in azurin labeled with M(II). These metals can be oxidized to the M(III) form by using the flash/quench methodology (see Chapter 2) where the excited state of M(II) is oxidized by bimolecular reaction with an electron acceptor [35]. If the azurin starts in its reduced form (Cu(I)), this method allows for measurement of ET between M(III) and Cu(I) yielding M(II) and Cu(II). Another benefit to this strategy is that the prominent MLCTs of the Ru and Os complexes and the well known blue Cu(II) absorption band make unambiguous observation of the donor and acceptor possible. Under these conditions, no species is generated that might interact with the protein non-specifically. That is, the reduced quencher is not sufficiently reactive (e.g.,  $E^0$  for  $\text{Ru(III)(NH}_3)_6/\text{Ru(II)(NH}_3)_6 \sim 0.1 \text{ V vs. NHE}$ ) to oxidize the copper; or to oxidize any other part of the protein. The study of the effect of temperature and driving force on the rate of ET in metal-labeled wild-type azurin yielded accurate measurements of the reorganization energy, found to be between 0.7 eV and 0.8 eV. This left only the distance dependence of the system to be examined [34].

Perhaps the best reason to use metallic photo-oxidants at histidines is the fact that the positions of these histidines in the protein can be varied by site-directed mutagenesis. Azurin is readily expressed in *E. coli* via inclusion of the appropriate gene in the bacterial DNA [36]. Mutations of the azurin sequence allow for the removal of the wild-type H83 (replaced with Q) and the inclusion of histidine at a number of locations. By using a variety of histidine mutants, the distance between the photo-active metal complex and the copper center can be systematically varied. Thus, by studying ET in mutants of azurin with

$[\text{Ru(II)(bpy)}_2(\text{im})(\text{HX})]^{2+}$  ( $X = 83, 107, 109, 122, 124, 126$ ) an accurate description of the distance dependence of the rate of electron transfer in azurin was obtained [37]. The net result showed that the exponential decay factor,  $\beta$ , was  $\sim 1.1 \text{ \AA}^{-1}$ , as predicted for single-step tunneling through a  $\sigma$ -bond network in a  $\beta$ -strand (using the TP model [38-40]).

With much of the basic information known about azurin, new aspects of charge transfer could be investigated. Semiclassical electron transfer theory suggests that if the driving force ( $-\Delta G^0$ ) in a poorly coupled acceptor/donor system is substantially larger than the reorganization energy ( $\lambda$ ), the rate of ET would actually be less than the rate when the driving force was equal to the reorganization energy (the so-called “inverted effect,” see Chapter 1) [1]. In an attempt to observe this effect, the same azurin mutants from the ruthenium study above were labeled at histidine with a Re(I) fragment [41]. A single surface histidine on each azurin mutant binds to a rhenium (I) tricarbonyl (4,7-dimethyl-1,10-phenanthroline)  $[\text{Re}(\text{CO})_3(\text{dmphen})]$  unit by displacing water from the labeling reagent,  $[\text{Re}(\text{CO})_3(\text{dmphen})(\text{H}_2\text{O})^+]$  ( $\text{OTf}^-$ ). Each of these Re-labeled azurins is readily purified by metal affinity chromatography and anion/cation exchange chromatography. The Re(I) and Cu(II) centers are not strongly coupled, as evidenced by the absorption spectrum of the Re-labeled mutant, H83Q/Q107H, which is a superposition of the blue copper spectrum and the Re(I) spectrum (Figure 3.2.2-1). Measured potentials of the model compound (see below) were used to estimate the driving force for ET from Cu(I) to the photogenerated “Re(II)” suggested that  $-\Delta G^0 \sim 1.5 \text{ eV}$ . Assuming that the inner sphere and outer sphere reorganization energy is similar for  $[\text{Re(I)}(\text{CO})_3(\text{dmphen})(\text{HX})]^+$  and



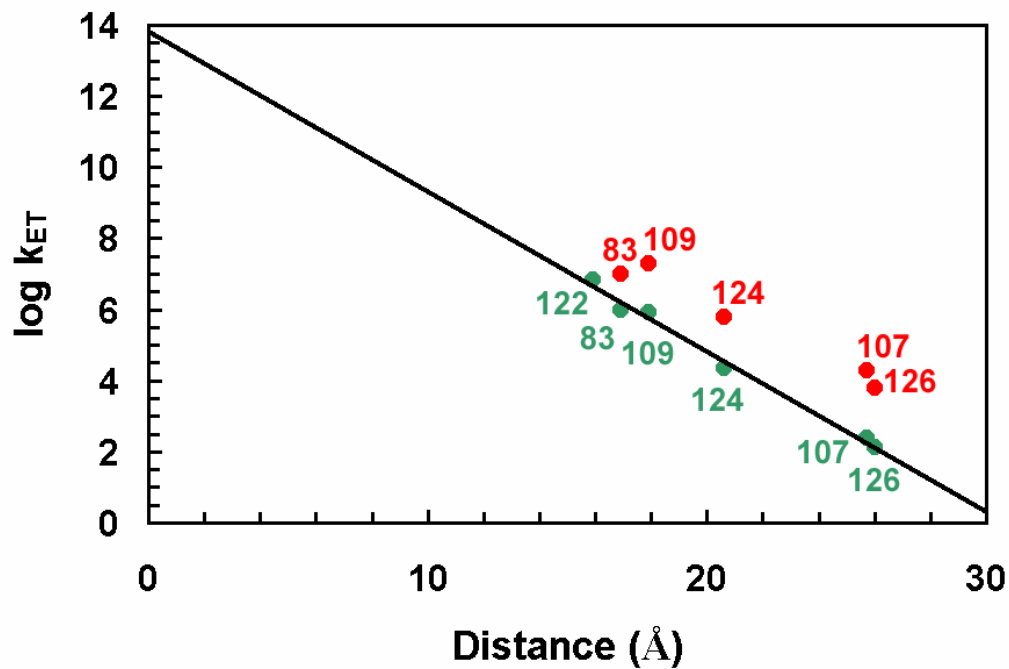
**Figure 3.2.2-1:** Absorption spectra of Re-labeled azurin in 50 mM KPi buffer, pH 7.2: (A) unlabeled H83Q/Q107H-Az; (B)  $[\text{Re}(\text{CO})_3(\text{phen})(\text{imidazole})]^+$  (sulfate salt) and (C)  $\text{Re}(\text{H107})\text{Az}$  [42].

$[\text{Ru(II)(bpy)}_2(\text{im})(\text{HX})]^{2+}$ ,  $\lambda \sim 0.7 \text{ eV}^1$ , the copper to rhenium ET should be in the inverted region of the Marcus curve. Instead of the expected decrease in rate, at every position measured, the rate of ET from Cu(I) to “Re(II)” was accelerated relative to reactions between Cu(I) and Ru(III) (Figure 3.2.2-2, [42]). As a possible suggestion for this unusual increase in rates, a multi-step mechanism was proposed [42]. As a single example, the accelerated rate for ET between the Re label at position 107 and Cu(I) could be explained by intermediate oxidation of Y108 in a mechanism demonstrated in Scheme 3.2.2-1.

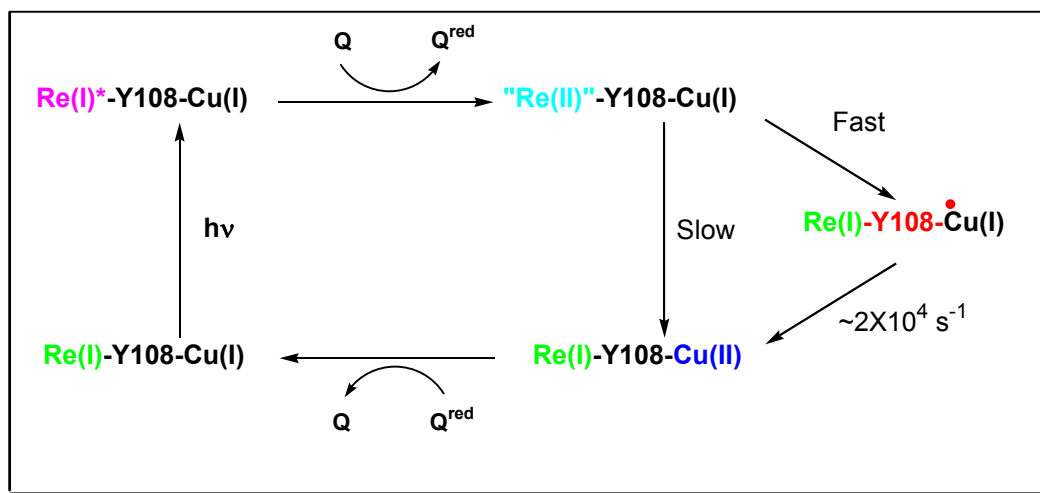
At this point, I began to work on the problems involved with multi-step ET in metal-modified azurins. Initially, the project was aimed at manipulating multi-step ET by altering the amino-acid residue sequence in the  $\beta$  strand from position 107 to the C112 copper ligand. To this end, three mutant azurins (Re(I)(CO)<sub>3</sub>(dmphen)-labeled H83Q/W48F/Y72F/Q107H/Y108W [Re(H107)(W108)AzM, M= Zn, Cu, Figure 3.2.2-3A] H83Q/W48F/Y72F/Q107H/Y108F/F110W [Re(H107)(W110)AzM, M= Zn, Cu, Figure 3.2.2-3B] and Y72F/Y108F [Re(H83)(W48)AzM, M= Zn, Cu, Figure 3.2.2-3C]) were examined incorporating tryptophan residues in the predicted electron transfer pathway. These mutants, along with some investigations on the Re-labeled wild-type protein [Re(H83)WTAz] (Figure 3.2.2-3D) were used to probe the role of the intervening amino-acid residues in multi-step tunneling. Ultimately, the mechanism proposed in Scheme 3.2.2-1 is not correct (see Chapter 6). In the course of showing Scheme 3.2.2-1 to be in error, the properties of a number of tryptophan radicals were elucidated.

---

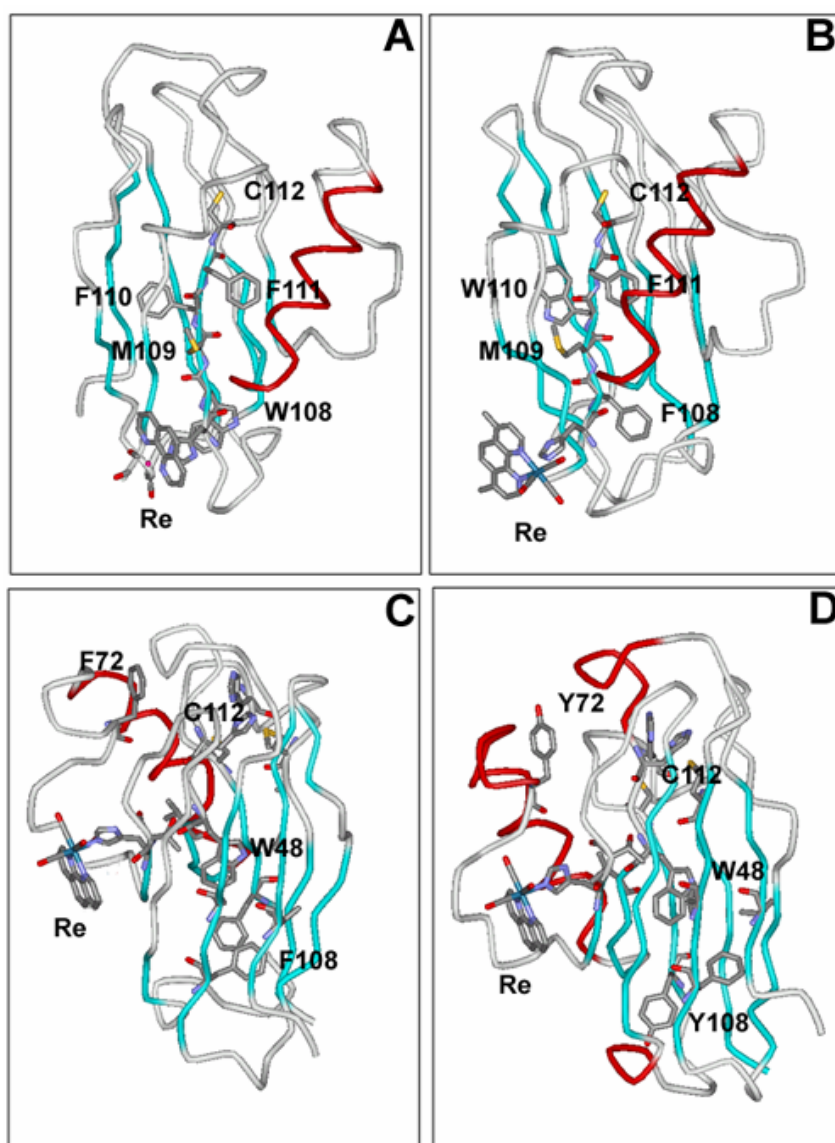
<sup>1</sup> For  $[\text{Ru}((\text{bpy})_2(\text{im})(\text{HX}))]^{2+}$  in azurin,  $\lambda = 0.74 \text{ eV}$  in H<sub>2</sub>O [43], while in  $[\text{ReCO}_3(\text{bpy})(\text{Etpy})]^+$   $\lambda = 0.72 \text{ eV}$  in MeOH/EtOH [44].



**Figure 3.2.2-2:** Electron tunneling timetable for Cu(I) to Ru(III) and “Re(II)” reactions in azurins: Ru-Cu (●) and Re-Cu (●) distances calculated from crystal structures and models [42].



**Scheme 3.2.2-1:** Multi-step tunneling mechanism for accelerated ET in [Re(I)(H107)AzCu(I)] [41, 42].



**Figure 3.2.2-3:** Structures of Re-labeled azurins. (A) [Re(H107)(W108)AzCu(II)], crystal structure [45] (B) [Re(H107)(W110)AzCu(II)], unoptimized model from crystal structure [45] (C) [Re(H83)(W48)AzCu(II)], unoptimized model from crystal structure [46] (D) [Re(H83)WTazCu(II)], crystal structure [46]. Red areas indicate  $\alpha$ -helical structure, while blue areas indicate  $\beta$ -strand character.

## Chapter 4

### SYNTHESIS AND CHARACTERIZATION OF RHENIUM-MODIFIED AZURIN

Note: Detailed procedures for the syntheses described in 4.1 and 4.2 can be found in 4.3.

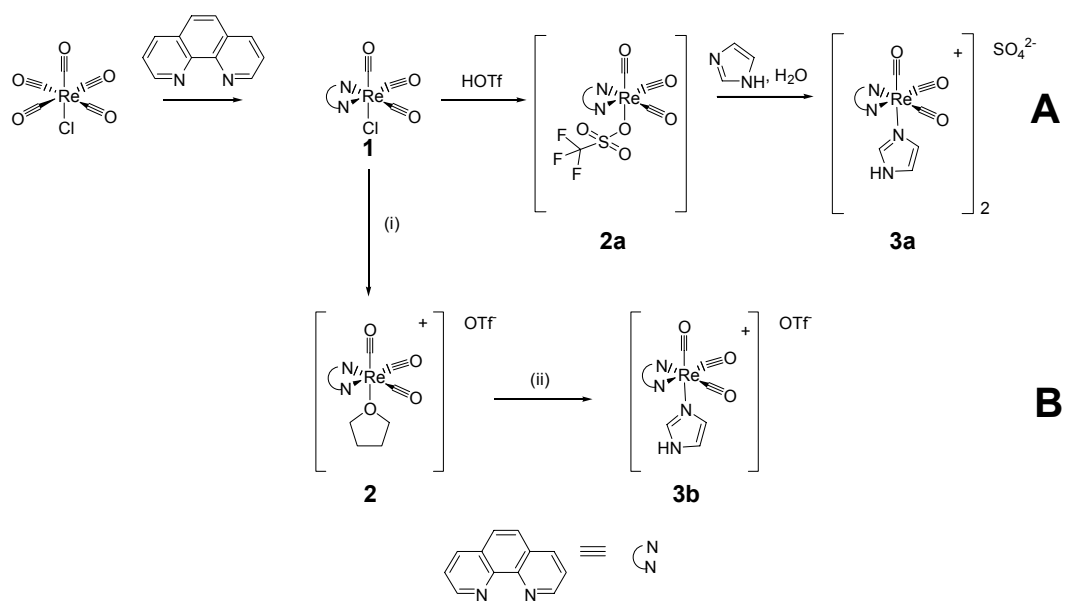
#### 4.1. *Synthesis and Characterization of the Rhenium Model Compound*

In order to fully understand the photophysics of the Re-labeled azurin systems, it is first necessary to understand the photophysics of the  $\text{Re(I)(CO)}_3(\text{dmphen})$  fragment. To investigate this moiety, the model  $\text{Re(I)(CO)}_3(\text{phen})(\text{imidazole})$  was synthesized (Scheme 4.1-1). Cyclic voltammetry of **3a** in nitromethane reveals a single, reversible oxidation wave at 1.87 V vs. Ag/AgCl (Figure 4.1-1)<sup>2</sup>. The one-electron reduction of the complex occurs at -1.06 V vs. Ag/AgCl in acetonitrile [47]. Both **3a** and **3b** exhibit similar electrochemistry, suggesting that the observed half-wave potentials are, in fact, the potentials for the rhenium complexes. The modified Latimer diagram for the Re(I) complex shows that it is a powerful excited-state oxidant [ $\text{Re(I)}^*/\text{Re(0)} \sim 1.3$  V] as well as an excited-state reductant [ $\text{Re(II)}/\text{Re(I)}^* \sim -0.5$  V] (Figure 4.1-2).

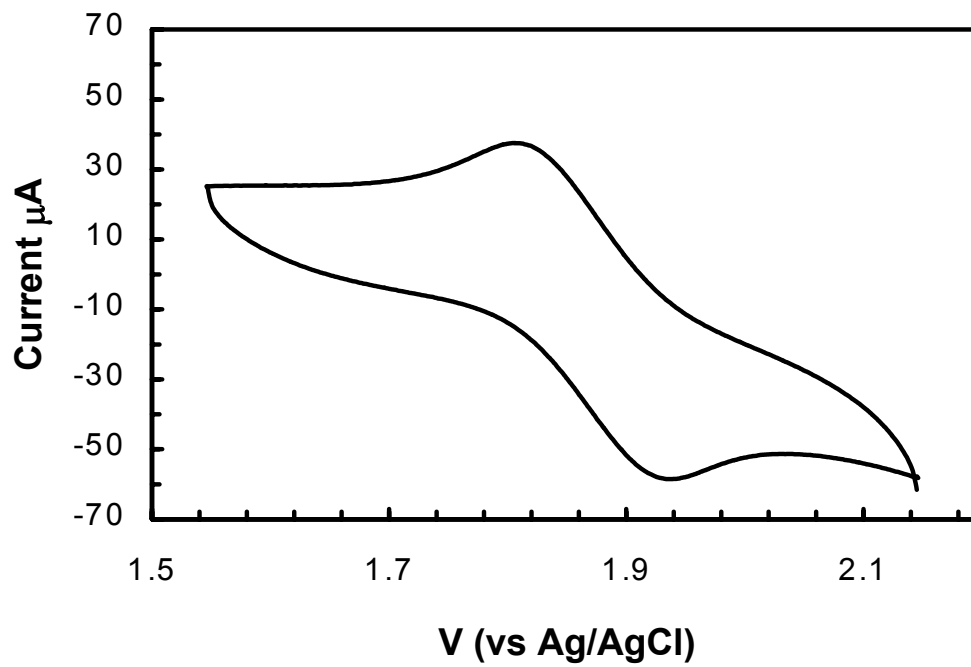
---

<sup>2</sup> In acetonitrile the wave is quasi-reversible at 1.85 V vs. Ag/AgCl [47].

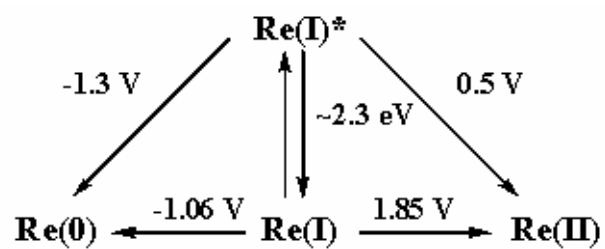




**Scheme 4.1-1:** Synthesis of  $\text{Re}(\text{I})(\text{CO})_3(\text{phen})(\text{imidazole})$  [**3a**]. (phen = 1,10-phenanthroline). (A) Synthetic pathway from [47]. (B) Novel synthetic pathway: (i)  $\text{AgOTf}$ , THF (ii) imidazole, THF.



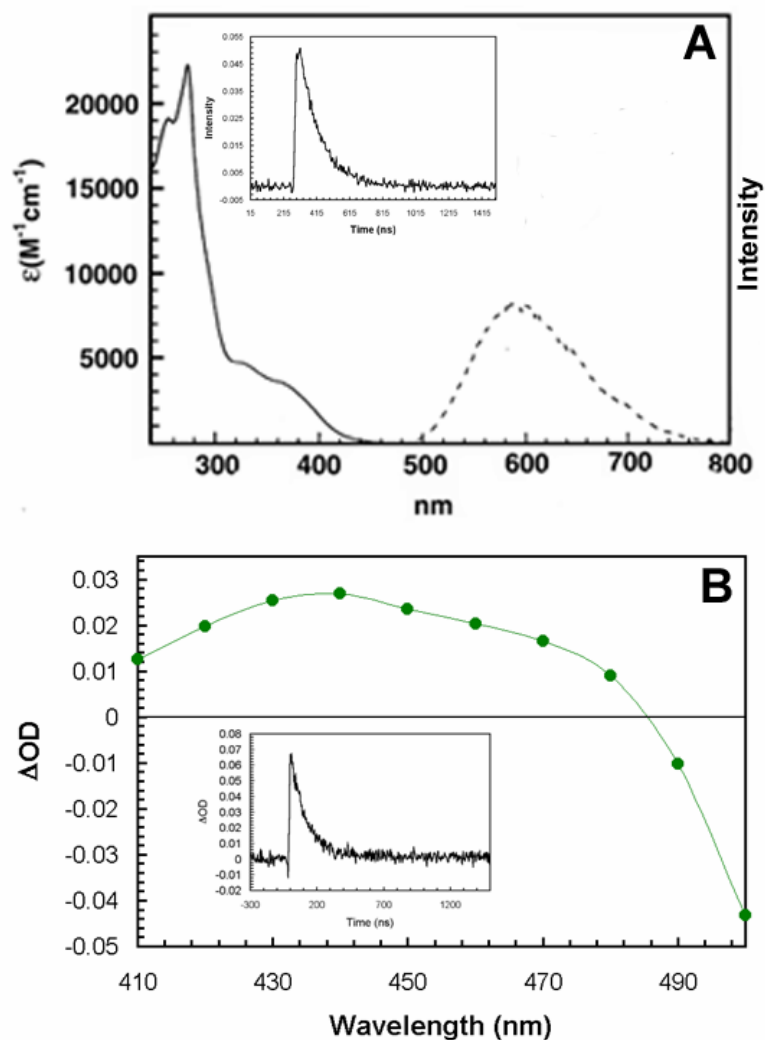
**Figure 4.1-1:** Cyclic voltammetry of **3a** (2 mM) in  $\text{CH}_3\text{NO}_2$  with 0.1 M TBAH.



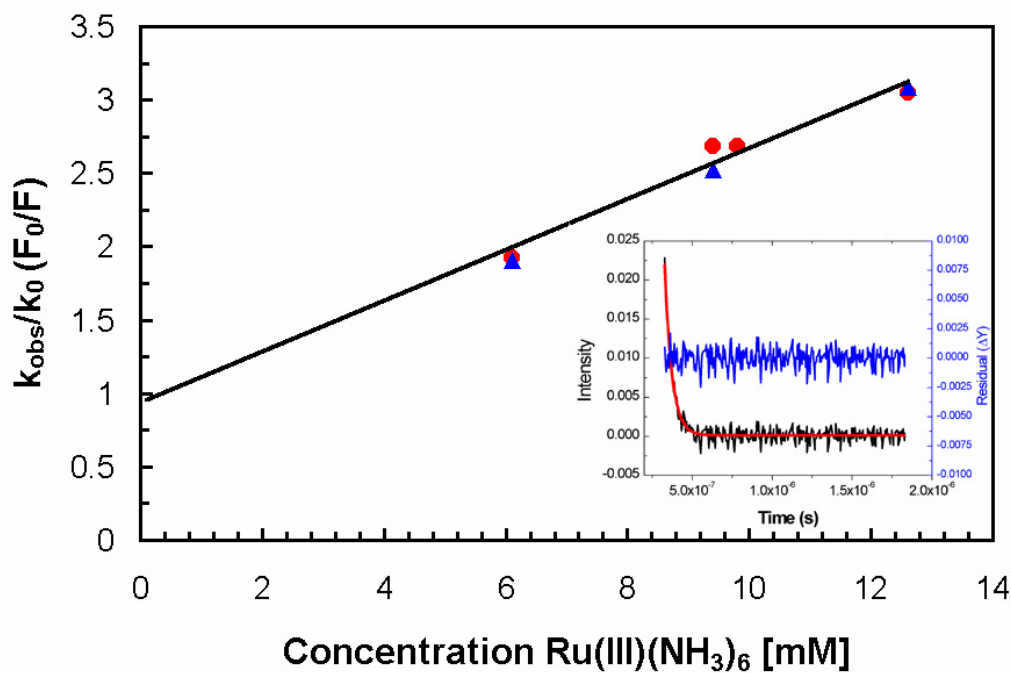
**Figure 4.1-2:** Modified Latimer diagram for **3a** (potentials vs. Ag/AgCl in acetonitrile)

[42].

Given the nicely reversible oxidation wave, and the fact that the excited state of **3a** is a modest reductant, it ought to be simple to oxidize the complex in the standard flash/quench fashion (Chapter 1). Characterization of the excited state of **3a** (**3a\***) has been accomplished both by steady-state and time-resolved means (Figure 4.1-3). The emission of **3a\*** exhibits a maximum at 595 nm and has a lifetime of  $\tau = 120$  ns ( $k = 8.3 \times 10^6 \text{ s}^{-1}$ ) (Figure 4.1-3A). The weak absorption band of **3a\*** is centered at  $\sim 440$  nm, showing an identical lifetime to the emission decay monitored at 595 nm (Figure 4.1-3B). Once the basic features of the excited state were known, flash quench oxidation of **3a\*** could be investigated. This oxidation was followed optically; by monitoring the decay of **3a\*** at 595 nm in the presence of varying concentrations of Ru(III)(NH<sub>3</sub>)<sub>6</sub> (an exogenous electron acceptor), the nature of excited state quenching was investigated. By plotting the observed decay rate constant at a given quencher concentration over the decay rate constant of the excited state without quencher ( $k_{\text{obs}}/k_0$ ) versus the concentration of quencher, the plot shown in Figure 4.1-4 (red circles) was generated. This plot is a standard Stern-Volmer plot [48]; part of the necessary data to show that in fact the quenching of the excited state is dynamic. The other piece of information necessary is a similar plot of the intensity of the emission without quencher over the emission intensity at a given quencher concentration ( $F_0/F$ ) versus the concentration of quencher, also shown in Figure 4.1-4 (blue triangles). In both cases, if the quenching is dynamic, the data for both the kinetics and intensity ought to fit to Equation 1, with an intercept  $C = 1$  and a similar slope  $k_Q\tau_0$ , where  $k_Q$  is the bimolecular rate of quenching and  $\tau_0$  is the lifetime of the unquenched excited state.



**Figure 4.1-3:** Optical characterization of **3a**. (A) (—) steady-state absorption (---) and emission of 20  $\mu M$  **3a**. Inset: emission decay of **3a**\* monitored at 595 nm,  $\tau = 120$  ns. (B) transient absorption spectrum of **3a**\* monitored every 10 nm at 15 ns after the pulse (NS1). Inset: transient absorption decay at 430 nm,  $\tau = 120$  ns. Time resolved measurements were made with 60  $\mu M$  **3a** in 0.1 M KPi pH 7.16.

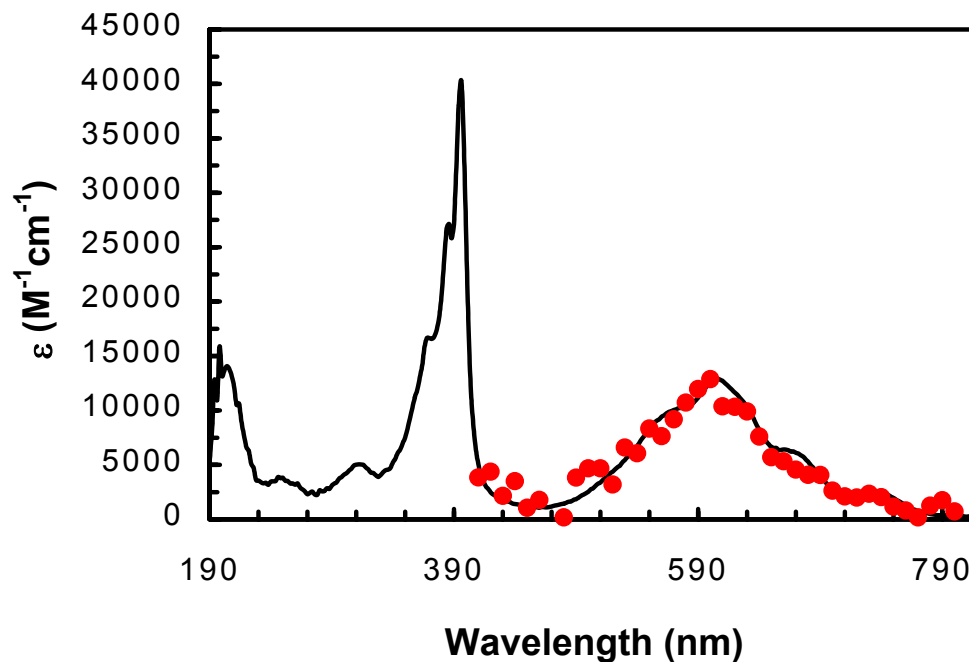


**Figure 4.1-4:** Quenching of **3a**\* by  $Ru(III)(NH_3)_6$ . Stern-Volmer plot of ratio of rates ( $k_{obs}/k_0$ , ●) and ratio of intensities ( $F_0/F$ , ▲) vs. concentration of quencher. (—) Fit according to Equation 1. Inset: (—) data for 1mM point (—) fit by linear least squares method;  $\tau = 121$  ns ( $k = 8.2 \times 10^6$  s<sup>-1</sup>) (—) residual for fit. All measurements performed on a 60  $\mu$ M solution of **3a** in 0.1 M KPi pH 7.16.

$$\frac{k_{obs}}{k_0} = \frac{F_0}{F} = C + k_Q \tau_0 [Q] \quad (1)$$

The fit shown in Figure 4.1-4 gives a  $C = 0.97$  and  $k_Q = 1.4 \times 10^9 \text{ M}^{-1}\text{s}^{-1}$ . A plot of the intensity alone is nearly identical leading to  $C = 0.81$  and  $k_Q = 1.5 \times 10^9 \text{ M}^{-1}\text{s}^{-1}$  (not shown). Thus, the quenching of **3a**\* by  $\text{Ru(III)(NH}_3)_6$  is collisional, with a bimolecular rate constant near the diffusion limit ( $10^{10} \text{ M}^{-1}\text{s}^{-1}$ ) of  $1.5 \times 10^9 \text{ M}^{-1}\text{s}^{-1}$ .

To show unequivocally that it is possible to abstract an electron from **3a** with the flash/quench methodology, the reaction of **3a**\* with methyl viologen (N,N-dimethyl-4,4'-bipyridinium,  $\text{MV}^{2+}$ ) was examined. The  $\text{MV}^{2+}$  di-cation is a standard electron acceptor with a well-known one-electron reduced absorption spectrum (solid line in Figure 4.1-5, courtesy of Randy Villahermosa [49]). Solutions of **3a** with  $\text{MV}^{2+}$  (chloride salt) were excited at 355 nm as above to generate **3a**\* which immediately reacted with the quencher to give the methyl viologen radical cation ( $\text{MV}^{+\bullet}$ ). Monitoring transient absorption of the solutions at 1.5  $\mu\text{s}$  after the pulse ensured that contributions from **3a**\* to the absorption spectra was inconsequential. This gives a spectrum that closely matches the spectroelectrochemically generated spectrum (Figure 4.1-5). Single-wavelength spectra recorded at 390 nm show identical formation and decay rate constants to spectra at 600 nm further indicating the formation of  $\text{MV}^{+\bullet}$ . By systematically varying the power of the laser, the relative concentration of **3a**\* could be manipulated, thus allowing for an estimation of the bimolecular quenching constant  $k_Q = 8 \times 10^{10} \text{ M}^{-1}\text{s}^{-1}$ . It should be noted that since the



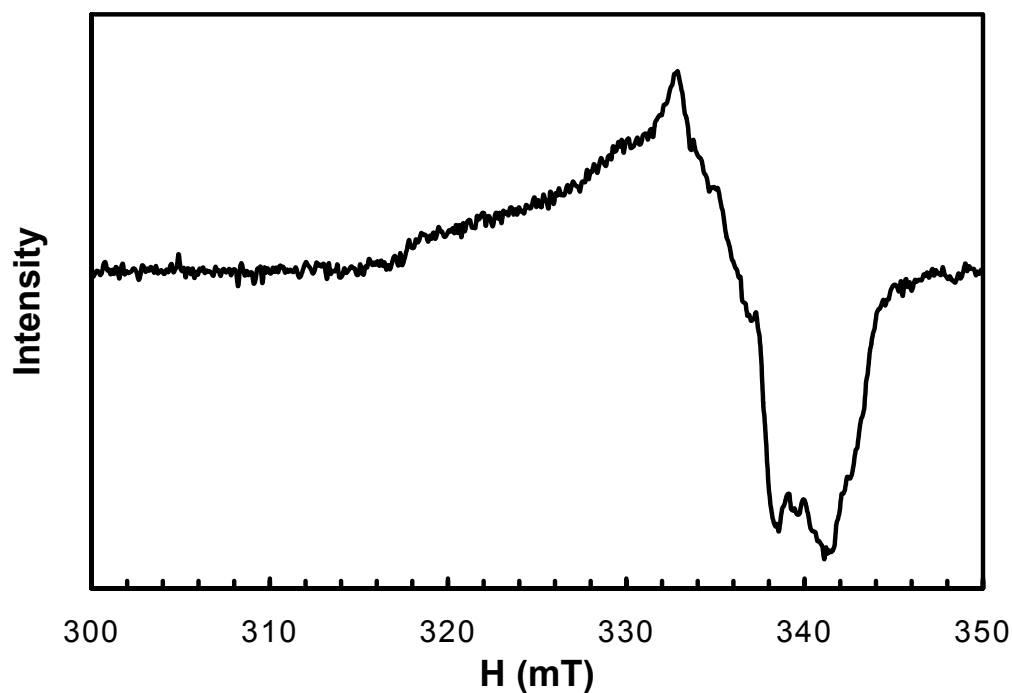
**Figure 4.1-5:**  $MV^{+\bullet}$  spectra. (—) generated by spectroelectrochemistry, of  $MV^{2+}(PF_6)_2$  in  $CH_3CN$  with 0.1M TBAH (R. Villahermosa). (●) generated by reduction of 5 mM  $MV^{2+}(Cl)_2$  by 80  $\mu M$  **3a** photo-excited in water, measured 1.5  $\mu s$  after laser pulse (NS1). Average calculated yield of  $MV^{+\bullet}$  is 4.5  $\mu M$ .



solutions used were not held at constant ionic strength, the derived value of  $k_Q$  is only approximate.

The same analysis could not be performed for the irreversible quencher  $\text{Co(III)(NH}_3)_5\text{Cl}$ . This is because when this quencher is reduced by  $\mathbf{3a}^*$ , it rapidly decomposes to form  $\text{Co(II)(H}_2\text{O)}_6$ , an extremely stable compound [50]. Therefore, the concentration of the quencher changes with each shot. Assuming that the reaction of  $\text{Co(III)}$  with  $\mathbf{3a}^*$  is about as efficient as the reaction between  $\text{MV}^{2+}$  and  $\mathbf{3a}^*$ ; at 5mM  $\text{Co(III)}$ , each laser shot results in the loss of  $\sim 5 \mu\text{M}$  quencher. In a typical experiment with 100 laser shots, the total molarity of the quencher is reduced from 5 mM to 4.5 mM. Fortunately, it is often the case that similar quenchers interact with a given molecule in the same way; so it seems plausible to expect that the  $\text{Co(III)(NH}_3)_5\text{Cl}$  will interact with  $\mathbf{3a}$  in the same way that  $\text{Ru(III)(NH}_3)_6$  did.

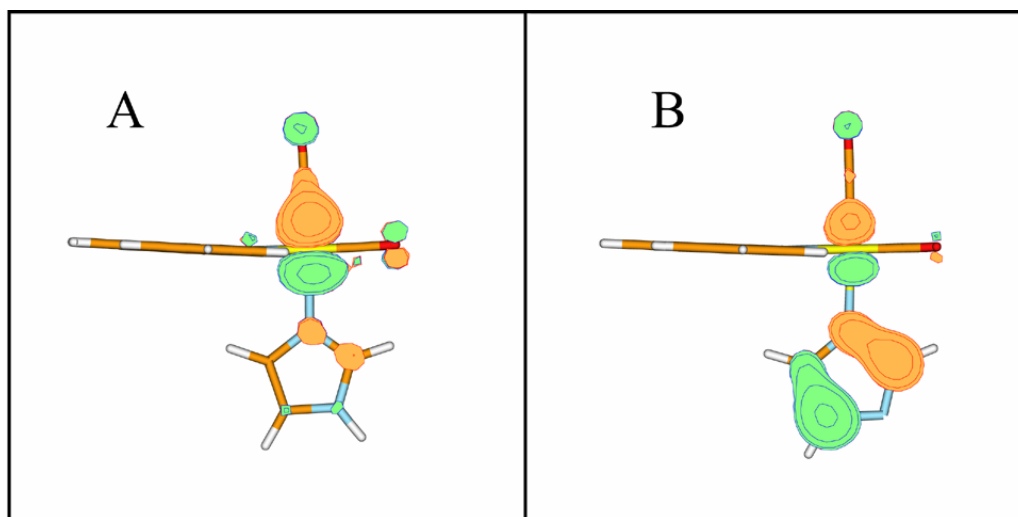
Throughout these experiments, a primary goal was to observe optical signals of oxidized  $\mathbf{3a}$  ( $\mathbf{3a}^{\text{ox}}$ ). A necessity for unambiguous kinetic measurements in these systems is the ability to observe both the electron donor and the electron acceptor. Ultimately, the  $\text{Re(II)(CO)}_3(\text{dmphen})$  (“Re(II)”) fragment will serve as the electron acceptor in the protein systems, so it is important to have some characteristic signals to identify the “Re(II)” species. Unfortunately, none of the laser experiments performed produced definitive signatures for  $\mathbf{3a}^{\text{ox}}$ . For an explanation, one can turn to data revealed by EPR. Flash/quench/freeze EPR experiments on  $\mathbf{3a}$  in pH 6.0 water saturated with  $\text{Co(III)(NH}_3)_5\text{Cl}$  revealed the EPR shown below (Figure 4.1-6).



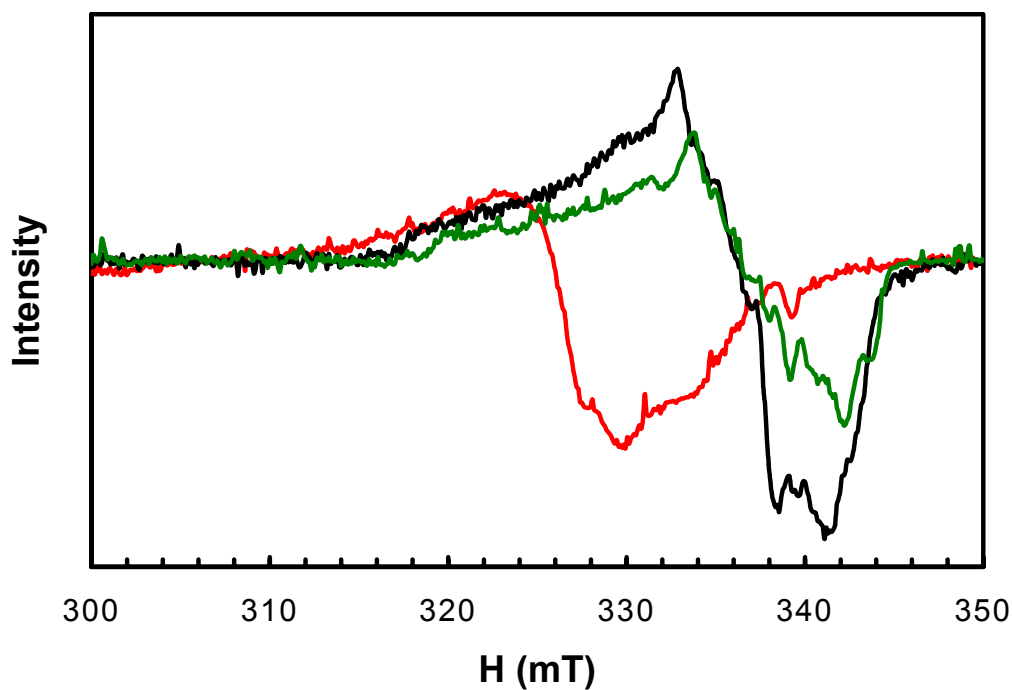
**Figure 4.1-6:** X-band EPR of **3a**/Co(III) at 77K. 3.4 mM **3a** in pH 6.11 water, with 1 mM Co(III)(NH<sub>3</sub>)<sub>5</sub>Cl (chloride salt). Settings:  $\nu$  = 9.474564 GHz; modulation frequency = 40 kHz; modulation amplitude = 5.0 G; microwave power = 8.03 mW; time constant = 20.48 ms; conversion time = 80.92 ms; 30 scans.

This spectrum is not straightforward to interpret: given the fact that rhenium has a quadrupolar nucleus, understanding the fine structure of an EPR with a contribution from this metal is certainly not simple. For instance, EPR of a Re(VI) oxo compound has been simulated, but only with significant effort [51]. Nonetheless, this spectrum can be qualitatively said to exhibit features common for both metal centered unpaired electrons and organic radicals; a substantial  $g_{\perp}$  region as well as  $g_{\parallel}$  centered around 2.0. This finding prompted an attempt to provide a theoretical explanation for the observed EPR spectrum (Figure 4.1-7, courtesy Professor Michael T. Green [42]). Calculations suggest that the spin density in **3a**<sup>ox</sup> is delocalized over both the metal center and the imidazole ligand. The distribution is heavily skewed by protonation state of the imidazole ligand: when the ligand is protonated at the amine nitrogen of the imidazole (i.e., the imidazole is neutral), spin resides primarily on the rhenium (Figure 4.1-7A); when the ligand is deprotonated (i.e., the imidazole is anionic), the spin resides primarily on the imidazole ring (Figure 4.1-7B). To test this theoretical result, flash/quench/freeze EPR spectra of **3a** with Co(III) were recorded at two other unbuffered pH's (Figure 4.1-8). Consistent with the prediction, there is a substantial change in the spectrum at low pH, but high pH produces less variation. At any rate, without high level calculations, ascribing the features of the EPR to any specific species remains an uncertain proposition.

The calculations suggest that the “hole” generated in the flash/quench could reside largely on the coordinated imidazole (or histidine in the protein systems). Thus, the true electron acceptor here could be essentially a one-electron oxidized histidine radical. The quest for absorption handles for the acceptor is at something of an impasse then; histidine



**Figure 4.1-7:** DFT calculations for  $3a^{ox}$ . Natural orbitals for the singly occupied levels of (A)  $3a^{ox}$  ( $[Re(II)(CO)_3(phen)(imidazole)]^{2+}$ ) and (B)  $3a^{ox}-H^+$  ( $[Re(II)(CO)_3(phen)(imidazolate)]^+$ ), showing radical character moving from the Re to the imidazole upon ligand deprotonation. Spin densities (A/B) are Re (0.81/0.25), imidazole (0.09/0.71). Structures were optimized at the B3LYP/LANL2DZ level using Gaussian 98 (Revision A.11.4).



**Figure 4.1-8:** X-band EPR of **3a**/Co(III) at 77K, various pH's. 3.4 mM **3a** with 1 mM Co(III)(NH<sub>3</sub>)<sub>5</sub>Cl (chloride salt). Settings: modulation frequency = 40 kHz; modulation amplitude = 5.0 G; microwave power = 8.03 mW; time constant = 20.48 ms; conversion time = 80.92 ms; 30 scans. (—) pH 2.1 water,  $\nu = 9.506044$  GHz; (—) pH 6.11 water,  $\nu = 9.474564$  GHz (—) pH 11.2 water,  $\nu = 9.502009$  GHz.

radicals show absorbance with  $\lambda_{\text{max}} = 300, 360$  ( $\epsilon = 5600, 2000 \text{ M}^{-1} \text{ cm}^{-1}$ ) [52]; signals that are largely obscured by excited state absorption and other species. In addition to this problem, the oxidation of **3a** cannot be followed by bleaching of the MLCT. Unfortunately, comparing the absorption spectrum of the **3a** with the spectrum of **3a\*** (Figure 4.1-3) it is apparent that there is significant excited state absorption at the MLCT. This absorption results in a masking of the bleach (occasionally visible as a negative “spike” in the NS1 data), so no useful information can be gained from the MLCT bleach. Therefore, the optical signal for the “Re(II)” species may not ever be observed.

However, this presents little problem for the general project at hand. The Stern-Volmer plot (Figure 4.1-4), reaction of **3a\*** with  $\text{MV}^{2+}$  (Figure 4.1-5) and EPR evidence (Figures 4.1-6 through 4.1-8) shows that **3a** may be oxidized efficiently in the flash/quench reaction. By extension the  $\text{Re(I)(CO)}_3(\text{dmphen})$  fragment ligated to surface histidine on azurin ought to be quenched by the exogenous electron acceptors employed.

## 4.2. *Synthesis and Characterization of Metal-Modified Azurins*

As mentioned in Chapter 3, the primary focus of the research in this section is to understand multi-step charge transfer processes in proteins, specifically azurin. In order to accomplish this work, a number of mutants were produced *via* site-directed mutagenesis; a standard microbiological procedure. Site-directed mutagenesis is most effective when performed a single mutation at a time; this means, for instance, that it takes five rounds of mutation to give W48F/H83Q/Y72F/Q107H/Y108W. To determine that the mutations had been made correctly, the plasmids for the relevant mutants were over-expressed in XL1 Blue *E. coli* and submitted for sequencing to the Sequence Analysis Facility at the California Institute of Technology. This method produces a trace showing the sequence of DNA bases in the plasmid fragment of interest (Appendix A). By comparing the DNA sequence with the wild-type sequence the exact composition of the resulting protein can be confirmed.

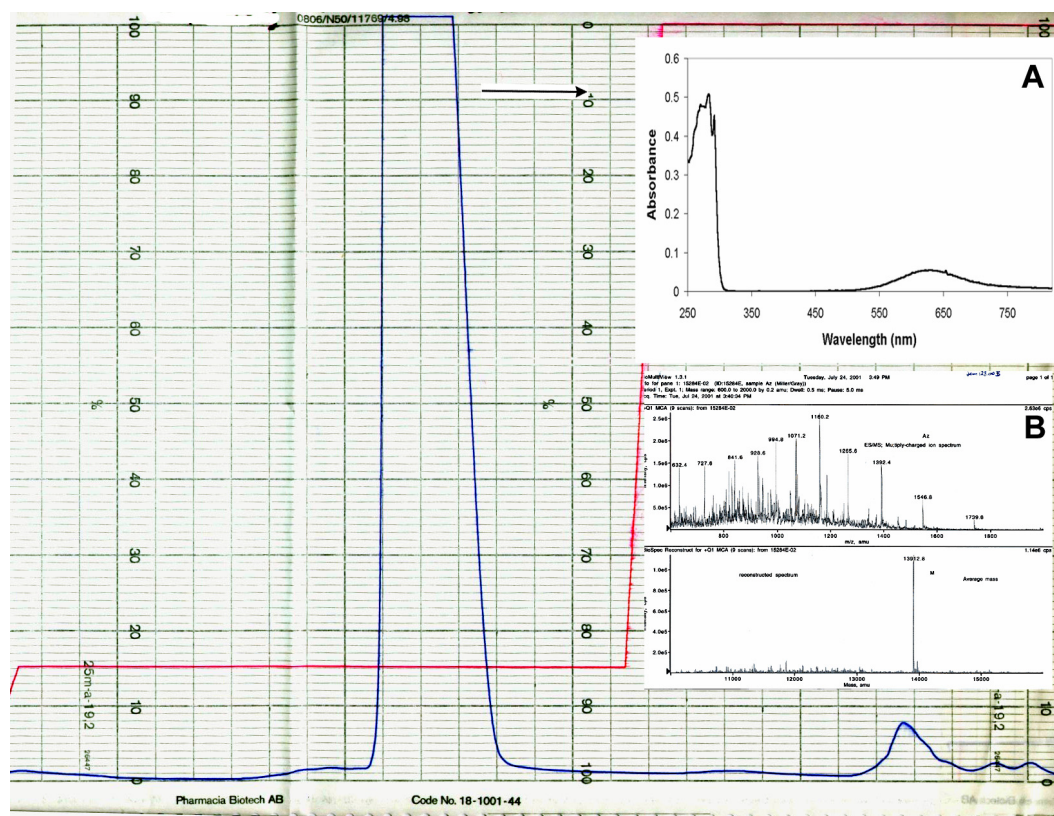
Once the sequence is known, the proteins can be expressed in *E. coli* and harvested. A detailed discussion of this procedure can be found in below in 4.3. Briefly, the bacteria were formed by heat shock inclusion of the appropriate plasmid in *E. coli* without nuclear DNA, then transferred to large cultures and allowed to incubate for 7-12 hrs. Then the *E. coli* were induced to begin expressing protein by addition of isopropyl- $\beta$ -thiogalactopyranoside (IPTG) to the growth media. The bacteria were allowed to manufacture protein for 2-4 hrs, collected, lysed by osmotic shock and the cell extrudate collected by centrifugation. This raw cellular extract was then incubated with either CuSO<sub>4</sub> or ZnSO<sub>4</sub> for

1 week at 4°C in a 25 mM NaOAC buffer, pH 4.5, to give either the Zn(II) or Cu(II) versions of the protein<sup>3</sup>. This mixture of proteins is then purified by application of the solution to cation or anion exchange resins on an FPLC apparatus. The purified azurin fraction can readily be identified by either (i) the characteristic blue copper absorption band at ~ 630 nm (Cu azurin) or (ii) diagnostic tryptophan absorption at ~ 290 nm (Zn azurin). In either case, definitive assignment of the nature of the protein comes from SDS-Page gel analysis and electro-spray mass spectroscopy (ESI-MS) performed at the Protein and Peptide Mass Analysis Laboratory at CalTech. The SDS-Page assay allows for the determination of relative purity by electrophoretic separation, and the mass spectrum is dependent on the amino-acid composition of the protein. Figure 4.2-1 shows the initial purification of W48F/H83Q/Y72F/Q107H/Y108W Az Cu(II) and analytic data. The exact strain of *E. coli* used for expression appears to have some effect on yield of the protein: BL21(DE3) varieties produced only 4 mg azurin/L growth media as compared with BL21\*(DE3) strains which produce 24 mg azurin/L growth media (for W48F/H83Q/Y72F/Q107H/Y108F/F110W). This is not the sole determinant of yield however, factors including incubation time before the addition of IPTG to induce protein expression, temperature and length of cell lysing all contributed to better or worse yields. In short, the protein yields were highly variable (4 mg/L growth media to 65 mg/L growth media) dependent on a number of interrelated factors. Once the mutant azurin had been

---

<sup>3</sup> Alternatively, the Zn(II) version could be prepared from the Cu(II) protein: the reduced Cu(I) version of the Re-labeled protein could be dialyzed against a solution of thiourea and reconstituted with ZnSO<sub>4</sub> [46, 53].





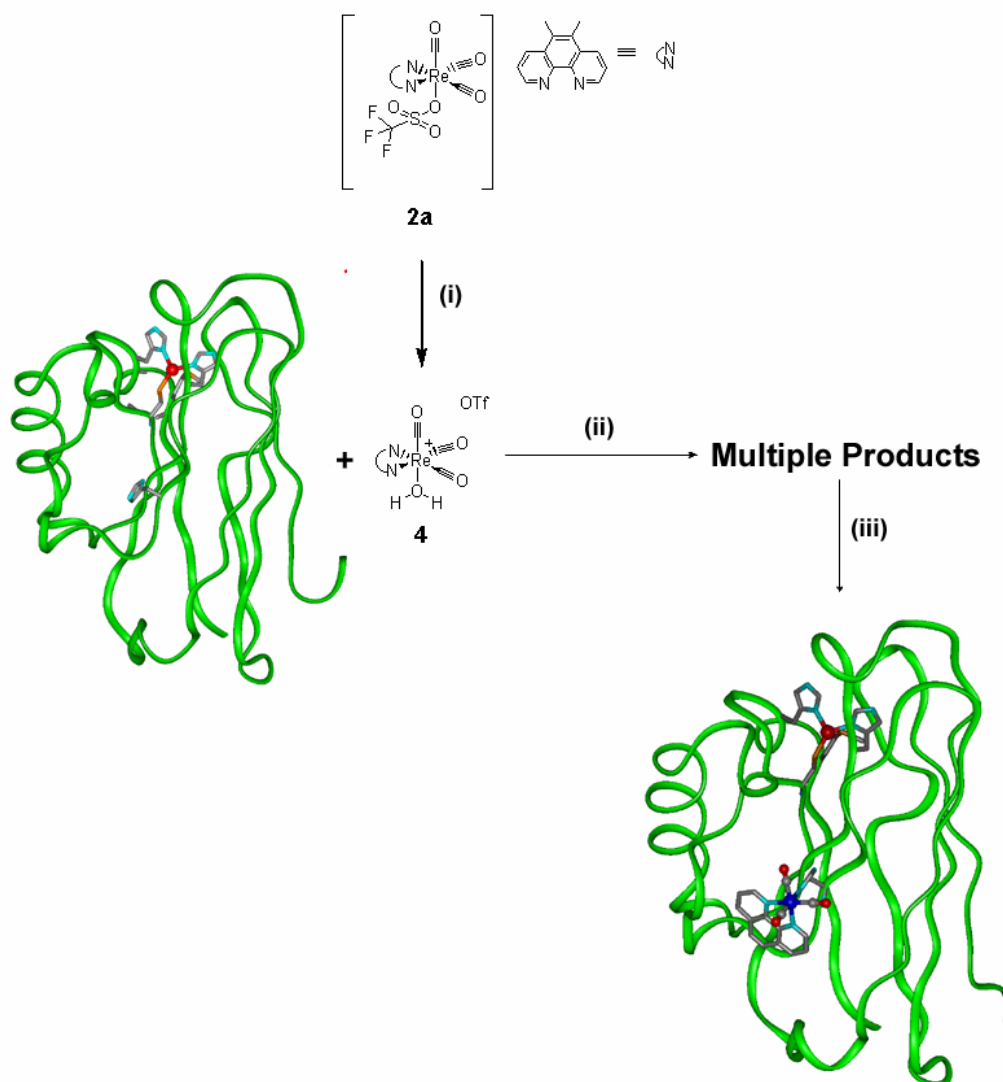
**Figure 4.2-1:** Purification of W48F/H83Q/Y72F/Q107H/Y108W AzCu(II). FPLC trace, cell extrudate on a cation exchange column (Mono-S, Pharmacia). Inset A: absorption spectrum of fraction from the indicated peak. Inset B: ESI-MS spectrum of the same fraction, showing a mass in accordance with the calculated value; calculated  $m/z$ : 13913.79 found  $m/z$ : 13912.8.

purified, it was readily labeled with rhenium complexes (Scheme 4.2-1, [46]). The pure protein was first exchanged into a HEPES based buffer after the cation or anion exchange column by elution from a PD-10 (Pharmacia) column equilibrated with the appropriate buffer. The solution was concentrated to  $\sim 15$  mM protein and then diluted to  $\sim 1$  mM protein with a 2 mM aqueous solution of  $\text{Re}(\text{CO})_3(\text{dmphen})(\text{H}_2\text{O})^+ \text{OTf}^-$ .<sup>4</sup> This solution was then warmed to 37 °C in the dark for 5-7 days (except for  $\text{Re}(\text{H83})\text{WTaz}$ , which must be kept at 37 °C for 30 days to go to 50% completion). The resulting mixture was then purified by means of a copper binding column (IMAC). The IMAC column binds copper which in turn will bind surface histidines on the protein. In this way the IMAC allows for separation of unlabeled and labeled azurin; azurin without rhenium at the surface histidine binds tightly to the column, while azurin with the surface histidine occupied by rhenium shows a relatively weak interaction with the IMAC. The resulting protein solution is then re-purified by FPLC cation/anion exchange. The final product was analyzed by absorption spectroscopy (the rhenium label shows a characteristic absorption at  $\sim 355$  nm, Figure 3.2.2-1B) and ESI-MS. This procedure gives the product with an absorption spectrum that is simply the sum of the protein and the label (Figure 3.2.2-1).

If these results presented in Chapters 5 and 6 are to have any relevance to the study of ET in natural protein, we must show that our systems are not unusually perturbed

---

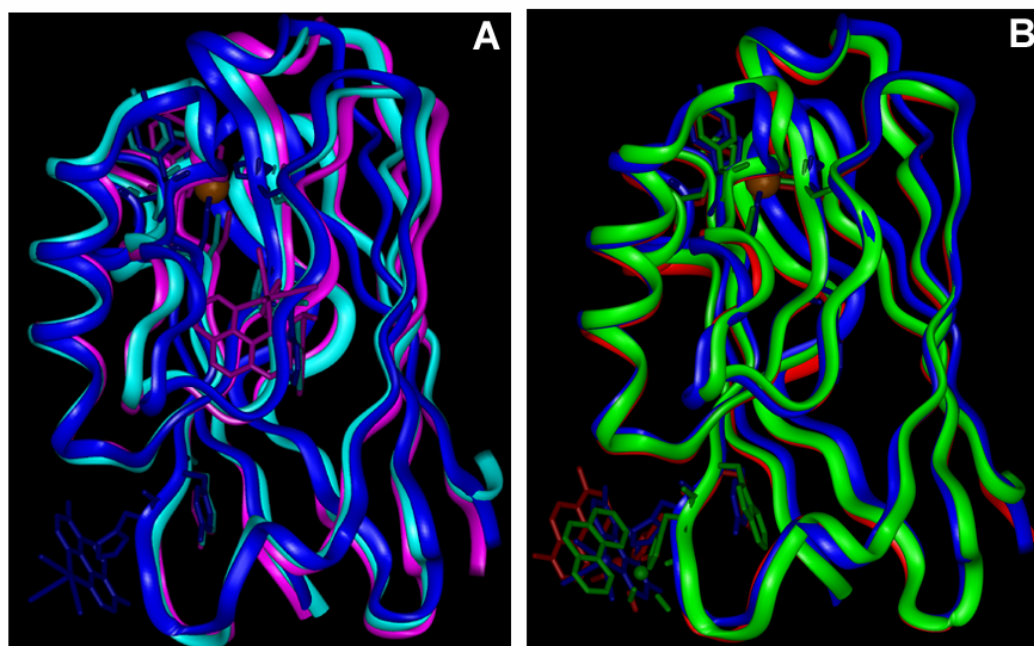
<sup>4</sup> All of the mutants constructed in this thesis employ a  $\text{Re}(\text{I})(\text{CO})_3(\text{dmphen})$  label. The wild-type protein studied (chapter 5) is labeled with a  $\text{Re}(\text{I})(\text{CO})_3(\text{phen})$  label as described previously [46]. The primary difference between these two labels is an enhancement of the lifetime of the excited state in the  $\text{Re}(\text{I})(\text{CO})_3(\text{dmphen})$  case ( $\tau \sim 360$  ns for dmphen,  $\tau \sim 100$  ns for phen).



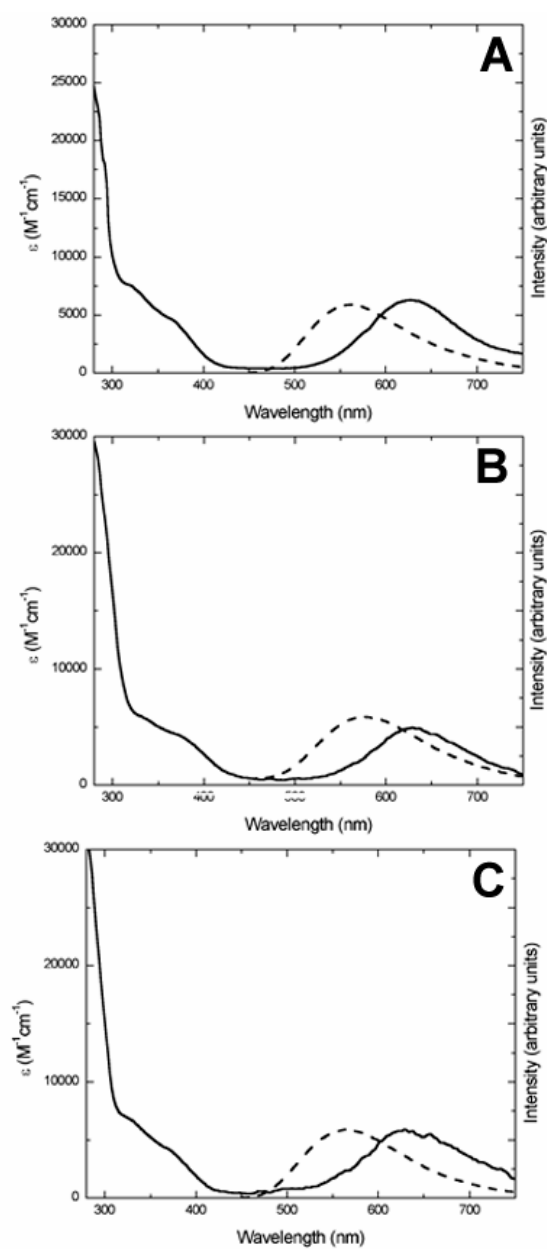
**Scheme 4.2-1:** Labeling of azurin. (i) H<sub>2</sub>O, reflux (ii) ~5 mM HEPES buffer, pH 7.2, 37 °C, 7 days (iii) IMAC/Mono-S FPLC purification.

relative to wild-type azurin. Crystal structures have been obtained for [Re(H107)(W108)AzCu(II)], [Re(H83)WTAzCu(II)]; the related Re-labeled mutant H83Q/Q107H, [Re(H107)(Y108)AzCu(II)] and the H83Q/W48F/Y72F/Q107H/Y108F Re(H107)(All Phe)AzCu(II) protein [32, 45, 46]. These crystal structures show remarkably little variation from one another (Figure 4.2-2), suggesting that the both the rhenium label and the site-specific mutations have little effect on the protein structure. Perhaps most revealing is the fact that [Re(H107)(All Phe)AzCu(II)] (4.2-2B, ●), a quintuple mutant, shows so little perturbation relative to the wild-type structure. This suggests that mutations carried out on the two proteins [Re(H107)(W110)AzCu(II)] and [Re(H83)(W48)AzCu(II)] should have a minimal effect on the tertiary structure of the azurin. Thus, Re-labeled proteins represent a reasonably accurate model for ET in a natural system.

The photophysics of the Re-labeled proteins are much the same as the photophysics for the model complex **3a**. Figure 3.2.2-1 above shows the minimal spectroscopic change associated with labeling; of particular importance is the fact that the spectrum of the labeled protein (Figure 3.2.2-1C) is simply the superposition of a spectrum of **3a** (Figure 3.2.2-1B) and the unlabeled H107 protein (Figure 3.2.2-1A). While Figure 3.2.2-1 only represents one protein; the others investigated in this study are the same (Figure 4.2-3). This suggests that there is no substantial electronic communication between the putative electron donor and acceptor. Upon excitation of the rhenium label (by irradiation at 355 nm) the Re-labeled protein behaves much the same as the model **3a**. The lifetime of the excited state is

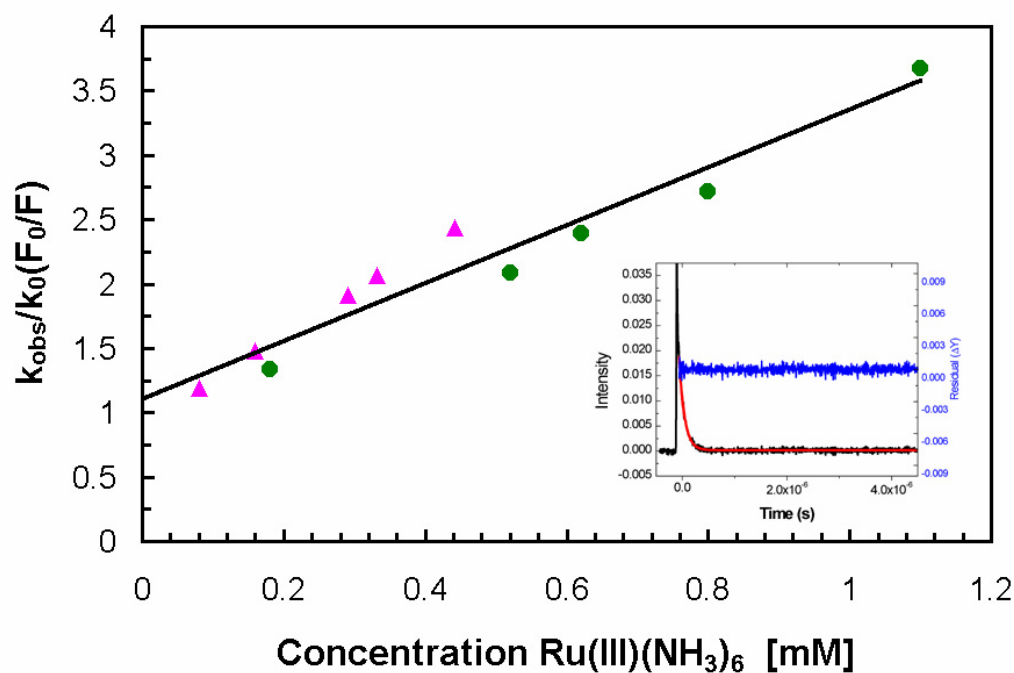


**Figure 4.2-2:** Overlay of azurin crystal structures. (A) (●) Apo-azurin; (●) Re(H83)WTaz Cu(II); (●) Re(H107)(Y108)AzCu(II) (B) (●) Re(H107)(Y108)AzCu(II); (●) Re(H107)(All Phe)AzCu(II); (●)Re(H107)(W108)AzCu(II). Data from references [28, 32, 45, 46].



**Figure 4.2-3:** Spectra of Re-labeled azurins. Solution (—) absorption spectra and (---) emission spectra in 50 mM KPi buffer, pH 7.2: (A) [Re(H83)(W48)AzCu(II)]; (B) [Re(H107)(W108)AzCu(II)] and (C) [Re(H107)(W110)AzCu(II)].

extended in the H107 labeled proteins to  $\tau \sim 360$  ns ( $k = 2.7 \times 10^6$  s<sup>-1</sup> [Re(H107)(W110)Az],  $k = 2.8 \times 10^6$  s<sup>-1</sup> [Re(H107)(W108)Az]) and to  $\tau = 770$  ns ( $k = 1.13 \times 10^6$  s<sup>-1</sup> [Re(H83)(W48)Az]) in the H83 labeled protein. It should be noted that even though the excited state of the rhenium label is predicted to be a powerful oxidant, it apparently does not oxidize the protein framework. This can be seen from the fact that the excited state lifetime in these mutants is not substantially different from the excited state lifetime of Re-labeled azurin that contains no easily oxidized amino-acids [32]. In order to verify that quenching occurred in the same dynamic fashion as the model complex above, a systematic quenching study was carried out on [Re(H107)(W110)AzCu(I)] in which varying amounts of the quencher Ru(III)(NH<sub>3</sub>)<sub>6</sub> was added to a 40  $\mu$ M solution of [Re(H107)(W110)AzCu(I)] showing once again simple collisional quenching (Figure 4.2-4). As discussed above, the relative intensity data for the quenching reactions measured by NS1 are unreliable due to variations in the sensitivity of the PMT on NS1. To get reliable intensity data for the quenching of this protein, steady-state fluorescence of the protein was monitored as a function of added quencher (▲, Figure 4.2-4). From a fit of this data,  $C = 1.11$  and the bimolecular quenching constant  $k_Q = 6.1 \times 10^9$  M<sup>-1</sup>s<sup>-1</sup> were found (in accordance with Equation 1, see above) This experiment has been indirectly repeated on the the [Re(H107)(W108)AzCu(I)] protein; over the course of a number of experiments, a slightly different concentration of quencher was used resulting in the same kind of behavior observed for [Re(H107)(W110)AzCu(I)]. Once again, to ensure the collisional nature of the quenching, steady-state experiments were undertaken. A Stern-Volmer analysis of this data yielded  $C = 0.78$  with a similar bimolecular rate constant,  $k_Q = 7.7 \times 10^9$  M<sup>-1</sup> s<sup>-1</sup>. While



**Figure 4.2-4:** Quenching of [Re(H107)(W110)AzCu(I)] by Ru(III)(NH<sub>3</sub>)<sub>6</sub>. Stern-Volmer plot of ratio of rates vs. concentration (●) and ratio of intensities (▲). (—) Fit according to Equation 1,  $k_Q \sim 7 \times 10^6 \text{ M}^{-1} \text{ s}^{-1}$ . Inset: (—) data for 1.1 mM point (—) fit by linear least squares method  $\tau = 100 \text{ ns}$  ( $k = 1.00 \times 10^7 \text{ s}^{-1}$ ) (—) residual for fit. (●) measurements performed on a 25  $\mu\text{M}$  solution of [Re(H107)(W110)AzCu(I)] in 0.05 M KPi pH 7.16, (▲) measurements performed on a 35  $\mu\text{M}$  solution of [Re(H107)(W110)AzZn(II)] in 0.05 M KPi pH 7.16.



identical experiments have not been performed for [Re(H83)(W48)AzCu(I)], it is expected to behave similarly. Also, since this protein was not designed to investigate charge transfer in any systematic way (see Chapter 6) the exact dynamics of the quenching are less important than the fact that quenching happens as can be seen from kinetic and steady-state observation of the protein with one concentration of quencher.

In [Re(H107)(W108)AzZn(II)] the excited state of the Re label exhibits the same absorption seen in **3a** with a slight extension of the red-edge of the band (Figure 4.2-5). The transients at 430 nm for this protein match the decay rate of the excited state ( $k = 2.8 \times 10^6 \text{ s}^{-1}$ ) as they do in [Re(H107)(W110)AzCu(I)] ( $k = 2.7 \times 10^6 \text{ s}^{-1}$ ). The excited state absorption spectrum of both [Re(H83)(W48)Az] and [Re(H107)(W110)Az] exhibit essentially the same spectrum. Although the results for individual proteins have been presented in the preceding figures, all of the proteins examined exhibited similar photophysical behavior, as well as appropriate mass spectra for their proposed composition (Table 4.2-1). A notable difference between the three mutants is the greatly extended lifetime of the excited state in [Re(H83)(W48)Az]. Given the slow labeling of H83, it seems likely that this site is protected from the bulk solution by the protein. Analysis of the protein structure supports this assertion: H83 is located in the middle of the protein, surrounded by part of the major  $\alpha$ -helical portion of the protein (Figure 3.2-1). This shielding may limit the interaction of the Re label with solvent, thus reducing the non-radiative decay pathways available for relaxation of the excited state. This, in turn, could lead to an observed increase in the lifetime of the excited state.

| <b>Protein</b>         | <b>Emission <math>\lambda_{\max}</math><br/>(nm) (<math>\tau</math> at 595<br/>nm)</b> | <b>Excited State <math>\lambda_{\max}</math><br/>(nm) (<math>\tau</math> at 440<br/>nm)</b> | <b><math>k_Q</math> (Ru(NH<sub>3</sub>)<sub>6</sub><sup>3+</sup>)</b> | <b><math>m/z</math></b> |
|------------------------|--|---|---|-------------------------|
| [Re(H107)<br>(W108)Az] | 570 (360 ns)   | 430 (360 ns)  | $6.1 \times 10^9 \text{ s}^{-1}$                                      | 14391.0                 |
| [Re(H107)<br>(W110)Az] | 564 (360 ns)   | 430 (360 ns)  | $7.7 \times 10^9 \text{ s}^{-1}$                                      | 14392.1                 |
| [Re(H83)<br>(W48)Az]   | 564 (770 ns)   | 430 (770 ns)  | n/a   | 14393.0                 |

**Table 4.2-1:** Properties of Re-labeled azurins.

### 4.3. Experimental

This section contains a detailed account of synthesis and characterization of the metal complexes and Re-labeled azurins discussed in 4.1 and 4.2 above. Also included are experimental details for EPR and laser sample preparation.

#### 4.3.1. Metal Complexes

##### *Rhenium (I) (1,10-phenanthroline) tricarbonyl chloride (1)*

0.166 g (0.92 mmol) of 1,10-phenanthroline (Aldrich) was dissolved in 15 ml toluene to give a colorless solution in a 25 ml round bottom flask equipped with a stir bar. Then, 0.300 g (0.83 mmol) rhenium pentacarbonyl chloride (Aldrich) was added to the flask with stirring to give a cloudy white suspension. In order to exclude water vapor, the flask was then equipped with a reflux condenser purged with a continuous flow of argon. The suspension was then warmed in a water bath to 70 °C. After 5 min, some yellow precipitate was observed. The suspension was allowed to stir at 70 °C for another 70 min, at which time the suspension was entirely yellow. The suspension was then filtered over fine porosity glass fritted funnel to give a yellow solid, washed several times with toluene. The solid was then dissolved in 20 ml methylene chloride leaving behind un-reacted rhenium pentacarbonyl chloride. The solvent was removed *in vacuo* to give 0.253 g yellow powder. The powder was readily recrystallized by slow evaporation of methylene chloride (63% yield). **<sup>1</sup>H NMR** (300 MHz CD<sub>3</sub>Cl) δ 9.42 (dd, J=4.8,1.5 2H), δ 8.61 (dd, J=8.5,1.5 Hz, 2H), δ 8.04 (s, 2H), δ 7.89 (dd, J=8.5,4.8 Hz, 2H) **IR** (CH<sub>2</sub>Cl<sub>2</sub>) 2045 cm<sup>-1</sup> (s, intense),

1985  $\text{cm}^{-1}$  (s, intense), 1920  $\text{cm}^{-1}$  (s), 1898  $\text{cm}^{-1}$  (s). **ESI-MS**  $[\text{M}+\text{Na}]^+$  509.0 (with Re isotope pattern, 1:1.6  $^{187}\text{Re}$ : $^{185}\text{Re}$ ).

*Rhenium (I) (1,10-phenanthroline) tricarbonyl  $\eta^1$ -tetrahydrofuran triflate (2)*

0.150 g (0.31 mmol) of **1** was suspended in 10 ml dry THF (Fluka) in a round bottom flask equipped with a stir bar. This yellow suspension was sparged with argon for 5 min and equipped with a reflux condenser also under an argon atmosphere. Then, 0.095 g (0.37 mmol) AgOTf was added to the suspension under a counter flow of argon. The suspension was heated to reflux in the dark for 4 hrs. After cooling to room temperature, a white precipitate was observed. The yellow solution was filtered over celite to remove the white precipitate and the solvent removed *in vacuo* to give a yellow oil. The oil was re-dissolved in 5 ml methylene chloride and added slowly to 50 ml pentane at 0 °C with stirring to give a fine yellow precipitate. The precipitate was collected by filtration over a fine porosity glass fritted funnel and dried under vacuum overnight to give 0.075 g yellow solid (soluble in diethyl ether). TLC of the product on silica gel with 9:1 methylene chloride:methanol eluent showed only a single spot. No further purification attempted (37% yield).

*Rhenium (I) (1,10-phenanthroline) tricarbonyl  $\eta^1$ -imidazole triflate (3b)*

0.075 g (0.11 mmol) **2** was dissolved in 15 ml dry methanol (Aldrich) to give a yellow solution. The solution was sparged with argon for 10 min, and equipped with a reflux condenser also under argon. Then, 0.030 g (0.44 mmol) imidazole was added to the

solution. The yellow solution was then heated to reflux in the dark for 5 hrs. Then, the solvent was removed *in vacuo* to give a yellow oil. The oil was transferred to a short (5 cm diameter, 5 cm height) silica gel column and washed with 20 column volumes of acetonitrile, eluting one yellow band (starting material) and leaving behind a yellow band at the top of the column. This second band was collected by elution with 8:2 acetonitrile:water, allowing for the separation of 3 additional bands. The final band was collected, and the solvent removed by rotary evaporation to give 0.03 g yellow solid.  $^1\text{H}$ -NMR revealed copious un-reacted imidazole. The solid was dissolved in 2 ml water and placed in 100 MWCO dialysis tubing (Spectrum Laboratories). The solution was dialyzed vs. nanopure water for 4 days. Then, the water was removed by rotary evaporation and the solid dried overnight under vacuum to give 0.017 g of the desired product as a yellow solid (25% yield).  $^1\text{H}$  NMR (300 MHz  $\text{CD}_3\text{OD}$ )  $\delta$  9.63 (d,  $J=5$  Hz 2H),  $\delta$  8.92 (d,  $J=8.7$  Hz, 2H),  $\delta$  8.24 (s, 2H),  $\delta$  8.14 (dd,  $J=8.7, 5$  Hz, 2H),  $\delta$  7.62 (s, 1H),  $\delta$  6.88 (s, 1H),  $\delta$  6.55 (s, 1H), agrees with reference [47].

#### 4.3.2. *Biological Buffers and Media*

A number of different buffers and media were employed in the synthesis of the mutant azurins. Formulas for these solutions are shown below.

|   |  |
|---|--|
| <p><i>50×TAE Buffer</i></p> <p>242 g tris base</p> <p>57.1 ml glacial acetic acid</p> <p>100 ml 0.5 M EDTA pH 8</p> <p>H<sub>2</sub>O to 1 L</p>                  | <p><i>NYZ+ Broth</i></p> <p>10 g NZ amine (casein hydrolysate)</p> <p>5 g yeast extract</p> <p>H<sub>2</sub>O to 1 L</p> <p>Autoclave</p> <p>Immediately before use, add:</p> <p>12.5 ml 1 M MgCl<sub>2</sub></p> <p>12.5 ml 1 M MgSO<sub>4</sub></p> <p>10 ml 2 M filter-sterilized glucose</p> |
| <p><i>5×LB Broth</i></p> <p>50 g NaCl</p> <p>50 g tryptone</p> <p>25g yeast extract</p> <p>H<sub>2</sub>O to 1 L</p> <p>pH 7.0 with 5 N NaOH</p> <p>Autoclave</p> | <p><i>Sucrose Solution</i></p> <p>200 g sucrose</p> <p>3.6 g tris</p> <p>0.27 g EDTA</p> <p>H<sub>2</sub>O to 1 L</p>  |
| <p><i>MgSO<sub>4</sub> Buffer</i></p> <p>1.23 g MgSO<sub>4</sub>•7H<sub>2</sub>O</p> <p>H<sub>2</sub>O to 1 L</p>   |  |

### 4.3.3. *Site-directed Mutagenesis*

Note: synthesis and purification of unlabeled and labeled wild-type protein will not be covered here as it has already been discussed in some detail [46].

In order to change an amino-acid in the expressed protein, PCR is used to replace the three-base codon of DNA for one amino-acid with another [2]. The three base-pair mismatch necessary to change the amino-acid must be surrounded by many bases which perfectly match the parental sequence (usually 10-11 bases on either side), allowing the primer to bind tightly to the parental DNA (template DNA). The polymerase then reads along the template and completes the primer, forming new DNA with the sequence appropriate for the desired mutant. The complement to the mutated DNA is produced in an analogous fashion, giving the double-stranded DNA necessary for protein production. This DNA can then be inserted into appropriate strains of *E. coli* for expression.

#### **Primer sequences:**

*H83Q/W48F/Y72F/Q107H/Y108W Az*

Beginning with the plasmid for H83Q/W48F/Y72F/Q107H/Y108F generously provided by W. Wehbi (see thesis [32], representation Figure 4.3.3-1) the mutation (mismatch in green) for F108 to W108 was provided with the following primer sequence (Life Technologies):

GCT GAA TGC TCC GTT GAT ATC CAG GGT AAT GAT CAG ATG CAG TTC AAC ACC AAC GCC ATC ACC GTC GAC  
 A E C S V D I Q G N D Q M Q F N T N A I T V D  
 1 23

AAG AGC TGC AAG CAG TTC ACT GTT AAC CTG TCT CAC CCA GGT AAC CTG CCG AAG AAC GTT ATG GGT CAC  
 K S C K Q F T V N L S H P G N L P K N V M G H  
 24 45 46

AAC TTC GTT CTG TCC ACC GCG GCT GAC ATG CAA GGC GTT GTC ACT GAC GGT ATG GCT AGC GGT CTG GAT  
 N F V L S T A A D M Q G V V T D G M A S G L D  
 47 48 69

AAA GAC TTC CTG AAG CCG GAT GAC TCT CGA GTT ATC GCC CAG ACC AAG CTG ATC GGA TCC GGT GAA AAA  
 K D F L K P D D S R V I A Q T K L I G S G E K  
 70 72 83 92

GAC TCC GTT ACT TTC GAC GTT TCC AAG CTT AAA GAA GGT GAA CAC TTC ATG TTC TTC TGC ACT TTC CCG  
 D S V T F D V S K L K E G E H F M F F C T F P  
 93 107 108 112 115

GGT CAC TCC GCA CTG ATG AAA GGT ACC CTG ACT CTG AAA  
 G H S A L M K G T L T L K  
 116 117 121 128

**Figure 4.3.3-1:** Sequence for H83Q/W48F/Y72F/Q107H/Y108F. **1** reference numbering; **46** Cu ligands; **107** mutations from the wild-type sequence. Note: this sequence only shows the sequence for protein expression; the entire plasmid is ~ 5000 bases.



Sense: GGT GAA CAC **TGG** ATG TTC TTC TGC

Anti-sense: GCA GAA GAA CAT CCA GTG TTC ACC

#### *H83Q/W48F/Y72F/Q107H/Y108F/F110W Az*

Once again, using the plasmid for H83Q/W48F/Y72F/Q107H/Y108F as a template (Figure 4.3.3-1), the mutation (mismatch in green) F110 to W110 was effected by the following primer sequence (Life Technologies) the PCR for this mutant was carried out by A. Katrine Museth.

Sense: CAC TTC ATG **TGG** TTC TGC ACT TTC

Anti-sense: GAA AGT GCA GAA GAA CAT CCA GTG

#### *Y72F/Y108F*

This time, I started with the plasmid for W48F/Y72F/ Y108F (again graciously provided by W. Wehbi, see thesis [32], Figure 4.3.3-2). Mutating (mismatch in green) F48 back to W48 was accomplished by use of the following primers (Life Technologies). PCR for this mutant was carried out by A. Katrine Museth.

Sense: GGT CAC AAC **TGG** GTT CTG TCC ACC

Anti-sense: GGT GGA CAG AAC CCA TTG GTG ACC

GCT GAA TGC TCC GTT GAT ATC CAG GGT AAT GAT CAG ATG CAG TTC AAC ACC AAC GCC ATC ACC GTC GAC  
 A E C S V D I Q G N D Q M Q F N T N A I T V D  
 1 23

AAG AGC TGC AAG CAG TTC ACT GTT AAC CTG TCT CAC CCA GGT AAC CTG CCG AAG AAC GTT ATG GGT CAC  
 K S C K Q F T V N L S H P G N L P K N V M G H  
 24 45 46

AAC TTC GTT CTG TCC ACC GCG GCT GAC ATG CAA GGC GTT GTC ACT GAC GGT ATG GCT AGC GGT CTG GAT  
 N F V L S T A A D M Q G V V T D G M A S G L D  
 47 48 69

AAA GAC TTC CTG AAG CCG GAT GAC TCT CGA GTT ATC GCC CAC ACC AAG CTG ATC GGA TCC GGT GAA AAA  
 K D F L K P D D S R V I A H T K L I G S G E K  
 70 72 92

GAC TCC GTT ACT TTC GAC GTT TCC AAG CTT AAA GAA GGT GAA CAG TTC ATG TTC TTC TGC ACT TTC CCG  
 D S V T F D V S K L K E G E Q F M F F C T F P  
 93 108 112 115

GGT CAC TCC GCA CTG ATG AAA GGT ACC CTG ACT CTG AAA  
 G H S A L M K G T L T L K  
 116 117 121 128

**Figure 4.3.3-2:** Sequence for W48F/Y72F/Y108F. **1** reference numbering; **46** Cu ligands; **108** mutations from the wild-type sequence. Note: this sequence only shows the sequence for protein expression; the entire plasmid is ~ 5000 bases.

**PCR:**

PCR was carried out by use of QuikChange™ Site-Directed Mutagenesis Kit (Catalog # 200518) from Stratagene (La Jolla, CA). A typical procedure is detailed below for the Y(F)108 to W108 mutation; this procedure is a slight variation of the procedure outlined in the Instruction Manual (Revision #108005h) accompanying the kit.

First, the concentration of the template plasmid was determined. To evaluate the template (in this case H83Q/W48F/Y72F/Q107H/Y108F) a UV/Vis absorption spectrum was acquired. In general, 1 AU at 280 nm corresponds to ~50 ng DNA/μl solution. Also, the ratio between the absorption at 260 nm and 280 nm should be in the range of 1.7-1.8, ensuring that there is little or no protein contamination. This procedure showed that the stock of plasmid contained 117 ng DNA/μl for the template. At the same time, solutions of the lyophilized primer strands of DNA were made to concentration of 48 ng/μl for the sense and 37 ng/μl for the anti-sense strand.

Then, in a 100 μl eppendorf tube all of the following were combined:

2 μl of 10× reaction buffer

20 ng template DNA (0.2 μl)

50 ng sense DNA primer (1.05 μl)

50 ng anti-sense DNA primer (1.37 μl)

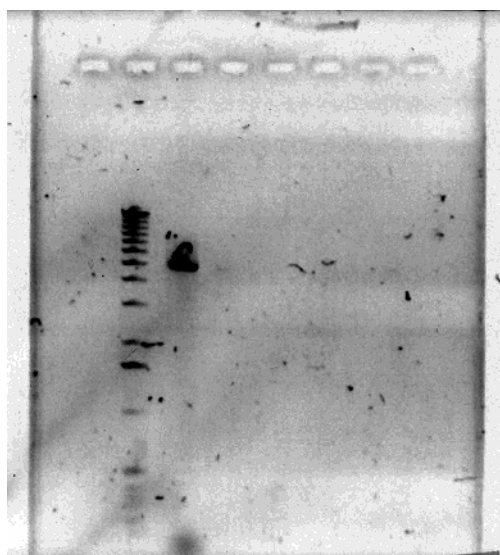
0.4 μl dNTP mix

15 μl H<sub>2</sub>O

0.4 μl *Pfu Turbo* DNA polymerase

The tube was chilled to 0 °C in an ice bucket before the addition of the enzyme. The tube was then placed in a thermocycler and subjected to the following program: Heat to 95 °C for 30 seconds, then 16 cycles of heat to 95 °C for 30 seconds, cool to 55 °C for 1 min, warm to 68 °C 10 min (2 min/kbase). Then the reaction was cooled to 4 °C and held there until workup. During the reaction, the template DNA was methylated, allowing it to be recognized and digested. To destroy the template DNA, 0.5 µl *Dpn I* restriction enzyme was added to the tube on ice and allowed to react for 2 min. The tube was then incubated at 37 °C for 1 hr.

To evaluate the success of the PCR reaction, an electrophoresis gel of the DNA was run. The gel itself was made by mixing 0.3 g ultrapure agarose (Pharmacia) with 30 ml H<sub>2</sub>O in a beaker, heating the solution to a boil in a microwave, and pouring the slightly cooled solution into a mold. The electrolytic solution for the gel was TAE buffer 50 fold dilution of 50×TAE buffer). Once the gel had solidified, it was placed in an electrophoresis tray. Two of the eight possible lanes were used: lane 2 contained 20 µl 1kbase DNA ladder (Stratagene), lane 3 contained 4 µl dye + 16 µl PCR product. Voltage was then applied to the gel for 1.4 hrs. The gel was removed, and a fluorescence photograph of the gel acquired showing only one PCR band of the appropriate size (Figure 4.3.3-3).



**Figure 4.3.3-3:** DNA Gel. Negative of a fluorescence photograph of PCR product of F108W mutation.

**Sequencing:**

In order to confirm that the mutations had in fact been inserted in the proper place, the PCR product had to be expressed in bacteria to provide enough copies to properly sequence the DNA. For this purpose, Epicurian Blue (aka XL1 Blue) *E. coli* (supercompetent, from Stratagene) were employed. An example procedure for the F108 to W108 mutant is given below.

XL1 Blue *E. coli* cells were thawed from -80 °C to 0 °C on ice. Then, 50 µl of cells were transferred to a pre-chilled 1.5 ml ependorf tube, the remainder of the cells were refrozen at -80 °C. The cells at 0 °C were mixed with 1 µl of the PCR product for the F108W mutation. The mixture was allowed to incubate at 0 °C for 30 min. Then, the tube was warmed to 42 °C in the thermocycler for 45 seconds, followed by 2 min at 0 °C. The chilled mixture was mixed with 250 µl NYZ+ broth, transferred to 10 ml falcon tube and placed in shaker at 37 °C for 1 hr. The cells were then transferred via pipetteman to LB agar plates inoculated with ampicillin (courtesy of the munificent W. Wehbi); glass beads were added to the plate and the whole plate rotated to evenly distribute the XL1 Blue cells. The plate was then placed in a 37 °C incubator in the dark for 16 hrs at which time colonies of bacteria were visible. In order to get a DNA sequence for the mutation, two colonies were selected with autoclaved toothpicks and grown in 0.8 ml 5×LB, 3.2 ml autoclaved H<sub>2</sub>O, 4 µl ampicillin (60 mg/ml) in a 10 ml falcon tube at 37 °C in a shaker for 18 hrs. At this time, the optical density was checked by light scattering at 600 nm and found to be 1.1. 0.4 ml of each batch was reserved, mixed with 100 µl 80% glucose (autoclaved) and frozen

at -80 °C. The remainder of each sample was worked up using the QIAprep<sup>®</sup> Miniprep (Qiagen) plasmid DNA purification kit; following the procedure outlined on p. 18-19 of the QIAprep<sup>®</sup> Miniprep Handbook (July 1999). The resulting two aqueous solutions of DNA contained 102 ng DNA/μl and 60 ng DNA/μl, judging from absorbance at 260 nm. The ratio  $A_{280}/A_{260}$  was in the desirable 1.7-1.8 range for each solution (1.7 for each). 10 μl from each batch was sent to Sequence and Structure Analysis Facility at the California Institute of Technology for DNA sequencing. The remainder of the solutions were stored at -20 °C. Sequences for both batches came back positive, showing the correct sequences (Figure 4.3.3-4). Raw output of these and other sequencing runs can be found in Appendix A.

#### 4.3.4. Protein Expression

Expressing the protein is a simple matter of placing the appropriate plasmid in *E. coli* designed to produce protein. For this purpose, BL21 (DE3) *E. coli* (supercompetent, from Stratagene) were employed. An example procedure for the F108 to W108 mutant is given below.

BL21 (DE3) *E. coli* cells were thawed from -80 °C to 0 °C on ice. Then, 20 μl of cells were transferred to a pre-chilled 1.5 ml ependorf tube, the remainder of the cells were refrozen at -80 °C. The cells at 0 °C were mixed with 1 μl of the sequenced DNA for the F108W mutation. The mixture was allowed to incubate at 0 °C for 5 min. Then, the tube was warmed to 42 °C in the thermocycler for 30 seconds, followed by 2 min at 0 °C. The

```

GCT GAA TGC TCC GTT GAT ATC CAG GGT AAT GAT CAG ATG CAG TTC AAC ACC AAC GCC ATC ACC GTC GAC
A  E  C  S  V  D  I  Q  G  N  D  Q  M  Q  F  N  T  N  A  I  T  V  D
1                                     23

AAG AGC TGC AAG CAG TTC ACT GTT AAC CTG TCT CAC CCA GGT AAC CTG CCG AAG AAC GTT ATG GGT CAC
K  S  C  K  Q  F  T  V  N  L  S  H  P  G  N  L  P  K  N  V  M  G  H
24                                     45 46

AAC TTC GTT CTG TCC ACC GCG GCT GAC ATG CAA GGC GTT GTC ACT GAC GGT ATG GCT AGC GGT CTG GAT
N  F  V  L  S  T  A  A  D  M  Q  G  V  V  T  D  G  M  A  S  G  L  D
47 48                                     69

AAA GAC TTC CTG AAG CCG GAT GAC TCT CGA GTT ATC GCC CAG ACC AAG CTG ATC GGA TCC GGT GAA AAA
K  D  F  L  K  P  D  D  S  R  V  I  A  Q  T  K  L  I  G  S  G  E  K
70 72                                     83                                     92

GAC TCC GTT ACT TTC GAC GTT TCC AAG CTT AAA GAA GGT GAA CAC TGG ATG TTC TTC TGC ACT TTC CCG
D  S  V  T  F  D  V  S  K  L  K  E  G  E  H  W  M  F  F  C  T  F  P
93                                     107 108                                     112 115

GGT CAC TCC GCA CTG ATG AAA GGT ACC CTG ACT CTG AAA
G  H  S  A  L  M  K  G  T  L  T  L  K
116 117                                     121                                     128

```

**Figure 4.3.3-4:** Sequence for H83Q/W48F/Y72F/Q107H/Y108W. **1** reference numbering; **46** Cu ligands; **108** mutations from the wild-type sequence. Note: this sequence only shows the sequence for protein expression; the entire plasmid is ~ 5000 bases.



chilled mixture was mixed with 80  $\mu$ l SOC buffer and transferred directly to LB agar plates inoculated with ampicillin; glass beads were added to the plate and the whole plate rotated to evenly distribute the cells. The plate was then placed in a 37 °C incubator in the dark for 16 hrs at which time colonies of bacteria were visible. The plate was then stored at 4 °C until it was needed for the next step.

To grow the protein on a sufficient scale, the cells were cultured on a 6 L scale. First, two single colonies were selected from the agar plate and grown in 0.8 ml 5 $\times$ LB, 3.2 ml autoclaved H<sub>2</sub>O, 4  $\mu$ l ampicillin (60 mg/ml) in each of two 10 ml falcon tube at 37 °C in a shaker for 7 hrs to an optical density at 600 nm of 0.7. 1 ml of these starter cultures were added to 6 $\times$ 4 L Erlenmeyer flasks each containing 1 L LB broth (autoclaved) with 4 ml ampicillin (60 mg/ml, added after autoclave and cooling of broth). 0.4 ml of the remaining starter culture was reserved, mixed with 100  $\mu$ l 80% glucose (autoclaved) and frozen at -80 °C. The 6 erlenmeyers were placed in a shaker at 37 °C for 12 hrs to an optical density at 600 nm of 1.2. Then, to induce protein expression, each erlenmeyer was inoculated with 1 ml 0.4 M isopropyl- $\beta$ -thiogalacto-pyranoside (IPTG) and allowed to continue mixing in a shaker at 37 °C for 3 hrs. The cells were then collected by ultra centrifugation (6 $\times$ 1 L centrifuge tubes in a JLA 8.1000 rotor, spun at 6000 rpm). The cells were then resuspended in 1.5 L sucrose solution in 6 $\times$ 250 ml centrifuge tubes, shaken at room temperature for 30 min in order to swell the cells. The bacteria were then recollected by ultra centrifugation, 7000 rpm. Resuspension of the cells in cold (4 °C) 1 L MgSO<sub>4</sub> buffer was followed by shaking at 4 °C for 1 hr with the effect of lysing the cells. The lysed cell remains were removed by centrifugation at 7000 rpm. The supernatant was acidified by addition of 200

ml of 200 mM NaOAc buffer, pH 4.5 to give a final concentration of 24 mM NaOAc buffer, pH 4.5. To make the Zn(II) version of the protein, 2.7 g  $\text{ZnSO}_4$  (10 mM) was added to the solution, to make the Cu(II) version, 4.2 g  $\text{CuSO}_4 \cdot 5\text{H}_2\text{O}$  (10 mM) was added to the solution. In either case, the cell extrudate was allowed to sit at 4 in the dark for 7 days. At the end of that time, a fair amount of precipitated protein was observable; hopefully only undesirable protein. This precipitate was separated from the supernatant by centrifugation and the now clear solution was concentrated by Amicon over a 10,000 MWCO membrane (YM-10 Millipore). The concentrated azurin was washed several times with 25 mM NaOAc pH 4.5 buffer. The concentrated Cu(II) protein was examined by UV/Vis spectroscopy. Assuming an extinction coefficient of  $5900 \text{ M}^{-1}\text{cm}^{-1}$  at 628 nm, the crude yield of protein was found to be 25 mg, suggesting a yield of  $\sim 4.2 \text{ mg azurin/L media}$ . The major impurity observable in this crude mixture was some sort of cytochrome protein with an absorption band with  $\lambda_{\text{max}} \sim 420 \text{ nm}$ . This crude extrudate was then purified by one of two FPLC methods.

#### *Method A: Anion exchange resin*

The first method used to purify the unlabeled azurin extracts was FPLC purification with anionic exchange resin (Mono-Q, Pharmacia). This resin consists of a surface quaternary amine, thus, it shows an affinity for negatively charged species. Given that the pI of azurin is 5.4 [54] (pH at which the protein has an overall neutral charge), to use this column the protein must be in a high pH solution. To affect this, the protein was exchanged by Amicon over a 10,000 MWCO membrane (YM-10 Millipore) into 25 mM DEA buffer

at pH 9.0. The protein was then applied to the anion exchange resin in 5 mg batches. The azurins do not bind tightly to the resin, nonetheless, the protein was eluted with a gradient between buffer A ( 25 mM DEA buffer, pH 9.0) and buffer B (25 mM DEA, 200 mM NaCl buffer, pH 9.0) shown in Table 4.3.4-1. This led to the elution of a single peak at 80% A, 20% B with (for cuproprotein) the characteristic blue copper spectrum of azurin. At 100 % B, a red band eluted, likely the cytochrome observed in the extrudate.

| Time (min) | %Buffer A | %Buffer B | Flow Rate (ml/min) |
|------------|-----------|-----------|--------------------|
| 0          | 100       | 0         | 1.5                |
| 15         | 100       | 0         | 1.5                |
| 20         | 80        | 20        | 1.5                |
| 40         | 80        | 20        | 1.5                |
| 45         | 0         | 100       | 1.5                |
| 60         | 0         | 100       | 1.5                |

**Table 4.3.4-1:** FPLC gradient for unlabeled protein purification by Mono-Q (anion exchange resin, Pharmacia).

*Method B: Cation exchange resin*

The preferred method for purification of the unlabeled azurin extracts was FPLC purification with cationic exchange resin (Mono-S, Pharmacia). This resin consists of a surface thiolate, thus, it shows an affinity for positively charged species. Once again, given the pI of 5.4, the azurin must be in acidic media. To affect this, the protein was exchanged by Amicon over a 10,000 MWCO membrane (YM-10 Millipore) into 25 mM NaOAc buffer at pH 4.5. The protein was then applied to the cation exchange resin in 5 mg batches.

In contrast to the anion exchange resin, the azurins bind tightly to the Mono-S column. This necessitated eluting the protein with a gradient between buffer A ( 25 mM NaOAc buffer, pH 4.5) and buffer B (300 mM NaOAc, buffer, pH 4.5) shown in Table 4.3.4-2. This led to the elution of a single peak at 85% A, 15% B with (for cuproprotein) the characteristic blue copper spectrum of azurin. At 100 % B, a red band eluted, likely the cytochrome observed in the extrudate. See Appendix A for FPLC traces for the relevant mutants.

| <b>Time (min)</b> | <b>%Buffer A</b> | <b>%Buffer B</b> | <b>Flow Rate (ml/min)</b> |
|-------------------|------------------|------------------|---------------------------|
| <b>0</b>          | 100              | 0                | 2                         |
| <b>20</b>         | 100              | 0                | 2                         |
| <b>40</b>         | 85               | 15               | 2                         |
| <b>75</b>         | 85               | 15               | 2                         |
| <b>90</b>         | 0                | 100              | 2                         |
| <b>130</b>        | 0                | 100              | 2                         |

**Table 4.3.4-2:** FPLC gradient for unlabeled protein purification by Mono-S (cation, exchange resin, Pharmacia).

After using either method A or B to purify the protein, the resulting fractions of protein were analyzed by absorption spectroscopy. The characteristic blue copper band with  $\epsilon = 5900 \text{ M}^{-1}\text{cm}^{-1}$  at 628 nm along with the characteristic tryptophan shoulder with  $\epsilon \sim 5000 \text{ M}^{-1}\text{cm}^{-1}$  at 292 nm were taken as evidence for the desired compound. Often times, the ratio of  $A_{628}/A_{292}$  did not equal 1.18. This is primarily for two reasons: one, the extinction coefficient of tryptophan depends to some extent on environment [55]. That is, changes in environment change the electronic structure of tryptophan and so may affect the extinction

coefficient. The other primary cause of this effect is the ready formation of Zn azurin from the cell extrudate, in competition with Cu inclusion. Since the affinity of azurin for these two metals is similar, both may be formed at the same time, leading to apparently more absorption at 292 nm than there should be. Another bit of spectroscopic evidence that suggests that these are in fact the desired proteins is the fluorescence spectrum of the tryptophan residues (see Figure 5.3-2). These emission spectra are typical of tryptophan residues, with the maxima showing a strong dependence on environment [56].

More compelling evidence for the purity of these proteins comes from an examination of the SDS-Page gel electrophoresis analysis. The protein mass can be roughly evaluated from the retention time on an electrophoretic gel when compared with a standard. The procedure for undertaking this analysis is described for H83Q/W48F/Y72F/Q107H/Y108W Az. First, 5  $\mu$ l protein of  $\sim 50$   $\mu$ M concentration was mixed with 5 ml 2 $\times$ TB dye in a 100  $\mu$ l ependorf tube. The tube is then heated to 100  $^{\circ}$ C for 5 min in the thermocycler. Then, the resulting solution is placed on a 8-25 Phast system gel (Pharmacia) along with protein ladder from 5 kDa to 30 kDa in a separate lane. The gel is then developed by standard techniques and stained to show bands of approximate molecular weight. In each protein studied, these gels showed only a single band after FPLC purification.

The best evidence for these proteins being the desired product comes from electrospray ionization mass spectroscopy (ESI-MS). Using a protein mass calculator ([http://cgi.uvm.edu/cgi-bin/mmaccos/aa\\_calc.pl](http://cgi.uvm.edu/cgi-bin/mmaccos/aa_calc.pl)) the mass of all single tryptophan containing mutants (that is, no tyrosines) was found to be 13913.79 (apo). ESI-MS carried

out at the Protein and Peptide Mass Analysis Laboratory at the California Institute of Technology found masses within 2  $m/z$  units of the predicted value for all the studied mutants (Table 4.3.4-3). It should be noted that the ESI-MS always shows the apo azurin mass. This is because the samples must be submitted in water instead of buffer; under these conditions, the copper or zinc does not bind tightly to the protein. Therefore, when the species is ionized, the metal center is lost, showing only fragments of the apo mass.

| <b>Azurin</b>                           | <b>Calculated</b> | <b>Found</b> |
|---|-------------------|--------------|
| <b>H83Q/W48F/Y72F/Q107H/Y108W</b>       | 13913.79          | 13912.8      |
| <b>H83Q/W48F/Y72F/Q107H/Y108F/F110W</b> | 13913.79          | 13913.0      |
| <b>Y72F/Y108F</b>                       | 13913.79          | 13911.8      |

**Table 4.3.4-3:** Mass spectra for unlabeled azurin mutants; calculated from [http://cgi.uvm.edu/cgi-bin/mmaccos/aa\\_calc.pl](http://cgi.uvm.edu/cgi-bin/mmaccos/aa_calc.pl); found by ESI-MS (PPMAL).

#### 4.3.5. Labeling Reaction

##### *Rhenium (I) (4,7-dimethyl-1,10-phenanthroline) tricarbonyl triflate (2a)*

2.0 g (3.9 mmol) Rhenium (I) (4,7-dimethyl-1,10-phenanthroline) tricarbonyl chloride (synthesized identically to **1**, 55% yield) was dissolved in 30 ml dry methylene chloride to give a yellow suspension in a 50 ml round bottom flask equipped with a stir bar. The solution was degassed by a 5 min argon sparge. To this suspension, trifluoromethane sulfonic acid (triflic acid, Aldrich) was added dropwise under a counter flow of argon until

the last of the solid had disappeared. The solution was allowed to stir open for ~ 2 hrs until a strip of indicator paper held over the top of the flask indicated a pH of ~ 5.0. Then, diethyl ether was added to the yellow solution slowly leading to the precipitation of an off yellow solid. The solid was collected by filtration over a fine porosity glass fritted funnel, and washed 3×50 ml with diethyl ether. The off yellow solid was dried under vacuum over night to give 2.2 g solid. No further characterization or purification was attempted. Note: investigations of the identical reaction with Rhenium (I) (1,10-phenanthroline) tricarbonyl chloride indicate very little spectroscopic distinction between the two chloride and the triflate compound suggesting there is in fact no covalent interaction of the triflate anion with rhenium. Further complicating the picture, the reaction most certainly does not go to completion as evidenced by the next step.

*Rhenium (I) (4,7-dimethyl-1,10-phenanthroline) tricarbonyl aquo triflate (4)*

From reference [57]. 2.2 g (~3 mmol) **2a** was suspended in 50 ml water in a 100 ml beaker equipped with a stir bar. Much of **2a** floated to the top of the vessel, forming a yellowish foam. The reaction was heated to 60 °C with stirring for 3 hrs. After this length of time, the solution phase had gone from clear to yellow and the foam was still present. The suspension was filtered over a medium porosity glass fritted funnel to give a yellow supernatant and a of yellow solid. The yellow solid was resuspended in water and the procedure repeated 10 times. The supernatants were combined, and the water removed by slow evaporation to give 1.1 g brown crystals (~50 % yield).

A standard labeling reaction is described for the H83Q/W48F/Y72F/Q107H/Y108W mutant below. 0.02 g (0.0014 mmol) H83Q/W48F/Y72F/Q107H/Y108W Az Cu(II) in 1 ml 25 mM HEPES buffer, pH 7.4 was divided in 5 aliquots of 200  $\mu$ l each in 5 $\times$ 1.7 ml eppendorf tubes. In parallel, 0.0084 g (0.013 mmol) **4** was dissolved in 6.5 ml water by gentle heating and stirring over 2 hrs. To each eppendorf tube containing protein, 1.3 ml of the solution of **4** was added leading to final concentrations of 3.3 mM HEPES, 0.9 mM azurin, and 1.7 mM **4**. These tubes were then placed in a heating block at 37 °C in the dark and allowed to incubate for 7 days. At the end of this time, the tubes were removed from the heating block and concentrated by centrifugation in 10000 MWCO Centricons (Pharmacia). The Re-labeled azurin was then exchanged into 25 mM NaOAc, pH 4.5 by passing the protein down a PD-10 gel filtration column (Pharmacia) equilibrated with the desired acetate buffer. The elution of the protein was followed by both observation of the characteristic blue color and by the observation of the yellow emission of the band stimulated by a standard UV B lamp. The collected protein was then concentrated by Centricon once again and allowed to stand for 3 days in the dark at 4 °C. Then, the tubes were centrifuged to remove the precipitated rhenium complex (e.g., rhenium that did not bind to the protein) and the protein was once more run down a PD-10 column equilibrated with 20 mM NaPi, 750 mM NaCl buffer, pH 7.2 to remove excess rhenium that did not bind or precipitate and to prepare the protein for purification. Both PD-10 columns are essential for this step: excess rhenium will bind strongly to the IMAC column. The methods for Zn proteins as well as all of the other mutants were very similar.



#### 4.3.6. *Purification of Labeled Azurins*

##### *Copper binding column*

The first stage of Re-labeled azurin purification was to remove any protein not labeled at the single surface histidine. To accomplish this goal, an IMAC column (Pharmacia) was employed. This column uses a surface composed of histidines to bind Cu(II) from a CuSO<sub>4</sub> solution injected before the protein. This resin-bound Cu(II) then binds tightly to any exposed surface histidine on the protein. In this way, azurins with an unlabeled surface histidine are held tightly by the column, while azurins with a Re-labeled surface histidine pass directly through the column. The protein was applied to the copper column in 5 mg batches, and eluted with a 20 mM NaPi, 750 mM NaCl buffer, pH 7.2. To remove the tightly bound unlabeled protein, after elution of the desired fraction, the column was washed with a 20 mM NaPi, 750 mM NH<sub>4</sub>Cl buffer, pH 7.2. This unlabeled fraction could be recovered and reused. See Appendix A for FPLC traces of the various mutants.

##### *Cation exchange resin*

In an approach analogous to purification of the unlabeled protein, after removal of the unlabeled protein, the remainder (“correctly labeled”) protein was purified by cationic exchange resin (Mono-S, Pharmacia). This resin consists of a surface thiolate, thus, it shows an affinity for positively charged species. Once again, given the pI of 5.4, the azurin must be in acidic media. To exchange the buffer, the fractions from the IMAC column were concentrated in Centricons and passed down a PD-10 gel filtration column

(Pharmacia) equilibrated with 25 mM NaOAc, pH 4.5. The resulting solution was then applied to the cation exchange resin in 2 ml batches. Since the Mono-S column binds as a function of charge, the addition of the positively charged rhenium label causes the rhenium-labeled protein to bind more strongly to the column than the unlabeled protein. This in turn requires a longer gradient against 300 mM NaOAc, pH 4.5 to move the protein off the column (Table 4.3.6-1). See Appendix A for FPLC traces of the various mutants.

| Time (min) | %Buffer A | %Buffer B | Flow Rate (ml/min) |
|------------|-----------|-----------|--------------------|
| 0          | 100       | 0         | 2.5                |
| 5          | 100       | 0         | 2.5                |
| 10         | 85        | 15        | 2.5                |
| 60         | 85        | 20        | 2.5                |
| 65         | 0         | 100       | 2.5                |
| 85         | 0         | 100       | 2.5                |

**Table 4.3.6-1:** FPLC gradient for Re-labeled Az purification by Mono-S (cation exchange resin, Pharmacia).

#### *Characterization*

After FPLC purification of the labeled protein, the resulting fractions were analyzed by absorption spectroscopy. The characteristic blue copper band with  $\epsilon = 5900 \text{ M}^{-1}\text{cm}^{-1}$  at 628 nm along with the characteristic rhenium absorption with  $\epsilon = 6000 \text{ M}^{-1}\text{cm}^{-1}$  at 355 nm (Figure 4.2-4) were taken as evidence for the desired compound. In addition to the absorption, yellow emission visible under short wavelength irradiation also suggested the compound was the desired one.

Better evidence for these proteins being the desired product comes from electrospray ionization mass spectroscopy (ESI-MS). Using a protein mass calculator ([http://cgi.uvm.edu/cgi-bin/mmaccos/aa\\_calc.pl](http://cgi.uvm.edu/cgi-bin/mmaccos/aa_calc.pl)) the mass of all single tryptophan containing mutants (that is, no tyrosines) was found to be 13913.79 (apo). Adding to that the calculated mass of the Re(I)(phen)(CO)<sub>3</sub> fragment (478.5) a total mass of 14392.29 is predicted for the apo form of each single tryptophan mutant. ESI-MS carried out at the Protein and Peptide Mass Analysis Laboratory at the California Institute of Technology found masses within 1 mass unit of the predicted value for all the studied mutants (Table 4.3.6-2). It should be noted that the ESI-MS always shows the apo azurin mass. This is because the samples must be submitted in water instead of buffer; under these conditions, the copper or zinc does not bind tightly to the protein. Therefore, when the species is ionized, the metal center is lost, showing only the apo mass.

One last method of characterization is crystallization. With collaborators at Cornell University, the crystal structure for [Re(H107)(W108)Cu(II)] has been solved (see 4.2 ). Unfortunately, not all mutants grow crystals so nicely, but by analogy the characterization data for the other proteins is taken to be enough.

| <b>Azurin</b>             | <b>Calculated</b> | <b>Found</b> |
|---------------------------|-------------------|--------------|
| <b>[Re(H107)(W108)Az]</b> | 14392.29          | 14391.0      |
| <b>[Re(H107)(W110)Az]</b> | 14392.29          | 14392.1      |
| <b>[Re(H83)(W48)Az]</b>   | 14392.29          | 14393.0      |

**Table 4.3.6-2:** Mass spectra for Re-labeled azurin mutants; calculated from unlabeled *m/z* values with additional mass for Re fragment; found by ESI-MS (PPMAL).

As noted above, simply incubating the cell extrudate with Cu(II) leads to a mixture of Cu(II) and Zn(II) azurin. To be quantitative about Cu(I) oxidation yields, and to remove obscuring signals from the EPR, it is desirable to have protein with only Zn(II) or only Cu(II) in the metal center. To do this, there are two available avenues.

*Method A: FPLC purification*

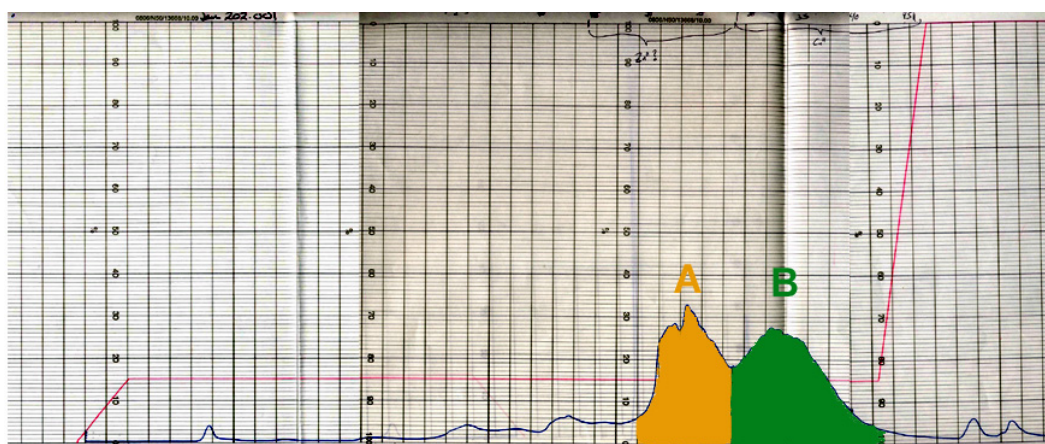
Beginning with a sample of [Re(H107)(W108)AzCu(II)] that is contaminated with Zn(II); one can remove the excess Zn(II) protein and bring the  $A_{628}/A_{355}$  did close to 1 by purification over cationic exchange resin (Mono-S, Pharmacia). Slow gradient conditions with A = 25 mM NaOAc, pH 4.5 and B = 25 mM NaOAc, pH 4.5 (Table 4.3.6-1) allow for separation of the Zn(II) protein from Cu(II) protein (Figure 4.3.6-1), confirmed by UV/Vis.

| Time (min) | %Buffer A | %Buffer B | Flow Rate (ml/min) |
|------------|-----------|-----------|--------------------|
| 0          | 100       | 0         | 2.0                |
| 5          | 85        | 15        | 2.0                |
| 50         | 85        | 15        | 2.0                |
| 55         | 0         | 100       | 2.0                |
| 70         | 0         | 100       | 2.0                |

**Table 4.3.6-3:** FPLC gradient for separation of Zn(II) and Cu(II) azurin.

*Method B: Cu removal*

Following the method of Blaszkak *et al.* [53] and Di Bilio *et al.* [46]; the reduced Cu(I) may be abstracted from the Re labeled azurin. Briefly, 4 ml of a 70  $\mu$ M solution of [Re(H83)(W48)AzCu(II)] in 25 mM NaOAc pH 4.5 was reduced by a slight excess of

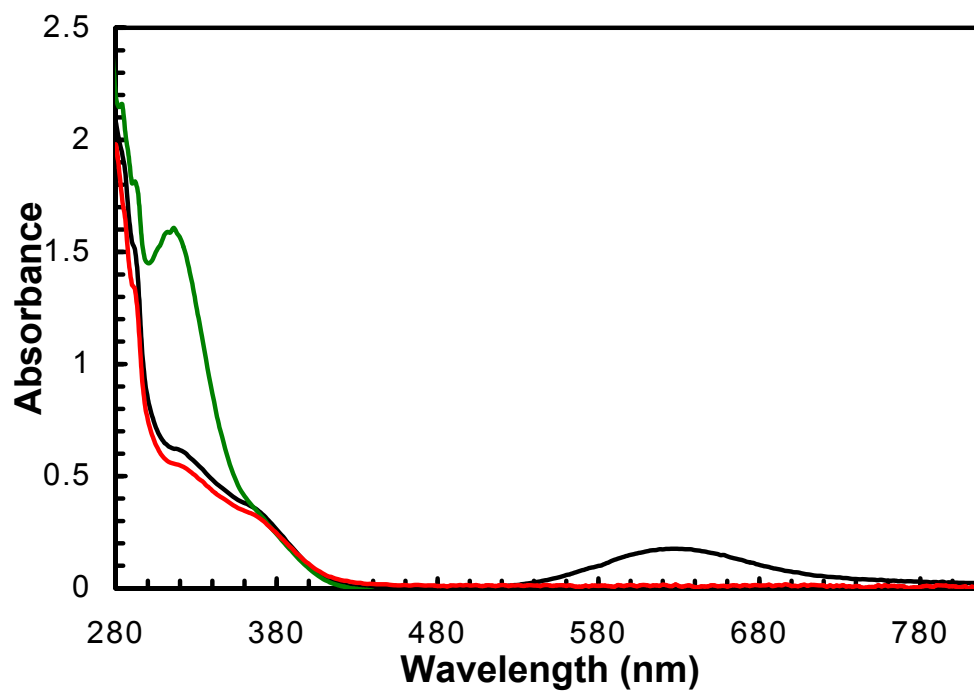


**Figure 4.3.6-1:** FPLC separation of Zn(II) and Cu(II) azurin (A) [Re(H107)(W108)AzZn(II)] from (B) [Re(H107)(W108)AzCu(II)].

sodium dithionite. The solution was then transferred into 3500 MWCO dialysis tubing (Pharmacia) and dialyzed against 400 ml of 250 mM NaCl, 100 mM thiourea and 25 mM NaOAc pH 4.5 at 4 °C for 18 hrs in the dark. The protein solution was then removed from the dialysis tubing and concentrated in a Centricon with 5 mM ZnSO<sub>4</sub> 25 mM NaOAc pH 5.3. After fully exchanging the dialysis buffer for the Zn replacement buffer, the protein was allowed to sit at 37 °C in a heating block in the dark for 12 hrs. The protein was then exchanged into 25 mM NaOAc buffer, pH 4.5 and examined by absorption spectroscopy showing no trace of Cu(II) absorption (Figure 4.3.6-2). Addition of the oxidant KCo(III)EDTA showed no increase at 630 nm indicating there was no Cu(I) present either. Based on absorption at 355 nm, it appears that the yield of this reaction was ~ 90%.

#### **4.3.7. *Measuring a Rate and Observing Radical Formation***

In order to examine rates of Cu(I) oxidation, the Cu(II) proteins first had to be reduced to their Cu(I) forms. To achieve this, a concentrated (~300 µM) solution of ReAzCu(II) in any of the buffers used in this thesis was reduced by careful addition of sodium dithionite to the solution. Sodium dithionite was added just until the blue color of the solution disappeared. Then, the protein was passed down a PD10 column (Pharmacia) equilibrated with the buffer to be used in the laser experiment; in this way excess dithionite was removed from the sample before the laser experiment. The concentration of the solution was evaluated by UV/Vis spectroscopy to determine concentration, then either concentrated in a centricon or diluted with excess buffer to reach the appropriate



**Figure 4.3.6-2:** UV/Vis absorption of metal removal from [Re(H83)(W48)AzM]. (—) M = Cu(II) (—) M = Cu(I) + sodium dithionite (—) Zn(II).

concentration of protein as determined by absorption at 355 nm. Immediately after the concentration was selected, the protein was placed in an atmosphere-controlled cuvette and degassed to prevent re-oxidation of the Cu(I) center to Cu(II).

All of the reported laser experiments use a 355 nm laser pulse at a power of 1-3 mJ/pulse to pump the samples. Broad-band spectra were acquired on NS2 (see Chapter 2), at delays of 16  $\mu$ s to 5 ms; unless substantial change of the spectra was observed, only one spectrum is reported. For kinetic experiments (radical formation rates, Cu(I) oxidation rates), NS1 (Chapter 2) was employed. For all wavelengths without substantial contribution from the excited state emission (<520 nm >710 nm) the probe was a Xe arc lamp, often equipped with a 355 nm long pass filter. For observation of the Cu(I) oxidation, a HeNe CW laser was used as described in Chapter 2.

To investigate the formation of radicals in these proteins, the following procedure was used. A dilute 1 ml (30  $\mu$ M-60  $\mu$ M, typically taken directly from the final Mono-S column) sample of Re-labeled azurin was reduced to  $\sim$  250  $\mu$ l by centricon. The sample was passed down a PD-10 gel filtration column equilibrated with the appropriate buffer. The concentration of the resulting solution was measured by absorption spectroscopy ( $\epsilon_{355}$  = 6000 M<sup>-1</sup>cm<sup>-1</sup>) and the volume reduced by centricon to 150-200  $\mu$ l (measured by microliter syringe or pipetteman) to give a final protein concentration of 300-600  $\mu$ M. The concentrated protein solution was allowed to incubate with a small amount of Co(III)(NH<sub>3</sub>)<sub>5</sub>Cl for 5 min at room temperature in the dark. The solution was then carefully removed from the remaining solid by pipette and added to an atmosphere-



controlled EPR tube, and subjected to the flash/quench/freeze EPR experiment (see Chapter 2).

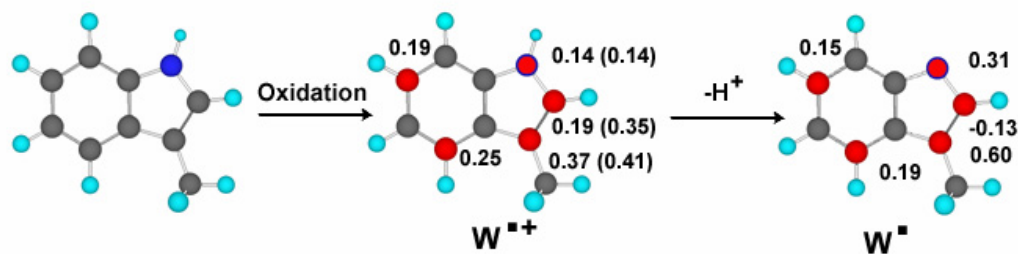
## Chapter 5

### TRYPTOPHAN RADICALS

#### 5.1. *Radical Formation in a Model System*

A key component of understanding multi-step ET in any system is being able to identify the intermediate charge carriers. As indicated to above, the majority of the work undertaken in this section focuses on the use of tryptophan as a charge (“hole”) carrier. As such, understanding the properties of one-electron oxidized tryptophan ( $W^{\bullet}$ ) is of paramount importance.

A few studies have addressed the nature of this radical. The oxidation potential of the amino-acid residue has been indirectly determined to be  $\sim 1$  V vs. NHE [58, 59], but this value is approximate because it relies on rates of reaction of the radical (generated by pulse radiolysis) with reductive quenchers of known potential. An important issue to consider along with the redox potentials of the radical is protonation state. As Figure 5.1-1 shows, the radical can exist as either the neutral radical or the radical cation. Upon oxidation the first species formed is a tryptophan radical cation ( $W^{\bullet+}$ ). As a monomer,  $W^{\bullet+}$  has a  $pK_a$  of 4.5 and rapidly loses a proton to give  $W^{\bullet}$  ( $\tau = 1.1 \mu s$ ) [60]. To accomplish a given reaction, proteins can stabilize either  $W^{\bullet}$  or  $W^{\bullet+}$ . Primarily, preference for one protonation state over



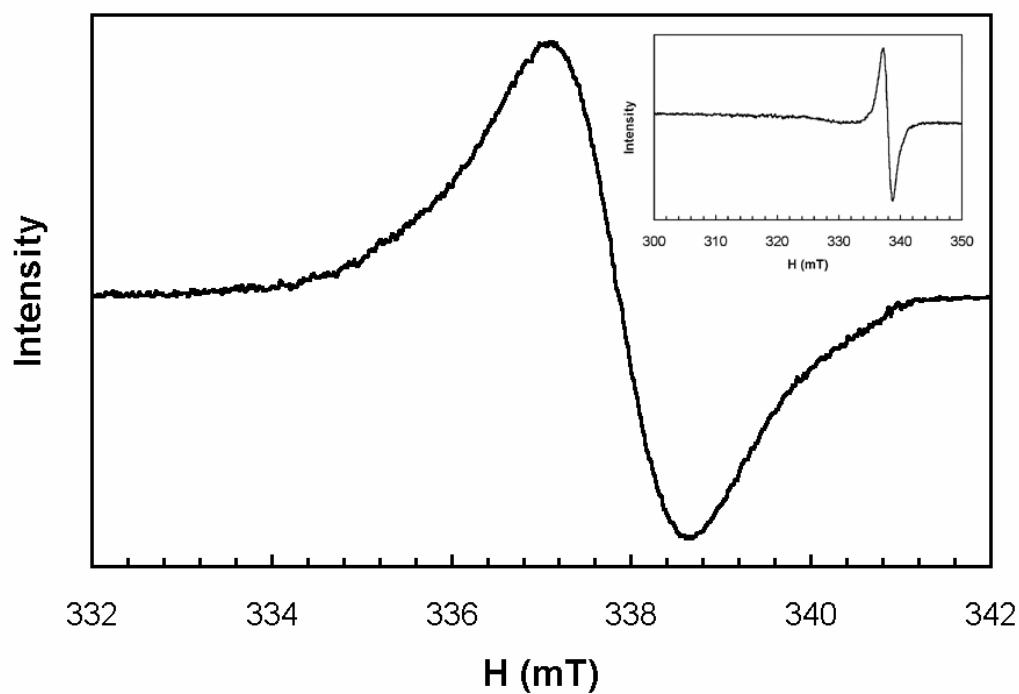
**Figure 5.1-1:** Schematic of a one-electron oxidation of tryptophan (the amide portion is truncated for clarity). Numbers correspond to spin density calculated by DFT methods [61] (experimental results cited from [62]). Color scheme: (●) proton (●) carbon (●) nitrogen (●) spin density.

the other is driven by the fact that the redox potentials differ by  $\sim 100$  mV [63], a biologically accessible difference in potential. Thus it is necessary to distinguish between the two states.

Calculations (Figure 5.1-1) suggest that there are substantial differences in the electronic structure of  $W^{\bullet+}$  and  $W^{\bullet}$ ; thus the spectroscopy of the two species is quite different. For the free monomer, paramagnetic resonance spectra (e.g., EPR, ENDOR, ESEEM) for the cationic and neutral radical have not been observed, although the theoretical framework for observing the differences with these techniques exists [64]. Absorption spectroscopy, on the other hand, has shown striking results. In pulse radiolysis experiments on tryptophan in phosphate buffered solutions at pH 3 and pH 7-10, significantly different absorption spectra have been observed [65]. At low pH, the absorption spectrum shows three maxima:  $\lambda_{\text{max}} = 335$  nm ( $4750 \text{ M}^{-1}\text{cm}^{-1}$ ), 560 nm ( $3000 \text{ M}^{-1}\text{cm}^{-1}$ ) and 600 nm ( $3000 \text{ M}^{-1}\text{cm}^{-1}$ ). At neutral or high pH, the absorption spectrum shows two maxima:  $\lambda = 335$  nm ( $3670 \text{ M}^{-1}\text{cm}^{-1}$ ) and 510 nm ( $2300 \text{ M}^{-1}\text{cm}^{-1}$ ). For acidic conditions, the two maxima around 580 nm correspond to a single broad absorption band with a “double hump” maximum; for neutral/basic conditions the red band shows no such fine structure. No theoretical explanation of this situation has been advanced, although preliminary calculations undertaken with D. R. Kent IV have suggested that the double maxima results from two nearly degenerate electronic states of the cation [66]. Thus, the two protonation states should be readily distinguishable by absorption spectroscopy and by appropriate paramagnetic resonance techniques.

The first order of business, then, is to show that the photogenerated “Re(II)” species will in fact be capable of oxidizing tryptophan. To establish this minimum benchmark, solutions of **3a** saturated with Co(III)(NH<sub>3</sub>)<sub>5</sub>Cl and with the dipeptide tryptophan-glutamate (Trp-Glu, chosen for its increased solubility in water relative to the tryptophan residue itself) were exposed to the flash/quench/freeze EPR experiment. The observed spectrum (Figure 5.1-2) shows only an inversion with g apparent at 2.003 with none of the associated structure seen in the EPR of **3a**<sup>ox</sup> (Figure 4.1-6); indicating that the “Re(II)” species was consumed by the reaction. This result suggests that the photogenerated “Re(II)” species is capable of oxidizing the tryptophan dipeptide, at least in a bimolecular reaction.

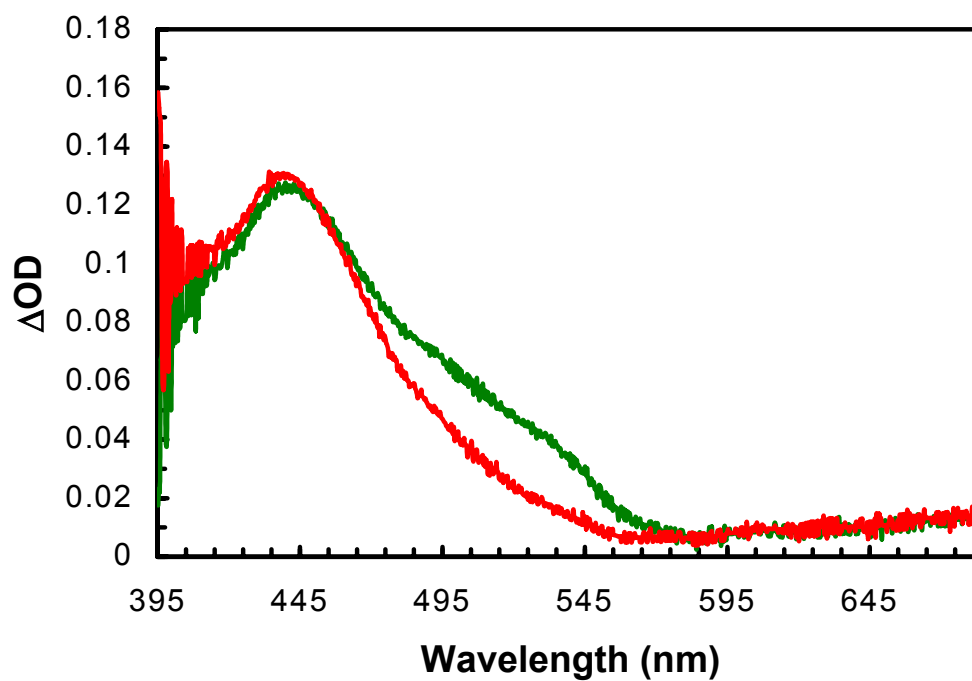
Next, it is necessary to observe the absorption spectrum of W<sup>•+</sup> and W<sup>•</sup> under the conditions that are important for the investigations of Re-labeled azurins. To acquire these data, buffered solutions of **3a** with Co(III)(NH<sub>3</sub>)<sub>5</sub>Cl and Trp-Glu were examined on NS2. These experiments show significant differences from the spectra for W<sup>•+</sup>/ W<sup>•</sup> reported in the literature [60, 65], exhibiting substantially blue shifted bands relative to the pulse radiolysis results (Figure 5.1-3). Due to limitations of the apparatus, as well as intense absorption from the excited state of **3a** only the red band of the spectrum was directly studied. This band showed a maximum at 437 nm with a shoulder at ~520 nm which disappeared over time. Single wavelength monitoring of a similar solution showed no absorption at 600 nm at timescales greater than 10 ns. This monitoring also showed that the signal at 450 nm decays with  $\tau \sim 20 \mu\text{s}$ , while the signal at 545 nm decays with  $\tau \sim 10 \mu\text{s}$ . In order to investigate these differences further, broad-band absorption spectra of the radical in buffered solution at a variety of



**Figure 5.1-2:** X-band EPR of  $W^{\bullet}$  in a dipeptide; 2.84 mM **3a** in pH 6 water with 2.5 mM  $\text{Co(III)(NH}_3)_5\text{Cl}$  and 10 mM Trp-Glu at 40 K. Inset: same signal with a larger field sweep. Settings:  $\nu = 9.474237$  GHz; modulation frequency = 40 kHz; modulation amplitude = 4.0 G; microwave power = 8.03 mW; time constant = 20.48 ms; conversion time = 80.92 ms; 30 scans.

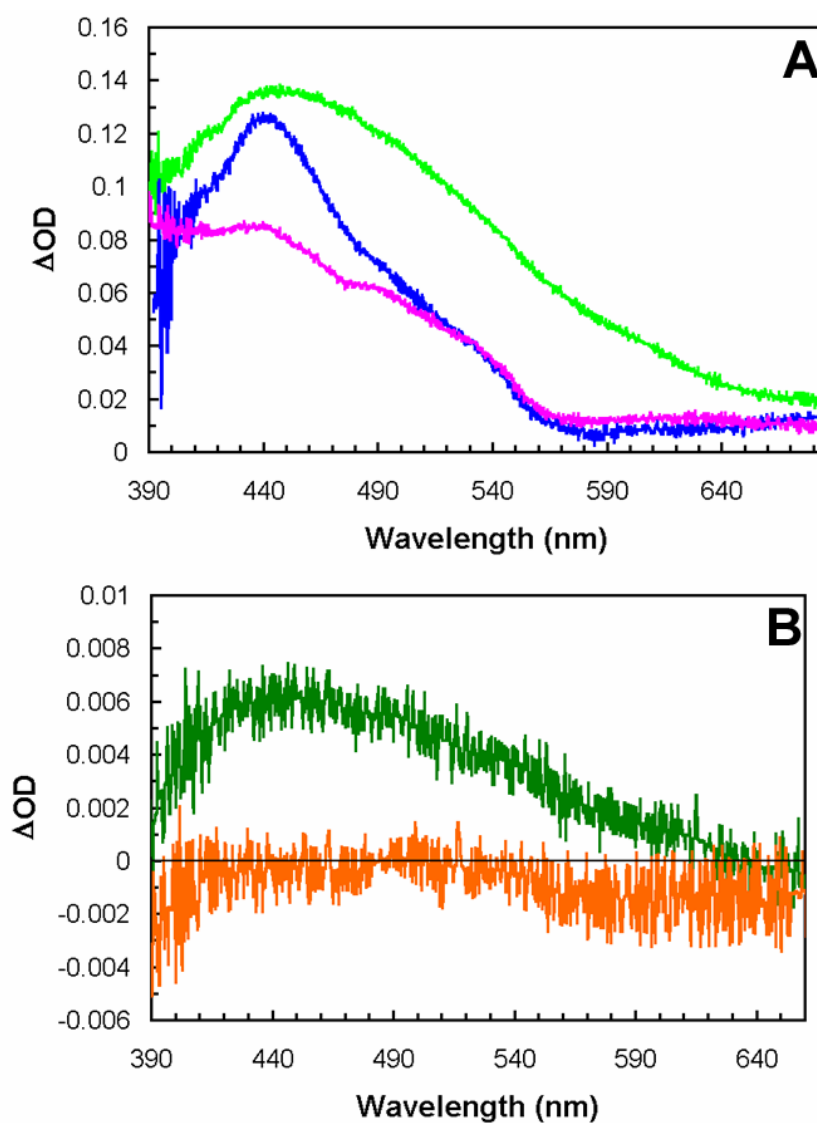
pHs were acquired (Figure 5.1-4A). Spectra at low pH are generally less featured than the neutral spectrum and show a maximum at 438 nm. At high pH, the spectrum is complex, perhaps complicated by oxidation of the glycine buffer. To confirm the nature of the high and low pH spectra, new transient absorption spectra were recorded in buffers other than glycine (Figure 5.1-4). These absorptions suggested that glycine was not innocent at high pH, although the low pH spectrum looks essentially the same.

In any case, it is apparent that this model system does not adhere to the previously published behavior for tryptophan radicals. Although this could be a limitation of the model system, these results for tryptophan radicals in azurin (5.2) suggests that there is simply a large amount of variation in the optical spectra of tryptophan radicals. In any case, it is apparent that this model system does not adhere to the previously published behavior for tryptophan radicals. Although this could be a limitation of the model system, these results for tryptophan radicals in azurin (5.2) suggests that there is simply a large amount of variation in the optical spectra of tryptophan radicals.



**Figure 5.1-3:** Transient absorption spectra of Trp-Glu; 80  $\mu M$  **3a**, 5 mM  $Co(III)(NH_3)_5Cl$  and 5 mM Trp-Glu in 50 mM KPi pH 7.16. (—) 16  $\mu s$  after the pulse, (—) 2 ms after the pulse.





**Figure 5.1-4:** NS2 spectra of  $W^{\bullet}$ , 20  $\mu$ s after the pulse, solutions of 80  $\mu$ M **3a**, 5 mM Co(III)(NH<sub>3</sub>)<sub>5</sub>Cl and (A) 5 mM Trp-Glu, (B) 1 mM Trp-Glu in a number of different buffers. (A) (—) 50 mM glycine, pH 3.60 (—) 50 mM KPi, pH 7.16 (—) 50 mM glycine, pH 9.25. (B) (—) 50 mM NaOAc, pH 4.03 (—) 50 mM NaHCO<sub>3</sub>, pH 9.8.

## 5.2. Tryptophan Radicals in Azurin

With some idea about the nature of tryptophan radicals in dipeptides, tryptophan radicals in azurin could be investigated.  $W^\bullet$  in proteins has been extensively studied by paramagnetic resonance techniques [46, 67-72]. There are, however, only a few EPR spectra of  $W^\bullet$  in environments where the radical is not obscured by other radicals or altered by coupling to a nearby paramagnetic metal center. Mutants of RNR containing tryptophans in place of tyrosines show some well-defined signals [69, 70]. The assignment of these radicals was accomplished by X-band EPR and ENDOR. The EPR shows a complicated multi-line structure with a  $g$  apparent at 2.003; simulations suggest that the fine structure is due to a substantial coupling to  $^{14}\text{N}$  as well as the  $C_\beta$  hydrogens. ENDOR of all the tryptophan radicals studied indicated that none of them were protonated. The other primary example of a “pure”  $W^\bullet$  comes from Re-labeled azurin [46]. In this case, using the same methodology to be employed here, an X-band EPR spectrum of  $W48^\bullet$  (see discussion below) was acquired; this time exhibiting a multi-line spectrum with  $g$  apparent at 2.006. Simulation of this spectrum suggested that the fine structure of the radical was due primarily to coupling of the spin to  $C_\beta$  hydrogens with little contribution from the  $^{14}\text{N}$  coupling. The remaining paramagnetic resonance investigations of tryptophan radicals deal with situations where the radical is coupled to iron in RNR [67, 71] or obscured by other radicals (e.g., a porphyrin radical) in cytochrome c peroxidase [68, 72].

There is noticeably less information on the absorption spectra of tryptophan radicals in proteins. Two examples of the absorption spectra of  $W^\bullet$  are the work on RNR [67] and a

chain of  $W^\bullet$  in DNA Photolyase [73]. The tryptophan radical in RNR for which the optical spectrum was determined is coupled to the nearby iron center, thus the EPR is somewhat difficult to interpret. In this case, the radical is formed by stopped-flow mixing of the RNR with appropriate initiators (hydrogen peroxide and/or mercaptol) allowing for time resolved spectroscopy on the millisecond timescale. By averaging the signals (from 4 ms to 14 ms) at individual wavelengths a broad-band spectrum in almost perfect agreement with that published for  $W^{\bullet+}$  [65] was obtained. The timescale of this observation highlights an important fact: protein environments are capable of stabilizing thermodynamically or kinetically unfavorable states. That is,  $W^{\bullet+}$  monomer is predicted to be 100 mV more oxidizing [63] and to decay much faster [60] than  $W^\bullet$ , yet  $W^{\bullet+}$  is apparently stable for at least milliseconds in RNR. In DNA photolyase, reduction of the DNA lesion is accomplished by the somewhat unstable  $FADH^-$  anion. In order to stabilize this anion, it is proposed that excited  $FADH^\bullet$  abstracts an electron from a surface-accessible tryptophan to give  $W^{\bullet+}$  which rapidly loses a proton to give  $W^\bullet$ . This assertion is supported by fast time resolved absorption spectroscopy, wherein the absorption spectra of  $FADH$  species subtracted from the broad-band spectrum composed of single wavelength spectra. This process gives a spectrum at short timescales (ns) that resembles the previously published cation radical spectrum of the monomer. At longer timescales (ms) this method shows a spectrum similar to the published deprotonated radical spectrum [65].

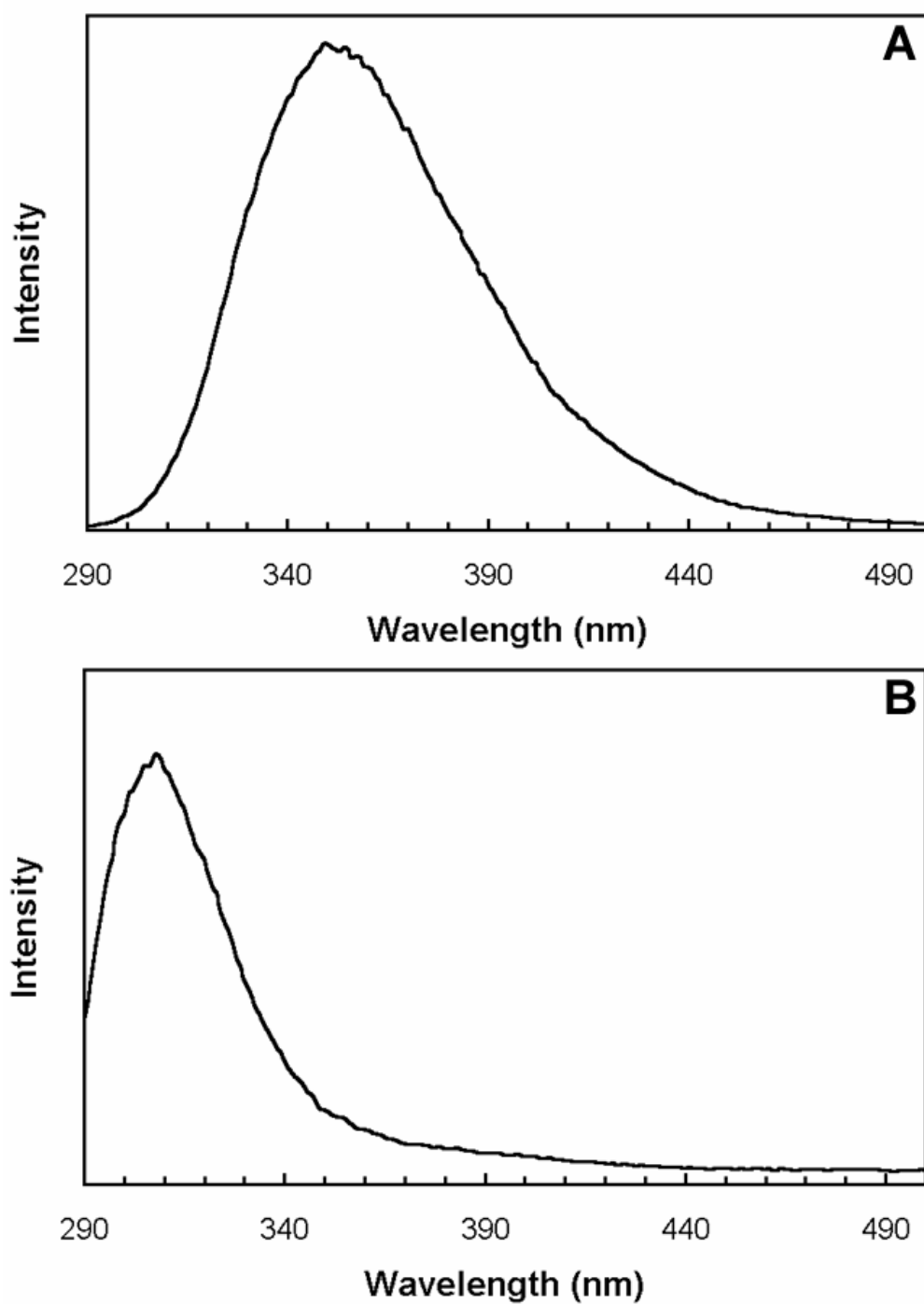
### 5.2.1. *[Re(H83)WTaz]* and *[Re(H83)(W48)Az]*

W48 in azurin is an interesting tryptophan residue; it is entirely encapsulated in the hydrophobic protein fold. This fact can be derived from an examination of the crystal structure of both the labeled and unlabeled versions of azurin and also from examination of the fluorescence of the tryptophan residue. Tryptophan fluoresces in the range of approximately 300-350 nm, with a maximum that is strongly dependent on the hydrophobicity of the surrounding environment [56, 74]. As an example, the dipeptide investigated above, Trp-Glu, shows a relatively strong fluorescence with a  $\lambda_{\text{max}} = 354$  nm ( $\lambda_{\text{ex}} = 280$  nm) in buffer (Figure 5.2.1-1A). The measured fluorescence of W48 in the wild-type azurin matches with the published value at  $\lambda_{\text{max}} = 308$  nm. This is the most strongly blue-shifted tryptophan fluorescence observed in proteins (Figure 5.2.1-1B) [75].

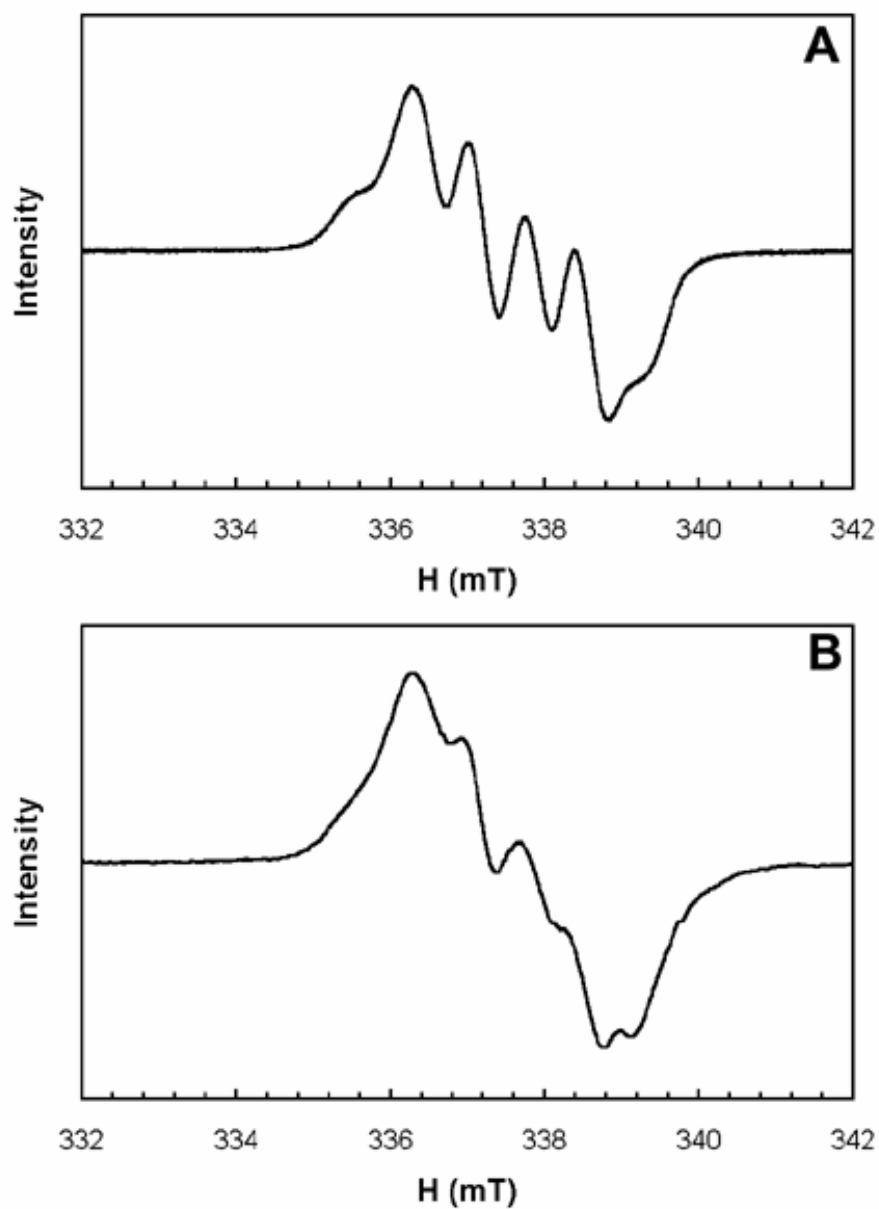
W48 is often implicated in electron transfer pathways, particularly in the work employing the C3-C26 disulfide radical anion [29, 31]. This, coupled with its unique protein environment, makes it worthwhile to understand the nature of the W48 radical (W48<sup>•</sup>). Some work on this radical has already been completed [46]: EPR spectra have been acquired for the flash/quench/freeze-generated radical in both standard buffer and in buffer with cryo-protectant (ethylene glycol) (Figure 5.2.1-2). The spectra are quite different; a change attributed primarily to effects on the local environment of the tryptophan by the inclusion of cryo-protectant. Fitting of Figure 5.2.1-2A suggested that the radical was deprotonated, but, as discussed above, EPR alone is not enough to unambiguously assign the protonation state of W48<sup>•</sup>. In order to understand the nature of W48<sup>•</sup> more completely,

optical absorption spectra were acquired using NS2 and NS1. broad-band absorption experiments showed a single, relatively intense signal at  $\lambda_{\text{max}} = 415 \text{ nm}$  for the reaction of [Re(H83)WTAzZn(II)] with  $\text{Co(III)(NH}_3)_5\text{Cl}$  after irradiation (Figure 5.2.1-3, the small band at  $\sim 630 \text{ nm}$  is most likely due to small amounts of Cu(II) impurities involved in a bimolecular reaction).

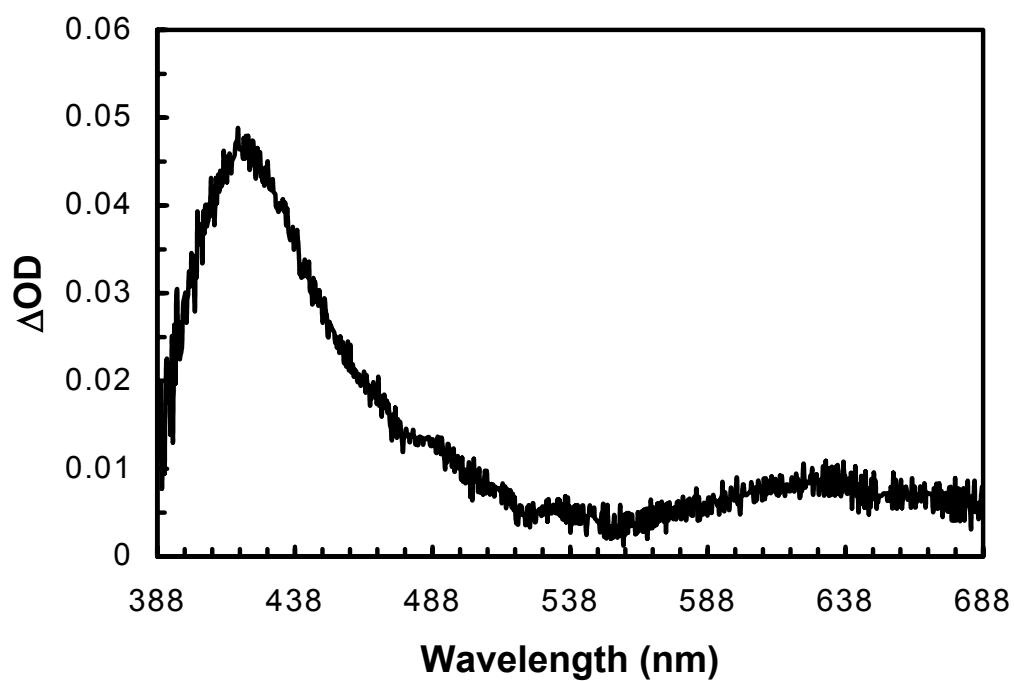
This absorption spectrum seems somewhat odd; first, it is much narrower than the band observed in the model system (Figure 5.1-3). Second, the wavelength of the primary absorbance is much closer to that of a tyrosine radical [76] than to either the signals observed in the model system or the published spectra of tryptophan radicals. However, since the environment of W48 is unique, it seemed plausible that the observed spectrum was  $\text{W48}^\bullet$ . In order to examine this hypothesis, [Re(H83)(W48)AzZn(II)] was subjected to the same set of experiments. The hypothesis did not withstand this test: to begin with, the EPR of the mutant without Y72 or Y108 is strikingly different (Figure 5.2.1-4). In addition to the qualitative differences in the spectrum, the decay of the signal is markedly different. In [Re(H83)WTAzZn(II)] the observed signal monitored at the maximum intensity disappeared on the order of milliseconds (A. Di Bilio, personal communication). The EPR spectrum for [Re(H83)(W48)AzZn(II)] on the other hand shows quite a bit of persistence at room temperature, remaining observable after more than 20 min at room temperature (Figure 5.2.1-4, inset). This is remarkable; the longest lasting tryptophan radical in a protein (excepting [Re(H107)(W108)AzZn(II)], see below) at room temperature is 49 s for a RNR mutant [69].



**Figure 5.2.1-1:** Tryptophan fluorescence,  $\lambda_{\text{ex}} = 280$  nm. (A) 4  $\mu\text{M}$  Trp-Glu in 50 mM KPi pH 7.16 (B) 4  $\mu\text{M}$  wild-type azurin tryptophan fluorescence (W48) in 50 mM KPi pH 7.16.

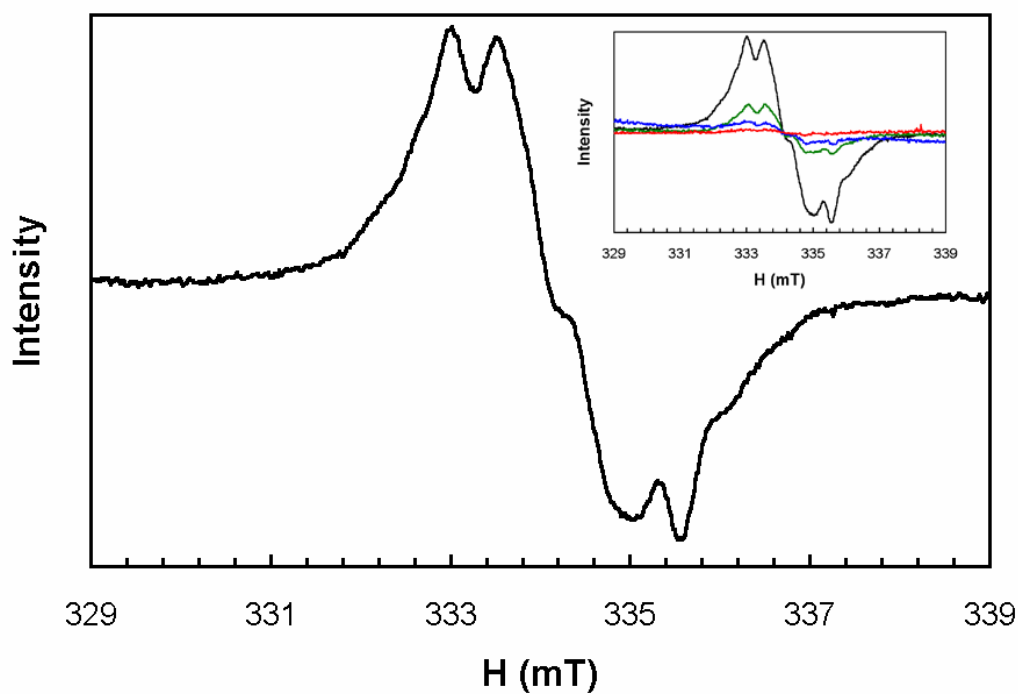


**Figure 5.2.1-2:** X-band EPR of  $[\text{Re}(\text{H83})\text{WTaz}]/\text{Co}(\text{III})$  at 100 K; (A) 1mM  $[\text{Re}(\text{H83})\text{WTaz}]$  25 mM KPi pH 7, 25% ethylene glycol, saturated  $\text{Co}(\text{III})(\text{NH}_3)_5\text{Cl}$  [46]. (B) 1mM  $[\text{Re}(\text{H83})\text{WTaz}]$  25 mM KPi pH 7, saturated  $\text{Co}(\text{III})(\text{NH}_3)_5\text{Cl}$  (A. Di Bilio, personal communication).



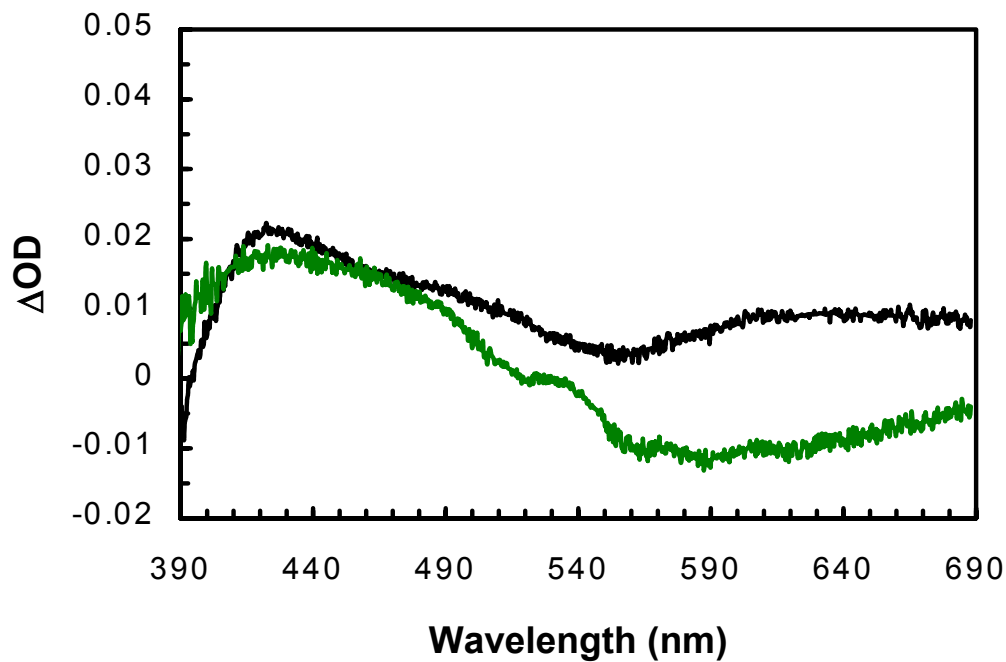
**Figure 5.2.1-3:** NS2 spectrum, [Re(H83)WTazZn(II)]/Co(III). 20  $\mu$ s after the pulse, 91  $\mu$ M [Re(H83)WTazZn(II)] with 5 mM Co(III)(NH<sub>3</sub>)<sub>5</sub>Cl in 50 mM KPi pH 7.16.



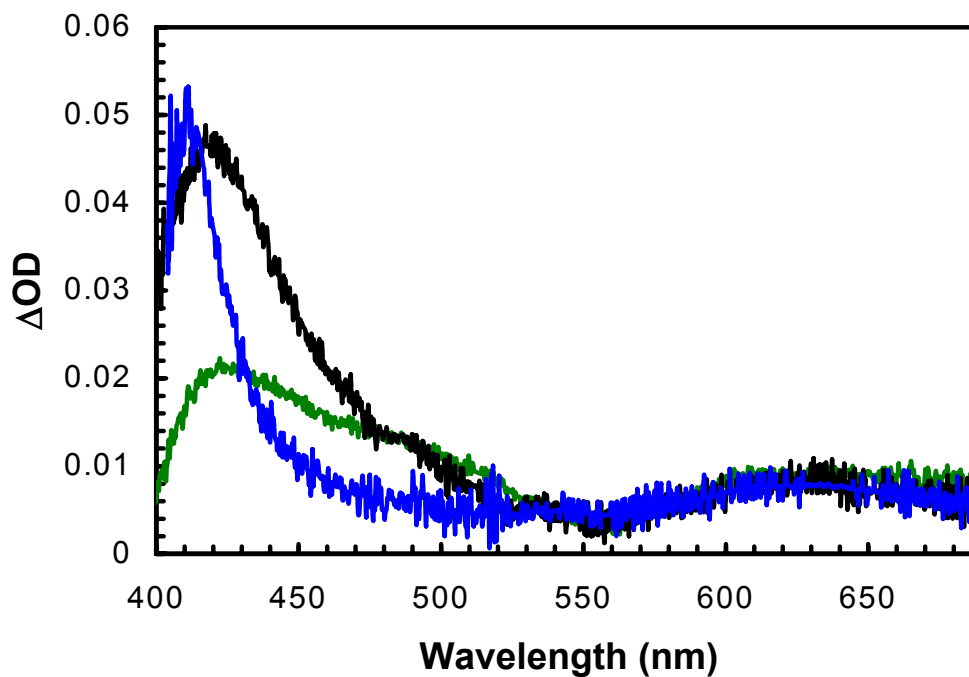


**Figure 5.2.1-4:** X-band EPR of  $[\text{Re}(\text{H}83)(\text{W}48)\text{AzZn}(\text{II})]$  with  $\text{Co}(\text{III})$  at 77 K. 600  $\mu\text{M}$   $[\text{Re}(\text{H}83)(\text{W}48)\text{AzZn}(\text{II})]$  in 50 mM KPi pH 7.16, saturated with  $\text{Co}(\text{III})$ . Inset: EPR spectrum taken after various amounts of time at room temperature (—) 0 min (—) 5 min (—) 25 min (—) 65 min. Settings:  $\nu = 9.375463$  GHz; modulation frequency = 100 kHz; modulation amplitude = 2.0 G; microwave power = 79.5  $\mu\text{W}$ ; time constant = 10.24 ms; conversion time = 40.96 ms; 25 scans.

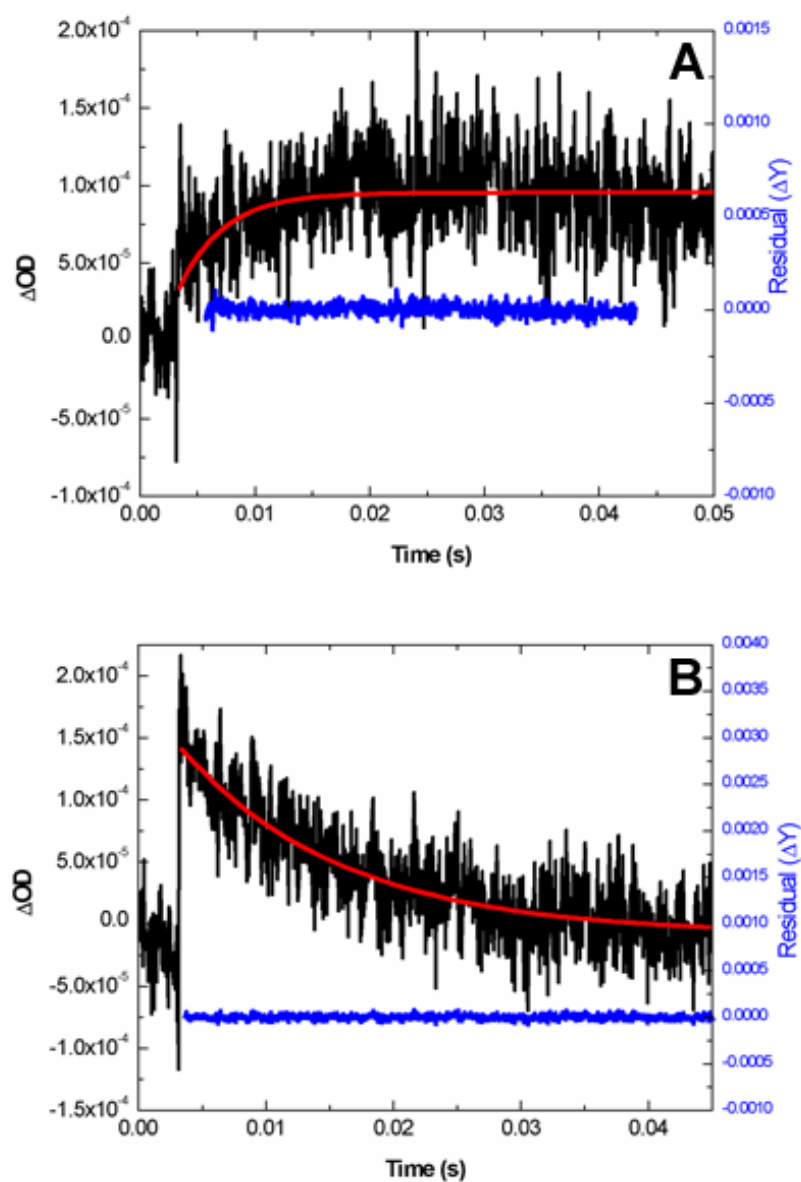
More telling even than the EPR spectrum is the optical absorption spectrum acquired from NS2 (Figure 5.2.1-5). In this spectrum, no strong absorption at  $\sim 415$  nm is observed (spectra with and without quencher differ very little at 415 nm). In fact, very little absorption at all is observed. From comparison of this spectrum with the spectra obtained for [Re(H83)WTAzZn(II)] and for the Re-labeled mutant H83Q/W48F/Y72F/Q107H Cu(II) azurin ([Re(H107)(Y108)AzCu(II)]) [32], it is quite clear that the majority of the spectrum shown in Figure 5.2.1-3 is in fact due to a tyrosine radical, most likely the Y108, although it could also be due to Y72 (Figure 5.2.1-6). The primary observable difference in the spectra shown in Figure 5.2.1-6 is a small positive absorption at with an approximate  $\lambda_{\text{max}}$  of 500 nm. Attempts to confirm this absorption as due to W48 $\bullet$  by point-by-point on NS1 met with little success, the signal being in general quite weak. If the slight change in the NS2 spectrum is accurate, this absorption is approximately in the range expected for a neutral tryptophan radical. In fact, single wavelength transient absorption spectroscopy of [Re(H83)WTAzCu(II)] show the signal with  $\lambda_{\text{max}} = 415$  nm appearing with a rate constant  $k = 2 \times 10^2 \text{ s}^{-1}$  (tyrosine is oxidized by W48 $\bullet$  Figure 5.2.1-7A), while a small signal at 500 nm decays with a rate of  $1 \times 10^2 \text{ s}^{-1}$  (W48 $\bullet$  reduced by tyrosine, Figure 5.2.1-7B). Given the relatively poor signal-to-noise ratio of the spectra in Figure 5.2.1-7, it seems possible that the signal at 420 nm is increasing at the same rate that the signal at 500 nm is decreasing, suggesting that the species which absorbs at 500 nm is converting to the species absorbing at 420 nm. Also strongly supporting this hypothesis, flash/quench reaction of



**Figure 5.2.1-5:** NS2 spectrum,  $[\text{Re}(\text{H83})(\text{W48})\text{AzZn}(\text{II})]$  with  $\text{Co}(\text{III})$ ; 20  $\mu\text{s}$  after the pulse, 40  $\mu\text{M}$   $[\text{Re}(\text{H83})(\text{W48})\text{AzZn}(\text{II})]$  (—) without 5 mM  $\text{Co}(\text{III})(\text{NH}_3)_5\text{Cl}$  and (—) with 5 mM  $\text{Co}(\text{III})(\text{NH}_3)_5\text{Cl}$  in 50 mM KPi pH 7.16.



**Figure 5.2.1-6:** NS2 comparison of radical spectra at 20  $\mu$ s after excitation. (—) 91  $\mu$ M [Re(H83)WTAzZn(II)] with 5 mM Co(III)(NH<sub>3</sub>)<sub>5</sub>Cl in 50 mM KPi pH 7.16 (—) 30  $\mu$ M [Re(H107)(Y108)AzZn(II)] with 5 mM Co(III)(NH<sub>3</sub>)<sub>5</sub>Cl in 50 mM KPi pH 7.16 (—) 40  $\mu$ M [Re(H83)(W48)AzZn(II)] with 5 mM Co(III)(NH<sub>3</sub>)<sub>5</sub>Cl in 50 mM KPi pH 7.16.



**Figure 5.2.1-7:** NS1 transient absorption, [Re(H83)WTAzZn(II)]/Co(III); 40  $\mu$ M [Re(H83)WTAzZn(II)] with 5 mM Co(III)(NH<sub>3</sub>)<sub>5</sub>Cl in 50 mM KPi pH 7.16. (A) Transient absorption at 420 nm, (—) linear least squares fit, ( $k = 2 \times 10^2 \text{ s}^{-1}$ ) (—) residual of the fit. (B) Transient absorption at 500 nm, (—) linear least squares fit, ( $k = 1 \times 10^2 \text{ s}^{-1}$ ) (—) residual of the fit.

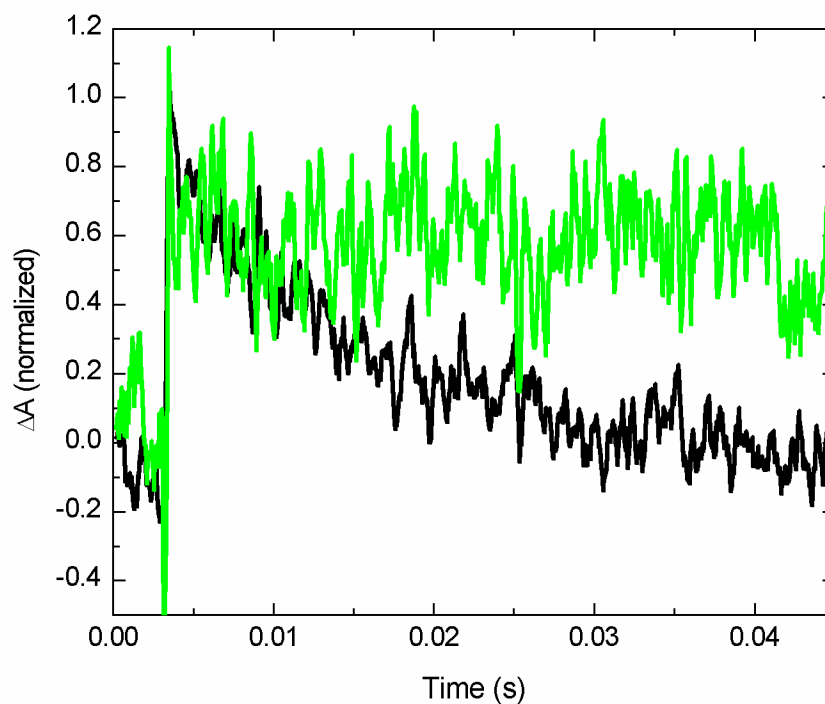
[Re(H83)(W48)AzCu(II)] with Ru(III)(NH<sub>3</sub>)<sub>6</sub> shows a small signal at 500 nm which apparently decays with a rate constant on the order of  $10^{-2} \text{ s}^{-1}$  (Figure 5.2-8).<sup>5</sup> Analysis of the crystal structure of [Re(H83)WTAzCu(II)] shows that the distance from W48 to Y108 is 12.1 Å and the distance from W48 to Y72 is 14.2 Å; a distance over which ET might proceed at a reasonable rate from either Y to the W48 radical, even with the small driving force predicted (~ 100-200 meV).

### 5.2.2. [Re(H107)(W108)Az]

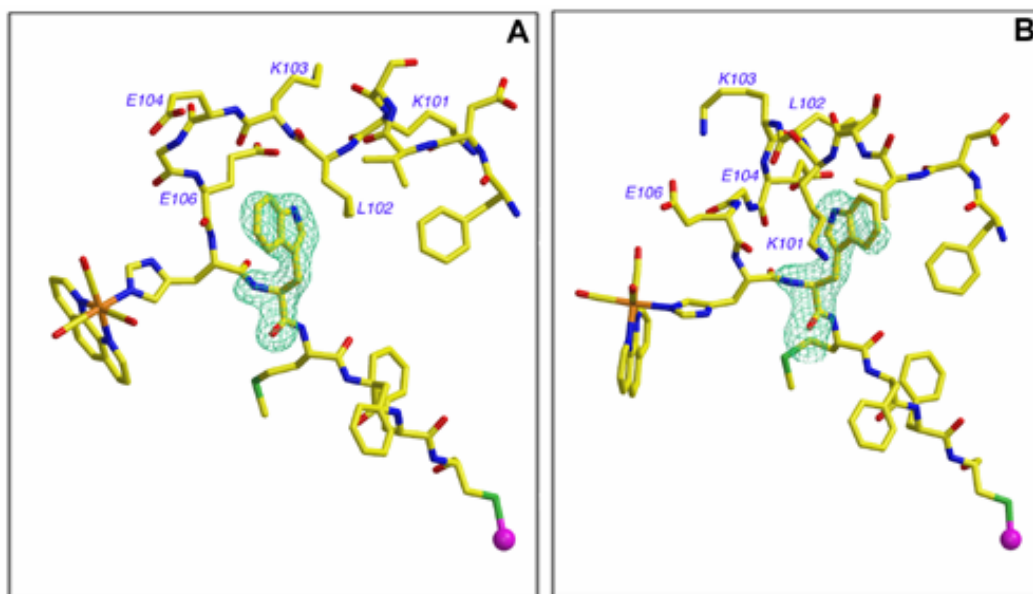
The first azurin mutant designed to specifically test the effect of an intermediate tryptophan radical on ET through a  $\beta$ -strand was the quintuple mutant H83Q/W48F/Y72F/Q107H/Y108W. The local environment of W108 in the rhenium-labeled version ([Re(H107)(W108)AzCu(II)]) was investigated by crystallographic analysis performed by our collaborators B. R. Crane and his student, Cristian Gradinaru at Cornell University [45]. The obtained structure of H83Q/W48F/Y72F/Q107H/Y108W labeled with the Re(I)(CO)<sub>3</sub>(phen) fragment is shown in Figure 5.2.2-1. The four independent azurin molecules contained in the asymmetric unit show two major conformations (Figure 5.2.2-1 A and B) for W108 ( $F_{\text{obs}} - F_{\text{calc}} = 1.9 \text{ Å}$  resolution omit-electron density in green). Rearrangement of the polypeptide in the surrounding loop (residues 101-107) accompanies the change in W108 conformation.

---

<sup>5</sup> Due to limitations of NS1, rates less than  $10^{-1} \text{ s}^{-1}$  cannot be reliably measured.



**Figure 5.2.1-8:** NS1 transient absorption,  $[\text{Re}(\text{H}83)(\text{W}48)\text{AzZn}(\text{II})]/\text{Ru}(\text{III})$  at 500 nm (—) 40  $\mu\text{M}$   $[\text{Re}(\text{H}83)\text{WTAzCu}(\text{II})]$  and (—) 42  $\mu\text{M}$   $[\text{Re}(\text{H}83)(\text{W}48)\text{AzCu}(\text{II})]$  both in 50 mM KPi pH 7.16 buffer with 5 mM  $\text{Ru}(\text{III})(\text{NH}_3)_6$ .



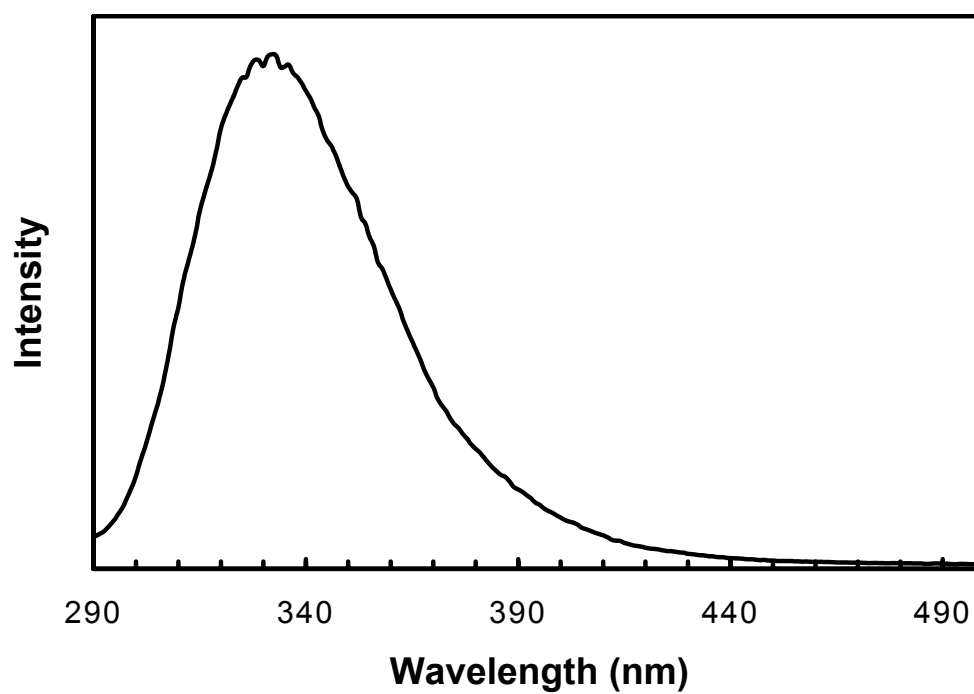
**Figure 5.2.2-1:** Two different tryptophan-108 environments in the crystal structure of  $[\text{Re}(\text{H107})(\text{W108})\text{AzCu}(\text{II})]$  [45].



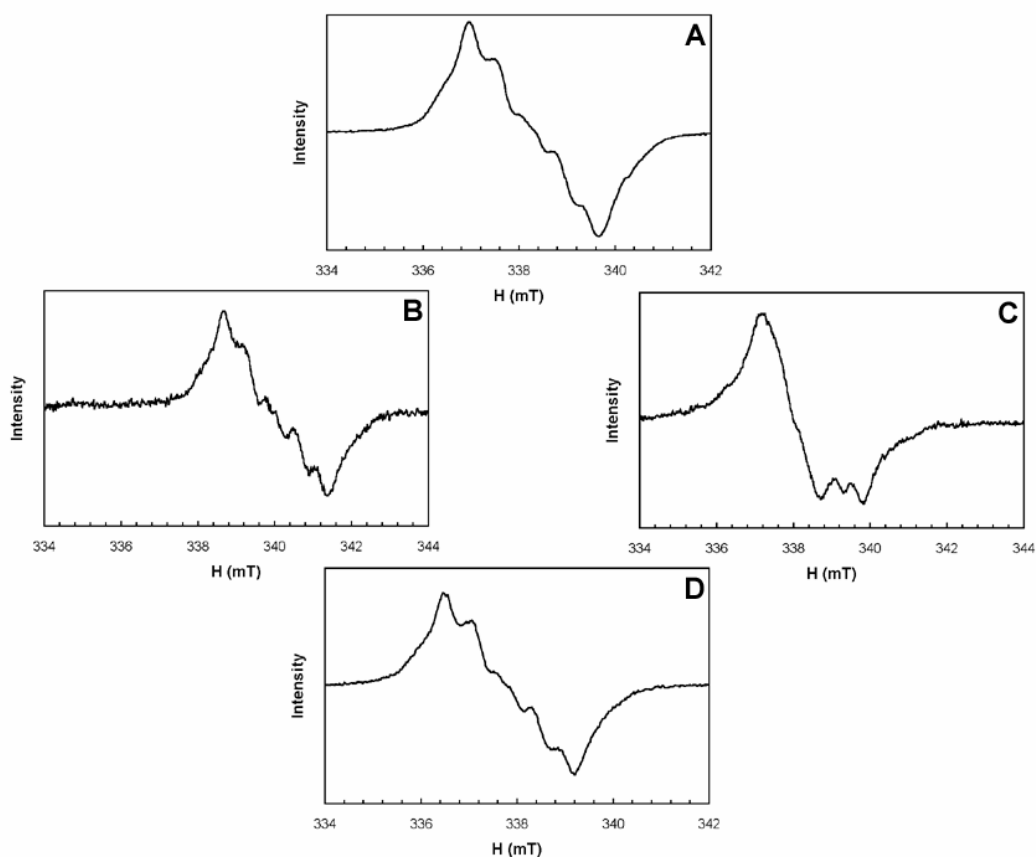
In the two molecules not shown, W108 has mainly the conformation shown in 5.2.2-1A, but in each case, the indole ring has less definition in the electron density than depicted above. In all cases, the W108 is relatively exposed to solvent. This is supported by the fluorescence spectrum which has  $\lambda_{\text{max}} = 332$  nm (Figure 5.2.2-2).

This mutant readily forms a tryptophan radical (W108<sup>•</sup>) under the flash/quench/freeze conditions, giving the EPR spectrum shown in Figure 5.2.2-3A. This signal shows little variation with temperature or power. The spectrum is insensitive to increases in pH (Figure 5.2.2-3B), although at acidic pH the spectrum changes markedly (Figure 5.2.2-3C). Deuteration also has little effect at neutral pD (Figure 5.2.2-3D). The spectrum at pH 4.03 (Figure 5.2.2-3C) shows substantial variation relative to the other spectra; attempts to fit this spectrum to that of a protonated radical have been largely unsuccessful, suggesting that the variation is due primarily to changes in the local protein fold, not to changes in the protonation state of the radical. W108<sup>•</sup> reacts readily with oxygen to give a peroxy radical, as indicated by the EPR spectrum with prominent features at  $g = 2.03$  and  $g = 2.01$  (Figure 5.2.2-4) [77]. This type of radical is often observed in H<sub>2</sub>O<sub>2</sub> reactions with myoglobin proteins [78]. The EPR spectrum of the peroxy radical looks similar at pH 4.03, pH 7.16, and pH 9.8.

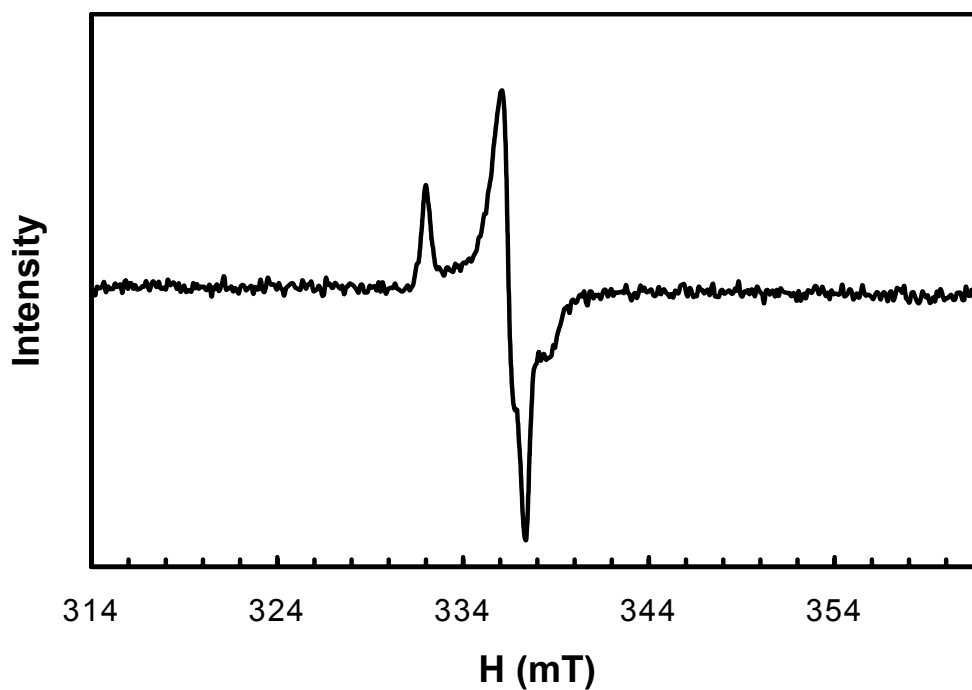
By far the most unusual property of W108<sup>•</sup> is its long persistence. At room temperature, the radical decay to a point below the detection limit of the EPR spectrometer took more than 5 hrs. In short peptide chains, tryptophan radicals persist for only ~400 ns [79], while the lifetimes are extended in DNA photolyase (~10 ms) [73] and an RNR mutant (49 s) [69]. Even so, the lifetimes of these tryptophan radicals pale in comparison to



**Figure 5.2.2-2:** Tryptophan fluorescence,  $\lambda_{\text{ex}} = 280 \text{ nm}$  4  $\mu\text{M}$  H83Q/W48F/Y72F/Y108W AzCu(II) in 50 mM KPi pH 7.16.



**Figure 5.2.2-3:** X-band EPR of  $[\text{Re}(\text{H107})(\text{W108})\text{AzZn}(\text{II})]/\text{Co}(\text{III})$  at 77K. 300  $\mu\text{M}$   $[\text{Re}(\text{H107})(\text{W108})\text{AzZn}(\text{II})]$  in different buffers, saturated with  $\text{Co}(\text{III})(\text{NH}_3)_5\text{Cl}$ . Settings: modulation frequency = 40 kHz; modulation amplitude = 1.5 G; microwave power = 202  $\mu\text{W}$ ; time constant = 20.48 ms; conversion time = 80.92 ms; 40 scans. (A)  $\nu = 9.488635$  GHz 50 mM KPi pH 7.16 (B)  $\nu = 9.536925$  GHz 50 mM  $\text{NaHCO}_3$  pH 9.8 (C)  $\nu = 9.492492$  GHz 50 mM NaOAc pH 4.03 (D)  $\nu = 9.475345$  GHz 50 mM KPi ( $\text{D}_2\text{O}$ ) pD 7.56.

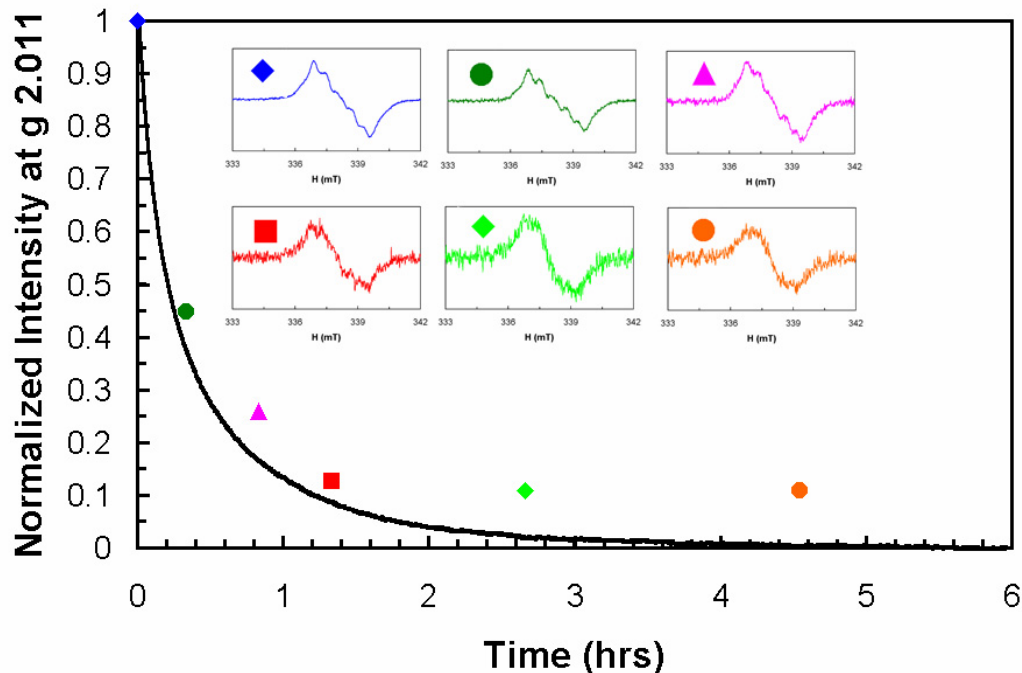


**Figure 5.2.2-4:** X-band EPR of  $[\text{Re}(\text{H107})(\text{W108})\text{AzZn}(\text{II})]/\text{Co}(\text{III})$ , aerated at 77 K. 300  $\mu\text{M}$   $[\text{Re}(\text{H107})(\text{W108})\text{AzZn}(\text{II})]$  in 50 mM NaOAc, pH 4.03, saturated with  $\text{Co}(\text{III})(\text{NH}_3)_5\text{Cl}$ , aerated. Settings:  $\nu = 9.480910$  GHz; modulation frequency = 40 kHz; modulation amplitude = 1.5 G; microwave power = 202  $\mu\text{W}$ ; time constant = 20.48 ms; conversion time = 81.92 ms; 40 scans.

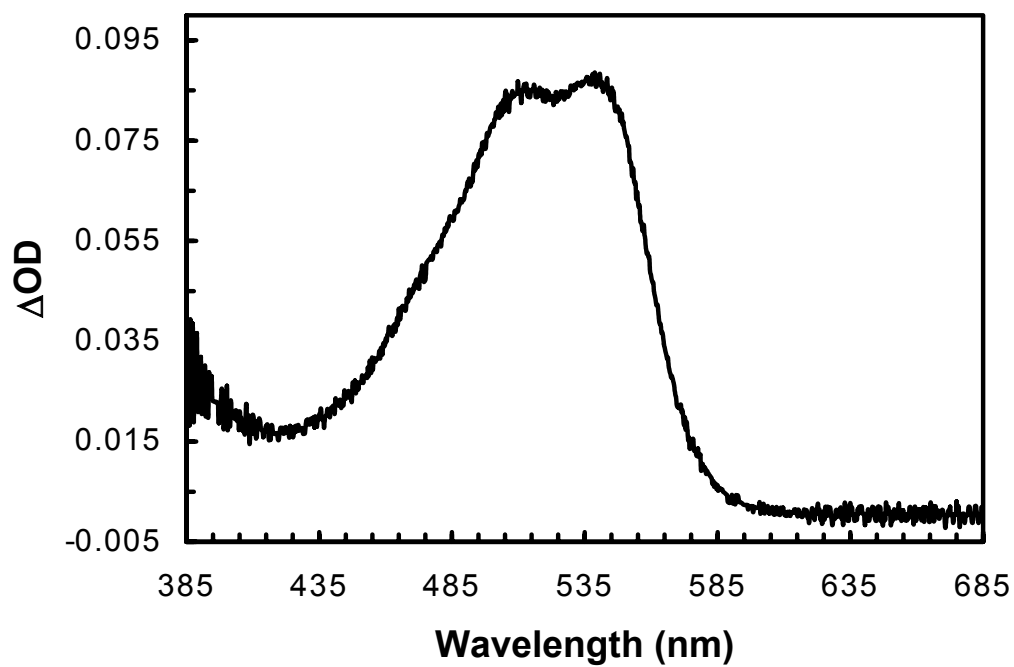
W108<sup>•</sup>; only TyrD in PSII persists on the same timescale [80]. The stability of this radical at room temperature can be monitored by EPR signal decay over time (Figure 5.2.2-5). Experiments wherein the radical was generated by flash/quench/freeze and then warmed to room temperature for specific intervals are shown as insets in Figure 5.2.2-5. These experiments demonstrate that no new organic radical species is formed in the decay.

To complete the picture of W108<sup>•</sup>, time resolved optical spectroscopy was carried out on both NS1 and NS2 on a solution of [Re(H107)(W108)AzZn(II)] with the irreversible Co(III)(NH<sub>3</sub>)<sub>5</sub>Cl quencher. A striking broad-band spectrum was observed, showing “double hump” maxima at  $\lambda = 510$  nm and  $\lambda = 535$  (Figure 5.2.2-6). Moreover, in keeping with the slight changes in the EPR spectrum, the transient absorption spectrum is remarkably insensitive to changes in pH or deuteration (Figure 5.2.2-7). Despite the prolonged decay of W108<sup>•</sup>, the radical formed quite quickly. Single wavelength monitoring at 500 nm (a convenient wavelength due to very little emission from Re and substantial absorption of the radical) of [Re(H83)(W108)AzZn(II)] gave a signal with a formation rate constant of  $k = 3 \times 10^6 \text{ s}^{-1}$  (Figure 5.2.2-8). Kinetic data collected from 510 nm to 540 nm showed the same rate of formation (data not shown). Importantly, no signal was detected at 600 nm, the putative maximum for a tryptophan cation radical [65]. This, taken with the fact that the EPR shows little difference between pH 7.16 and pH 9.8, suggests that at times greater than 10 ns (the resolution of NS1) W108<sup>•</sup> is a deprotonated tryptophan radical.

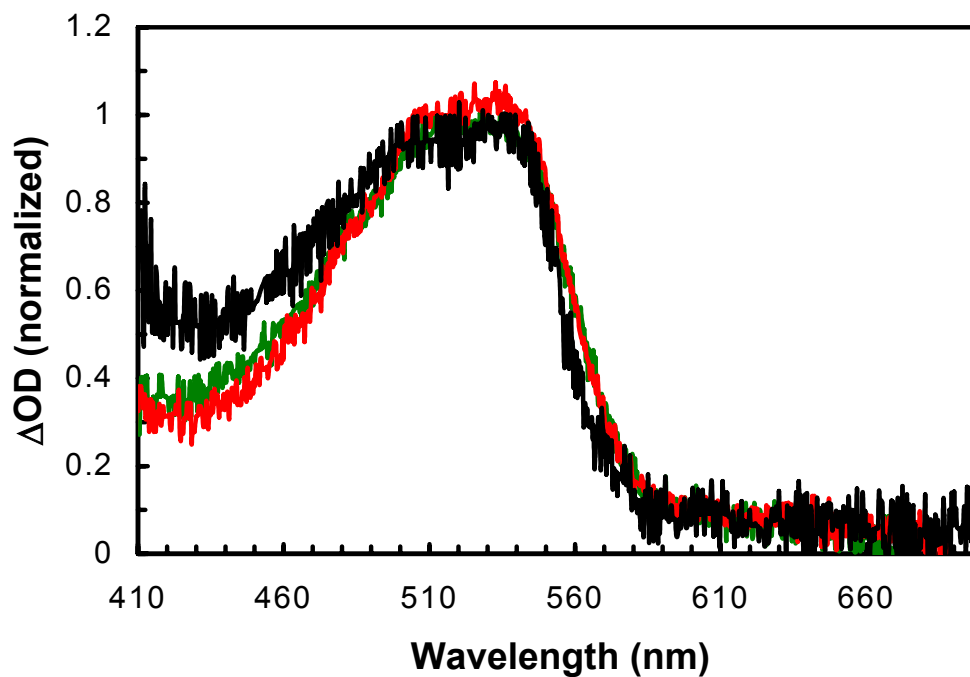
The explanation for the observed stability of W108<sup>•</sup> is not straightforward. Initially, it was suspected that the reason for its prolonged lifetime was thermodynamic; that is,



**Figure 5.2.2-5:** EPR decay of  $W108^{\bullet}$  at room temperature. (—) X-band single frequency kinetic monitoring of the decay of the EPR signature for  $W108^{\bullet}$  at room temperature; generated in 200  $\mu\text{M}$   $[\text{Re}(\text{H107})(\text{W108})\text{AzZn}(\text{II})]$  in 50 mM KPi pH 7.16 saturated with  $\text{Co}(\text{III})(\text{NH}_3)_5\text{Cl}$ . Settings:  $\nu = 9.797195$  GHz; modulation frequency = 100 kHz; modulation amplitude = 3.5 G; microwave power = 6.38 mW; time constant = 2.62 s; conversion time = 5.24 s; 1 scan. Inset: X-band EPR spectra of  $W108^{\bullet}$  at 77 K; generated in 300  $\mu\text{M}$   $[\text{Re}(\text{H107})(\text{W108})\text{AzZn}(\text{II})]$  in 50 mM KPi pH 7.16 saturated with  $\text{Co}(\text{III})(\text{NH}_3)_5\text{Cl}$  after standing at room temperature. (♦) 0 hrs (●) 0 hrs, 20 min (▲) 0 hrs, 50 min (■) 1 hr, 29 min (◆) 2 hrs 40 min (●) 4 hrs 32 min. Settings:  $\nu = 9.486858$  GHz; modulation frequency = 40 kHz; modulation amplitude = 1.5 G; microwave power = 202  $\mu\text{W}$ ; time constant = 20.48 ms; conversion time = 81.92 ms; 40 scans.

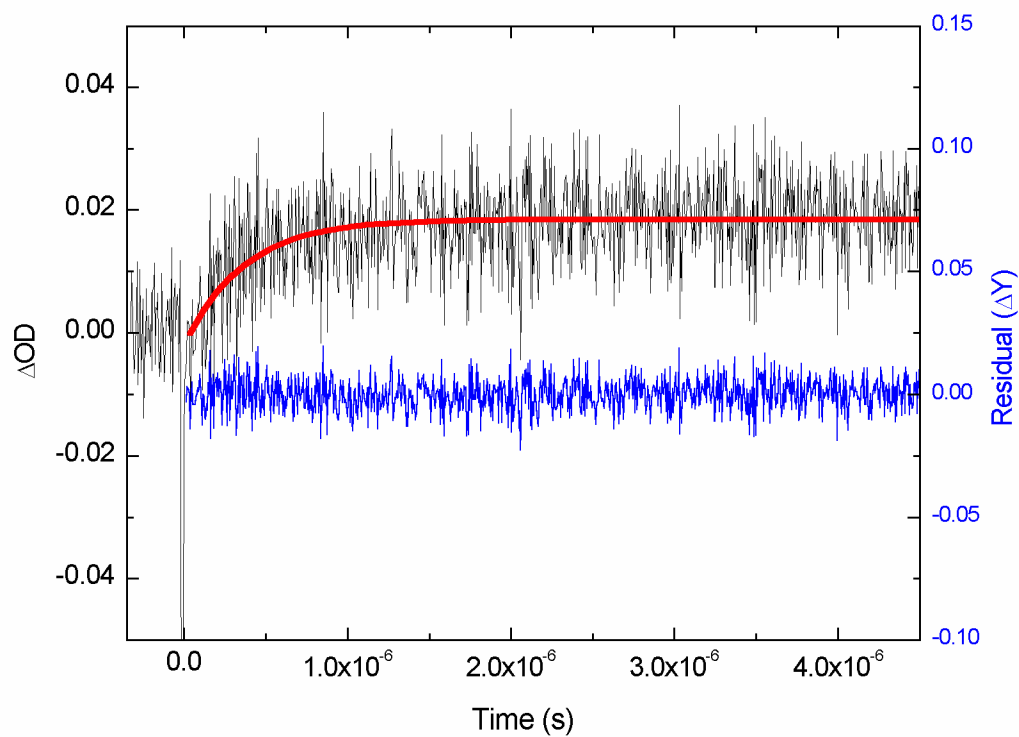


**Figure 5.2.2-6:** NS2 spectrum of  $[\text{Re}(\text{H107})(\text{W108})\text{AzZn}(\text{II})]/\text{Co}(\text{III})$ ; 20  $\mu\text{s}$  after the pulse, 60  $\mu\text{M}$   $[\text{Re}(\text{H107})(\text{W48})\text{AzZn}(\text{II})]$  with 5 mM  $\text{Co}(\text{III})(\text{NH}_3)_5\text{Cl}$  in 50 mM KPi pH 7.16.



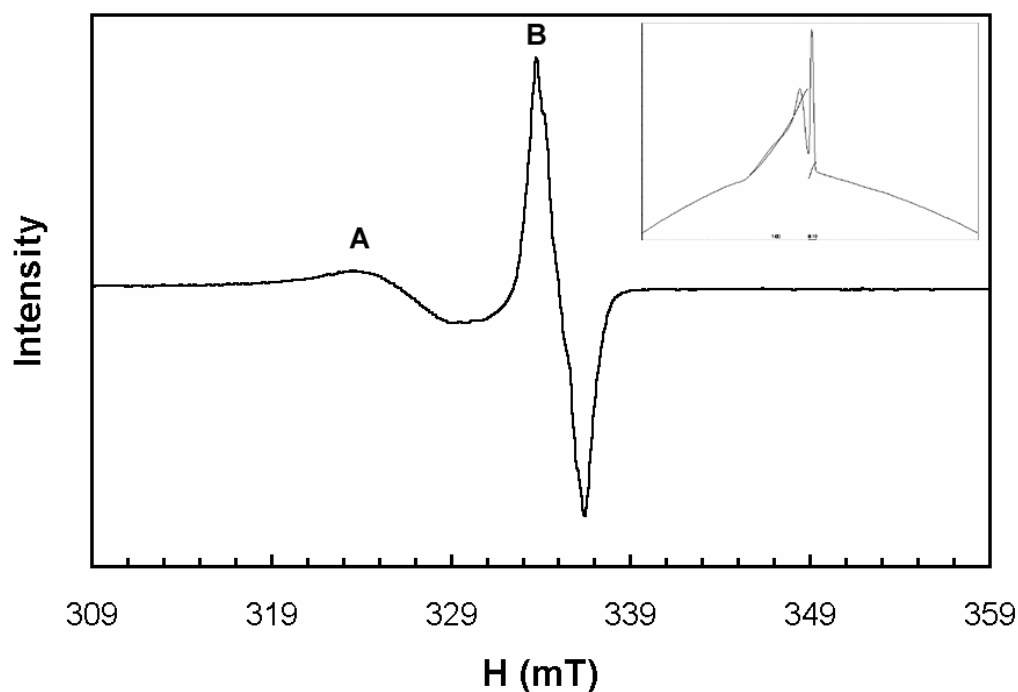
**Figure 5.2.2-7:** NS2 spectrum of  $[\text{Re}(\text{H107})(\text{W108})\text{AzZn}(\text{II})]/\text{Co}(\text{III})$ , various pH's. 20  $\mu\text{s}$  after the pulse, 40  $\mu\text{M}$   $[\text{Re}(\text{H83})(\text{W108})\text{AzZn}(\text{II})]$  with 5 mM  $\text{Co}(\text{III})(\text{NH}_3)_5\text{Cl}$  in a variety of buffers. (—) 50 mM NaOAc pH 4.03 (—) 50 mM KPi ( $\text{D}_2\text{O}$ ) pD 7.56 (—) 50 mM  $\text{NaHCO}_3$  pH 9.8.





**Figure 5.2.2-8:** NS1 transient absorption  $[\text{Re}(\text{H107})(\text{W108})\text{AzZn}(\text{II})]/\text{Co}(\text{III})$  at 500 nm. 40  $\mu\text{M}$   $[\text{Re}(\text{H83})(\text{W48})\text{AzZn}(\text{II})]$  with 5 mM  $\text{Co}(\text{III})(\text{NH}_3)_5\text{Cl}$  in 50 mM KPi pH 7.16. (—) linear least squares fit of data ( $k = 3 \times 10^6 \text{ s}^{-1}$ ) (—) residual for fit.

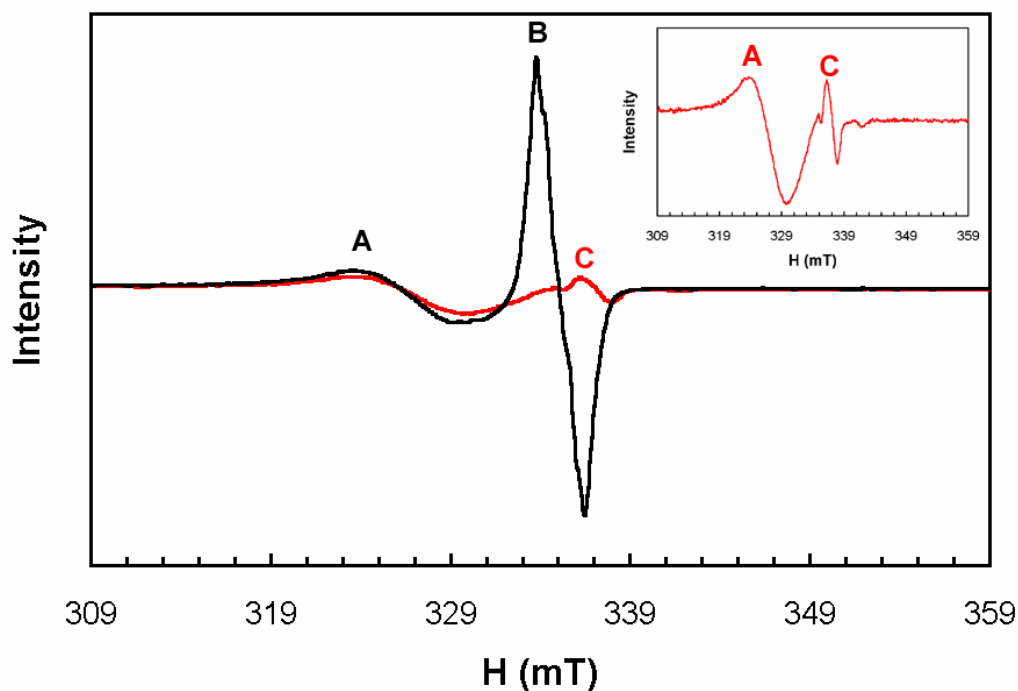
the local environment of W108 was lowering the oxidation potential of the radical from the expected 1 V vs. NHE to a much lower number, perhaps 300 mV vs. NHE. This would render the radical much less reactive, and could (in theory) prolong its existence at room temperature. To test this hypothesis, we needed a method to determine the approximate redox potential of the radical. Since W108<sup>•</sup> was so long lived, it seemed possible that it might be generated by flash/quench/freeze, thawed long enough to add a chemical agent which might reduce the radical, re-frozen and monitored by EPR. By using [Re(H107)(W108)AzCu(II)] as the protein source, it was possible to do spin-integration relative to Cu(II) [81] to determine roughly the amount of radical generated. In a solution of 240  $\mu$ M [Re(H107)(W108)AzCu(II)] in 50 mM KPi pH 7.16 saturated with Co(III)(NH<sub>3</sub>)<sub>5</sub>Cl,  $\sim$  45  $\mu$ M W108<sup>•</sup> was formed (Figure 5.2.2-9). This number is approximate due to the fact that the irradiation and freezing are not homogeneous. Upon warming, mixing of the solution may lead to a lower total concentration of radical. K<sub>4</sub>Mo(IV)(CN)<sub>8</sub> was employed as a reductant. This species has a Mo(IV)/Mo(V) couple of 0.867 V vs. NHE [82], within the expected range of W<sup>•</sup> potentials. In addition, Mo(IV)(CN)<sub>8</sub><sup>4-</sup> is diamagnetic (d<sup>2</sup>) and so shows no EPR spectrum, while Mo(V)(CN)<sub>8</sub><sup>3-</sup> is paramagnetic (d<sup>1</sup>) with a characteristic EPR spectrum [83]. The radical shown in Figure 5.2.2-9 was warmed to room temperature for 3 min. Under a counter flow of argon, a solution of K<sub>4</sub>Mo(IV)(CN)<sub>8</sub> in 50 mM KPi pH 7.16 was added to the EPR tube to give a final concentration of K<sub>4</sub>Mo(IV)(CN)<sub>8</sub> of 160  $\mu$ M. The tube was re-sealed, inverted several times, and re-frozen in liquid nitrogen, having spent a total of 8 min at room temperature.



**Figure 5.2.2-9:** X-band EPR of  $[\text{Re}(\text{H107})(\text{W108})\text{AzCu}(\text{II})]/\text{Co}(\text{III})$  at 77 K, 240  $\mu\text{M}$   $[\text{Re}(\text{H107})(\text{W108})\text{AzCu}(\text{II})]$  in 50 mM KPi, pH 7.16, saturated with  $\text{Co}(\text{III})(\text{NH}_3)_5\text{Cl}$ . (A) signal from Cu(II); (B) signal from W108 $^\bullet$ . Inset: integration of absorption spectrum with Cu(II) set to 1 and W108 $^\bullet$  integrating to 0.17 ( $\sim 45 \mu\text{M}$  radical). Settings:  $\nu = 9.396953$  GHz; modulation frequency = 100 kHz; modulation amplitude = 1.5 G; microwave power = 202  $\mu\text{W}$ ; time constant = 20.48 ms; conversion time = 81.92 ms; 15 scans.

The resulting EPR showed no trace of W108<sup>•</sup>, revealing only Cu(II) absorption and the characteristic Mo(V) EPR spectrum with features at  $g$  1.997 and  $g$  1.976 (Figure 5.2.2-10).

The fact that the radical is completely reduced even at the relatively low concentration ratio of  $\sim 4:1$  Mo(IV): W108<sup>•</sup> indicates that the oxidation potential of W108<sup>•</sup> is greater than or equal to 0.867 V vs. NHE. This value is in accordance with the predicted potentials showing that the stabilization of W108<sup>•</sup> is not thermodynamic. Rather, the likely explanation for this unprecedented stability is a kinetic one. The exact nature of this kinetic stabilization is still unclear. The time course of the EPR signal amplitude (Figure 5.2.2-5) clearly indicates that the pathways associated with radical decay are complex (e.g., it is not nicely fit by 1, 2 or 3 exponentials or by assuming a bimolecular reaction). In general, radicals decay by three major pathways: bond formation between two radicals, hydrogen atom abstraction from some other component or electron transfer between the radical and a reductant or oxidant [84]. In proteins, pulse radiolysis studies have suggested that radicals are often quenched by sidechain scission or dimerization [85, 86]. Given the available information, none of these pathways can be ruled out. However, there seems to be a few possibilities that are consistent with the available information. To start with, ESI-MS of the products of the reaction show only the  $m/z$  for [Re(H107)(W108)Az] and a peak for [Re(H107)(W108)Az] + 16  $m/z$  units; suggesting no substantial decomposition of the protein results from W108<sup>•</sup> decay. Perhaps more telling, the rapid reaction of the radical with Mo(V) suggests that the rate of decay of W108<sup>•</sup> is determined by electron transfer from Mo(IV) to the radical. This argument is bolstered by the fact that in [Re(H107)(W108)AzCu(I)], no ET is observed between the copper center and the oxidized

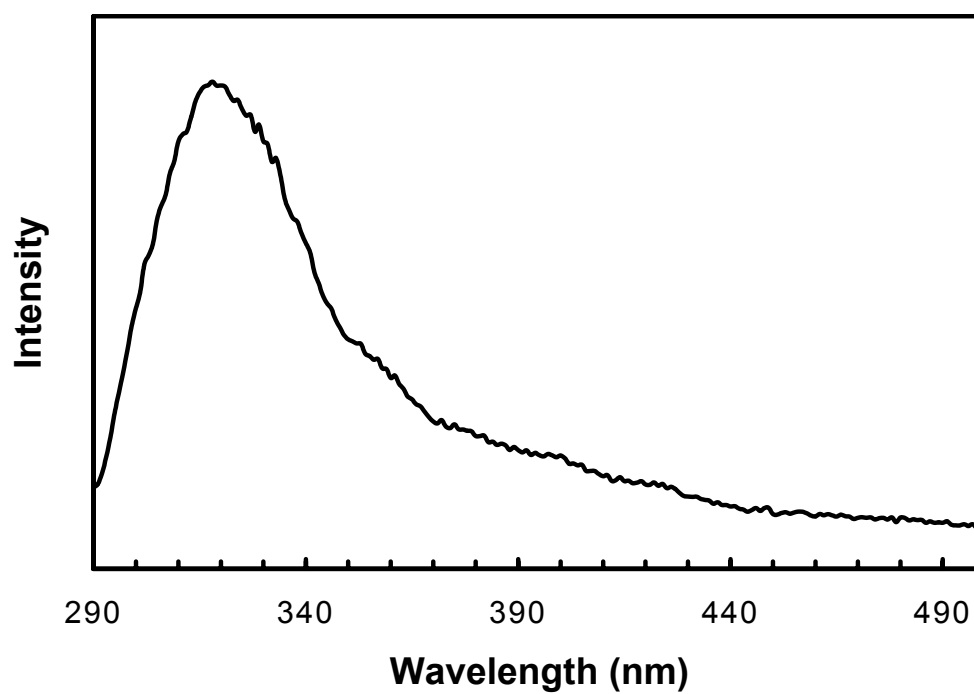


**Figure 5.2.2-10:** X-band EPR of  $[\text{Re}(\text{H}107)(\text{W}108)\text{AzCu}(\text{II})]/\text{Co}(\text{III})/\text{Mo}(\text{IV})$ , with  $\text{Mo}(\text{IV})$ . 240  $\mu\text{M}$   $[\text{Re}(\text{H}107)(\text{W}108)\text{AzCu}(\text{II})]$  in 50 mM KPi, pH 7.16, saturated with  $\text{Co}(\text{III})(\text{NH}_3)_5\text{Cl}$  (—) before and (—) after mixing with  $\text{K}_4\text{Mo}(\text{IV})(\text{CN})_8$ . (A)  $\text{Cu}(\text{II})$  signal; (B)  $\text{W}108^\bullet$  signal; (C)  $\text{Mo}(\text{V})$  signal. Inset:  $\text{Mo}(\text{V})$  EPR fine structure (with  $\text{Cu}(\text{II})$  signal). Settings:  $\nu = 9.398667$  GHz; modulation frequency = 100 kHz; modulation amplitude = 1.5 G; microwave power = 202  $\mu\text{W}$ ; time constant = 20.48 ms; conversion time = 81.92 ms; 15 scans.

W108<sup>•</sup> (see Chapter 6). This can be taken to mean that the conformation of the protein prevents intramolecular electron transfer, perhaps by raising the reorganization energy ( $\lambda$ ) of the system. Even at increased  $\lambda$ , if the radical comes into Van der Waals contact with the Mo(IV) species, ET can still occur (see the example of Fe(II)/Fe(III) self exchange in Chapter 1). Another possible kinetic explanation for the unusual stability of W108<sup>•</sup> is that a cage formed by the residues from 101-107 disfavors reprotonation of the neutral radical in the folded polypeptide structure. Since formation of the tryptophan anion is unfavorable, a high barrier for protonation would slow the decay. This explanation fails to account for the acceleration of the decay of the EPR signal observed in Figure 5.2.2-10; the pH of the buffer is identical with and without the Mo(IV) species. Ultimately, both of these explanations rely on a unique effect of the local protein environment around W108. One possible conformation of the protein that could stabilize W108<sup>•</sup> is that the nearby E106 residue could easily rotate in order to interact with W108<sup>•</sup>, thereby either increasing the reorganization energy for the reduction or to preventing protonation from occurring readily. In any case, the stabilization of the radical is substantial. Given a reduction potential  $\geq 0.867$  V vs. NHE, the persistence of this radical for more than 5 hours implies a significant perturbation of the physical properties of the radical relative to a tryptophan monomer or dipeptide.

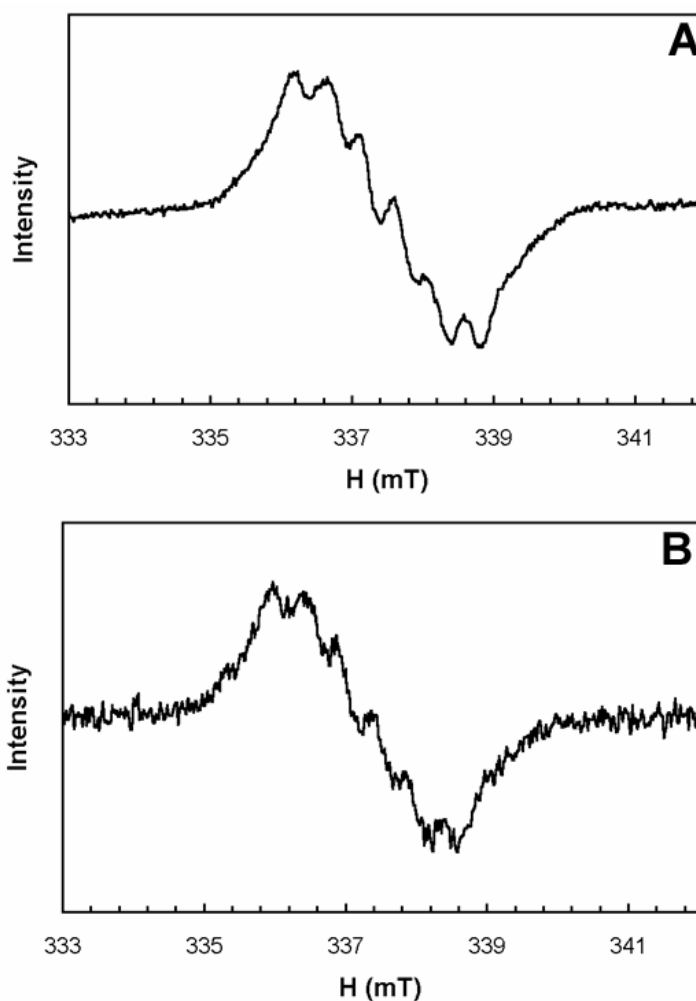
### 5.2.3. *[Re(H107)(W110)Az]*

Another mutant chosen for its possible contribution to multi-step ET is H83Q/W48F/Y72F/Q107H/Y108F/F110W. The Re-labeled version of this protein *[Re(H107)(W110)Az]* did not readily crystallize, so the conformation of the lone tryptophan at position 110 (W110) can only be estimated. It is, however, certain that W110 resides in an environment of intermediate polarity relative to W48 and W108: the fluorescence maximum for W110 is  $\lambda = 319$  nm between the values for W48 ( $\lambda = 308$  nm) and W108 ( $\lambda = 332$  nm) (Figure 5.2.3-1). Once again, it is straightforward to generate the one-electron oxidized W110 (W110<sup>•</sup>) by means of the flash/quench/freeze technique (Figure 5.2.3-2A). The EPR spectrum of W110<sup>•</sup> shows better defined fine structure than W108<sup>•</sup>, perhaps indicating a smaller number of conformations for the radical in the frozen solution. The EPR spectrum shows only slight variation in deuterated buffer (Figure 5.2.3-2B). This radical disappears much more quickly than either W48<sup>•</sup> (~ 30 min) or W108<sup>•</sup> (~5 hr), the signal is gone after only a few min at room temperature (Figure 5.2.3-3). Optically, the absorption spectrum was somewhat difficult to interpret, showing a broad-band centered at ~ 460 nm and a smaller feature centered at ~ 624 nm. The red-shifted band is likely a small amount of Cu(I) impurity oxidized by the reaction (Figure 5.2.3-4). This assertion is supported by the fact that at different pHs the red band is largely unaffected, while the blue band blue shifts under both acidic and basic pHs (Figure 5.2.3-5). The formation of the band with  $\lambda_{\text{max}} = 460$  nm is fast, as shown by the observation of the single wavelength absorption at 440 nm (Figure 5.2.3-6). The kinetic analysis of this signal is

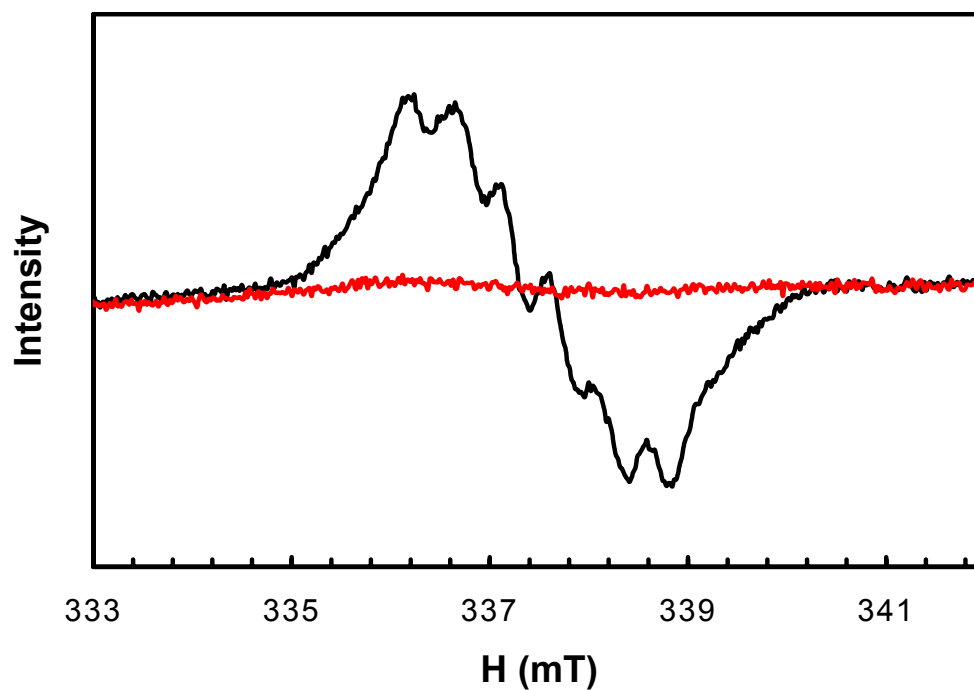


**Figure 5.2.3-1:** Tryptophan fluorescence,  $\lambda_{\text{ex}} = 280 \text{ nm}$  4  $\mu\text{M}$  H83Q/W48F/Y72F/Y108F/F110W AzCu(II) in 50 mM KPi pH 7.16.

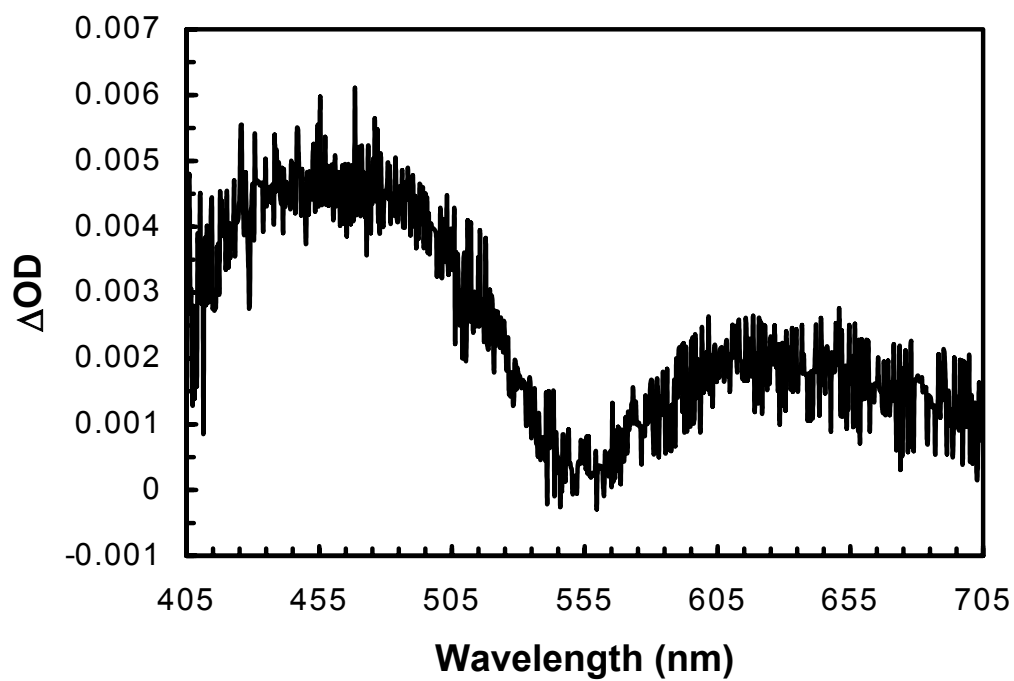




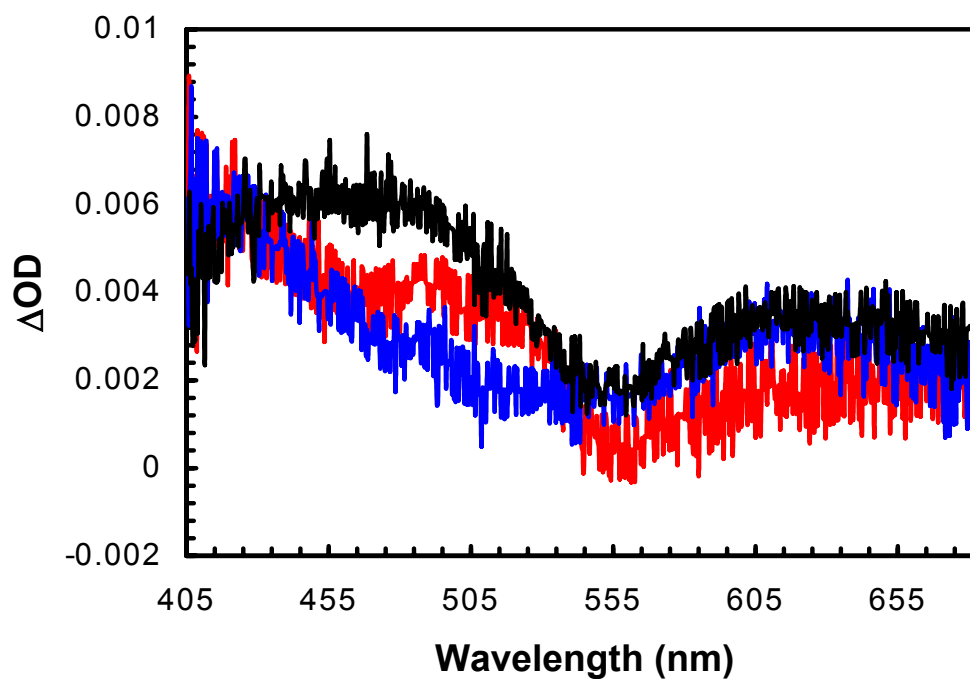
**Figure 5.2.3-2:** X-band EPR of  $[\text{Re}(\text{H107})(\text{W110})\text{AzZn}(\text{II})]/\text{Co}(\text{III})$  in protic and deuterated buffer saturated with  $\text{Co}(\text{III})(\text{NH}_3)_5\text{Cl}$  at 77K. (A) 300  $\mu\text{M}$   $[\text{Re}(\text{H107})(\text{W110})\text{AzZn}(\text{II})]$ , 50 mM KPi, pH 7.16,  $\nu = 9.465794$  GHz (B) 200  $\mu\text{M}$   $[\text{Re}(\text{H107})(\text{W110})\text{AzZn}(\text{II})]$ , 50 mM KPi ( $\text{D}_2\text{O}$ ), pD 7.16,  $\nu = 9.457586$  GHz. Settings: modulation frequency = 100 kHz; modulation amplitude = 1.0 G; microwave power = 202  $\mu\text{W}$ ; time constant = 10.24 ms; conversion time = 40.96 ms; 15 scans.



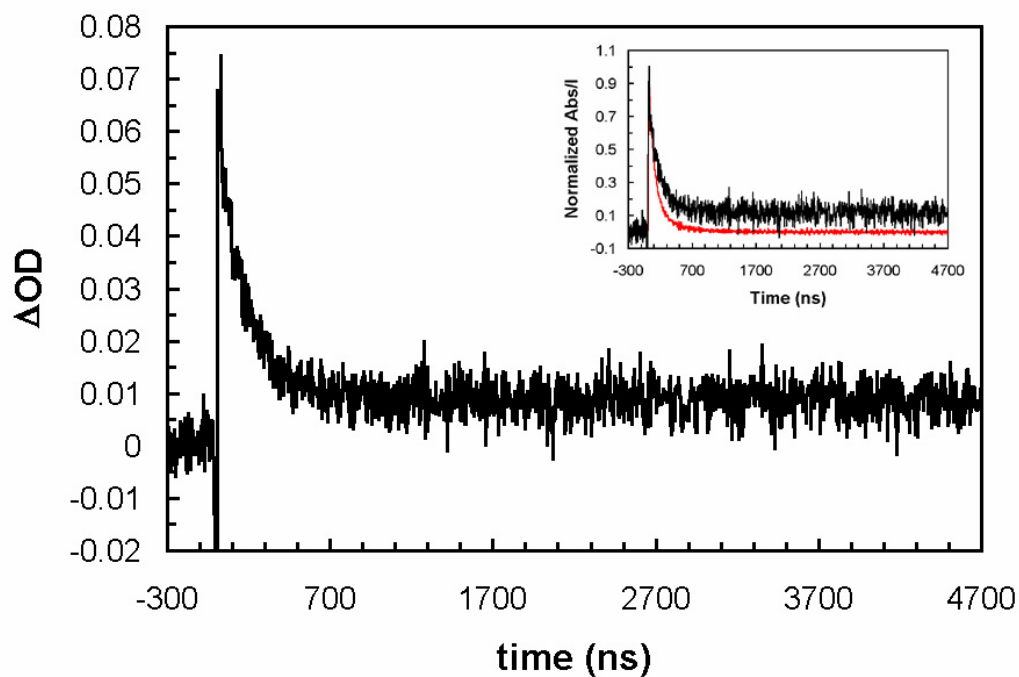
**Figure 5.2.3-3:** X-band EPR decay of  $[\text{Re}(\text{H107})(\text{W110})\text{AzZn}(\text{II})]/\text{Co}(\text{III})$ ,  $300\ \mu\text{M}$   $[\text{Re}(\text{H107})(\text{W110})\text{AzZn}(\text{II})]$  in  $50\ \text{mM}$  KPi, pH 7.16 saturated with  $\text{Co}(\text{III})(\text{NH}_3)_5\text{Cl}$  at  $77\text{K}$  (—) after generation (—) after 3 min at room temperature. Settings:  $\nu = 9.465794\ \text{GHz}$ ; modulation frequency =  $100\ \text{kHz}$ ; modulation amplitude =  $1.0\ \text{G}$ ; microwave power =  $202\ \mu\text{W}$ ; time constant =  $10.24\ \text{ms}$ ; conversion time =  $40.96\ \text{ms}$ ; 15 scans.



**Figure 5.2.3-4:** NS2 spectrum,  $[\text{Re}(\text{H107})(\text{W110})\text{AzZn}(\text{II})]/\text{Co}(\text{III})$ , 20  $\mu\text{s}$  after the pulse, 20  $\mu\text{M}$   $[\text{Re}(\text{H107})(\text{W110})\text{AzZn}(\text{II})]$  with 5 mM  $\text{Co}(\text{III})(\text{NH}_3)_5\text{Cl}$  in 50 mM KPi pH 7.16.



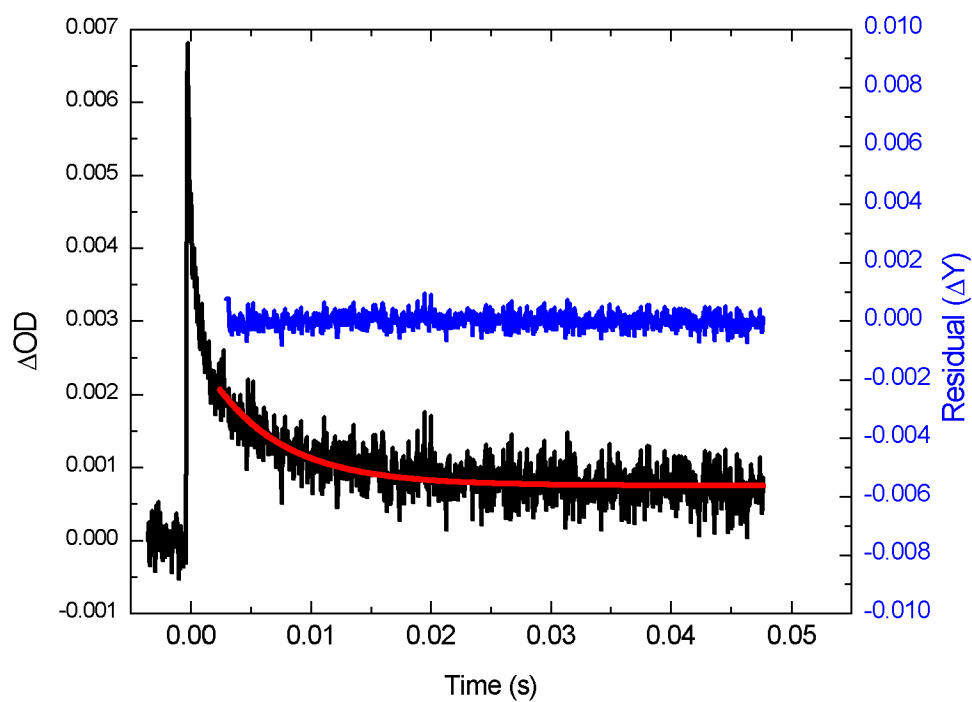
**Figure 5.2.3-5:** NS2 spectra,  $\text{Re}(\text{H107})(\text{W110})\text{AzZn}(\text{II})/\text{Co}(\text{III})$ , various pH's, 20  $\mu\text{s}$  after the pulse, 20  $\mu\text{M}$   $[\text{Re}(\text{H107})(\text{W110})\text{AzZn}(\text{II})]$  with 5 mM  $\text{Co}(\text{III})(\text{NH}_3)_5\text{Cl}$  in (—) 50 mM KPi pH 7.16 (—) 50 mM NaOAc pH 4.03 (—) 50 mM NaHCO3 pH 9.8.



**Figure 5.2.3-6:** NS1 transient absorption,  $[\text{Re}(\text{H107})(\text{W110})\text{AzZn}(\text{II})]/\text{Co}(\text{III})$ , 57  $\mu\text{M}$   $[\text{Re}(\text{H107})(\text{W110})\text{AzZn}(\text{II})]$  with 5 mM  $\text{Co}(\text{III})(\text{NH}_3)_5\text{Cl}$  in 50 mM KPi pH 7.16. Monitoring at 440 nm. Inset: overlay of (—) transient absorption at 440 nm and (—) emission decay at 595 nm.

complicated by absorption of the Re excited state (as observed for the model complex, inset Figure 5.2.3-6). Subtraction of the excited state profile from the transient absorption yields an approximate of formation constant  $k \sim 1 \times 10^5 \text{ s}^{-1}$ . The signal at 440 nm decays with a rate constant of  $k = 2 \times 10^2 \text{ s}^{-1}$  (a lifetime comparable to DNA photolyase) (Figure 5.2.3-7). This is a much faster decay than that observed for W108<sup>•</sup>.

These results, particularly the changes in the absorption spectrum of the radical and its shortened persistence suggest that this radical is somewhat different than the other two azurin-based radicals covered in this thesis. W110<sup>•</sup> is not likely to be protonated; high and low pH optical spectra show approximately the same trace. This suggests that the issue is again perhaps one of local protein environment. That is, it is well known that azurin shows conformational differences at high (9.0) and low (5.5) pH [87]. Although these changes in the wild-type structure occur mainly at a site remote from the 110 residue environment, in the mutant investigated here, the changes at W110 as a result of pH variation may be substantial.



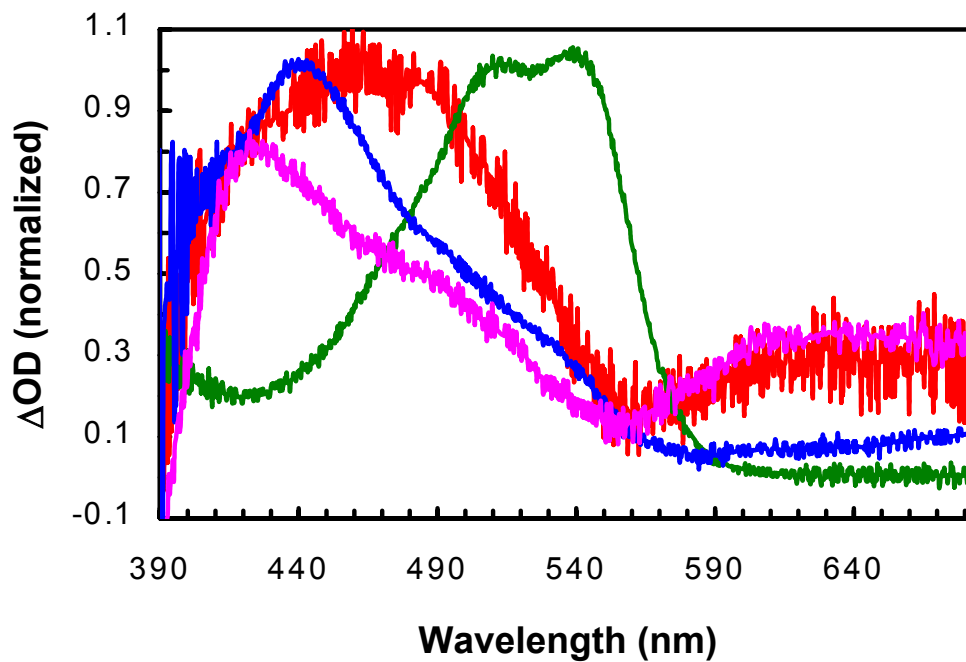
**Figure 5.2.3-7:** NS1 transient absorption  $[\text{Re}(\text{H107})(\text{W110})\text{AzZn}(\text{II})]/\text{Co}(\text{III})$ , 41  $\mu\text{M}$   $[\text{Re}(\text{H107})(\text{W110})\text{AzZn}(\text{II})]$  with 5 mM  $\text{Co}(\text{III})(\text{NH}_3)_5\text{Cl}$  in 50 mM KPi pH 7.16. Monitoring at 440 nm. (—) linear least squares fit of data ( $k = 2 \times 10^2 \text{ s}^{-1}$ ) (—) residual for fit.

### 5.3. *Comparison of Tryptophan Radicals*

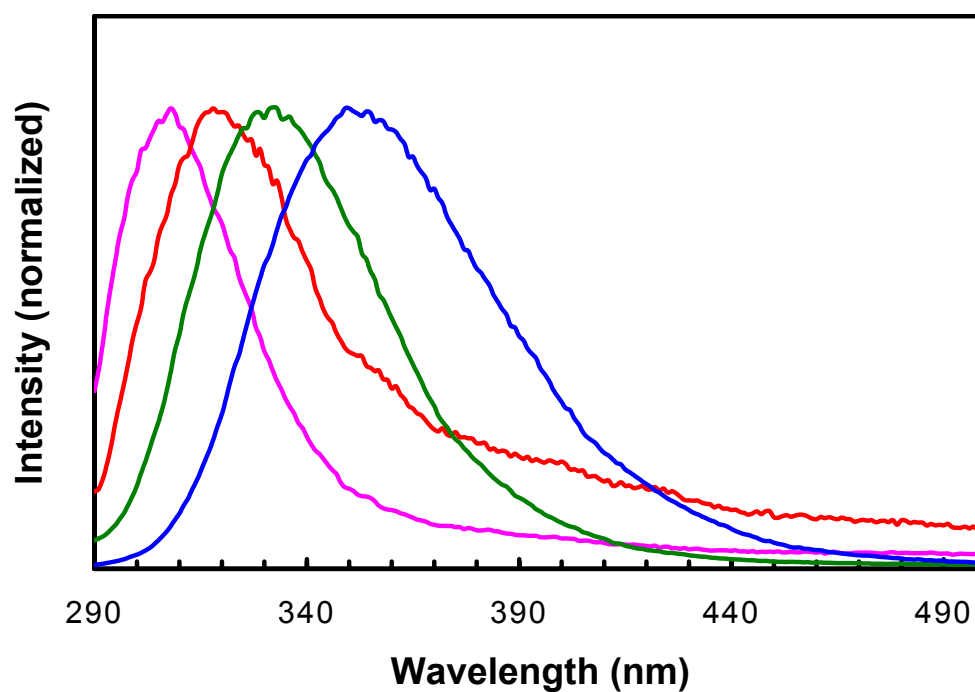
Overall, this analysis of tryptophan radicals has some important consequences for the study of proteins which contain such radicals; particularly on the optical front. Of paramount importance is the variability of the absorption maxima of the tryptophan radicals. By comparing normalized spectra of the model dipeptide Trp-Glu, W48<sup>•</sup>, W108<sup>•</sup> and W110<sup>•</sup>, it is clear that neutral tryptophan radicals exhibit red absorption maxima that span a range of more than 50 nm in the protein environment (100 nm if the dipeptide is considered) (Figure 5.3-1). Furthermore, the absorbance of the radicals in the protein seems to be somewhat correlated with emission maxima and, therefore, with hydrophobicity of the residue environment (W48<sup>•</sup> does not appear to strictly fit this model since it absorbs at ~ 500 nm), though not simply with access to water: the dipeptide, though the most red-shifted in fluorescence is the most blue-shifted in absorbance (Figure 5.3-2). All of this combines to make analysis of a tryptophan radical by absorption spectroscopy alone a dicey proposition. If the spectrum of the radical can shift more 50 nm based solely on protein environment, assigning protonation state of a purported tryptophan radical on the basis of absorption spectra alone [73] is likely to encounter a fair amount of error. In order to fully assign protonation state, and even character of the radical, absorption spectroscopy must be used in concert with a variety of paramagnetic resonance techniques.

Another important result of this work is the understanding that tryptophan radicals may be stabilized for a surprising length of time, and that that stabilization appears to be intimately linked to the electron transfer properties of the environment. The W48<sup>•</sup> in the





**Figure 5.3-1:** NS2 spectra, W48<sup>•</sup>, W108<sup>•</sup>, W110<sup>•</sup>, comparison. 20  $\mu$ s after the pulse, comparison of (—) 60  $\mu$ M [Re(H83)(W48)AzZn(II)] (—) 80  $\mu$ M [Re(H107)(W110)AzZn(II)] (—) 50  $\mu$ M [Re(H83)(W48)AzZn(II)] (—) 80  $\mu$ M **3a** and 5 mM Trp-Glu all with 5 mM Co(III)(NH<sub>3</sub>)<sub>5</sub>Cl in 50 mM KPi pH 7.16.



**Figure 5.3-2:** Normalized fluorescence spectra,  $\lambda_{\text{ex}} = 280$  nm of (—) wild-type azurin Cu(II) (—) H83Q/W48F/Y72F/Q107H/Y108F/F110W Azurin Cu(II) (—) H83Q/W48F/Y72F/Q107H/Y108W Azurin Cu(II) (—) Trp-Glu in 50 mM KPi pH 7.16.

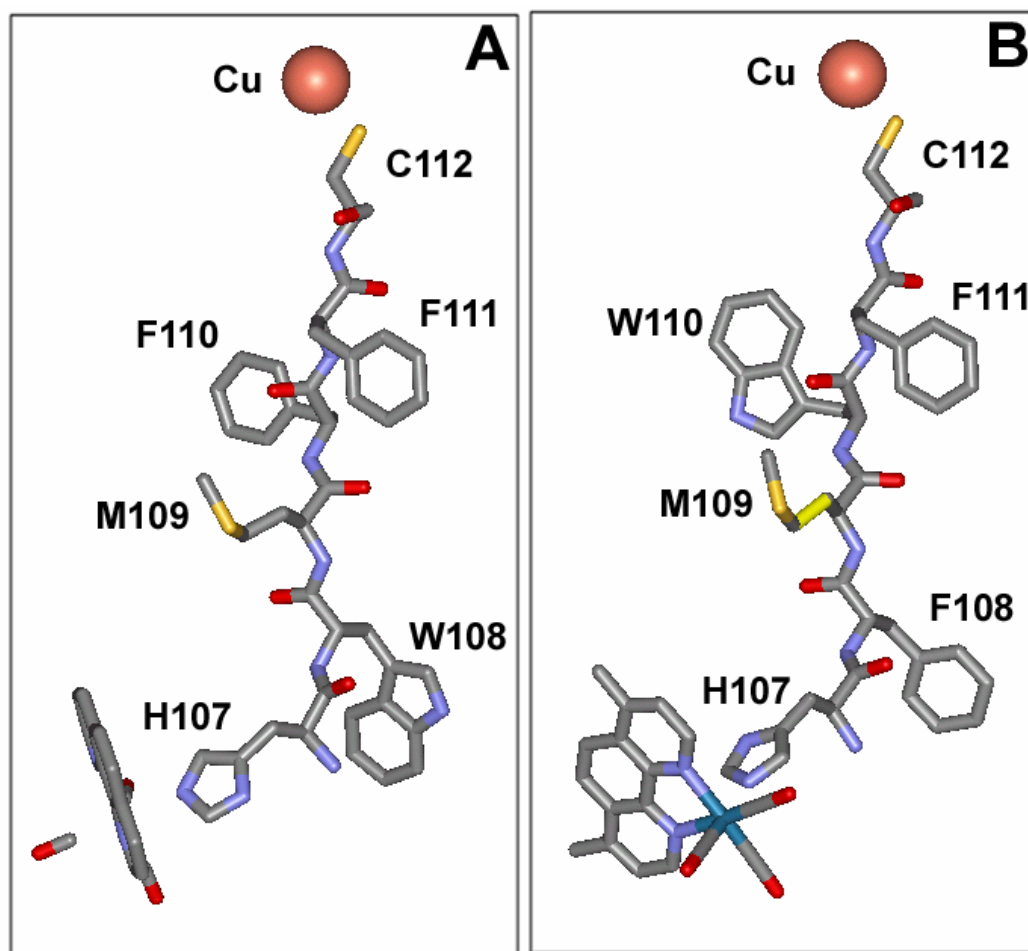
wild-type protein decays quickly, with  $\tau \sim 5$  ms, apparently converted to a tyrosine radical; but if all the tyrosine donors are removed (as in [Re(H83)(W48)Az]), the halflife of the radical increases by 10000 to be on the order of minutes. W108<sup>•</sup> behaves in a similar fashion: in the absence of a readily available electron donor (even Cu(I) in the protein is not sufficient, see chapter 6), the radical persists for hrs. Once an exogenous electron donor (e.g., Mo(IV)(CN)<sub>8</sub><sup>4-</sup>) is added to the radical, it disappears at most on a timescale of minutes. Thus, it is likely that the factor which is dominant in the persistence of these radicals (at least in azurin) is their ability to acquire the necessary electron for reduction. In the case of W48<sup>•</sup>, perhaps the limiting factor is the shielding of the protein environment; if no nearby residues may be oxidized, its contact with the external (to the protein) environment is sufficiently limited to prolong the lifetime of the radical. For W108<sup>•</sup>, perhaps the operative limitation is an increase in reorganization energy of the protein. A locked conformation of the radical would require a large amount of energy to break in order to allow a return to the reduced state. In any case, these results highlight the sophistication of protein evolution when it comes to the control of the physical properties of proteins.

## *Chapter 6*

### **COPPER OXIDATION IN RE-LABELED AZURINS**

Owing to the unusual rates of copper oxidation found in the histidine only mutants of azurin (Figure 3.2.2-2), investigations of proteins with varied internal compositions were necessary. The focus of this chapter is on the electron transfer along the  $\beta$ -strand between Q105 and the copper-ligating C112. This pathway was chosen for its well defined  $\beta$ -strand character, direct coupling to copper, and for the relatively slow rate of ET between Cu(I) and “Re(II)” at position 107 in the mutant H83Q/Q107H ( $k = 2 \times 10^4 \text{ s}^{-1}$  [41, 42]). This “slow” rate means that reactions along this pathway would be well within the monitoring capabilities of the available instrumentation (NS1) and therefore modification of this rate would be immediately obvious.

Of the mutants investigated, two were designed specifically to understand ET through this  $\beta$ -strand mediated by a multi-step mechanism: [Re(H107)(W108)Az] and [Re(H107)(W110)Az] (Figure 6-1). In both cases, the Re-labeled proteins contain only one easily oxidized amino-acid residue, W108 or W110; Y72, Y108 and W48 having been removed. “Easily oxidized” in this context refers to the indirectly determined one electron oxidation potential of tryptophan, found to be  $\sim 1\text{V}$  vs. NHE [58, 59]. The oxidation potentials of the other residues (excepting tyrosine,  $\sim 0.8\text{ V}$  vs. NHE [11]) are all in a



regime less likely to participate in multi-step ET.<sup>6</sup> Ultimately, this paucity of energetically accessible intermediate charge carriers should help ensure that alterations of the rate of ET are due only to the specifically placed tryptophans.

As demonstrated in Chapter 5 above, these proteins readily form tryptophan radicals in the absence of another intramolecular electron donor (e.g., Cu(I)). In the case of [Re(H107)(W108)Az] the tryptophan radical has been determined to have a redox potential  $\geq 0.867$  V vs. NHE. Given the redox potential of the copper center (0.310 V vs. NHE) and the measured reorganization energy of the ruthenium and osmium labeled proteins (0.7 eV [34], see Chapter 3), this radical ought to provide a driving force for Cu(I) oxidation of  $\sim 0.6$  eV, near the maximum of the Marcus curve for metal-labeled azurin. W110<sup>•</sup> appears to be more reactive than W108<sup>•</sup>, at least based on the rates of radical decay, thus it might have an even higher driving force to complete the ET reaction. In both cases, the distance between the copper center and the radical is short (19.8 Å for C $\alpha$  W108 to Cu [crystal structure distance], 12 Å for C $\alpha$  W110 to Cu [estimated]); suggesting that ET at a reasonable rate should occur between the radicals and the reduced copper center. Given that both radicals are formed quickly ( $\sim 10^6$  s<sup>-1</sup> for W108<sup>•</sup> and  $\sim 10^5$  s<sup>-1</sup> for W110<sup>•</sup>, see Chapter 5) and that W110 is much closer to the copper than W108; the rate of Cu(I) oxidation in [Re(H107)(W110)AzCu(I)] should be substantially faster than the same rate in [Re(H107)(W108)AzCu(I)], if there is multi-step ET. It is also possible, however, that the rate-limiting step in Cu(I) oxidation in [Re(H107)(W110)AzCu(I)] would be radical

---

<sup>6</sup> In fact, only cysteine (1.33 V vs. NHE) and glycine (1.22 V vs. NHE) potentials fall below the measured 1.85 V vs. NHE oxidation potential of the Re fragment [11]

formation. In this case, the observed rate of Cu(I) oxidation would be the same as the rate of W110 oxidation. This problem does not arise with the W108 mutant because the W108-Cu distance is so much longer, making ET from Cu(I) to W108<sup>•</sup> with a rate constant of  $\sim 10^6 \text{ s}^{-1}$  unlikely. Both of these systems were examined carefully to determine what effect, if any, the formation of an intermediate tryptophan radical has on Cu(I) oxidation by “Re(II).”

### 6.1. Copper Oxidation in *[Re(H107)(W108)AzCu(I)]*

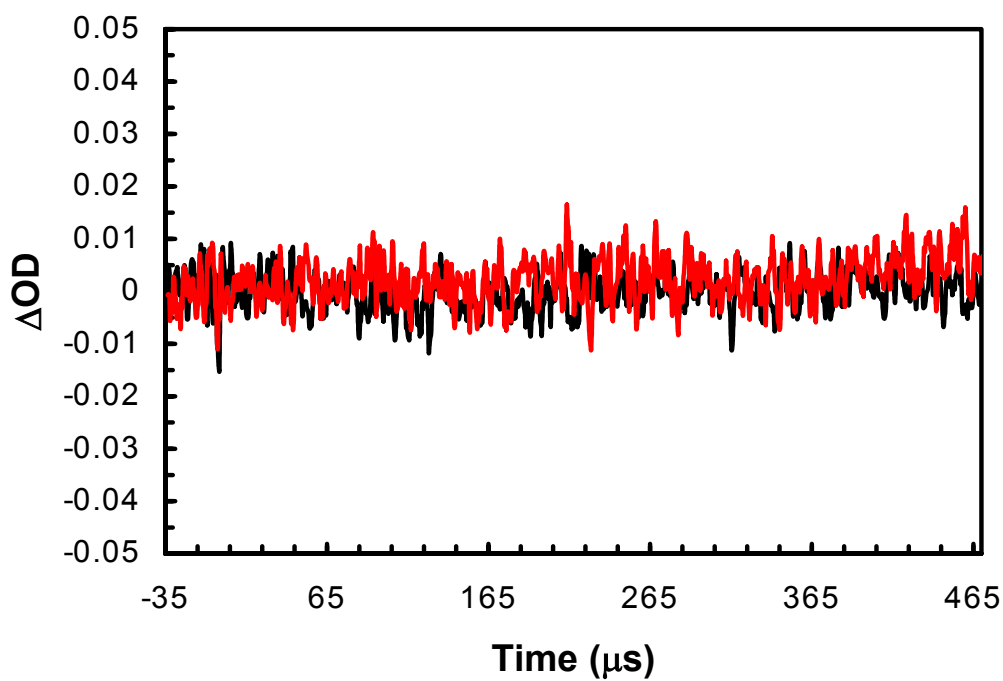
Since the initial mechanism postulated for the observed enhanced rates in Re(H107)-labeled azurin involved the transient generation of a Y108 radical (Scheme 3.2.2-1); the logical first method to test this hypothesis was to construct a mutant with an oxidizable amino-acid residue at position 108. In addition, in order to ensure that this residue was the only viable radical intermediate, all other tyrosines and tryptophans were removed. As described in Chapter 4, this mutant was readily purified and labeled to give *[Re(H107)(W108)AzCu(II)]*. This protein is easily reduced by addition of sodium dithionite followed by gel filtration of the protein on a PD10 column (Pharmacia). The reduction is accompanied by a change in the ground state absorption spectrum: the intense ( $\epsilon = 5900 \text{ M}^{-1}\text{cm}^{-1}$ ) Cu(II) absorption at  $\lambda_{\text{max}} = 628 \text{ nm}$  disappears.

Using NS1 to monitor single wavelength kinetic transformations, changes in intensity at 632.8 nm could be monitored in order to assess the formation of Cu(II) from a flash/quench reaction of *[Re(H107)(W108)AzCu(I)]* with Ru(III)(NH<sub>3</sub>)<sub>6</sub>. Surprisingly, no

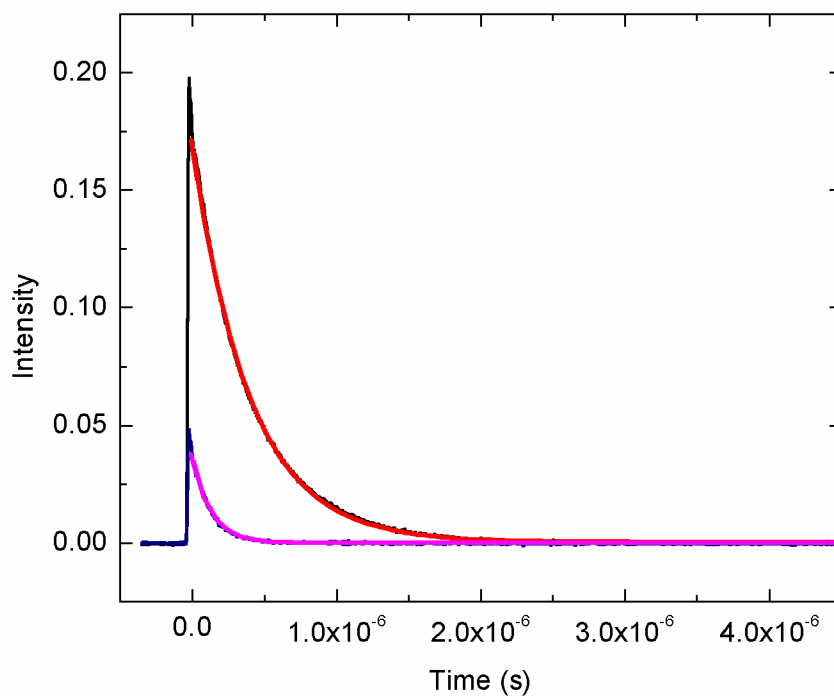
oxidation of Cu(I) was observed (Figure 6.1-1). The decay of the excited state was clearly quenched, showing a change in the rate constant from  $\tau = 395$  ns ( $k = 2.53 \times 10^6$  s<sup>-1</sup>) to  $\sim 129$  ns ( $k_{\text{obs}} = 7.75 \times 10^6$  s<sup>-1</sup>) (Figure 6.1-2). Changing the pH to 9.8 had no measurable effect on this process; still, there was no change in the absorbance at 632.8 nm despite effective quenching of the excited state ( $k = 2.9 \times 10^6$  s<sup>-1</sup> to  $k_{\text{obs}} = 8.4 \times 10^6$  s<sup>-1</sup>, Figure 6.1-3).

The possible answer to this mystery came in the form of a small signal at 500 nm. This absorption is in the appropriate region to be W108<sup>•</sup> ( $\lambda_{\text{max}} = 510, 535$  nm, see Chapter 4); the signal is formed with a rate constant  $k = 5.8 \times 10^6$  s<sup>-1</sup> and decays with  $k_{\text{obs}} = 20$  s<sup>-1</sup> (assuming a first order decay process). It should be noted at this point that the same signal is apparent at pH 9.8, but it is smaller in amplitude and decays somewhat faster ( $k_{\text{obs}} = 3 \times 10^2$  s<sup>-1</sup>). This finding suggests that the barrier to Cu(I) oxidation comes from the inability of the W108<sup>•</sup> to obtain an electron from copper. The sample continues to generate the radical as demonstrated by the absorption at 500 nm, but this signal slowly decays without concomitant Cu(II) formation. A plausible explanation, then, is that W108<sup>•</sup> reacts preferentially with Ru(II)(NH<sub>3</sub>)<sub>6</sub> over extracting an electron from the reduced Cu(I) center. This mechanism is shown in Scheme 6.1-1. For this mechanism to explain the observed behavior,  $k_{\text{HOP}} > k_{\text{Q}} > k_{\text{ET}}$ . That is, the radical reacts more quickly with reduced quencher in solution than with Cu(I). If the transient absorption data is re-plotted for a bimolecular reaction, the rate constant for the putative reduction of W108<sup>•</sup> by Ru(II) is found to be  $k = 3.64 \times 10^7$  M<sup>-1</sup>s<sup>-1</sup> (Figure 6.1-4,  $k = 1.2 \times 10^8$  M<sup>-1</sup>s<sup>-1</sup> for pH 9.8 [data not shown]). This same signal at 500 nm with an identical decay is observed in

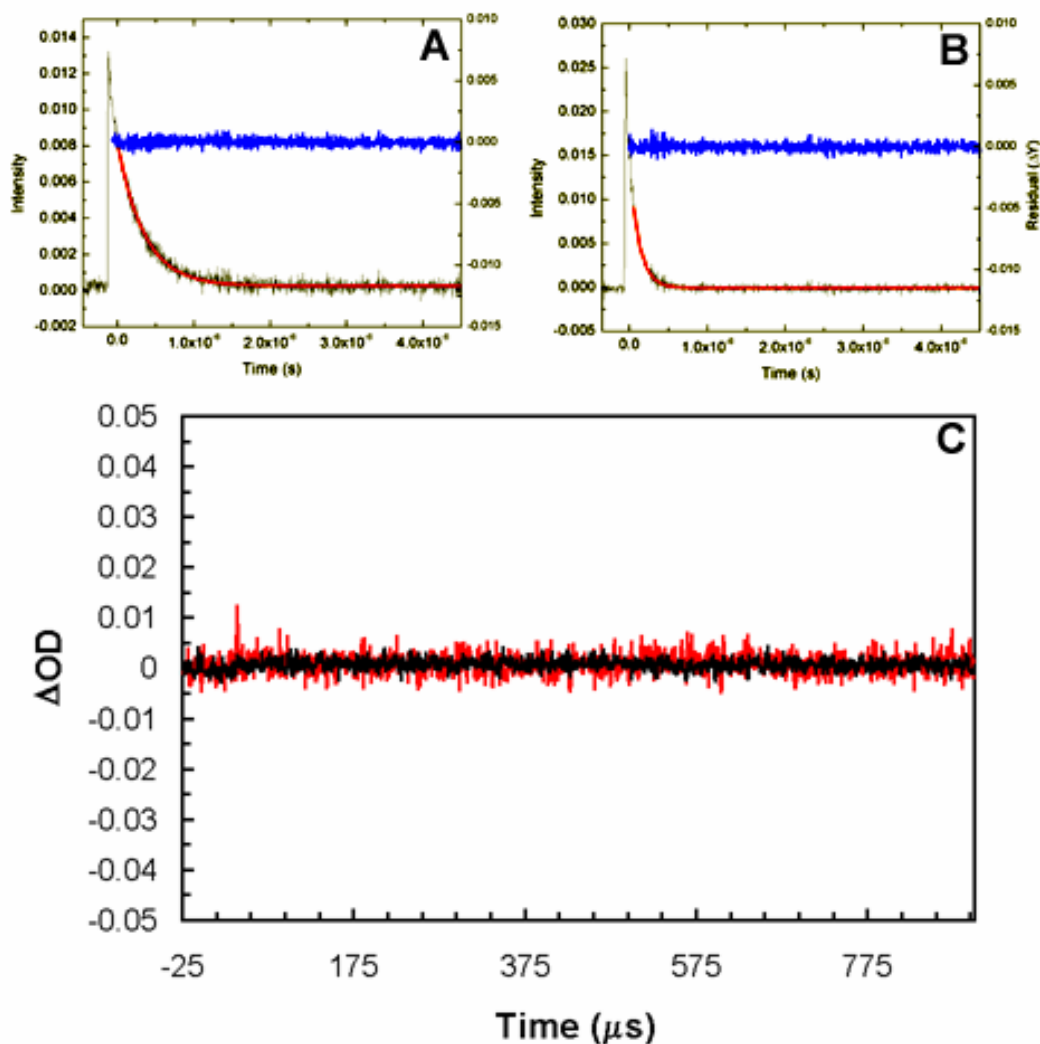




**Figure 6.1-1:** NS1 transient absorption,  $[\text{Re}(\text{H107})(\text{W108})\text{AzCu}(\text{I})]/\text{Ru}(\text{III})$  at 632.8 nm 43  $\mu\text{M}$   $[\text{Re}(\text{H107})(\text{W108})\text{AzCu}(\text{I})]$  in 50 mM KPi pH 7.16. (—) without 5 mM  $\text{Ru}(\text{III})(\text{NH}_3)_6$  (—) with 5 mM  $\text{Ru}(\text{III})(\text{NH}_3)_6$ .

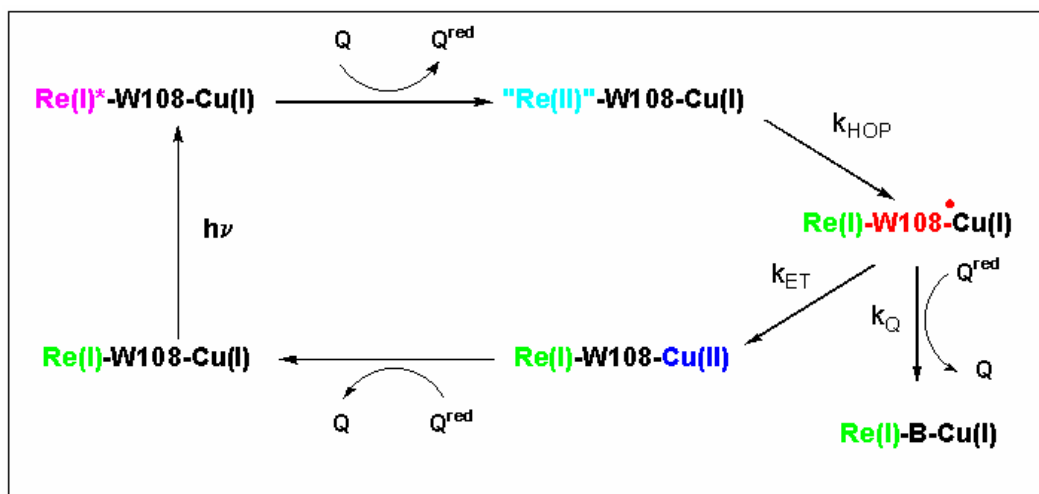


**Figure 6.1-2:** NS1 emission spectra,  $[\text{Re}(\text{H107})(\text{W108})\text{AzCu}(\text{I})]/\text{Ru}(\text{III})$ , at 595 nm. 43  $\mu\text{M}$   $[\text{Re}(\text{H107})(\text{W108})\text{AzCu}(\text{I})]$  in 50 mM KPi pH 7.16. (—) without 5 mM  $\text{Ru}(\text{III})(\text{NH}_3)_6$  (—) linear least squares fit ( $k = 2.53 \times 10^6 \text{ s}^{-1}$ ). (—) with 5 mM  $\text{Ru}(\text{III})(\text{NH}_3)_6$  (—) linear least squares fit ( $k = 7.75 \times 10^6 \text{ s}^{-1}$ ).

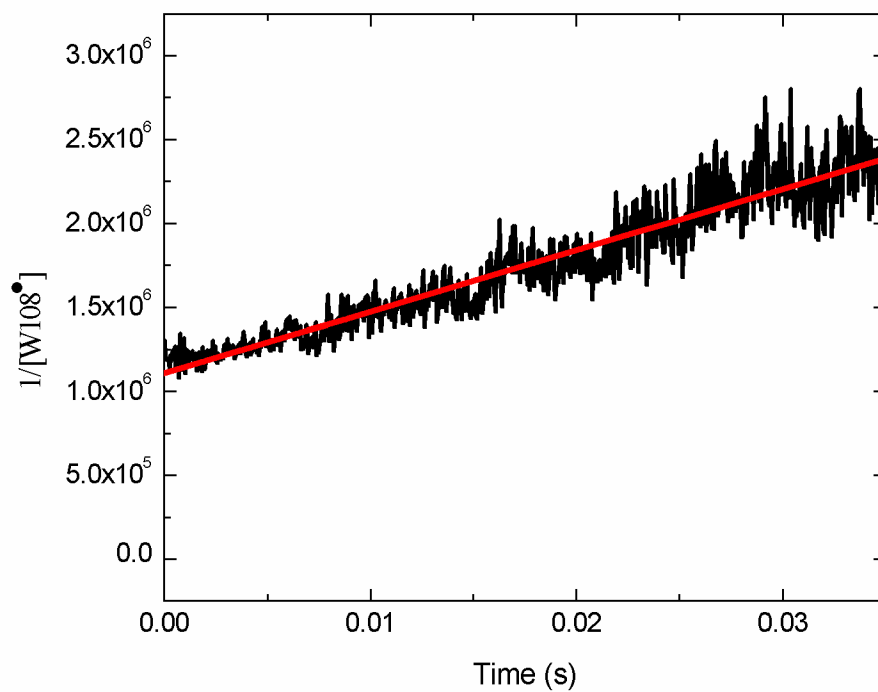


**Figure 6.1-3:** NS1 spectra, 35  $\mu\text{M}$   $[\text{Re}(\text{H107})(\text{W108})\text{AzCu}(\text{I})]$  in 50 mM  $\text{NaHCO}_3$  pH 9.8.

(A) emission at 595 nm, without 5 mM  $\text{Ru}(\text{III})(\text{NH}_3)_6$  (—) linear least squares fit ( $k = 2.9 \times 10^6 \text{ s}^{-1}$ ) (—) residual of fit. (B) emission at 595 nm, with 5 mM  $\text{Ru}(\text{III})(\text{NH}_3)_6$  (—) linear least squares fit ( $k = 8.4 \times 10^6 \text{ s}^{-1}$ ) (—) residual of fit. (C) transient absorption at 632.8 nm (—) without 5 mM  $\text{Ru}(\text{III})(\text{NH}_3)_6$  (—) with 5 mM  $\text{Ru}(\text{III})(\text{NH}_3)_6$ .



**Scheme 6.1-1:** Explanatory mechanism for the lack of Cu(I) oxidation in  $[\text{Re}(\text{H107})(\text{W108})\text{AzCu(I)}]$ .  $Q = \text{Ru(III)}(\text{NH}_3)_6$ ,  $Q^{\text{red}} = \text{Ru(III)}(\text{NH}_3)_6$ .



**Figure 6.1-4:** Reciprocal plot of concentration of W108<sup>•</sup> vs. time. Data from NS1 transient absorption at 500 nm of 43  $\mu\text{M}$  [Re(H107)(W108)AzCu(I)] in 50 mM KPi pH 7.16 with 5 mM Ru(III)(NH<sub>3</sub>)<sub>6</sub>; assuming  $\epsilon_{500} = 2000 \text{ M}^{-1}\text{cm}^{-1}$  (—) linear fit ( $k = 1.82 \times 10^4 \text{ M}^{-1}\text{s}^{-1}$ ). Fit parameter:  $R = 0.946$ .

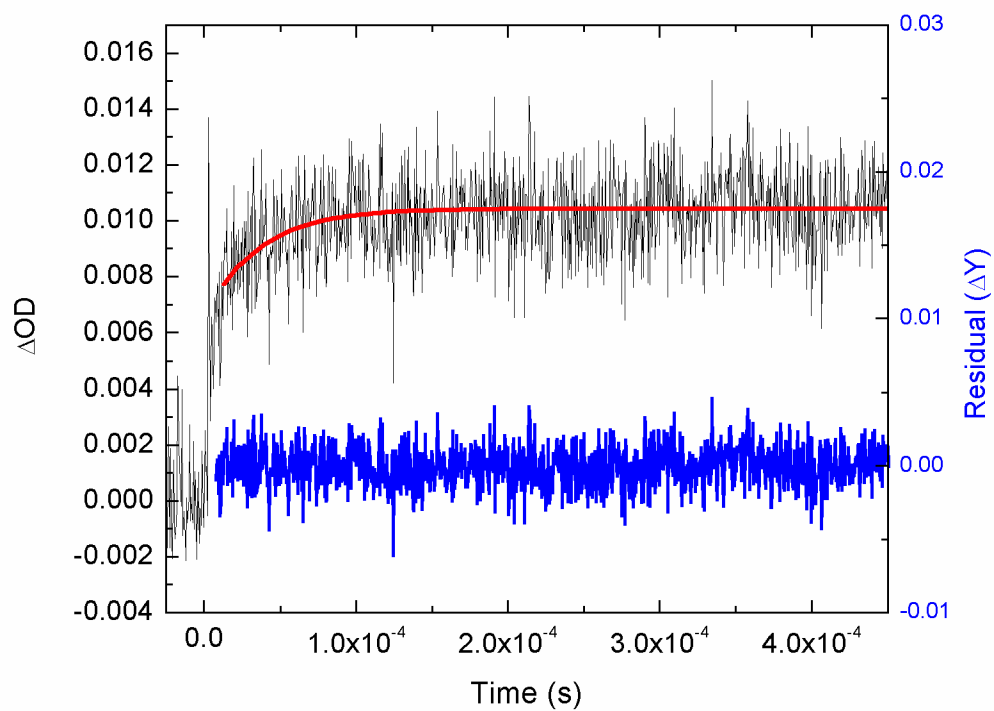
the flash/quench reaction of [Re(H107)(W108)AzZn(II)] with Ru(III)(NH<sub>3</sub>)<sub>6</sub> demonstrating that the decay is not dependent on the nature of the metal center. This result supports the assertion that the decay of the signal at 500 nm is not due to copper oxidation. If correct, this mechanism (Scheme 6.1-1) is quite surprising; that a bimolecular reaction occurring at such a slow rate could out-compete intramolecular reaction between Cu(I) and W108<sup>•</sup> separated by 19.8 Å with a driving force of at least 0.6 eV is certainly counterintuitive. One fact that is not completely explained by the mechanism in Scheme 6.1-1 is the increase in the rate of decay of the 500 nm signal at high pH. The change in the rate constant is a factor of ~ 3, a value which could easily be explained as a function of pH; since, as noted above, changes in pH induce changes in the protein structure. Perhaps these changes alter the exposure of the W108 residue, leading to increased efficiency of the Ru(II)/W108<sup>•</sup> reaction.

The initial reason for examining this protein was to investigate a system which underwent an acceleration of the rate of ET due to multi-step tunneling. Instead, this mutant exhibits a dramatic decrease in the rate of Cu(I) oxidation as the result of radical formation. This finding underlines the elegance of nature: through protein evolution the enzymes that make use of a multi-step mechanism to transfer charge have been carefully tuned.

## 6.2. Copper Oxidation in $[Re(H107)(W110)AzCu(I)]$

As a second attempt for understanding multi-step ET in azurin, a tryptophan residue was placed much closer to the copper site. This mutant,  $[Re(H107)(W110)Az]$ , has a  $C_{\alpha}W$ -Cu distance of approximately 12 Å as estimated from an unoptimized model of the protein from a crystal structure of the W108 mutant. Thus, as noted above, ET mediated by  $W110^{\bullet}$  should show a much faster rate of Cu(I) oxidation than that observed for the Re-labeled H83Q/Q107H mutant, with a maximum possible observable rate of  $\sim 10^5 \text{ s}^{-1}$  (the rate of formation of the radical). Once again, the expected result was not observed. Instead, for a flash/quench reaction of  $[Re(H107)(W110)AzCu(I)]$  with  $Ru(III)(NH_3)_6$ , a very similar rate to that of the simple mutant H83Q/Q107H [42] was found, giving a rate constant  $k = 2.8 \times 10^4 \text{ s}^{-1}$  (Figure 6.2-1)

At this point, an issue must be addressed. The rates of copper oxidation observed in  $[Re(H107)(W110)AzCu(I)]$  and in the Re-labeled H83Q/Q107H are slow enough that it is possible that the observed oxidation is actually a bimolecular reaction between two proteins. That is, it is possible that the photogenerated “Re(II)” species on one protein is in fact coming into contact with another protein without a photo-oxidized rhenium fragment and then oxidizing the Cu(I) of this second azurin. Although this process would require a large bimolecular rate constant, it is not outside the realm of possibility. To exclude this hypothesis as the reason that the Cu(I) oxidation rates are the same in both  $[Re(H107)(W110)AzCu(I)]$  and the Re-labeled H83Q/Q107H, flash/quench reactions of

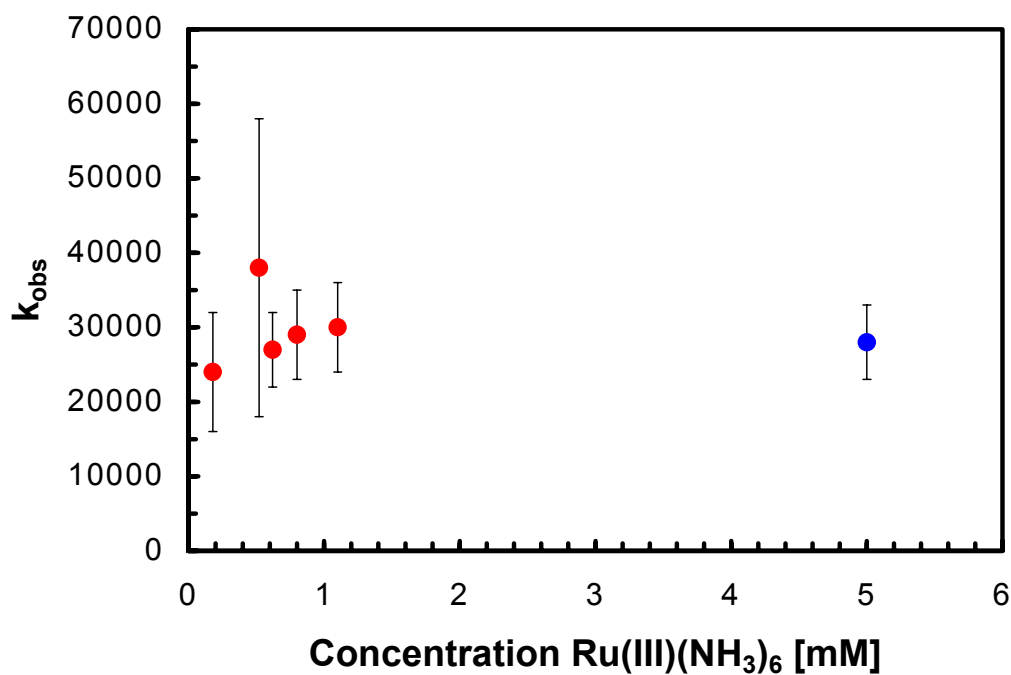


**Figure 6.2-1:** NS1 transient absorption,  $[\text{Re}(\text{H107})(\text{W110})\text{AzCu}(\text{I})]/\text{Ru}(\text{III})$  at 632.8 nm, 47  $\mu\text{M}$   $[\text{Re}(\text{H107})(\text{W110})\text{AzCu}(\text{I})]$  in 50 mM KPi pH 7.16 with 5 mM  $\text{Ru}(\text{III})(\text{NH}_3)_6$  (—) linear least squares fit ( $k = 2.8 \times 10^4 \text{ s}^{-1}$ ). (—) residual for fit.



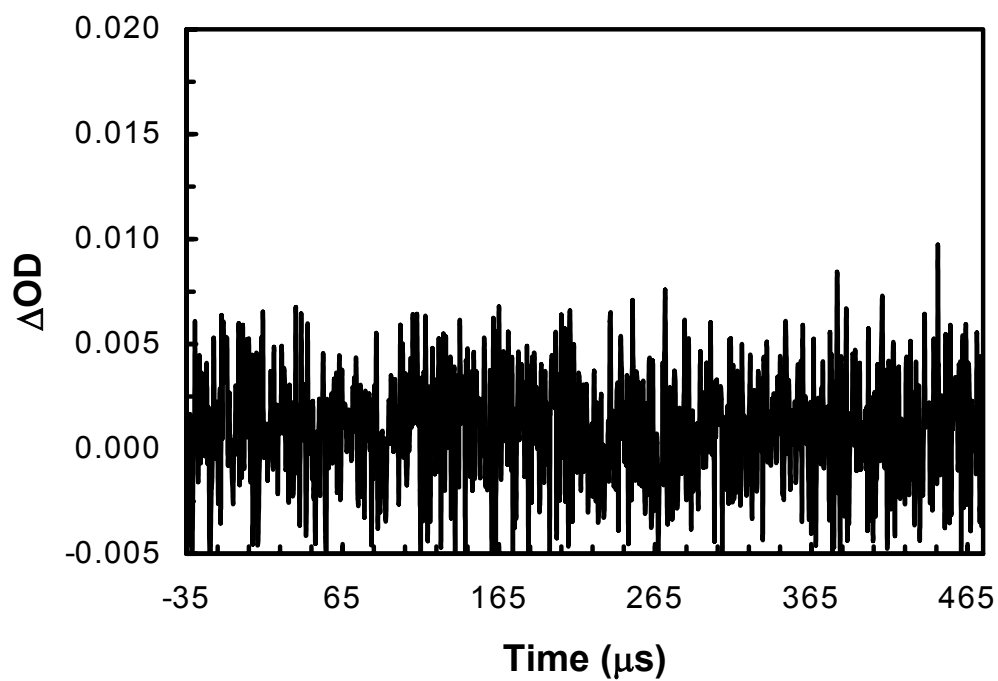
[Re(H107)(W110)AzCu(I)] with varying concentrations of  $\text{Ru(III)(NH}_3)_6$  were performed. Since the amount of quenching of the excited state is proportional to the amount of quencher (see Figure 4.2-5), varying the amount of quencher in effect varies the concentration of “Re(II).” Thus, if there is no dependence of the rate of copper oxidation on the amount of quencher, there is no dependence of the rate on “Re(II)” concentration and so the reaction is not bimolecular as described above. The results of this experiment clearly indicate that the reaction is intramolecular, there is no dependence of the rate on quencher in Figure 6.2-2. A parallel attempt to confirm this finding was undertaken: monitoring the rate of Cu(I) oxidation as a function of protein concentration. Unfortunately, at high concentrations of protein ( $> 90 \mu\text{M}$ ) some irreversible process took place. Therefore, all of the subsequent dilutions showed a fast-decaying positive signal at 632.8 nm in addition to the standard copper oxidation signal. This problem complicated the kinetic analysis, but as a rough approximation, at azurin concentrations below  $\sim 60 \mu\text{M}$  the rate of copper oxidation was independent of azurin concentration. Over the course of the flash/quench experiments with [Re(H107)(W110)AzCu(I)], protein concentrations from  $25 \mu\text{M}$  to  $47 \mu\text{M}$  were used (Figure 6.2-2). In these cases, no variation in the rate of Cu(I) oxidation was observed, further bolstering the assertion that the rate of copper oxidation is independent of the concentration of azurin. Hence, it is clear that the observed Cu(I) oxidation is an intramolecular process with a rate constant  $k = 2.8 \times 10^4 \text{ s}^{-1}$ .

Now, the question arises: why is the rate of copper oxidation nearly identical in both [Re(H107)(W110)AzCu(I)] and Re-labeled H83Q/Q107HAz Cu(I)? One possibility is



**Figure 6.2-2** Rate constants for Cu(I) oxidation in  $[\text{Re(H107)(W110)AzCu(I)}]$  by the flash/quench reaction of (●) 25  $\mu\text{M}$   $[\text{Re(H107)(W110)AzCu(I)}]$  and (●) 47  $\mu\text{M}$   $[\text{Re(H107)(W110)AzCu(I)}]$  plotted against concentration of  $\text{Ru(III)(NH}_3)_6$ . Error bars represent errors in the fit of the rate constant, due largely to poor signal-to-noise ratios.

that based on the physical properties of  $W110^\bullet$ , the rate of  $Cu(II)$  formation by reduction of  $W110^\bullet$  is accidentally identical with the rate of  $Cu(II)$  formation by reduction of  $Y108^\bullet$ . This seems unlikely, since  $Y108$  is  $\sim 8 \text{ \AA}$  further from the copper than  $W110$ . Fortunately, this hypothesis can be directly tested: given that  $W110^\bullet$  absorbs in a characteristic region, and that it is formed much more quickly than the  $Cu(II)$ , then a signal at 440 nm decaying at an identical rate to the formation of  $Cu(II)$  ought to be observable if this hypothesis is correct. No such signal can be seen; in fact, no  $W110^\bullet$  is even formed (Figure 6.2-3).

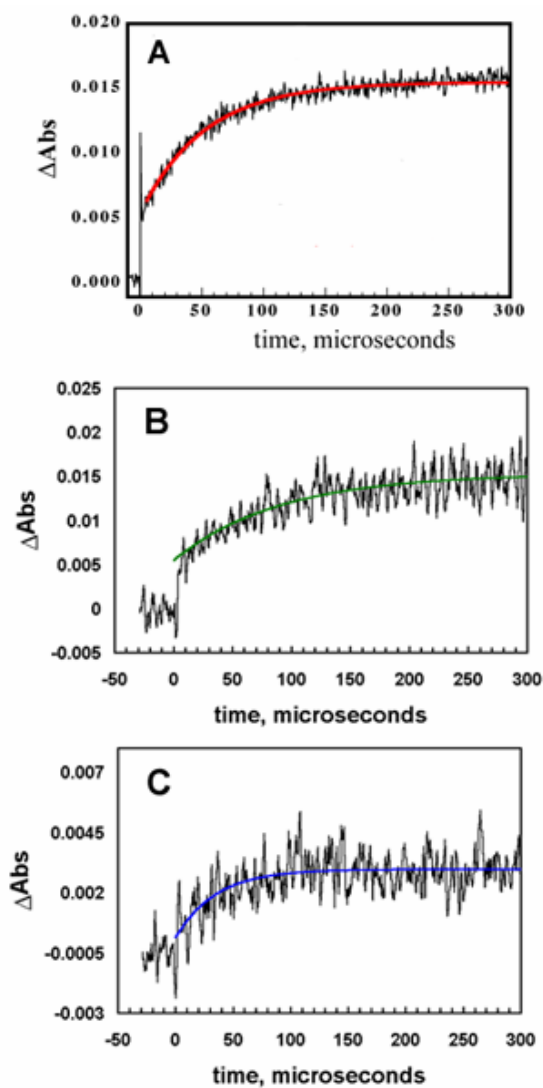


**Figure 6.2-3:** NS1 transient absorption,  $[\text{Re}(\text{H107})(\text{W110})\text{AzCu}(\text{I})]/\text{Ru}(\text{III})$  at 440 nm, 43  $\mu\text{M}$   $[\text{Re}(\text{H107})(\text{W110})\text{AzCu}(\text{I})]$  in 50 mM KPi pH 7.16 with 5 mM  $\text{Ru}(\text{III})(\text{NH}_3)_6$ .

### 6.3. Summary

In order to truly understand the observed rates, it is helpful to consider the Cu(I) oxidation rate in the Re-labeled H83Q/W48F/Y72F/Q107H/Y108F mutant [32]. In this mutant, the rate constant of Cu(II) formation ( $k = 1 \times 10^4 \text{ s}^{-1}$ ) is nearly identical to the rate constants for Re-labeled H83Q/Q107H Az Cu(I) and [Re(H107)(W110)AzCu(I)] (Figure 6.3-1 [42]). This fact, coupled with the observations in Chapters 4 and 5, suggests that the operative copper oxidation mechanism is electron abstraction by the histidine coordinated to the rhenium (for a more detailed discussion, see the thesis of W. Wehbi [32]). This hypothesis still presents some problems for the results obtained for copper oxidation in [Re(H107)(W110)AzCu(I)]; primarily that the formation of W110<sup>•</sup> in the Zn(II) version of the protein is two orders of magnitude faster than the Cu(II) formation, it should still be oxidized in the Cu protein. One possibility is that the charge of the metal center has a large effect on the redox potential of W110. That is, the columbic interactions of the W110 with the nearby metal may change its potential enough to affect the rate of oxidation, thus removing it from the ET pathway. This hypothesis has not been tested and so remains only speculation.

Ultimately, these investigations of Cu(I) oxidation in Re-labeled mutants of azurin have shown that nature is much more efficient at designing ET pathways which incorporate multiple steps than we are. In several cases in the natural world (see Chapter 3), biological molecules apparently make use of multi-step ET to transfer charge over long distances. The



**Figure 6.3-1:** Kinetics of Cu(I) oxidation by “Re(II)”: (A) Re-labeled H83Q/Q107H azurin (— fit with  $k = 2 \times 10^4 \text{ s}^{-1}$ ); (B) 35  $\mu\text{M}$  Re-labeled H83Q/W48F/Y72F/Q107H/Y108F (— fit with  $k = 1 \times 10^4 \text{ s}^{-1}$ ) and (C) 25  $\mu\text{M}$  [Re(H107)(W110)Az] (— fit with  $k = 3 \times 10^4 \text{ s}^{-1}$ ). All fittings were by a linear least squares method [42].

work discussed above has shown one case in which ET over a reasonable distance is shut off ([Re(H107)(W108)Az]) and a case where ET may be mediated by a radical, but not by the intended radical ([Re(H107)(W110)Az]). Thus, without the careful tuning of the protein environment available to nature, artificial approaches must rely on luck. Fortune still may smile upon a researcher occasionally; work recently begun with A. Katrine Museth (not covered here) seems to suggest that ET by a direct photo-induced mechanism mediated by tryptophan may be occurring, although the jury is still out.

## *Chapter 7*

### **CONCLUSIONS**

Through the course of these investigations of rhenium-labeled azurins, a few interesting facts have become apparent. For one, the optical spectra of tryptophan radicals are highly dependent on the local environment. As such, they cannot be relied on to positively identify such a radical, let alone to establish important features of the radical (e.g., protonation state). At the very least, paramagnetic resonance techniques are necessary for identification, and ideally they should be accompanied by site directed mutagenesis studies that remove suspected radical sources. In this work, both the sharp feature at 415 nm in the absorption spectrum and the EPR spectrum of [Re(H83)WTAzZn(II)] were misidentified as a W48 radical at first. It was not until undertaking the spectroscopy of the mutant [Re(H83)(W48)AzZn(II)] that it became apparent that this signal was in fact due to a tyrosine radical.

A key finding that has resulted from the investigations of Re-labeled azurins is that radicals may be stabilized for a substantial period, even in “unnatural” environments. That is, the site-specific azurin mutants studied here have shown at least two tryptophan radicals that persist for much longer than any thus far reported (W108<sup>•</sup> persists for more than 5 hrs at room temperature, W48<sup>•</sup> lasts for at least 20 min at room temperature). The implication here is that sustaining a tryptophan radical is relatively simple in a protein environment. As



discussed in Chapters 5 and 6 above, it seems likely that the source of this stabilization is a lack of ET partners. Perhaps this hypothesis can be generalized: the other routes to radical decomposition (dimerization, H atom abstraction [84]) are sufficiently disfavored in the protein that all nature must do to control the reactivity of an amino-acid radical is restrict its ability to acquire (or lose) the electron necessary to return it to the ground state. This explanation could account for the stability and utility of the many radical enzymes covered briefly in Chapter 3.

Another important finding of these studies is that not just any radical will participate in a charge transfer reaction. W110<sup>•</sup> failed to participate at all in charge transfer from Cu(I); even though the radical is generated quickly in the Zn(II) version of the protein and is in close proximity to the copper center. Even if a radical does participate, its contributions are just as likely to impede the reaction as to accelerate it. W108<sup>•</sup> shut off efficient ET in a system that seemed perfectly poised to express multi-step ET. Finally, the protein environment is unique as compared to a bulk solution. Perhaps this seems somewhat trivial, but there is a model that would pay little attention to the protein environment (UB model, see Chapter 1), simply treating it as a medium slightly more favorable to charge transfer than solvent [88]. Based on my observations of the deviation in absorption spectra, EPR spectra and charge transfer properties of the tryptophan radicals investigated; in my view it is beyond question that the specific local environment of proteins involved in ET is crucial to the success of any charge transfer event. That is, the pathway for any given ET event (particularly a multi-step ET event) is carefully constructed to promote the transfer of an electron from one site to another. An analogous

situation can be found in the brief review of PSII in Chapter 3. Although there are two symmetrically located tyrosine residues, only one of them, TyrZ, is oxidized efficiently by  $P_{680}$  in native PSII. Nature tuned the protein environment to control this process so that only the amino-acid residue directly involved in the generation of  $O_2$  would be oxidized and so allow photosynthesis to occur. The real trick here lies in nature's ability to select the appropriate environment to stabilize or destabilize amino-acid residues to exactly the extent required for the enzyme to function. This is a skill that is currently beyond the reach of molecular biology; although it is possible to replace single amino-acid residues, the understanding of the higher order structure effects is not advanced enough to predict changes which might affect any number of the physical properties of that residue (e.g., oxidation potential). To better understand these factors, much more research on the properties of radicals in proteins and their ability to mediate charge transfer is necessary.

## REFERENCES

- [1] Marcus, R. A.; Sutin, N. Electron Transfers in Chemistry and Biology *Biochim. Biophys. Act.* **1985**, *811*, 265-322.
- [2] Voet, D.; Voet, J. G. *Biochemistry*; 2nd ed.; John Wiley & Sons Inc.: New York, 1995 1361.
- [3] Tommos, C.; Hoganson, C. W.; Di Valentin, M.; Lydakis-Simantiris, N.; Dorlet, P.; Westphal, K.; Chu, H. A.; McCracken, J.; Babcock, G. T. Manganese and Tyrosyl Radical Function in Photosynthetic Oxygen Evolution *Curr. Opin. Chem. Biol.* **1998**, *2*, 244-252.
- [4] Kamiya, N.; Shen, J.-R. Crystal structure of Oxygen-Evolving Photosystem II from *Thermosynechococcus vulcanus* at 3.7 Å Resolution *Proc. Natl. Acad. Sci. U.S.A.* **2003**, *100*, 98-103.
- [5] Faller, P.; Debus, R. J.; Brettel, K.; Sugiura, M.; Rutherford, A. W.; Boussac, A. Rapid Formation of the Stable Tyrosyl Radical in Photosystem II *Proc. Natl. Acad. Sci. U.S.A.* **2001**, *98*, 14368-14373.
- [6] Berthomieu, C.; Hienerwadel, R.; Boussac, A.; Breton, J.; Diner, B. A. Hydrogen Bonding of Redox-Active Tyrosine Z of Photosystem II Probed by FTIR Difference Spectroscopy *Biochemistry* **1998**, *37*, 10547-10554.
- [7] Ahlbrink, R.; Haumann, M.; Cherepanov, D.; Bogershausen, O.; Mulkidjanian, A.; Junge, W. Function of Tyrosine Z in Water Oxidation by Photosystem II: Electrostatic Promoter Instead of Hydrogen Abstractor *Biochemistry* **1998**, *37*, 1131-1142.
- [8] Barry, B. A.; Eldeeb, M. K.; Sandusky, P. O.; Babcock, G. T. Tyrosine Radicals in Photosystem-II and Related Model Compounds – Characterization by Isotopic Labeling and EPR Spectroscopy *J. Biol. Chem.* **1990**, *265*, 20139-20143.
- [9] Yamasato, A.; Kamada, T.; Satoh, K. Random Mutagenesis Targeted to the psbAII Gene of *Synechocystis* sp. PCC 6803 to Identify Functionally Important Residues in the D1 Protein of the Photosystem II Reaction Center *Plant Cell Phys.* **2002**, *43*, 540-548.
- [10] Debus, R. J.; Barry, B. A.; Sithole, I.; Babcock, G. T.; McIntosh, L. Directed Mutagenesis Indicates that the Donor to P<sub>680</sub><sup>+</sup> in Photosystem II is Tyrosine-161 of the D1 Polypeptide *Biochemistry* **1988**, *27*, 9071-9074.
- [11] Stubbe, J.; van der Donk, W. A. Protein Radicals in Enzyme Catalysis *Chem. Rev.* **1998**, *98*, 705-762.

- [12] Berman, H. M.; Westbrook, J.; Feng, Z.; Gilliland, G.; Bhat, T. N.; Weissig, H.; Shindyalov, I. N.; Bourne, P. E. The Protein Data Bank *Nuc. Acid. Res.* **2000**, 28, 235-242.
- [13] Andersson, J.; Bodevin, S.; Westman, M.; Sahlin, M.; Sjoberg, B.-M. Two Active Site Asparagines Are Essential for the Reaction Mechanism of the Class III Anaerobic Ribonucleotide Reductase from Bacteriophage T4 *J. Biol. Chem.* **2001**, 276, 40457-40463.
- [14] Eklund, H.; Uhlin, U.; Farnegardh, M.; Logan, D. T.; Nordlund, P. Structure and Function of the Radical Enzyme Ribonucleotide Reductase *Prog. Biophys. Mol. Biol.* **2001**, 77, 177-268.
- [15] Yee, C. S.; Gie, J.; Chang, M. C. Y.; Nocera, D. G.; Stubbe, J. Radical Initiation by the Class I Ribonucleotide Reductases: Long-Range Proton-Coupled Electron Transfer?, *225th ACS National Meeting*, **2003**
- [16] Shi, W.; Hoganson, C. W.; Espe, M.; Bender, C. J.; Babcock, G. T.; Palmer, G.; Kulmacz, R. J.; Tsai, A.-I. Electron Paramagnetic Resonance and Electron Nuclear Double Resonance Spectroscopic Identification and Characterization of the Tyrosyl Radicals in Prostaglandin H Synthase 1 *Biochemistry* **2000**, 39, 4112-4121.
- [17] Whittaker, M. M.; Ekberg, C. A.; Peterson, J.; Sendova, M. S.; Day, E. P.; Whittaker, J. W. Spectroscopic and Magnetochemical Studies on the Active Copper Complex in Galactose Oxidase *J. Mol. Catal. B: Enzym.* **2000**, 8, 3-15.
- [18] Sawers, G.; Watson, G. A Glycyl Radical Solution: Oxygen-Dependent Interconversion of Pyruvate Formate-Lyase *Mol. Microbiol.* **1998**, 29, 945-954.
- [19] Rich, P. R.; Rigby, S. E. J.; Heathcote, P. Radicals Associated with the Catalytic Intermediates of Bovine Cytochrome C Oxidase *Biochim. Biophys. Act.* **2002**, 1554, 137-146.
- [20] Brash, D. E.; Rudolph, J. A.; Simon, J. A.; Lin, A.; McKenna, G. J.; Baden, H. P.; Halperin, A. J.; Ponten, J. A Role for Sunlight in Skin-Cancer - UV-Induced P53 Mutations in Squamous-Cell Carcinoma *Proc. Natl. Acad. Sci. U.S.A.* **1991**, 88, 10124-10128.
- [21] Olsson, M. H. M.; Ryde, U. The Influence of Axial Ligands on the Reduction Potential of Blue Copper Proteins *J. Biol. Inorg. Chem.* **1999**, 4, 654-663.
- [22] Salgado, J.; Jimenez, H. R.; Donaire, A.; Moratal, J. M. <sup>1</sup>H-NMR Study of a Cobalt-Substituted Blue Copper Protein - *Pseudomonas aeruginosa* Co(II)-Azurin *Eur. J. Biochem.* **1995**, 231, 358-369.

- [23] Donaire, A.; Salgado, J.; Moratal, J. M. Determination of the Magnetic Axes of Cobalt(II) and Nickel(II) Azurins from  $^1\text{H}$  NMR Data: Influence of the Metal and Axial Ligands on the Origin of Magnetic Anisotropy in Blue Copper Proteins *Biochemistry* **1998**, *37*, 8659-8673.
- [24] Moratal, J. M.; Romero, A.; Salgado, J.; Peralesalarcon, A.; Jimenez, H. R. The Crystal-Structure of Nickel(II)-Azurin *Eur. J. Biochem.* **1995**, *228*, 653-657.
- [25] Sjolín, L.; Tsai, L. C.; Langer, V.; Pascher, T.; Karlsson, G.; Nordling, M.; Nar, H. Structure of *Pseudomonas aeruginosa* Zinc-Azurin Mutant Asn47asp at 2.4-Angstrom Resolution *Acta Crystallogr. Sect. D-Biol. Crystallogr.* **1993**, *49*, 449-457.
- [26] Lowery, M. D.; Solomon, E. I. Axial Ligand Bonding in Blue Copper Proteins *Inorg. Chim. Acta* **1992**, *200*, 233-243.
- [27] Guckert, J. A.; Lowery, M. D.; Solomon, E. I. Electronic-Structure of the Reduced Blue Copper Active-Site - Contributions to Reduction Potentials and Geometry *J. Am. Chem. Soc.* **1995**, *117*, 2817-2844.
- [28] Nar, H.; Messerschmidt, A.; Huber, R.; Vandekamp, M.; Canters, G. W. Crystal-Structure of *Pseudomonas aeruginosa* Apo-Azurin at 1.85 Angstrom Resolution *FEBS Lett.* **1992**, *306*, 119-124.
- [29] Farver, O.; Skov, L. K.; Pascher, T.; Karlsson, B. G.; Nordling, M.; Lundberg, L. G.; Vaenngaard, T.; Pecht, I. Intramolecular Electron Transfer in Single-Site-Mutated Azurins *Biochemistry* **1993**, *32*, 7317-7322.
- [30] Farver, O.; Pecht, I. The Role of the Medium in Long-Range Electron Transfer *J. Biol. Inorg. Chem.* **1997**, *2*, 387-392.
- [31] Farver, O.; Skov, L. K.; Young, S.; Bonander, N.; Karlsson, B. G.; Vaenngård, T.; Pecht, I. Aromatic Residues May Enhance Intramolecular Electron Transfer in Azurin *J. Am. Chem. Soc.* **1997**, *119*, 5453-5454.
- [32] Wehbi, W. A. Amino Acid Radicals in Rhenium-Modified Copper Proteins *California Institute of Technology*, **2003**.
- [33] Kostic, N. M.; Margalit, R.; Che, C. M.; Gray, H. B. Kinetics of Long-Distance Ruthenium-to-Copper Electron Transfer in [pentaammineruthenium histidine-83]Azurin *J. Am. Chem. Soc.* **1983**, *105*, 7765-7767.
- [34] Di Bilio, A. J.; Hill, M. G.; Bonander, N.; Karlsson, B. G.; Villahermosa, R. M.; Malmstroem, B. G.; Winkler, J. R.; Gray, H. B. Reorganization Energy of Blue Copper:

Effects of Temperature and Driving Force on the Rates of Electron Transfer in Ruthenium- and Osmium-Modified Azurins **1997**, 119, 9921-9922.

[35] Bjerrum, M. J.; Casimiro, D. R.; Chang, I. J.; Dibilio, A. J.; Gray, H. B.; Hill, M. G.; Langen, R.; Mines, G. A.; Skov, L. K.; Winkler, J. R.; Wuttke, D. S. Electron Transfer in Ruthenium-Modified Proteins *J. Bioenerg. Biomembr.* **1995**, 27, 295-302.

[36] Van de Kamp, M.; Hali, F. C.; Rosato, N.; Agro, A. F.; Canters, G. W. Purification and Characterization of a Nonreconstitutable Azurin, Obtained by Heterologous Expression of the *Pseudomonas aeruginosa* Azu Gene in *Escherichia coli* **1990**, 1019, 283-292.

[37] Langen, R.; Chang, I. J.; Germanas, J. P.; Richards, J. H.; Winkler, J. R.; Gray, H. B. Electron Tunneling in Proteins: Coupling Through a  $\beta$  Strand *Science* **1995**, 268, 1733-1735.

[38] Skourtis, S. S.; Beratan, D. N. In *Electron Transfer: From Isolated Molecules to Biomolecules, Part I*, 1999; Vol. 106, pp 377-452.

[39] Beratan, D. N.; Betts, J. N.; Onuchic, J. N. Protein Electron-Transfer Rates Set by the Bridging Secondary and Tertiary Structure *Science* **1991**, 252, 1285-1288.

[40] Beratan, D. N.; Onuchic, J. N.; Hopfield, J. J. Electron-Tunneling through Covalent and Noncovalent Pathways in Proteins *J. Chem. Phys.* **1987**, 86, 4488-4498.

[41] Winkler, J. R.; Di Bilio, A. J.; Farrow, N. A.; Richards, J. H.; Gray, H. B. Electron Tunneling in Biological Molecules *Pur. Appl. Chem.* **1999**, 71, 1753-1764.

[42] Miller, J. E.; Di Bilio, A. J.; Wehbi, W. A.; Green, M. T.; Winkler, J. R.; Gray, H. B. Electron Tunneling in Rhenium-Modified *Pseudomonas aeruginosa* Azurins *Biochim. Biophys. Act.* **Submitted**.

[43] Gray, H. B.; Winkler, J. R. *Electron Transfer in Metalloproteins*; Verlag GmbH: Weinheim, 2001; Vol. 3 3-23.

[44] Fujita, E.; Brunschwig, B. S. *Homogeneous Redox Catalysis in CO<sub>2</sub> Fixation*; Verlag GmbH: Weinheim, 2001; Vol. 4 88-123.

[45] Miller, J. E.; Gradinaru, C.; Crane, B. R.; Di Bilio, A. J.; Wehbi, W. A.; Winkler, J. R.; Gray, H. B. Photogeneration of a Kinetically Stable Tryptophan Radical in a Structurally Defined Protein Environment *J. Am. Chem. Soc.* **Submitted**.

[46] Di Bilio, A. J.; Crane, B. R.; Wehbi, W. A.; Kiser, C. N.; Abu-Omar, M. M.; Carlos, R. M.; Richards, J. H.; Winkler, J. R.; Gray, H. B. Properties of Photogenerated Tryptophan

and Tyrosyl Radicals in Structurally Characterized Proteins Containing Rhenium(I) Tricarbonyl Diimines *J. Am. Chem. Soc.* **2001**, *123*, 3181-3182.

[47] Connick, W. B.; DiBilio, A. J.; Hill, M. G.; Winkler, J. R.; Gray, H. B. Tricarbonyl(1,10-phenanthroline)(imidazole)rhenium(I): A Powerful Photooxidant for Investigations of Electron Tunneling in Proteins *Inorg. Chim. Acta* **1995**, *240*, 169-173.

[48] Lakowicz, J. R. *Principles of Fluorescence Spectroscopy*; 1st ed.; Plenum Press: New York, 1983 258-297.

[49] Villahermosa, R. M. Electron Tunneling through Phenylene Bridges PhD *California Institute of Technology*, **2002**, 242.

[50] Berglund, J.; Pascher, T.; Winkler, J. R.; Gray, H. B. Photoinduced Oxidation of Horseradish Peroxidase *J. Am. Chem. Soc.* **1997**, *119*, 2464-2469.

[51] Brewer, J. C.; Thorp, H. H.; Slagle, K. M.; Brudvig, G. W.; Gray, H. B. Electronic Structure of Trans-Dioxorhenium(VI) *J. Am. Chem. Soc.* **1991**, *113*, 3171-3173.

[52] Rao, P. S.; Simic, M.; Hayon, E. Pulse-Radiolysis Study of Imidazole and Histidine in Water *J. Phys. Chem.* **1975**, *79*, 1260-1263.

[53] Blaszkak, J. A.; McMillin, D. R.; Thornton, A. T.; Tennent, D. L. Kinetics of Copper(II) Uptake by Apoazurin in Complexing Media *J. Biol. Chem.* **1983**, *258*, 9886-9892.

[54] Kim, S. W.; Kim, J. A.; Kim, E.; Ro, Y. T.; Song, T.; Kim, Y. M. Purification and Some Properties of a Blue Copper Protein from *Methylobacillus* sp Strain SK1 DSM 8269 *Mol. Cells* **2002**, *14*, 214-223.

[55] Strickland, E. H.; Billups, C.; Kay, E. Effects of Hydrogen-Bonding and Solvents Upon Tryptophanyl 1-L<sub>a</sub> Absorption-Band - Studies Using 2,3-Dimethylindole *Biochemistry* **1972**, *11*, 3657-&.

[56] Clayton, A. H. A.; Sawyer, W. H. Site-Specific Tryptophan Fluorescence Spectroscopy as a Probe of Membrane Peptide Structure and Dynamics *Eur. Biophys. J.* **2002**, *31*, 9-13.

[57] Connick, W. B.; Di Bilio, A. J.; Schaefer, W. P.; Gray, H. B. The red form of [Re(phen)(CO)<sub>3</sub>(H<sub>2</sub>O)]-CF<sub>3</sub>SO<sub>3</sub>-H<sub>2</sub>O *Acta Crystallogr. Sect. C-Cryst. Struct. Commun.* **1999**, *55*, 913-916.

[58] Harriman, A. Further Comments on the Redox Potentials of Tryptophan and Tyrosine *J. Phys. Chem.* **1987**, *91*, 6102-6104.

- [59] Jovanovic, S. V.; Harriman, A.; Simic, M. G. Electron-Transfer Reactions of Tryptophan and Tyrosine Derivatives *J. Phys. Chem.* **1986**, *90*, 1935-1939.
- [60] McGimpsey, W. G.; Gorner, H. Photoionization of Indole, N-methylindole and Tryptophan in Aqueous Solution upon Excitation at 193 nm *Photochem. Photobiol.* **1996**, *64*, 501-509.
- [61] Jensen, G. M.; Goodin, D. B.; Bunte, S. W. Density functional and MP2 calculations of spin densities of oxidized 3-methylindole: Models for tryptophan radicals *J. Phys. Chem.* **1996**, *100*, 954-959.
- [62] Huyett, J. E.; Doan, P. E.; Gurbiel, R.; Houseman, A. L. P.; Sivaraja, M.; Goodin, D. B.; Hoffman, B. M. Compound Es of Cytochrome-C Peroxidase Contains a Trp Pi-Cation Radical – Characterization by Cw and Pulsed Q-Band EPR Spectroscopy *J. Am. Chem. Soc.* **1995**, *117*, 9033-9041.
- [63] DeFelippis, M. R.; Murthy, C. P.; Broitman, F.; Weinraub, D.; Faraggi, M.; Klapper, M. H. Electrochemical Properties of Tyrosine Phenoxyl and Tryptophan Indolyl Radicals in Peptides and Amino Acid Analogs *J. Phys. Chem.* **1991**, *95*, 3416-3419.
- [64] Walden, S. E.; Wheeler, R. A. Distinguishing Features of Indolyl Radical and Radical Cation: Implications for Tryptophan Radical Studies *J. Phys. Chem.* **1996**, *100*, 1530-1535.
- [65] Solar, S.; Getoff, N.; Surdhar, P. S.; Armstrong, D. A.; Singh, A. Oxidation of Tryptophan and N-Methylindole by  $\text{N}_3^-$ ,  $\text{Br}_2^-$ , and  $(\text{SCN})_2^-$  Radicals in Light-Water and Heavy-Water Solutions – a Pulse-Radiolysis Study *J. Phys. Chem.* **1991**, *95*, 3639-3643.
- [66] IV, D. R. C. K. New Quantum Monte Carlo Algorithms to Efficiently Utilize Massively Parallel Computers PhD *California Institute of Technology*, **2003**, 131.
- [67] Baldwin, J.; Krebs, C.; Ley, B. A.; Edmondson, D. E.; Huynh, B. H.; Bollinger, J. H. Mechanism of Rapid Electron Transfer during Oxygen Activation in the R2 Subunit of *Escherichia coli* Ribonucleotide Reductase. 1. Evidence for a Transient Tryptophan Radical *J. Am. Chem. Soc.* **2000**, *122*, 12195-12206.
- [68] Rigby, S. E. J.; Junemann, S.; Rich, P. R.; Heathcote, P. Reaction of Bovine Cytochrome C Oxidase with Hydrogen Peroxide Produces a Tryptophan Cation Radical and a Porphyrin Cation Radical *Biochemistry* **2000**, *39*, 5921-5928.
- [69] Potsch, S.; Lendzian, F.; Ingemarson, R.; Hornberg, A.; Thelander, L.; Lubitz, W.; Lassmann, G.; Graslund, A. The Iron-Oxygen Reconstitution Reaction in Protein R2-tyr-177 Mutants of Mouse Ribonucleotide Reductase – EPR and Electron Nuclear Double



Resonance Studies on a new Transient Tryptophan Radical *J. Biol. Chem.* **1999**, *274*, 17696-17704.

[70] Lendzian, F.; Sahlin, M.; MacMillan, F.; Bittl, R.; Fiege, R.; Potsch, S.; Sjoberg, B. M.; Graslund, A.; Lubitz, W.; Lassmann, G. Electronic Structure of Neutral Tryptophan Radicals in Ribonucleotide Reductase Studied by EPR and ENDOR Spectroscopy *J. Am. Chem. Soc.* **1996**, *118*, 8111-8120.

[71] Sahlin, M.; Lassmann, G.; Potsch, S.; Slaby, A.; Sjoberg, B. M.; Graslund, A. Tryptophan Radicals Formed by Iron/Oxygen Reaction with *Escherichia coli* Ribonucleotide Reductase Protein R2 Mutant Y122f *J. Biol. Chem.* **1994**, *269*, 11699-11702.

[72] Fishel, L. A.; Farnum, M. F.; Mauro, J. M.; Miller, M. A.; Kraut, J.; Liu, Y. J.; Tan, X. L.; Scholes, C. P. Compound-I Radical in Site-Directed Mutants of Cytochrome-C Peroxidase as Probed by Electron-Paramagnetic Resonance and Electron Nuclear Double-Resonance *Biochemistry* **1991**, *30*, 1986-1996.

[73] Aubert, C.; Vos, M. H.; Mathis, P.; Eker, A. P. M.; Brettel, K. Intraprotein Radical Transfer during Photoactivation of DNA Photolyase *Nature* **2000**, *405*, 586-590.

[74] Voges, K.-P.; Jung, G.; Sawyer, W. H. Depth-dependent Fluorescent Quenching of a Tryptophan Residue at Defined Positions on a Rigid 21-Peptide Helix in Liposomes **1987**, *896*, 64-76.

[75] Sweeney, J. A.; Harmon, P. A.; Asher, S. A.; Hutnik, C. M.; Szabo, A. G. UV Resonance Raman Examination of the Azurin Tryptophan Environment and Energy Relaxation Pathways *J. Am. Chem. Soc.* **1991**, *113*, 7531-7537.

[76] Prutz, W. A.; Land, E. J. Charge-Transfer in Peptides – Pulse-Radiolysis Investigation of One-Electron Reactions in Dipeptides of Tryptophan and Tyrosine *Int. J. Radiat. Biol.* **1979**, *36*, 513-520.

[77] Sahlin, M.; Cho, K.-B.; Potsch, S.; Lytton, S. D.; Huque, Y.; Gunther, M. R. G.; Sjoberg, B.-M.; Mason, R. P.; Graslund, A. Peroxyl Adduct Radicals Formed in the Iron/Oxygen Reconstitution Reaction of Mutant Ribonucleotide Reductase R2 Proteins from *Escherichia coli* *J. Biol. Inorg. Chem.* **2002**, *7*, 74-82.

[78] Svistunenko, D. A. An EPR Study of the Peroxyl Radicals induced by Hydrogen Peroxide in the Haem Proteins *Biochim. Biophys. Acta-Protein Struct. Molec. Enzym.* **2001**, *1546*, 365-378.

- [79] Jones, G.; Lu, L. N. Photoactive Peptides. 8. Long-Lived Charge-Separated Species Observed on Flash Photolysis of Peptide Conjugates. Interplay of Local and Radical Ion Pair Triplet States *J. Org. Chem.* **1998**, *63*, 8938-8945.
- [80] Vass, I.; Styring, S. Ph-Dependent Charge Equilibria between Tyrosine-D and the S-States in Photosystem (II). Estimation of Relative Midpoint Redox Potentials *Biochemistry* **1991**, *30*, 830-839.
- [81] Weil, J. A.; Bolton, J. R.; Wertz, J. E. In *Electron Paramagnetic Resonance: Elementary Theory and Practical Applications*; John Wiley & Sons Inc.: New York, 1994, pp 492-510.
- [82] Fu, Y. S.; Swaddle, T. W. Electrochemical Kinetics of Cyanometalate Complexes in Aqueous Solution at High Pressures *Inorg. Chem.* **1999**, *38*, 876-880.
- [83] McGarvey, B. R. Structure of Octacyanomolybdate(V) and -Tungstate(V) Ions from Electron Spin Resonance *Inorg. Chem.* **1966**, *5*, 476-&.
- [84] Lowry, T. H.; Richardson, K. S. *Mechanism and Theory in Organic Chemistry*; 3rd ed.; Harper Collins Publishers: New York, 1987 737-811.
- [85] Headlam, H. A.; Davies, M. J. Beta-Scission of Side-Chain Alkoxy Radicals on Peptides and Proteins Results in the Loss of Side-Chains as Aldehydes and Ketones *Free Radic. Biol. Med.* **2002**, *32*, 1171-1184.
- [86] Garrison, W. M. Reaction-Mechanisms in the Radiolysis of Peptides, Polypeptides, and Proteins *Chem. Rev.* **1987**, *87*, 381-398.
- [87] Nar, H.; Messerschmidt, A.; Huber, R.; Vandekamp, M.; Canters, G. W. Crystal-Structure Analysis of Oxidized *Pseudomonas aeruginosa* Azurin at pH 5.5 and pH 9.0 - a pH-Induced Conformational Transition Involves a Peptide-Bond Flip *J. Mol. Biol.* **1991**, *221*, 765-772.
- [88] Moser, C. C.; Page, C. C.; Dutton, P. L. *Photosynthesis: Bacterial Reaction Center*; Verlag GmbH: Weinheim, 2001; Vol. 3 24-38.

## *Appendix A*

### PROTEIN MUTATION AND PURIFICATION

The following appendix contains reproductions of the DNA sequences for H83Q/W48F/Y72F/Q107H/Y108W (Figure A-1) and Y72F/Y108F (Figure A-2) from the Chromas program (v. 1.61, Techneylisum Ltd.). It also contains the FPLC purification of labeled and unlabeled H83Q/W48F/Y72F/Q107H/Y108W (Figure A-3, A-4, A-5); labeled and unlabeled H83Q/W48F/Y72F/Q107H/Y108F/F110W (Figure A-6, A-7, A-8); and labeled and unlabeled Y72F/Y108F (Figure A-9, A-10, A-11).

The tables below show FPLC conditions for the three purifications of the labeled and unlabeled protein. For the Mono-S purifications, buffer A is 25 mM NaOAc, pH 4.5 and buffer B is 300 mM NaOAc, pH 4.5. For the IMAC column, buffer A is 750 mM NaCl, 20 mM NaPi pH 7.2, buffer B is 750 mM NH<sub>4</sub>Cl, 20 mM NaPi pH 7.2.

| <b>Time (minutes)</b> | <b>%Buffer A</b> | <b>%Buffer B</b> | <b>Flow Rate (ml/min)</b> |
|-----------------------|------------------|------------------|---------------------------|
| <b>0</b>              | 100              | 0                | 1.5                       |
| <b>15</b>             | 100              | 0                | 1.5                       |
| <b>20</b>             | 80               | 20               | 1.5                       |
| <b>40</b>             | 80               | 20               | 1.5                       |
| <b>45</b>             | 0                | 100              | 1.5                       |
| <b>60</b>             | 0                | 100              | 1.5                       |

**Table A-1:** FPLC purification of unlabeled protein on a Mono-S column (cation exchange column, Pharmacia)

| <b>Time (minutes)</b> | <b>%Buffer A</b> | <b>%Buffer B</b> | <b>Flow Rate (ml/min)</b> |
|-----------------------|------------------|------------------|---------------------------|
| <b>0</b>              | 100              | 0                | 3                         |
| <b>10</b>             | 100              | 0                | 3                         |
| <b>15</b>             | 0                | 100              | 2                         |

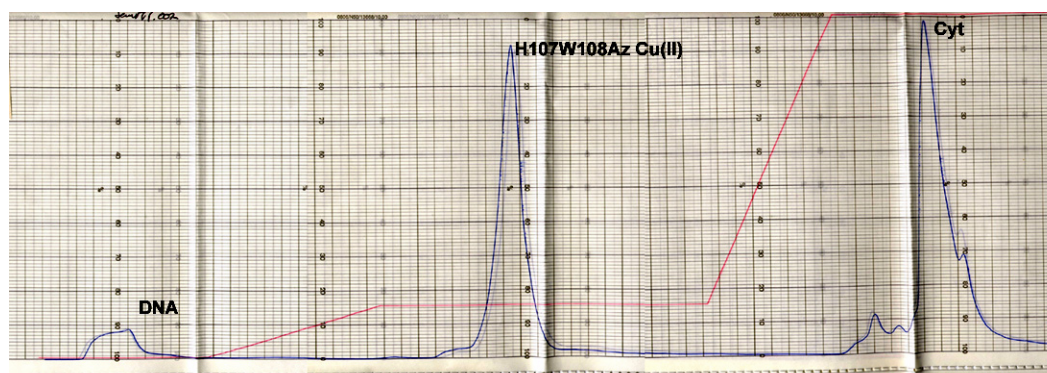
**Table A-2:** FPLC purification of labeled protein by IMAC column (metal affinity column, Pharmacia)

| <b>Time (minutes)</b> | <b>%Buffer A</b> | <b>%Buffer B</b> | <b>Flow Rate (ml/min)</b> |
|-----------------------|------------------|------------------|---------------------------|
| <b>0</b>              | 100              | 0                | 2                         |
| <b>20</b>             | 100              | 0                | 2                         |
| <b>40</b>             | 85               | 15               | 2                         |
| <b>75</b>             | 85               | 15               | 2                         |
| <b>90</b>             | 0                | 100              | 2                         |
| <b>130</b>            | 0                | 100              | 2                         |

**Table A-3:** FPLC purification of labeled protein on a Mono-S column (cation exchange column, Pharmacia)

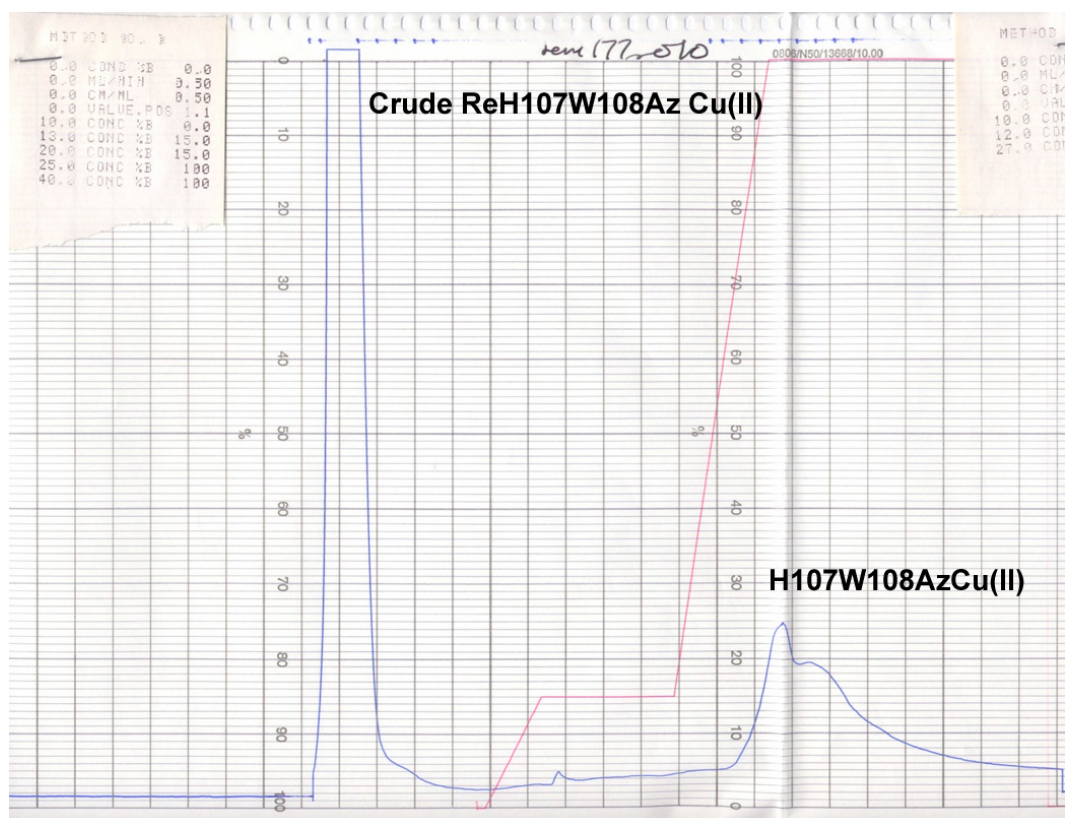
**Figure A-1:** Sequence data for H83Q/W48F/Y72F/Q107H/Y108W.

**Figure A-2: Sequence for Y72F/Y108F.**



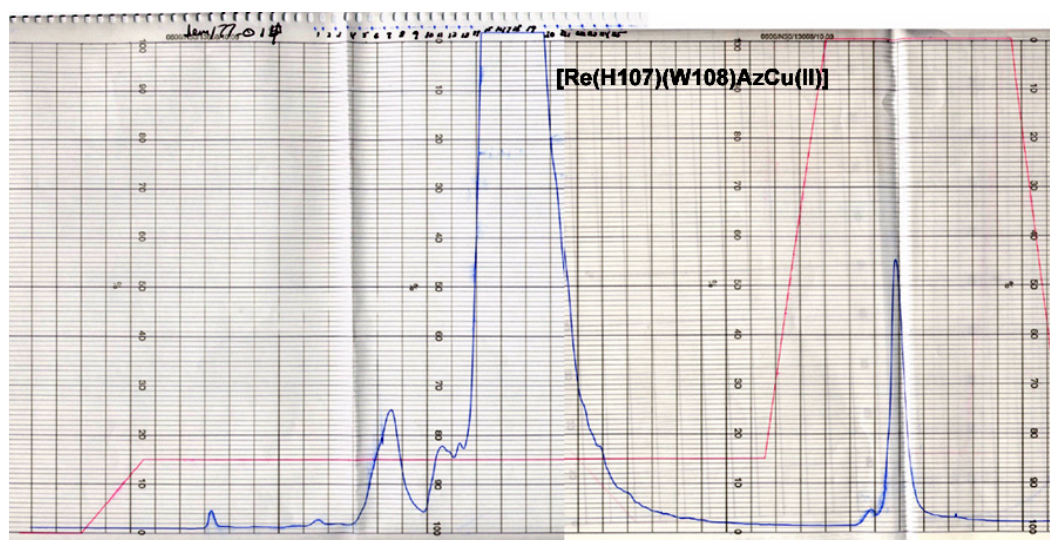
**Figure A-3:** FPLC purification of H83Q/W48F/Y72F/Q107H/Y108W AzCu(II), Mono-S, according to Table A-1 (Pharmacia).



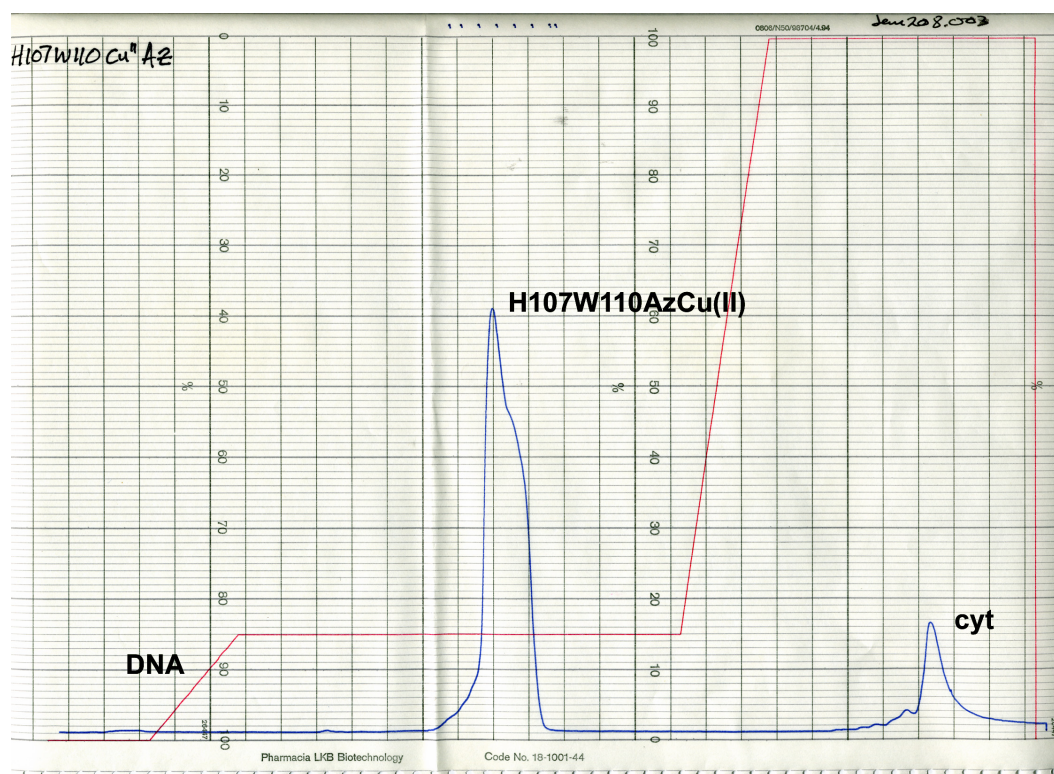


**Figure A-4:** FPLC purification of  $[\text{Re}(\text{H107})(\text{W108})\text{AzCu}(\text{II})]$ , IMAC according to Table A-2 (Pharmacia).

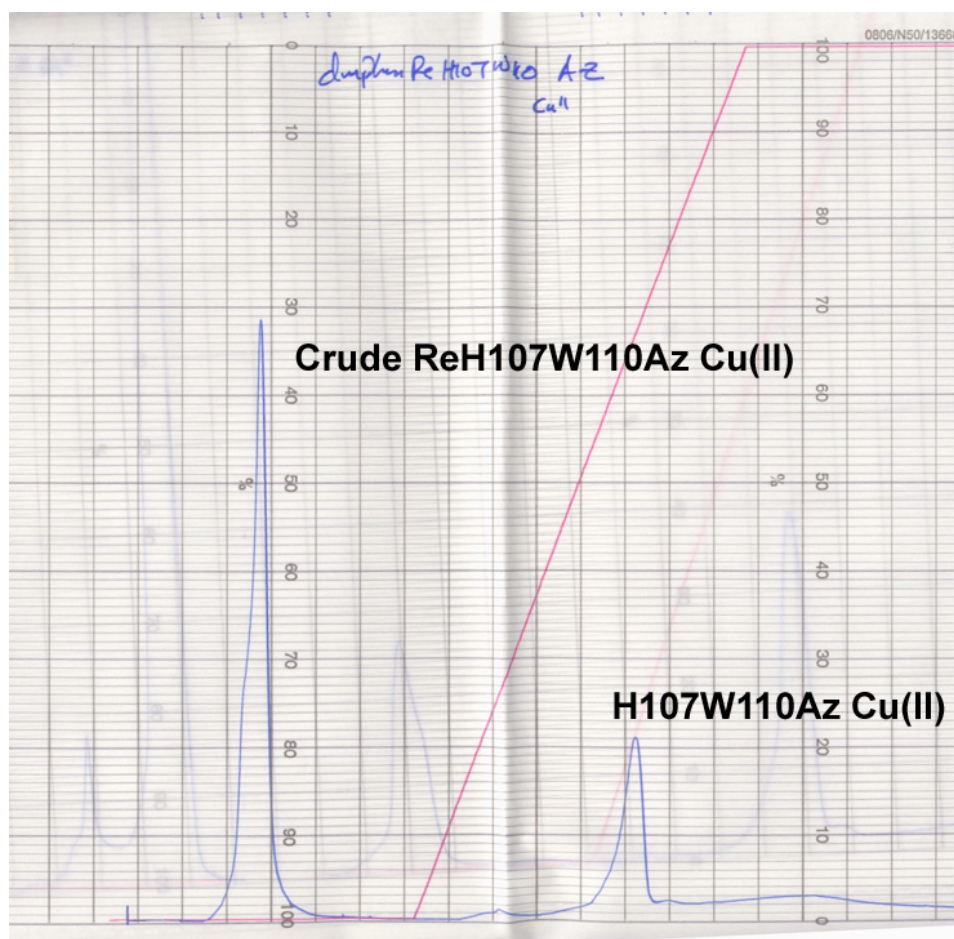




**Figure A-5:** FPLC purification of  $[Re(H107)(W108)AzCu(II)]$ , Mono-S, according to Table A-3 (Pharmacia).

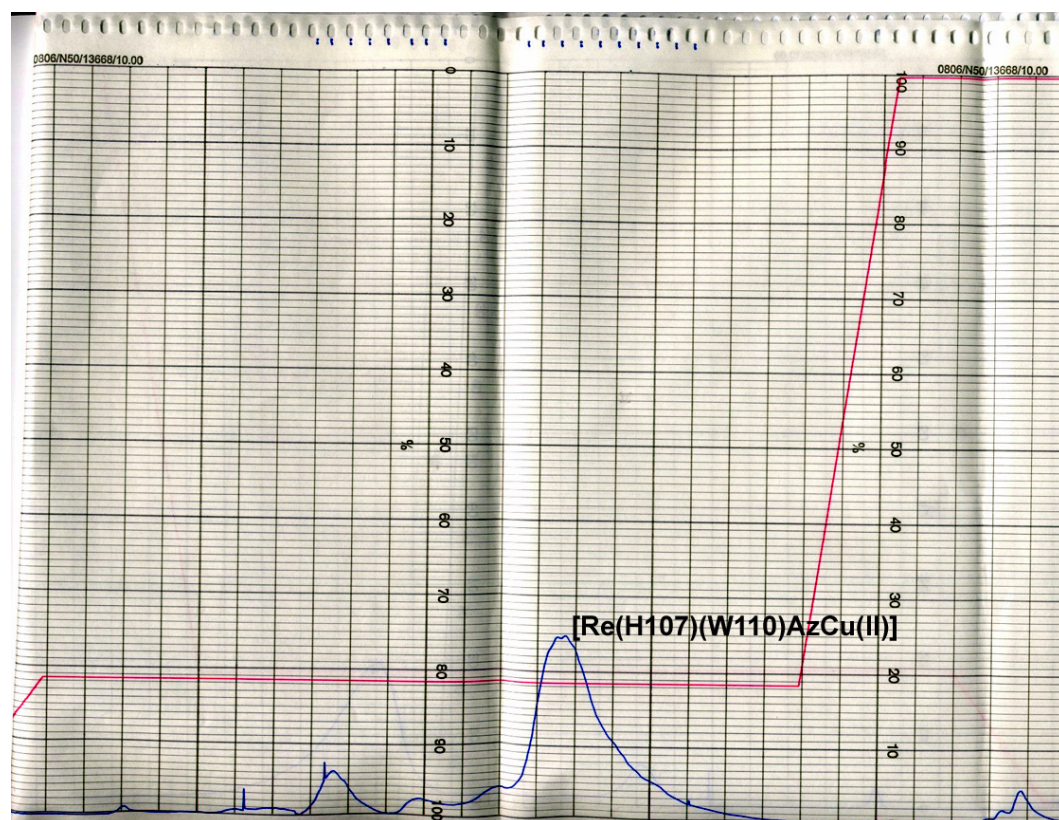


**Figure A-6:** FPLC purification of H83Q/W48F/Y72F/Q107H/Y108F/F110W AzCu(II), Mono-S, according to Table A-1 (Pharmacia).

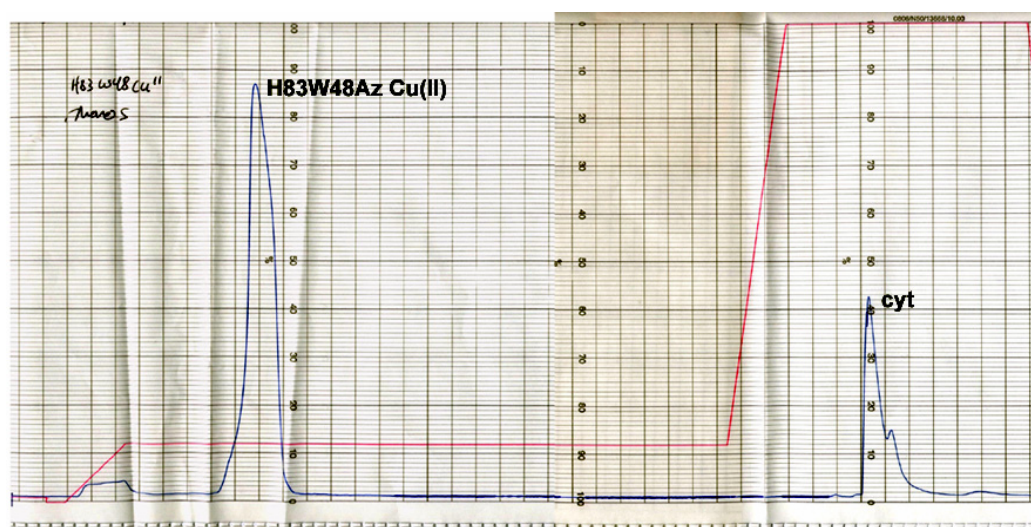


**Figure A-7:** FPLC purification of  $[\text{Re}(\text{H107})(\text{W110})\text{AzCu}(\text{II})]$ , IMAC, according to Table A-2 (Pharmacia).

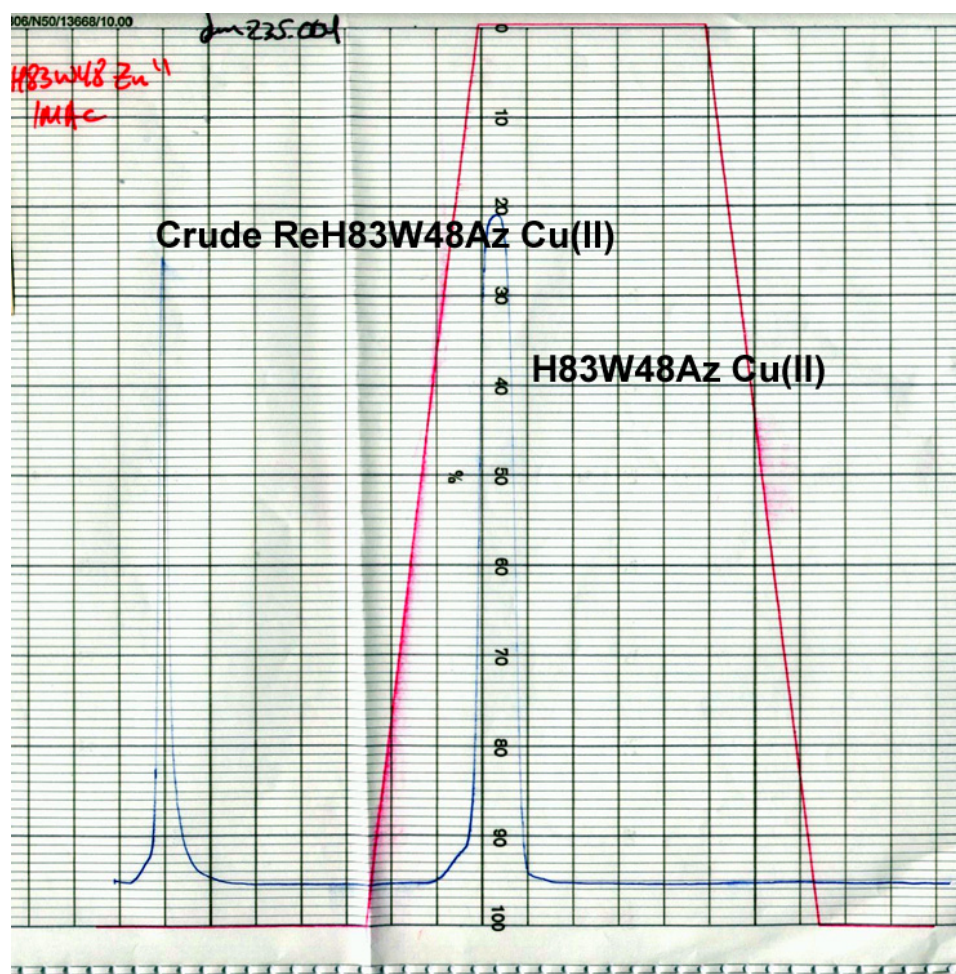




**Figure A-8:** FPLC purification of  $[\text{Re}(\text{H107})(\text{W110})\text{AzCu}(\text{II})]$ , Mono-S, according to Table A-3 (Pharmacia).

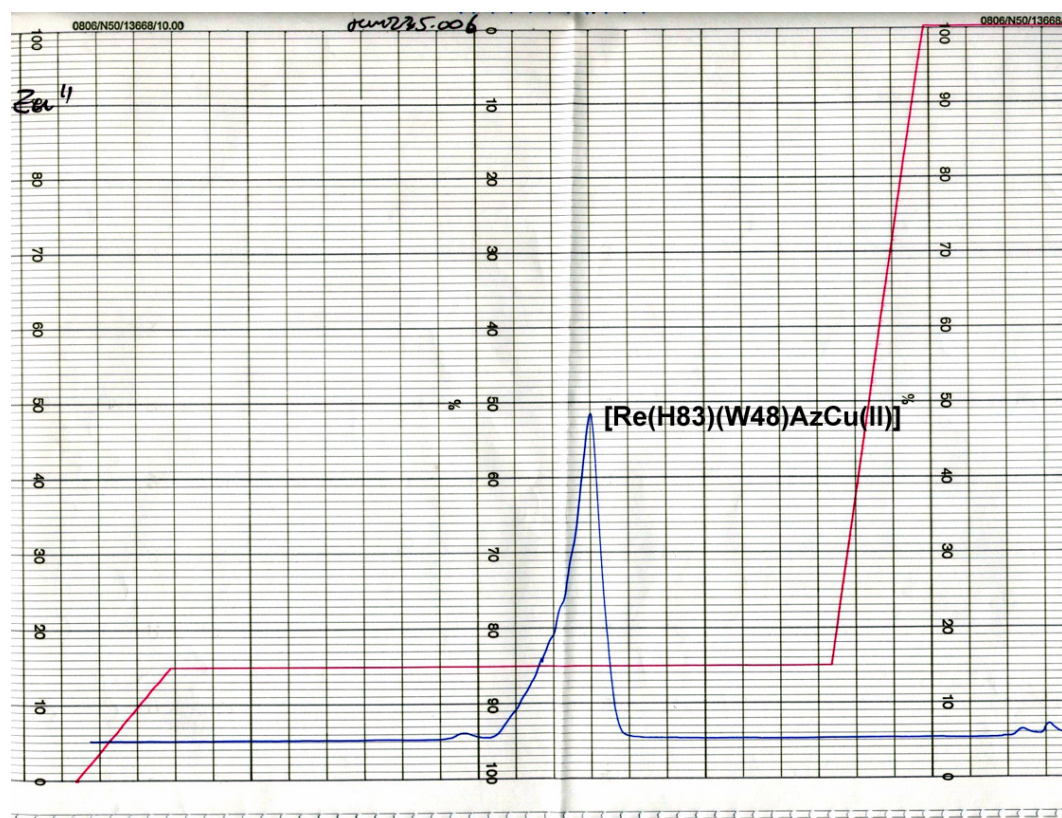


**Figure A-9:** FPLC purification of Y72F/Y108F Az Cu(II), Mono-S, according to Table A-1 (Pharmacia).



**Figure A-10:** FPLC purification of  $[\text{Re}(\text{H}83)(\text{W}48)\text{AzCu}(\text{II})]$ , IMAC, according to Table A-2 (Pharmacia).





**Figure A-11:** FPLC purification of [Re(H83)(W48)AzCu(II)], Mono-S, according to Table A-3 (Pharmacia).

### **III. Guanine Radical Formation and Electron Transfer in Metal-Modified DNA**



## *Chapter 8*

### **INTRODUCTION**

Charge transfer in DNA is a disputed process. There are many studies which show that long-range ET is possible [1-4], but only a few indications that this, in fact, is a physiologically important process: the binding of endonuclease BamHI to chromosomal DNA seems to play a part in restricting oxidative charge transport [5] and there are some intimations that long-range ET may be involved in DNA repair [6]. Recent work on the distance dependence of the rate of ET and the effect of driving force on the rate of ET suggest that in non-inverted systems, a single-step electron tunneling mechanism cannot account for observed long-range charge migration [7-10].

A number of models have been proposed to explain long-range ET through DNA. One model holds that the system may be viewed as an extended linear array of overlapping base pair  $\pi$  orbitals [1]. If the observed long-range electron transfer through DNA is in fact due to significant  $\pi$  system overlap of the intervening bases with the donor and acceptor,  $\beta$  (see Chapter 1) will be far less than  $1 \text{ \AA}^{-1}$ . That is, if the donor, acceptor and bridge are all well coupled electronically, charge migration up and down the strand will be relatively efficient and suffer little decrease in rate as a function of distance. This implies that long-range charge transport by single-step electron tunneling is possible. Another model holds that the electronic structure of DNA is much more like proteins, that is, it is essentially

electronically coupled through a  $\sigma$  bonding framework [11]. With this situation,  $\beta$  ought to be much nearer to  $1 \text{ \AA}^{-1}$ , resulting in a steep distance dependence of the rate of electron transfer. Therefore, charge migration over significant distances by single-step electron tunneling should not happen (e.g., assuming  $\Delta G^0 \sim \lambda$ , no ET over distances greater than  $\sim 14 \text{ \AA}$ ). These extremes have each encountered some problems: The model postulating that DNA is “protein like” is faced with some apparently contradictory evidence that charge migration will in fact occur over long distances easily [1, 12, 13]; while the “pi-way” model is weakened by the fact that single-step ET in DNA has been shown to occur with a  $\beta \sim 1 \text{ \AA}^{-1}$  [10].

To explain these somewhat inconsistent results, a third model has been proposed [14-17]. If the observed charge transport is due to a multi-step electron tunneling mechanism, wherein the charge migrates via the  $\sigma$  bond network for short distances; long distance charge transport could be achieved without significant  $\pi$  system overlap. The hopping mechanism can be explained as follows. The donor and first acceptor (Gu for example) are separated by a short distance (the intervening bases constitute the energetically distant bridge states) over which the charge migrates by tunneling. The next acceptor is a short distance from the first and the process is repeated. In this way, the charge moves along the DNA, from station to station as it were.  $\beta$  for the individual steps will still be on the order of  $1 \text{ \AA}^{-1}$ , but over the entire segment the process may show little dependence on distance. Such a model is supported by much of the current research in the field of electron transfer through DNA.

The theory that long-range ET is mediated by radical formation is a logical one: DNA is prone to radical formation under a variety of light induced conditions. Irradiation of a range of metal complexes, from ruthenium to vanadium will lead to oxidation of the nucleobase by the production of singlet oxygen; as will irradiation of small molecule organic compounds such as anthraquinones and azides [18]. In addition to the photo-oxidations involving cofactors, DNA is directly damaged by UV B and UV C radiation (240 nm-320 nm) [19]. The mechanism for one type of resulting damage, the pyrimidine <6-4> pyrimidone lesion, is believed to involve the transient generation of a di-radical intermediate [20, 21].

Using Gu oxidation to study charge transport in DNA is currently an active area of research. Some of the most recent highlights are discussed below. A one-electron “hole” at the sugar base can be created by the use of a photo-active pivaloyl moiety on the sugar backbone.<sup>1</sup> From careful HPLC analysis of the products of such radical chemistry, the researchers were able to back calculate relative rates of electron transfer through DNA (e.g., rates over 4 base pairs relative to rates over 5 base pairs). By making some assumptions about these rates relative to the addition of water to the radical (e.g., sequence does not influence the rate of addition) they estimated absolute rates. In addition to rates of sugar “hole” quenching by Gu, these studies revealed some information about “hole” hopping between Gu and the more easily oxidized GGG sequences. By placing GGG regions after the mono Gu region closest to the radical and watching product formation, they were able to formulate the distance dependence of the rate of positive charge

---

<sup>1</sup> This fragment can be cleaved photochemically to produce, among other things, a radical at the sugar [12, 13].

migration through DNA. From these experiments it was concluded that long-range charge transport through DNA is most likely a hopping process [14]. Further, analysis of this data suggested that the  $\beta$  value for sugar radical quenching by Gu was  $1.0 \text{ \AA}^{-1}$ . For the Gu to Gu ET process  $\beta$  was found to be  $0.7 \text{ \AA}^{-1}$ .

Another area of research in charge transport phenomena in DNA is the examination of DNA hairpins containing a stilbene dicarboxamide moiety at the turn of the hairpin [22, 23]. From a crystal structure of a representative duplex the stilbene linker is  $3.4 \text{ \AA}$  from the closest base pair [7]. The crystal structure also shows the  $\pi$  system of the stilbene linker to be well aligned with the  $\pi$  stack of the DNA hairpin. By the use of a pulsed laser source, short time scale (ps) observation of the decay of the stilbene excited state can be observed. By careful choice of the sequence of the synthetic DNA, Lewis and co-workers were able to investigate the dynamics of charge transfer from Gu, GG and GGG to the stilbene; as well as the dynamics of the charge movement between them, showing a  $\beta = 0.7 \text{ \AA}^{-1}$ .

Also working on the ultra-fast time scale (fs to ps), researchers examining a system consisting of non-natural guanine analogs along with guanine and adenine in 13 unit strands of DNA [10] support the notion that there is no efficient long-range ET in DNA in a single-step. Changes in the excited state decay of aminopurine attributable to charge transfer to G were monitored by ultra-fast emission spectroscopy. By comparing many strands with varying placement of G's, they determined that no superexchange occurred greater than  $14 \text{ \AA}$ , suggesting that single-step ET in DNA proceeds with a  $\beta \sim 1 \text{ \AA}^{-1}$ .

With this background in mind, investigations of the nature of ET in DNA by means of site-specific covalent attachment of donor-acceptor complexes to DNA bases were

begun [11]. There are some important requirements to be considered when attempting to construct a donor and acceptor system to study charge transport phenomena in DNA. First, the donor and acceptor must not interfere with the higher order structure of the DNA. The goal is to discover how natural DNA might be involved in ET events, so a system that closely resembles the natural structure of DNA is desirable. Second, the donor and acceptor must be incorporated into the DNA at well defined sites, particularly for investigating the distance dependence of the rate of electron transfer. Unless the exact locations of the donor and acceptor complexes are known, the data abstracted from the experiments will be approximate at best. Furthermore, the donor and acceptor must also be spectroscopically distinct; that is, the electronic transitions of the donor and acceptor must not be energetically similar. Without distinct donor and acceptor moieties, analysis of the reactants and products of the electron transfer reaction is extremely difficult. Ensuring the electronic isolation of the donor and acceptor also excludes other processes that can compete with electron transfer, including energy transfer, intermolecular quenching and the decay of the donor and acceptor excited state.

Ultimately, it is desirable to examine systems that exhibit both multi-step ET mechanisms and single-step ET mechanisms. To achieve this goal, it is necessary to first establish the relevant redox potentials of the acceptor (in this case a metal complex) and the possible intermediate donor (in this case, a guanine base). Then, one must construct a separate donor, a complex which should be easily oxidized by the acceptor. By using both acceptors which can oxidize guanine and acceptors which cannot oxidize guanine, systems that can be used to distinguish between multi-step and single-step mechanisms can be

constructed. In either case, the ultimate donor needs to meet the criteria discussed above: no spectral overlap with either the initial or intermediate acceptors and a well characterized redox potential. Many forays into this arena have been made [1-4, 10, 24-28], some of which have been successful. Early strategies employing non-covalently bound donors and acceptors [1] suggested long-range transport was occurring with an extremely small distance dependence ( $\beta \sim 0.1 \text{ \AA}^{-1}$ ). Following up on these studies, covalently bound intercalating and non-intercalating analogs were prepared [25-28]. When the DNA investigated in these experiments has included guanine as part of the bridge with an acceptor capable of directly or indirectly oxidizing the base, the small value of  $\beta$  has been confirmed; when the strands have not met these criteria, the distance dependence has been much closer to the value commonly found for proteins.

In order to meet these requirements, the following course of action has been pursued. First, by using metal-labeled thymine residues, DNA duplexes with unambiguous donor and/or acceptor incorporation can be synthesized. Second, one can exploit the relatively low oxidation potential of guanine moieties (Gu) ( $\sim 1.3 \text{ V}$  vs NHE [29, 30]) and the capacity to vary the location of these bases in strands of synthetic DNA; to design a system studying both single-step and multi-step ET. This system was to be investigated optically; therefore, we constructed an oxidizing complex with no spectral overlap with the Gu radical spectrum ( $\lambda=310 \text{ nm}$  ( $\epsilon=6800$ ),  $\lambda=390 \text{ nm}$  ( $\epsilon=2700$ ),  $\lambda=520 \text{ nm}$  ( $\epsilon=1500$ ) [31]).

The scientific community appears to be approaching an agreement on the nature of charge transport through DNA [32]. This agreement has yet to be fine tuned, and in order

to finalize it more data is needed. My work on synthetic radical formation and charge transfer in DNA will in some small way help to settle the question

## *Chapter 9*

# **SYNTHESIS AND CHARACTERIZATION OF METAL-MODIFIED THYMINE COMPLEXES AND METAL-MODIFIED DNA**

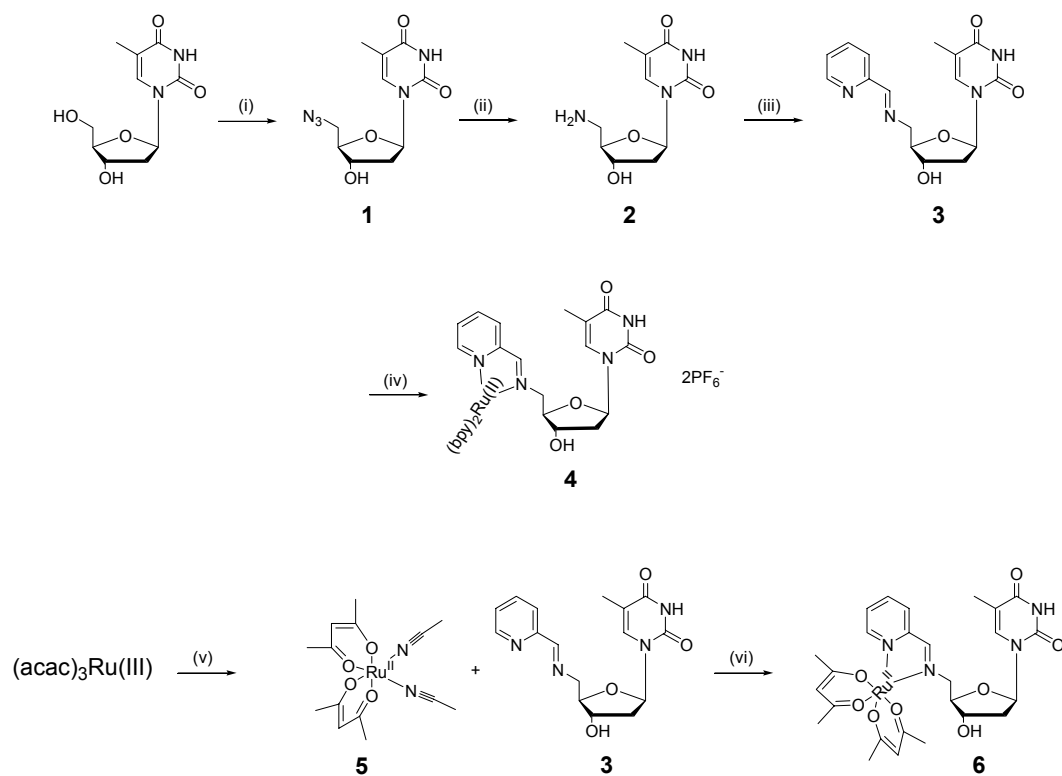
### **9.1. *Metal-Modified Thymine Complexes***

In order to construct a system with site specific metal complex incorporation, a scheme was pursued that would allow for solid phase inclusion of the complex into DNA. Using tris-(2,2'-bipyridine) ruthenium as a model; a synthetic route was developed involving the synthesis of a diimine ligand attached to the sugar of thymine ( $T_{\text{impy}}$ , Scheme 9.1-1) [25]. Building on this same motif, one more donor (**8**) and two more acceptor (**9,10**) complexes were synthesized (Scheme 9.1-2 ). As suggested in Chapter 8, one of the goals of this project was to generate intervening radicals that might act as charge carriers for the electron transfer event; the two high potential thymine complexes (**9,10**) are perfect candidates to oxidize Gu (Table 9.1-1). The Rhenium complex **9** crystallized readily from vapor diffusion of heptanes into acetone (Figure 9.1-1).<sup>2</sup>

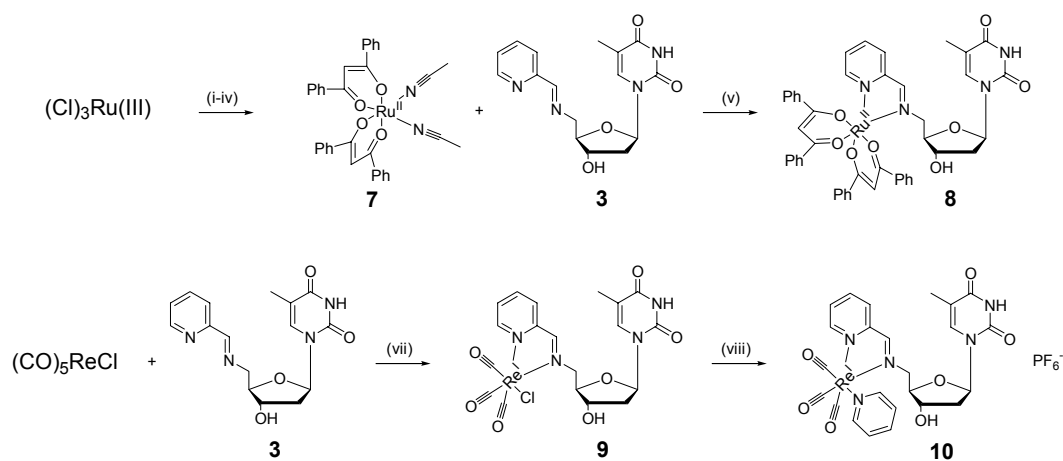
---

<sup>2</sup> The heptanes lead to some disorder in the crystal structure due to the many possible isomers.





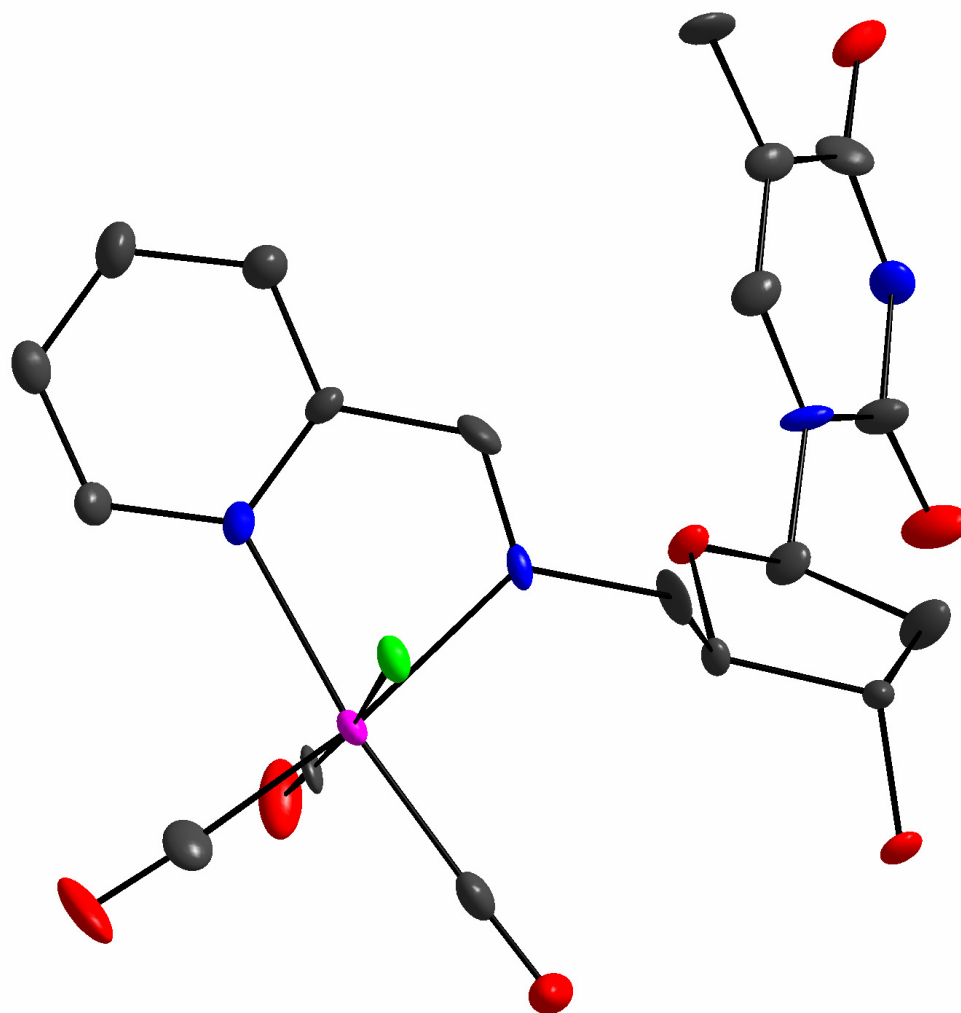
**Scheme 9.1-1:** Synthesis of acceptor and donor ruthenium complexes. (i)  $\text{PPh}_3$ ,  $\text{CBr}_4$ ,  $\text{NaN}_3$ , DMF, reflux; (ii)  $\text{H}_2$ , Pd/C, EtOH; (iii) 2-pyridine carboxaldehyde, mol sieves, EtOH; (iv)  $(\text{bpy})_2\text{RuII}(\text{Cl})_2$ , EtOH, reflux; (v)  $\text{ZnHg}$ ,  $\text{H}_2\text{O}$ ,  $\text{CH}_3\text{CN}$ , reflux; (vi) EtOH, reflux [25].



**Scheme 9.1-2:** Synthesis of a new ruthenium donor and new rhenium acceptors. (i)  $\text{H}_2\text{O}$ , EtOH, reflux; (ii)  $\text{NaHCO}_3$ ; (iii) dibenzoylmethane, reflux; (iv)  $\text{ZnHg}$ ,  $\text{H}_2\text{O}$ ,  $\text{CH}_3\text{CN}$ , reflux; (v) **3**, EtOH, reflux; (vii) EtOH, reflux; (viii)  $\text{AgPF}_6$ , THF, pyridine, room temperature.

| Complex | <sup>1</sup> H-NMR<br>(CD <sub>3</sub> Cl) | UV/Vis<br>(CH <sub>3</sub> OH)  | E <sub>1/2</sub> <sup>0</sup><br>(0.1 TBAH,<br>CH <sub>3</sub> CN) | E <sub>1/2</sub> <sup>0</sup><br>(0.8 M NaCl,<br>0.05 NaPi,<br>pH 7.0) | λ <sub>em</sub> | τ   |
|---------|--|---|--|--|-----------------|-----|
|         | vs. TMS                                    | λ <sub>max</sub> nm (ε)   | V<br>(vs. NHE)   | V<br>(vs. NHE)   | nm              | ns  |
| 4       | δ 5.65 t<br>(J=7Hz, 1H)                    | 210 (42,000)<br>246 (25,000)<br>288 (49,000)<br>486 (7,500)               | 1.61   | 1.41   | 720             | 53  |
| 6       | δ 6.15 t<br>(J=7Hz, 1H)                    | 208(27,000) <sup>a</sup><br>264 (25,000)<br>402 (4,600)<br>586 (4,600)    | 0.350  | 0.278  | n/a             | n/a |
| 8       | δ 6.27 t<br>(J=7Hz, 1H)                    | 256 (23,400) <sup>b</sup><br>316 (20,100)<br>474 (4,400)<br>598 (5,200)   | 0.327  | 0.252  | n/a             | n/a |
| 9       | δ 6.23 t<br>(J=7Hz, 1H)                    | 202 (26,000)<br>266 (17,600)<br>388 (3,400)<br>400 (3,100)<br>420 (2,100) | 1.67   | n/a  | 770             | ~6  |
| 10      | δ 6.01 t<br>(J=7Hz, 1H)                    | 202 (56,500)<br>266 (25,000)<br>388 (3,900)<br>400 (3,500)<br>420 (2,200) | n/a  | n/a  | 705             | 13  |

**Table 9.1-1:** Selected physical data for metal-labeled thymine complexes. Reported <sup>1</sup>H-NMR shifts are the 1'H on the ribose, an apparent triplet. a: in ethanol b: in methylene chloride.

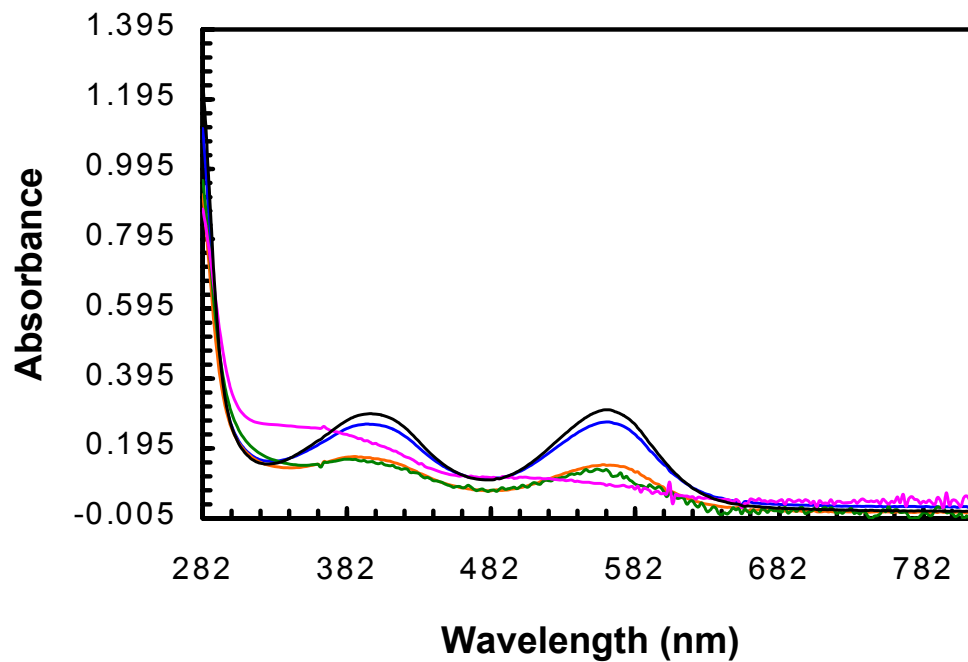


**Figure 9.1-1:** Crystal structure of compound **9**. Monoclinic crystal system, space group  $C 12 1$ , unit cell dimensions:  $a = 18.9576(10) \text{ \AA}$ ;  $b = 9.5095(5) \text{ \AA}$ ;  $c = 12.4516(8) \text{ \AA}$ ;  $\beta = 100.5^\circ$ . Ellipsoids drawn at 50% probability. (●) carbon, (●) nitrogen, (●) oxygen, (●) chlorine, (●) rhenium. Structure solved and refined by L. Henling and M. Day at the Beckman Institute X-ray Crystallography Facility.

This library of model compounds (Table 9.1-1) makes it possible to examine a variety of ET scenarios. First, by using electron acceptor complexes (e.g., **4**) at or below the oxidation potential of guanine, single-step electron transfer through a DNA bridge may be examined. The two donors **6** and **8** are similar in potential, so a system with a donor acceptor pair of any of the combinations of **4**, **6**, **8** will give an estimated driving force of  $-\Delta G^\circ \sim 1.1$  eV vs. NHE. This suggests that the rate of ET will be slightly in the inverted region, assuming that the measured reorganization energy of DNA with intercalators ( $\lambda \sim 0.66$  eV [2]) is approximately applicable to this system.

Second, the acceptors **4**, **9** and **10** all are potentially capable of oxidizing intermediate Gu residues in the DNA strand. Thus, systems may be designed which study either (i) single-step electron transfer from Gu in the strand or (ii) exploit a multi-step mechanism wherein the electron is abstracted first from guanine and then from one of the electron donor complexes **6** or **8**. Case (i) is particularly tantalizing since the distance between donor and acceptor can be strictly controlled.

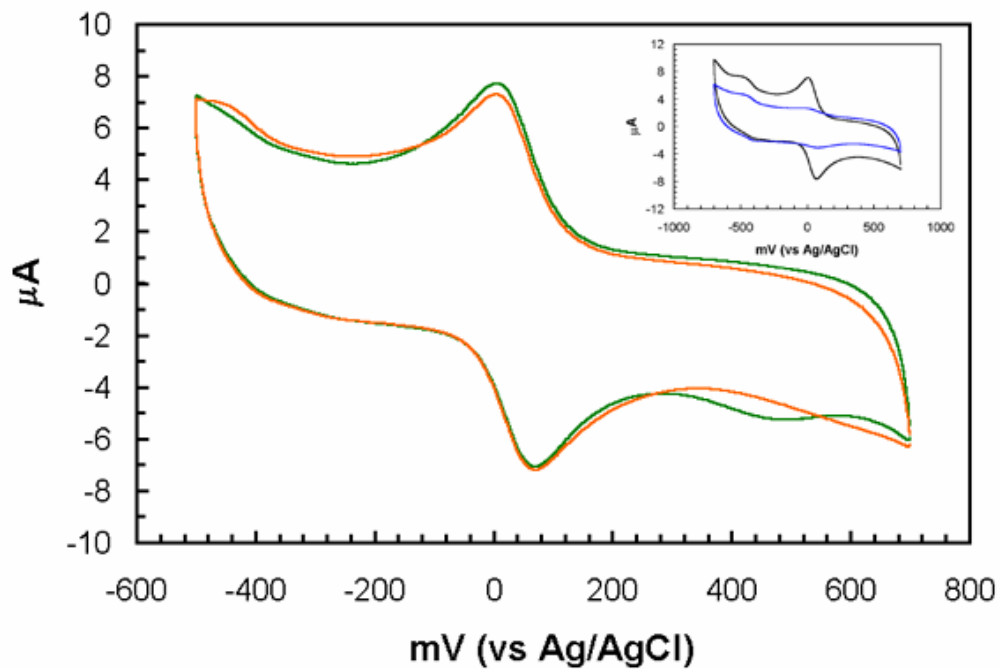
The donor **6** has some less than desirable properties. Most disturbing, the complex undergoes an irreversible reaction with water. To investigate this problem two different approaches were employed. First, the UV/Vis spectrum of **6** in water was monitored over time. For the absorption experiments, the MLCT absorption at 400 nm and 562 nm show substantial decrease over even 1 hr, 40 min. At extremely long times (53 days) the absorption spectra is totally different, showing a maximum at  $\sim 360$  nm and no discernable absorption at 560 nm (Figure 9.1-2). Mass spectra taken at 100 min and 43 hrs 23



**Figure 9.1-2:** Absorption spectra of 45  $\mu\text{M}$  **6** in 95:5 800 mM NaCl 50 mM NaPi pH 7.0 : MeOH. (—) 30 s (—) 1 hr 40 min (—) 43 hr 23 min (—) 70 hr 45 min (—) 53 days

min showed no change from the initial mass spectrum ( $[M+H]^+ = 630$ ). However, a mass spectrum at 53 days showed a new species at  $m/z = 647$ . Earlier experiments that attempted to oxidize **6** by iodine followed by treatment with ammonium hydroxide gave similar results. Regardless of the oxidation state it is clear from this experiment that given enough time some decomposition of **6** will result.

Second, **6** was monitored electrochemically over time in a water buffer (800 mM NaCl, 50 mM NaPi, pH 7.0). Cyclic voltammetry of these solutions showed significant decomposition of the metal-labeled nucleoside. Using a 1 mM solution of **6** in buffer (800 mM NaCl, 50 mM NaPi, pH 7.0), potentials for the Ru(II)/Ru(III) couple were obtained at varying times (Figure 9.1.3). These voltammograms, when compared with the methylene chloride case show a second wave apparent even at 9 min. This reduction wave disappears over time as a new oxidation wave appears (around 62 min). The technique was somewhat limited by the available potential window (0.700 V to either  $-0.500$  V or  $-0.700$  V). A separate voltammogram of the solution used for the UV/Vis experiments above (a 60  $\mu$ M solution of **6** in 95:5 buffer: MeOH) at 66 days after mixing shows a small amount of the original compound with a significant new wave (Figure 9.1-3, inset). These experiments once again do not necessarily suggest an oxidation, but certainly something changes when the complex is added to water. Given the available evidence, it is likely that the decomposition observed is due to addition of water to the complex in some way. In particular, hydrolysis of the imine bond of  $T_{\text{impy}}$  could cause the observed loss of MLCT as well as account for the 17  $m/z$  increase in the ESI-MS data.

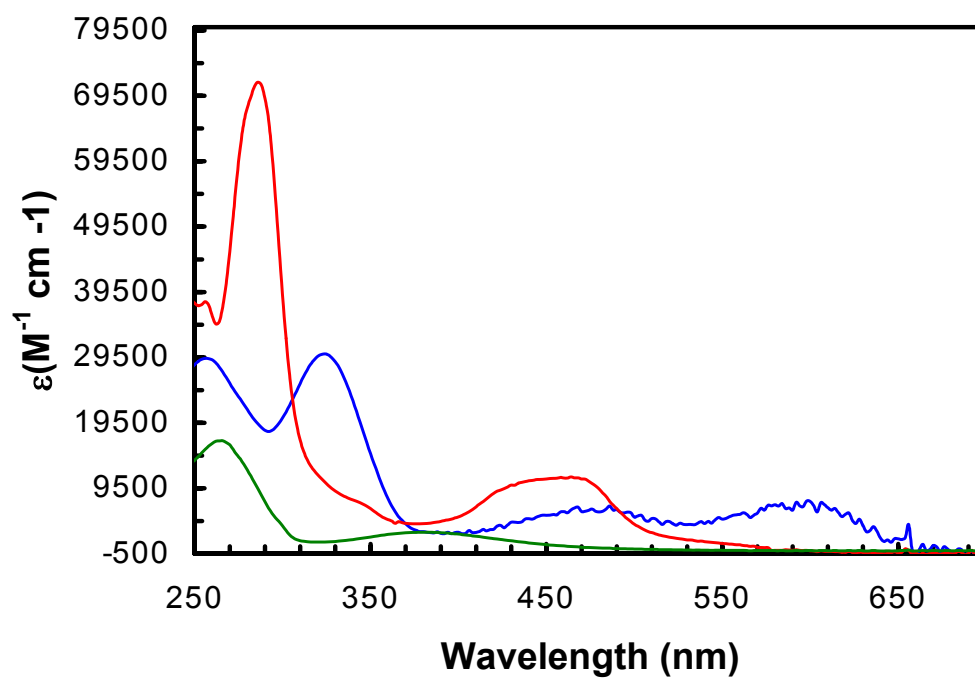


**Figure 9.1-3:** CV data for 1.5 mM **6** in 800 mM NaCl 50 mM NaPi pH 7.0 buffer. (—) 9 min after mixing (—) 62 min after mixing. Inset: (—) 105 min after mixing (—) 66 days after mixing.



The obvious alternative to **6** is **8**; this compound has an oxidation potential that is only 26 mV less positive than **6** (Table 9.1-1). To ensure that **8** would not be susceptible to the same sort of reaction with water, it was carefully evaluated for its behavior in water. UV/Vis monitoring proved ineffective for **8** because of solubility problems. By observing a 60  $\mu$ M solution of **8** in 95:5 H<sub>2</sub>O: MeOH over a period of 100 min (taking a spectrum every minute) it was apparent that some change was taking place. All regions of the spectra showed a significant decrease in absorption intensity. Upon examination of the cuvette it was clear that some material had precipitated from solution. Mass spectrum and <sup>1</sup>H-NMR of the suspension confirmed that **8** remained unaltered. Therefore it was concluded that **8** is poorly soluble in water, but is not hydrolyzed by water.

In addition to its poor solubility in water, another issue raised by **8** is the problem of band overlap. Unfortunately, addition of the conjugated system to the acetylacetonate ligands lead to a large shift of the more blue MLCT (402 nm for **6** to 474 nm for **8**). This caused some overlap between the acetylacetonate MLCT of **8** and the MLCT of **4**. This issue does not arise if the intended donor acceptor pair are **8** and **9** or **10**. The rhenium-modified nucleosides still show some overlap with **8** but not to the extent of **4** (Figure 9.1-4).



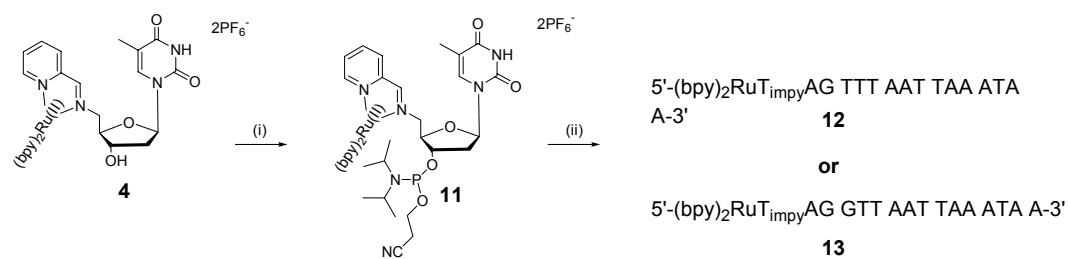
**Figure 9.1-4:** Absorption spectra of (—) 4, (—) 8, (—) 9.

## 9.2. Metal-Modified DNA

Compound **4** exhibits a Ru(II)/Ru(III) redox couple that is just strong enough (1.41 V vs. NHE in buffer, Table 9.1-1) to oxidize guanine [29] alone in solution. Given the fact that the predicted oxidation potential of G is lower in DNA [30], it seemed possible that complex **4** would, in fact, produce G radicals under appropriate conditions. In addition, the spectroscopic handles for G radicals [31] do not overlap with the metal to ligand charge transfer (MLCT) band of **4**. With these auspicious omens, two different strands of DNA were synthesized (Scheme 9.2-1).

**12** and **13** were purified by HPLC to give small amounts of the DNA single-strands. Mass spectra acquired by MALDI-TOF were within 0.5 mass units of the calculated  $m/z$  ratios. The complements to **12** and **13** (**14** and **15** respectively) as well as the non-metalated analogs of **12** and **13** (**16** and **17**) were synthesized and purified by the Biopolymer Synthesis and Analysis Resource Center (Figure 9.2-1). Mass spectra of these strands (**14-17**) showed only signals for the correct  $m/z$  ratio; therefore, the strands were used without further purification.

In order to verify that the metal complex had not been modified by the DNA synthesizer, strands **12** and **13** were subjected to enzymatic digestion. Two enzymes were employed. Phosphodiesterase (rattle snake venom) an exonuclease that cleaves 3'-5' internucleotide phosphate bonds, leaving 5' monophosphate nucleotides; and alkaline phosphatase (calf intestinal mucosa) which effects the hydrolysis of 5' monophosphate nucleotides. By using these enzymes individual nucleosides are regenerated. These



**Scheme 9.2-1:** Synthesis of single-stranded DNA incorporating complex **4**. (i) [(i-pr)<sub>2</sub>N]<sub>2</sub>P(OCH<sub>2</sub>CH<sub>2</sub>CN), 1-H tetrazole, CH<sub>3</sub>CN (ii) DNA synthesizer X.

5'-TTA TTT AAT TAA ACT A-3'  
**14**

5'-TTA TTT AAT TAA CCT A-3'  
**15**

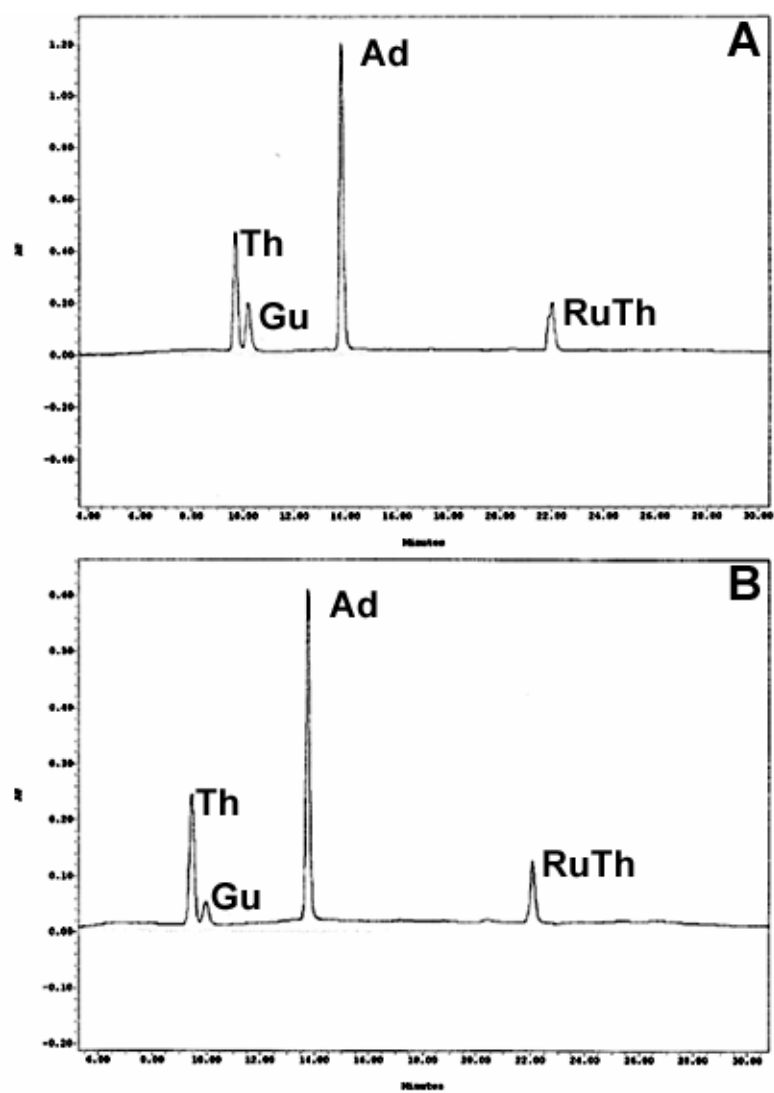
5'-TAG TTT AAT TAA ATA A-3'  
**16**

5'-TAG GTT AAT TAA ATA A-3'  
**17**

**Figure 9.2-1:** Non-metallated DNA strands.

enzymes were incubated with strands of **12** and **13** separately. The enzymes were then filtered away and the supernatant subjected to HPLC analysis. Comparison of a standard solution (containing thymine (Th), guanosine (Gu), adenosine (Ad), and **4**) with the digestion showed only the expected ratio of bases and complex **4** (Figure 9.2-2).

The synthesized strands of DNA were annealed to form duplex DNA fragments. In general, DNA forms three kinds of helical structures: A-form, B-form and Z-form [33]. The distinguishing characteristics of these structures are handedness of the turn and the properties of the resulting major and minor grooves in the helix. B-form DNA is the naturally occurring structure with a right hand turn incorporating  $\sim 10$  base pairs per turn with a wide, deep major groove and narrow, deep minor groove. A-form is also right handed, but the turn is somewhat less tight, incorporating  $\sim 11$  base pairs per turn, with a narrow, deep major groove and a wide, shallow minor groove. Z-form DNA is left handed with 12 base pairs per turn, no major groove and a narrow and deep minor groove. Not surprisingly, these differences result in substantially different macroscopic behavior of DNA. Investigating electron transfer processes in DNA strands that are as close as possible to the natural form (B-form) requires checking the structure of the duplexes. The first method employed was monitoring the absorbance at 260 nm as a function of temperature. The point at which the first derivative of the slope is zero is referred to as the melting temperature. For the metallated duplex **12/14** the melting temperature was found to be  $47.8 \pm 0.4$  °C. The corresponding un-metallated duplex **16/14** gave a melting temperature of  $47.7 \pm 0.7$  °C, suggesting very little difference between the two. The metallated duplex **13/15** had an inflection point at  $51.3 \pm 0.5$  °C, while **17/15** had a

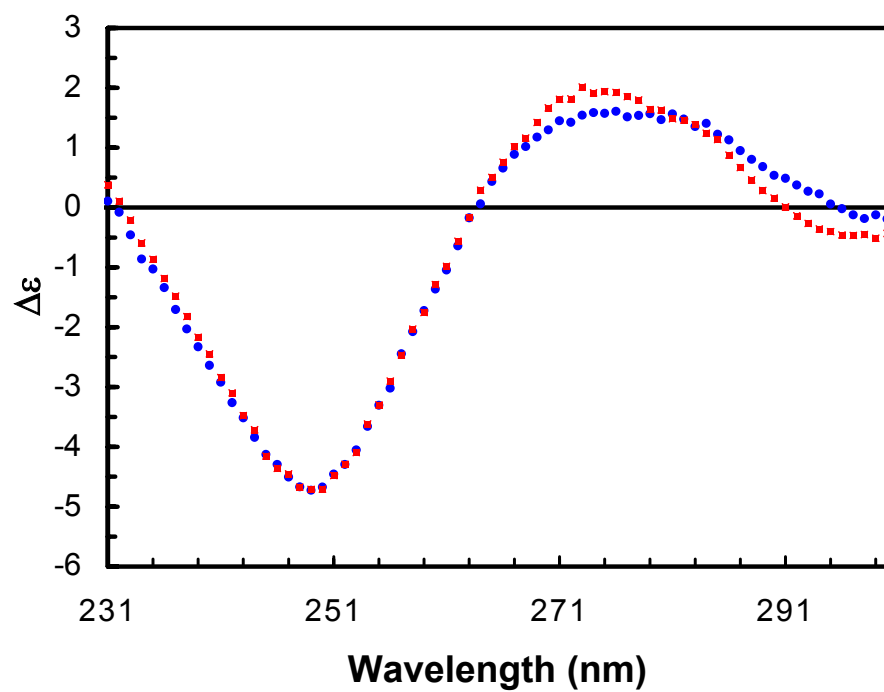


**Figure 9.2-2:** Enzyme digestion HPLC traces of (A) 4 nmol **13** (RuTh = Ru(II)(bpy)<sub>2</sub>(T<sub>imp</sub>)) and (B) 3 nmol **12** (RuTh = Ru(II)(bpy)<sub>2</sub>(T<sub>imp</sub>)). Retention time and intensity of these peaks correspond exactly to the standard composed of unmodified DNA bases and Ru(II)(bpy)<sub>2</sub>(T<sub>imp</sub>).

melting temperature of  $49.7 \pm 0.5$  °C, also suggesting very little difference between the two. However, it should be noted that a melting temperature only reveals that the absorbance at 260 nm starts at one point, increases with temperature to a certain value and levels out. The assumption is that the absorbance of a base is quenched when there is significant hydrogen bonding with its complement; therefore, when the absorbance is at a minimum the duplex is tightly bound and when it is a maximum the duplex is split apart [34]. Therefore this method does not ensure that the duplex is well formed.

Given the ambiguity in the melting temperature structure analysis, further investigations of the structure of the synthesized duplexes were undertaken. Another technique often used to understand tertiary structure in DNA is circular dichroism (CD) [35-39]. CD makes use of the fact that chiral molecules absorb one kind of circularly polarized light better than another to generate an absorption spectrum related to that chirality. A method for distinguishing A-form DNA from B-form DNA by comparing the positive lobe area to the negative lobe area has been developed [35]. Spectra with an approximate positive/negative ratio of 0.2 to 0.6 can be considered B-form. A ratio of approximately 2.1 to 5.7 suggests A-form. A ratio between 0.6 and 2.1 indicates a structure that is neither the canonical B-form nor the canonical A-form but some mixture of the two. Duplex **13/15** produced a typical spectrum of B-form DNA with a positive/negative ratio of 0.37. Comparison of **17/15** with **13/15** shows very little perturbation of structure due to the metal complex (Figure 9.2-3). On the other hand, **12/14** gave a spectrum that was much more consistent with DNA that has both B-form sections and Z-form sections [38]. The trough at 294 nm is diagnostic for Z-form DNA, while the rest of the spectrum

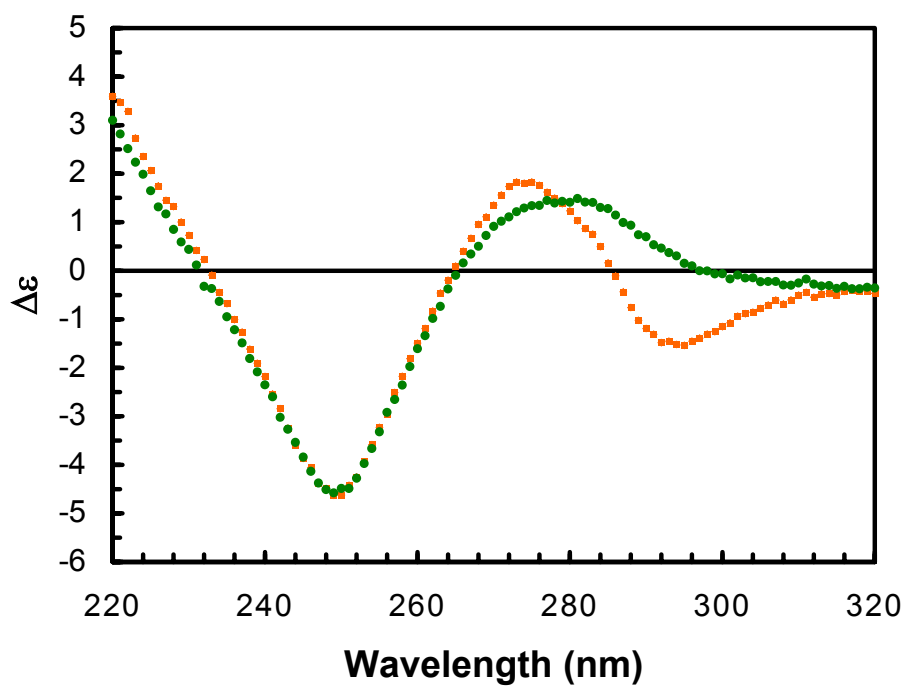




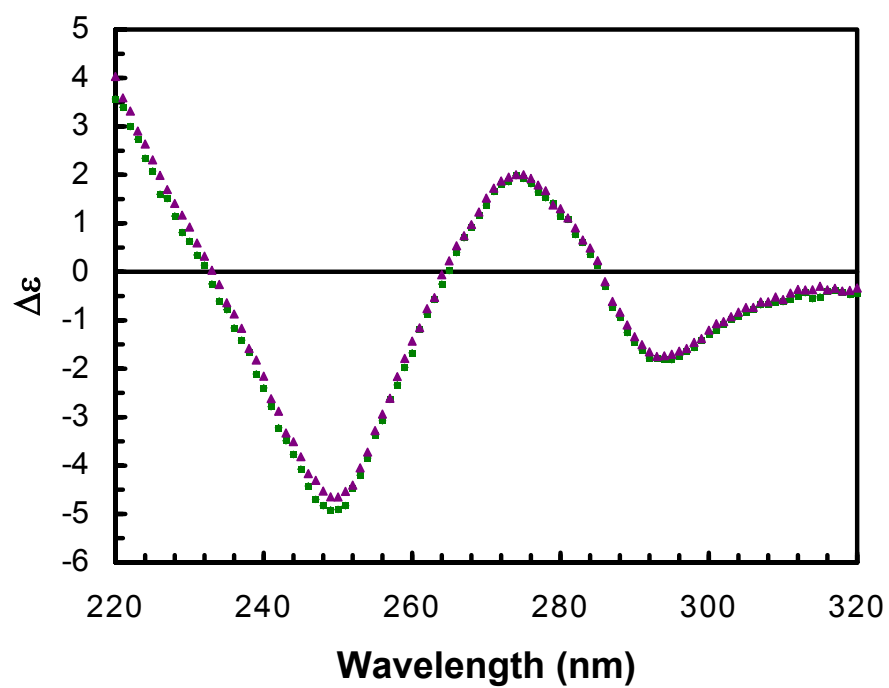
**Figure 9.2-3:** CD spectra of the double-stranded DNA **13/15** and **17/15**. 2  $\mu$ M **13/15** (■) and 2  $\mu$ M **17/15** (●) in 800 mM NaCl, 50 mM NaPi pH 7.0.

looks very much like B-form DNA. This result does not automatically make **12/14** useless; the most important thing is for **12/14** to be unperturbed relative to the control **16/14**. Unfortunately, **16/14** appears to be strictly B-form DNA (Figure 9.2-4).

One possibility for this difference is that the salt concentration of the buffer (800 mM NaCl) was too high. It has been demonstrated that high enough ( $> 1.5$  M) salt concentrations can induce just such a B/Z junction [38]. To investigate this possibility, the salt concentration was lowered by a 75% (to 200 mM NaCl). Unfortunately, the spectrum was virtually identical. Another possibility was that the sample was poorly annealed. To check this, a CD spectrum was acquired of a sample, that sample was then subjected to a melting temperature experiment. After 8 hrs of heating and cooling, the sample was re-examined by CD. The spectra show no difference (Figure 9.2-5); the melting temperature was found to be  $46.6 \pm 0.5$  °C, not statistically different than the original measurements. Without an explanation of this phenomenon, it was decided that further experiments would only be done on the duplex **13/15**.



**Figure 9.2-4:** CD spectra of the double-stranded DNA **12/14** and **16/14**. 2  $\mu\text{M}$  **12/14** (■) and 1.5  $\mu\text{M}$  **16/14** (●) in 800 mM NaCl, 50 mM NaPi pH 7.0.



**Figure 9.2-5:** CD spectra of the double-stranded DNA **12/14**. 2  $\mu$ M **12/14** before melting (■) and after melting (▲) in 800 mM NaCl, 50 mM NaPi pH 7.0.

### 9.3. *Experimental*

**Materials and Methods.** Anhydrous solvents from Fluka were used without further purification. Water was de-ionized and then distilled with a Barnstead Fishteam II still. All other solvents were “Omnisolve” grade reagents from EM Science. Preparative chromatography was performed using either activated aluminum oxide, Brockman I, from Fluka or silica, 60 Å, EM Science. *Cis*-bis (2,2'-bipyridene) ruthenium (II) dichloride and ruthenium (III) chloride were purchased from Strem Chemicals (Newburyport, MA). Oligonucleotide synthesis was carried out on an ABI 394 DNA synthesizer. DNA synthesis reagents were purchased from Glen Research. Digestion reagents were purchased from Pharmacia. Unless otherwise specified, materials from commercial suppliers were used without further purification.

#### 9.3.1. *Thymine Complexes*

##### *5'-azido-5'-deoxythymine (1)*

1.52 g (6.3 mmol) of 5'-deoxythymine was dissolved in 10 ml of anhydrous pyridine under argon. The pyridine was removed *in vacuo*, giving a white solid. The solid was then washed with anhydrous toluene and dried under vacuum. The flask was purged with argon for 5 min. The solid was dissolved in 40 ml anhydrous dimethyl formamide under argon. 1.65 g (6.3 mmol) triphenylphosphine was then added to the solution with an argon counter flow. Immediately afterward, 2.0 g (31.4 mmol) sodium azide was added to

the solution to give a slightly cloudy colorless solution. Then 2.1 g (6.3 mmol) carbon tetrabromide was added in two portions to the suspension, resulting in a cloudy yellowish solution. The reaction mixture was stirred for 18.5 hrs under argon, then quenched with 6 ml methanol. The solution was frozen and lyophilized on a 4.5 L bench top model Labconco lyophilizer. Column Chromatography on silica (95% methylene chloride: 5% methanol) afforded 1.42 g white crystals. Recrystallization from hot ethanol gave 1.3g (4.9 mmol) of the desired product (78% yield). **<sup>1</sup>H NMR** (300 MHz CD<sub>3</sub>OD) δ 7.47 (m, 1H), δ 6.23 (t, J=6 Hz, 1H), δ 4.49 (brs, 1H), δ 4.30 (dt, J=6,3 Hz, 1H), δ 3.95 (dd, J=6,3 Hz, 1H), δ 3.60 (ABX, J<sub>AB</sub>=24 Hz, J<sub>AX</sub>=12 Hz, J<sub>BX</sub>=6Hz, 2H), δ 2.20 (m, 2H) δ 1.87 (s, 3H). **<sup>13</sup>C NMR** (500 MHz, CD<sub>3</sub>OD) δ 166.5 (s), δ 152.5 (s), δ 137.9 (s), δ 112.0 (s), δ 86.5 (s), δ 86.4 (s), δ 72.6 (s), δ 53.5 (s), δ 40.4 (s), δ 12.6 (s). **IR** (CH<sub>3</sub>CN) 1192 cm<sup>-1</sup> (s), 1271 cm<sup>-1</sup> (s), 1693 cm<sup>-1</sup> (s, intense), 2106 cm<sup>-1</sup> (s, intense), 3271 cm<sup>-1</sup> (br), 3539 cm<sup>-1</sup> (br). **ESI-MS** [M+Cl]<sup>-</sup> 302.0. **EA** (Desert Analytics) Calculated C, 44.94; H, 4.90; N, 26.21; Found C, 44.45; H, 4.97; N, 25.01.

#### *5'-amino-5'-deoxythymine (2)*

1.00 g (3.7 mmol) **1** was suspended in 200 ml anhydrous ethanol. The suspension was then placed in a 500 ml Parr-Shaker bottle. 0.100 g of palladium on carbon was added to the slurry resulting in a black suspension. The bottle was evacuated/filled three times with 40 psi H<sub>2</sub>. The slurry was then agitated for 3.5 hrs. The apparatus was stopped at 1.5 hrs and a pressure of 15 psi H<sub>2</sub> and checked by TLC; some starting material remained. The bottle was re-sealed and re pressurized with 40 psi H<sub>2</sub> and agitated for 2 more hrs. TLC

showed no further starting material. The black suspension was filtered over celite and the ethanol was removed *in vacuo* to give 0.85 g of a yellowish powder (95% yield) **<sup>1</sup>H NMR** (300 MHz CD<sub>3</sub>OD) δ 7.47 (s, 1H), δ 6.21 (t, J=6 Hz, 1H), δ 4.25 (m, 1H), δ 3.82 (m, 1H), δ 2.88 (brs, 2H), δ 2.24 (m, 2H), δ 1.89 (s, 3H). **<sup>13</sup>C NMR** (500 MHz, CD<sub>3</sub>OD) δ 165.1 (s), δ 151.1 (s), δ 136.9 (s), δ 110.6 (s), δ 87.2 (s), δ 85.2 (s), δ 71.7 (s), δ 43.5 (s), δ 39.1 (s), δ 11.7 (s). **ESI-MS** [M+H]<sup>+</sup> 242.4

*1-(4-hydroxy-5-[(pyridin-2-ylmethylene)-amino]-methyl]-tetrahydro-furan-2-yl)-5-methyl-1H-pyrimidine-2,4-dione (3)*

0.800 g (3.3 mmol) **2** was dissolved in 75 ml ethanol and placed over 4 Å molecular sieves. Then, 0.450 g, 0.40 ml (4.2 mmol) of 2-pyridine carboxaldehyde was added to the solution. After sitting for 1 hr, the solution was heated to 70 °C in an oil bath under argon for 2 hrs. After cooling, the reaction mixture was left for 12 hrs. Some white precipitate was observed; the solution was filtered over a fine glass frit and the resulting yellow supernatant concentrated to dryness *in vacuo*. The oil was washed several times with hexanes and then dried over night under vacuum to give 1.02 g off-white powder (94% yield). **<sup>1</sup>H NMR** (300 MHz CDCl<sub>3</sub>) δ 8.70 (d, J=1.5 Hz 1H), δ 8.51 (s, 1H), δ 7.9 (m, 1H), δ 7.78 (td, J=7.5, 1.5 Hz, 1H), δ 7.4 (m, 2H), δ 6.38 (t, J=7 Hz, 1H), δ 4.6 (m, 1H) δ 4.3 (m, 1H), δ 4.02 (m, 2H), δ 2.4 (m, 1H), δ 1.60 (s, 3H). **<sup>13</sup>C NMR** (500 MHz, CD<sub>3</sub>OD) δ 165.4 (s), δ 150.4 (s), δ 137.7 (s), δ 136.5 (s), δ 126.0 (s), δ 121.5 (m), δ 110.9 (s), δ 100.8 (s), δ 86.8 (s), δ 85.1 (s), δ 72.8 (s), δ 62.7 (s), δ 40.5 (s), δ 12.6 (s). **IR** (CH<sub>3</sub>CN) 1193 cm<sup>-1</sup> (s),

1270  $\text{cm}^{-1}$  (s), 1698  $\text{cm}^{-1}$  (s, intense), 3280  $\text{cm}^{-1}$  (br), 3526  $\text{cm}^{-1}$  (br). **ESI-MS**  $[\text{M}+\text{H}]^+$  331.1,  $[\text{M}+\text{Na}]^+$  353.2.

*Bis (2,2'-bipyridine) ruthenium (II) (1-(4-hydroxy-5-[(pyridin-2-ylmethylene)-amino]-methyl]-tetrahydro-furan-2-yl)-5-methyl-1H-pyrimidine-2,4-dione) bis hexafluorophosphate (4)*

0.400 g (1.2 mmol) **3** was dissolved in 50 ml anhydrous ethanol and degassed by an argon sparge for 1 hr. Then, 0.700 g (1.4 mmol) of *cis*-bis (2,2'-bipyridine) ruthenium (II) dichloride was added to the reaction giving a dark purple solution. This purple solution was degassed for an additional 10 min. The flask was equipped with a reflux condenser and heated to reflux under argon for 3 hrs. At the end of this time, the solution had turned dark red. The ethanol was then removed *in vacuo* to give a red glass. The crude mixture was then purified by column chromatography on silica gel (80%  $\text{CH}_3\text{CN}$ : 16%  $\text{H}_2\text{O}$ : 4% saturated  $\text{KNO}_3$  solution) to give a deep red microcrystalline material. The diastereomers could not be separated by column chromatography (from the NMR it appears to be a 1:1 mixture). The solid was dissolved in 100 ml  $\text{H}_2\text{O}$  and 0.67 g (3.6 mmol) potassium hexafluorophosphate was added. The dark red solution was extracted 25 times with 25 ml  $\text{CH}_2\text{Cl}_2$ . The organic phases were combined and the solvent removed *in vacuo* to give 0.336 g (0.32 mmol) of a deep red crystalline material (26% yield)  $^1\text{H}$  NMR (300 MHz  $\text{CDCl}_3$ )  $\delta$  9.15 (s, 1H),  $\delta$  8.71 (m, 1H),  $\delta$  8.6 (m, 7H),  $\delta$  8.5 (m, 2H),  $\delta$  8.4 (m, 1H),  $\delta$  8.3 (m, 2H),  $\delta$  8.01 (m, 11H)  $\delta$  7.8 (m, 4H),  $\delta$  7.6 (m, 14H),  $\delta$  5.99 (dd,  $J=6,7$  Hz, 1H),  $\delta$  5.65 (t,  $J=7$  Hz, 1H),  $\delta$  4.20 (m 1H),  $\delta$  4.0 (m, 4H)  $\delta$  3.8 (m, 1H)  $\delta$  3.6 (m, 1H),  $\delta$  2.9 (m, 1H),  $\delta$



2.3 (m, 2H),  $\delta$  2.08 (m, 1H),  $\delta$  1.90 (s, 3H),  $\delta$  1.88 (s, 3H). **ESI-MS**  $[M-PF_6]^{+}$  889.2. **UV** ((Methanol)  $\lambda_{max}$  nm ( $\epsilon$ )) 210 (42,000), 246 (25,000), 288 (49,000), 468 (7,500). **Emission** (Methanol)  $\lambda_{EM}=720$  nm ( $\lambda_{EX}=480$  nm). **Lifetime** (in 800 mM NaCl, 50 mM NaPi, pH=7.02)  $\lambda_{EX}=480$  nm;  $\tau=53$  ns. **Quantum Yield**  $\Phi=3.5 \times 10^{-3}$  **Redox Potential** by cyclic voltammetry in 0.1 M tetrabutylammonium hexafluorophosphate in  $CH_3CN$ , scan rate of 50 mV/s, found to be 1.37 V vs. Ag/AgCl (1.61 V vs. NHE); in 800 mM NaCl, 50 mM NaPi, pH=7.0, scan rate of 50 mV/s, found to be 1.17 V vs. Ag/AgCl (1.41 V vs. NHE) .

#### *ZnHg Amalgam*

10.5 g (161 mmol) mossy zinc was washed with 1 M HCl to clean the surface . After 5 min of sitting in 1 M HCl, the acid was decanted and the metal was washed twice with 20 ml  $H_2O$  and left sitting under  $H_2O$ . In a separate flask, 0.347 g (1.61 mmol) mercuric oxide was dissolved into 1 ml concentrated HCl to give a colorless solution. This solution was added to the zinc in water. The suspension was swirled for 10 min by hand. The supernatant was decanted and the amalgam washed 5X50 ml  $H_2O$  and dried over night under vacuum. The resulting amalgam was then stored under argon.

#### *Bis-(acetylacetonate) ruthenium (II) cis-bis(acetonitrile) (5)*

2.0 g (5 mmol) tris-(acetylacetonate) ruthenium (III) was dissolved in 125 ml  $CH_3CN$ , 25 ml  $H_2O$  to give a purple solution. This solution was degassed by argon sparge for 20 min. After degassing, 6.04 g ZnHg amalgam was added. Then, the flask was equipped with a reflux condenser with an argon inlet. The suspension was heated to reflux

for 30 min, resulting in a deep orange solution with white precipitate. Refluxing was continued for 6 hrs. The suspension was then quickly filtered over a fine porosity glass frit and the supernatant collected. The solvent removed *in vacuo* to give orange oil. The oil was washed with 2X50 ml hexanes and sonicated twice in 50 ml hexanes to give 1.52 g (4.0 mmol) of an orange powder, stored under argon (80% yield). **<sup>1</sup>H NMR** (300 MHz CD<sub>3</sub>OD)  $\delta$  5.39 (s, 2H),  $\delta$  2.58 (s, 6H),  $\delta$  1.95 (s, 6H),  $\delta$  1.90 (s, 6H). **ESI-MS** [M-2CH<sub>3</sub>CN+H]<sup>+</sup> 300.4

*Bis-(acetylacetonate) ruthenium (II) (1-(4-hydroxy-5-[(pyridin-2-ylmethylene)-amino]-methyl]-tetrahydro-furan-2-yl)-5-methyl-1H-pyrimidine-2,4-dione) (6)*

0.355 g (1.1 mmol) **3** was dissolved anhydrous ethanol to give a faintly green solution. The solution was degassed for 30 min with an argon sparge. Then 0.373 g (0.98 mmol) **5** was added to give an orange solution. The flask was then equipped with a reflux condenser with an argon inlet. The flask was heated in an oil bath at 75 °C for 2 hrs to give a very dark purple solution. The ethanol was removed *in vacuo* to give a purple solid. The solid was purified by column chromatography on silica gel (67% CH<sub>2</sub>Cl<sub>2</sub>: 33% THF) to give the two diastereomers pure as 0.403 g (combined mass) (0.64 mmol) blue/green powder, stored under argon at -20 °C (66% yield). **<sup>1</sup>H NMR** (300 MHz CDCl<sub>3</sub>) **diastereomer I**:  $\delta$  7.88 (d, J=8 Hz, 1H),  $\delta$  7.6 (m, 4H),  $\delta$  7.13 (s, 1H),  $\delta$  6.30 (t, J=7 Hz, 1H),  $\delta$  5.50 (brs, 2H)  $\delta$  4.4 (m, 2H),  $\delta$  4.12 (brs, 2H),  $\delta$  2.2 (m, 2H),  $\delta$  1.39 (s, 12H),  $\delta$  1.28 (s, 3H); **diastereomer II**:  $\delta$  7.84 (d, J=7 Hz, 1H),  $\delta$  7.4 (m, 3H),  $\delta$  7.12 (s, 1H),  $\delta$  6.92 (s, 1H),  $\delta$  6.15 (t, J=6 Hz, 1H),  $\delta$  5.40 (brs, 2H)  $\delta$  4.3 (m, 4H),  $\delta$  2.3 (m, 2H),  $\delta$  1.39 (s, 12H),  $\delta$

1.28 (s, 3H). **IR** ( $\text{CH}_3\text{CN}$ )  $1195\text{ cm}^{-1}$  (s),  $1265\text{ cm}^{-1}$  (s),  $1570\text{ cm}^{-1}$  (s),  $1693\text{ cm}^{-1}$  (s, intense),  $3540\text{ cm}^{-1}$  (br). **ESI-MS**  $[\text{M}+\text{H}]^+$  630.2. **UV** ((ethanol)  $\lambda_{\text{max}}$  nm ( $\epsilon$ )) 208 (26,000), 274 (25,000), 402 (4,600), 586 (4,600). **Redox Potential** by cyclic voltammetry in 0.1 M tetrabutylammonium hexafluorophosphate in  $\text{CH}_2\text{Cl}_2$ , scan rate of 100 mV/s, found to be 0.109 V vs. Ag/AgCl (0.350 V vs. NHE); in 0.1 M ammonium hexafluorophosphate in ethanol, scan rate of 50 mV/s, found to be 0.036 V vs. Ag/AgCl (0.277 V vs. NHE). Attempts to get potentials in buffer failed- even after only 9 min additional waves appear.

*Tris-(dibenzoate methane) ruthenium (III) (Precursor to 7)*

Following the method of Endo et al. [42]; 1.00 g (4.8 mmol) ruthenium (III) chloride was dissolved in 100 ml ethanol/ 50 ml  $\text{H}_2\text{O}$  to give a dark red-brown solution. The flask was equipped with a reflux condenser with an argon inlet. Then, the solution was heated to reflux for 4 hrs, resulting in a deep blue/green solution (“ruthenium blue”). The solution was cooled to room temperature and 4.32 g (19.2 mmol) dibenzoyl methane was added to the solution under a counter flow of argon. The flask was then heated to reflux for 45 min, resulting in a deep red solution. The solution was again cooled to room temperature, and 1.21 g (14.5 mmol) sodium carbonate was added under a counter flow of argon with some gas evolution evident. The suspension was heated to reflux for 1.5 hrs, and then cooled to room temperature. Another portion of 1.21 g (14.5 mmol) sodium carbonate was added, this time no gas evolution was observed. After refluxing for an additional 1.5 hrs, the now brownish solution was cooled to room temperature. The solvent was removed *in vacuo* until 50 ml remained and filtered over a fine porosity glass frit to

give a black sticky precipitate and a clear brown supernatant. The solid was air dried briefly. 18X20 ml toluene was added to the frit and agitated. The toluene was collected as a deep red solution. The solvent was removed *in vacuo* to give a red solid. Further washings (7X25 ml) of the remaining solid with acetone gave a solution that contained the product by TLC. The organic fractions were combined and the solvent removed by vacuum to give a red solid. The solid was purified by column chromatography on alumina (neat toluene) to give 0.390 g (0.50 mmol) red crystals (11% yield). Proton NMR was acquired in accordance with Baird [39]. <sup>1</sup>H NMR (300 MHz C<sub>6</sub>D<sub>6</sub>) δ -32.76 (brs) ESI-MS [M+H]<sup>+</sup> 772.2, [M+Na]<sup>+</sup> 794.2.

*Bis-(dibenzoate methane) ruthenium (II) cis-bis(acetonitrile) (7)*

0.190 g (0.25 mmol) **precursor to 7** was suspended in 42.5 ml CH<sub>3</sub>CN, 7.5 ml H<sub>2</sub>O. The suspension was then degassed by argon sparge. To this orange suspension, 1.3 g ZnHg amalgam was added. The flask was then equipped with a reflux condenser with an argon inlet. The suspension was heated to 60 °C for 30 min resulting in dissolution of **precursor to 7** and a change in color to dark blue. The solution was then heated to reflux for 5.5 hrs, resulting in a color change to deep red. The suspension was cooled to room temperature and filtered over a fine porosity glass frit to give a clear red supernatant. The solvent was removed *in vacuo* to give 0.250 g red oil. The oil was washed 2X25 ml petroleum ether and then sonicated twice in 25 ml petroleum ether to give 0.12 g (0.19 mmol) red powder, stored under argon (77% yield). <sup>1</sup>H NMR (300 MHz CDCl<sub>3</sub>) δ 7.82 (s,

2H),  $\delta$  7.80 (s, 2H),  $\delta$  7.4 (m, 16H),  $\delta$  6.69 (s, 2H),  $\delta$  2.56 (s, 6H). **ESI-MS**  $[M-2CH_3CN+H]^+$  548.0.

*Bis-(dibenzoate methane) ruthenium (II) (1-(4-hydroxy-5-[(pyridin-2-ylmethylene)-amino]-methyl]-tetrahydro-furan-2-yl)-5-methyl-1H-pyrimidine-2,4-dione) (8)*

0.088 g (0.22 mmol) **3** was dissolved anhydrous ethanol to give a colorless solution. The solution was degassed for 45 min with an argon sparge. Then 0.100 g (0.16 mmol) **7** was added to give a dark red solution. The flask was then equipped with a reflux condenser with an argon inlet. The flask was heated in an oil bath at 60 °C for 45 min, resulting in no color change. The flask was then heated to 75 °C for 1.5 hrs to give a very dark blue solution. The ethanol was removed *in vacuo* to give a blue solid. The solid was purified by column chromatography on silica gel (67% CH<sub>2</sub>Cl<sub>2</sub>: 33% THF) to give one diastereomer pure and the other mixed as 0.100 g (combined mass) (0.11 mmol) blue powder, stored at –20 °C (71% yield). **<sup>1</sup>H NMR** (300 MHz CD<sub>3</sub>OD) **diastereomer I**:  $\delta$  8.0 (m, 8H),  $\delta$  7.5 (m, 4H),  $\delta$  7.3 (m, 8H),  $\delta$  7.04 (s, 1H),  $\delta$  6.9 (m, 2H),  $\delta$  6.27 (s, 1H),  $\delta$  5.4 (brs, 2H)  $\delta$  4.3 (m, 2H),  $\delta$  3.7 (m, 2H),  $\delta$  2.2 (m, 2H),  $\delta$  1.30 (s, 3H); **ESI-MS**  $[M+H]^+$  878.2. **UV** ((CH<sub>2</sub>Cl<sub>2</sub>)  $\lambda_{\max}$  nm ( $\epsilon$ )) 256 (23,400), 316 (20,100), 474 (4,400), 598 (5,200). **Redox Potential** by cyclic voltammetry in 0.1 M tetrabutylammonium hexafluorophosphate in CH<sub>2</sub>Cl<sub>2</sub>, scan rate of 1000 mV/s, found to be 0.086 V vs. SCE (0.327 V vs. NHE); in 0.1 M ammonium hexafluorophosphate in ethanol, scan rate of 1000 mV/s, found to be 0.011 V vs. SCE (0.252 V vs. NHE)

*Rhenium (I) tricarbonyl chloride (1-(4-hydroxy-5-[(pyridin-2-ylmethylene)-amino]-methyl]-tetrahydro-furan-2-yl)-5-methyl-1H-pyrimidine-2,4-dione) (9)*

0.240 (0.66 mmol)  $\text{Re}(\text{CO})_5\text{Cl}$  and 0.240 g (0.73 mmol) **3** were dissolved in 15 ml THF, to give a clear greenish solution with white solid. This solution was degassed by an Ar sparge and equipped with a reflux condenser, under Ar. The solution was heated to reflux in a water bath. All solid was dissolved after 5 min. Reflux was continued for an additional 70 min. At the end of this time, the greenish solution turned deep orange and cloudy. The orange suspension was filtered over a fine porosity frit to give an orange solution and a greenish tarry solid. The solid was washed with THF and the washings were combined with the filtrate. The THF was removed *in vacuo* to give an orange solid. Thin layer chromatography on silica gel with a 90:10  $\text{CH}_2\text{Cl}_2$ :MeOH eluent showed a deep yellow spot ( $R_f = 0.57$ ), and 4 UV active spots. The bulk solid was purified on silica gel with the same eluent to give 0.234 g of **9** (53%). Crystals were obtained from vapor diffusion of heptanes into acetone.  **$^1\text{H}$  NMR** (300 MHz  $\text{CD}_3\text{CN}$ ) **diastereomer I**:  $\delta$  9.03 (m, 2H),  $\delta$  8.92 (m, 1H),  $\delta$  8.20 (m, 1H),  $\delta$  8.10 (m, 1H),  $\delta$  7.70 (m, 1H),  $\delta$  7.30 (brs, 1H),  $\delta$  6.23 (t,  $J=7$  Hz 1H)  $\delta$  4.4 (m, 6H),  $\delta$  3.74 (d,  $J=4$  Hz 2H),  $\delta$  2.40 (m, 2H),  $\delta$  2.30 (m, 2H),  $\delta$  1.83 (d,  $J=1.5$  Hz 3H)  **$^{13}\text{C}$  NMR** (125.7 MHz  $\text{CD}_3\text{CN}$ ) **diastereomer I**:  $\delta$  171.4 (s),  $\delta$  164.6 (s),  $\delta$  155.7 (s),  $\delta$  155.7 (s),  $\delta$  154.2 (s),  $\delta$  151.4 (s),  $\delta$  141.4 (s),  $\delta$  137.6 (s),  $\delta$  130.3 (s),  $\delta$  111.8 (s),  $\delta$  86.5 (s),  $\delta$  84.6 (s),  $\delta$  72.5 (s),  $\delta$  66.9 (s),  $\delta$  39.0 (s),  $\delta$  12.4 (s) **UV/Vis** (( $\text{H}_2\text{O}$ )  $\lambda_{\text{max}}$  nm ( $\epsilon$ )) 202 (26,000), 266 (17,600), 388 (3,400), 400 (3,100), 420 (2,100). **IR:** ( $\text{CH}_2\text{Cl}_2$ )  $\nu$  2025.6  $\text{cm}^{-1}$ ,  $\nu$  1925.4  $\text{cm}^{-1}$ ,  $\nu$  1905.0  $\text{cm}^{-1}$ ,  $\nu$  1712.5  $\text{cm}^{-1}$ ,  $\nu$  1693.3  $\text{cm}^{-1}$ ,  $\nu$  1602.6  $\text{cm}^{-1}$ . **ESI-MS**  $[\text{M}+\text{H}]^+$  601.0 (Re isotope pattern apparent). **Redox Potential** by

cyclic voltammetry in 0.1 M tetrabutylammonium hexafluorophosphate in CH<sub>3</sub>CN, scan rate of 1000 mV/s, found to be 1.43 V vs. SCE (1.67 V vs. NHE).

*Rhenium (I) tricarbonyl pyridine (1-(4-hydroxy-5-[(pyridin-2-ylmethylene)-amino]-methyl]-tetrahydro-furan-2-yl)-5-methyl-1H-pyrimidine-2,4-dione) hexafluorophosphate (10)*

0.200 g (0.30 mmol) **9** was dissolved in 10 ml dry THF in a 20 ml scintillation vial with a teflon cap equipped with a stir bar, to give an orange solution. 0.075 g (0.30 mmol) AgPF<sub>6</sub> was then added to this solution to give an orange suspension. This suspension was stirred for 48 hrs at room temperature. The suspension was filtered over celite to remove the precipitated AgCl to give a clear orange solution. The THF was removed *in vacuo* to give an orange oil. The oil was redissolved in 5 ml THF and 0.75 ml (9.3 mmol) pyridine and stirred at room temperature for 24 hrs. The solvent was removed in *vacuo* once again to give an orange oil. This oil was applied to silica gel with a 90:10 CH<sub>2</sub>Cl<sub>2</sub>:MeOH eluent. Three orange bands were removed from the column, none of which proved to be the desired product. The column conditions were then changed to 90:7:3 CH<sub>3</sub>CN:H<sub>2</sub>O:sat'd KNO<sub>3</sub>. The orange band eluted this time was the desired product. The fraction containing the orange band was evaporated to dryness to give an orange solvent. Dry CH<sub>3</sub>CN was added to the solid leaving behind white solid KNO<sub>3</sub>. the orange solution was evaporated to dryness leaving an orange solid behind, 0.194 g (60% yield). **<sup>1</sup>H NMR** (300 MHz CD<sub>3</sub>CN) **diastereomer I**: δ 9.28 (m, 1H), δ 9.2 (m, 1H), δ 8.42 (m, 1H), δ 8.36 (m, 2H), δ 8.18 (m, 1H), δ 7.98 (m, 1H), δ 7.88 (m, 1H), δ 7.44 (m, 3H), δ 6.01 (t, J=7 Hz 1H) δ 4.4 (m, 6H), δ

3.74 (d, J=4 Hz 2H),  $\delta$  2.65 (m, 2H),  $\delta$  2.30 (m, 2H),  $\delta$  1.83 (d, J=1.5 Hz 3H) **UV/Vis**  
 ((H<sub>2</sub>O)  $\lambda_{\text{max}}$  nm ( $\epsilon$ )) 202 (56,500) 266 (25,000) 388 (3,900) 400 (3,500) 420 (2,200)

*Bis (2,2'-bipyridine) ruthenium (II) (1-(4-hydroxy-5-[(pyridin-2-ylmethylene)-amino]-methyl]-tetrahydro-furan-2-yl)-5-methyl-1H-pyrimidine-2,4-dione) bis hexafluorophosphate Phosphoramidite (13)*

0.270 g (0.26 mmol) **4** was dissolved in 5 ml anhydrous, degassed (via argon sparge) CH<sub>3</sub>CN to give a dark red solution. 0.018 g (0.26 mmol) 1H-tetrazole was then added with stirring and a counter flow of argon. After 5 min, 0.165 g, 174  $\mu$ l, (0.55 mmol) 2-cyanoethyl-tetraisopropylphosphoramidite was added with a syringe. The solution was allowed to stir at room temperature for 5 hrs. The solvent was removed *in vacuo* and the resulting oil purified by flash column chromatography on alumina (80% CH<sub>3</sub>CN: 15% H<sub>2</sub>O: 5% Saturated KNO<sub>3</sub> solution) to give a red solid. The solid was washed with 200 ml CH<sub>2</sub>Cl<sub>2</sub>. The organic washings were combined and the solvent removed *in vacuo* to give 0.240 g (0.19 mmol) red oil (73% yield). **<sup>31</sup>P NMR** (300 MHz CD<sub>3</sub>CN)  $\delta$  152.4 (s),  $\delta$  151.8 (s),  $\delta$  -140.27 (septet). **IR** (CH<sub>3</sub>CN) 846 cm<sup>-1</sup> (s), 1630 cm<sup>-1</sup> (s), 1693 cm<sup>-1</sup> (s, intense), 3541 cm<sup>-1</sup> (br). **ESI-MS** [M-PF<sub>6</sub>]<sup>+</sup> 1089.2.

### 9.3.2. Metallated DNA



*Oligonucleotide Synthesis and Purification of 5'-(bpy)<sub>2</sub>RuT<sub>impy</sub>AG TTT AAT TAA ATA A-3' (12), 5'-(bpy)<sub>2</sub>RuT<sub>impy</sub>AG GTT AAT TAA ATA A-3' (15), 5'-T TAT TTA ATT AAA CTA-3' (14), 5'-T TAT TTA ATT AAC CTA-3' (15), 5'-TAG TTT AAT TAA ATA A-3' (16) and 5'-TAG GTT AAT TAA ATA A-3' (17)*

Control and modified oligonucleotides were prepared on a 1.0  $\mu$ mol scale on a 500 Å CPG support. Modified nucleoside couplings were carried out directly in the DNA synthesizer. CH<sub>3</sub>CN solutions of the modified phosphoramidite (**5**) (0.095 M) were introduced at the 5' end of the oligonucleotide, trityl protecting group still in place; with a manual cleavage cycle. Coupling times were extended to 30 min with single delivery. The cleavage of the protecting groups was carried out manually by placing the CPG beads in 30% NH<sub>4</sub>OH solution followed by standing at 25 °C for 12 hrs. The solvent was removed *in vacuo* to give small pellets of orange material. The pellets were re-dissolved in H<sub>2</sub>O and the solvent removed two times. The samples were then taken up in nano-pure H<sub>2</sub>O and subjected to HPLC purification on a Dionex Nucleopac PA-100 using a mobile phase of 1.5 M NH<sub>4</sub>Cl, 20 mM tris, 0.5% CH<sub>3</sub>CN, pH=7.0 gradient in 20 mM tris, 0.5% CH<sub>3</sub>CN pH=7.0. The samples were collected based on a UV band at 260 nm and a visible band (MLCT) at 465 nm. The solvent was removed *in vacuo* to give salt and the desired oligonucleotides. The samples were desalted by dissolving the samples in water and passing them down a SepPak cartridge (Waters Corporation). (**14**), (**15**), (**16**) and (**17**) were synthesized and purified at the DNA synthesis facility. **MALDI-TOF** (**12**) [M-1]<sup>-</sup> 5398.6, (**13**) [M-1]<sup>-</sup> 5426.1, (**14**) [M-1]<sup>-</sup> 4852.0, (**15**) [M-1]<sup>-</sup> 4827.8, (**16**) [M-1]<sup>-</sup> 4902.9, (**17**) [M-1]<sup>-</sup>

4926.1 UV ( $\lambda_{\max}$  nm ( $\epsilon$ )) (**13**) 260 (210,029) 465 (7,300) **Lifetime** (**13**) ( $\lambda_{\text{EM}}$ =720 nm,  $\lambda_{\text{EX}}$ =480 nm)  $\tau$ =67 ns.

#### *Hybridization of 12/14 and 13/15*

30 nmol (determined by UV/Vis quantitation) each of **12** and **14** were combined in 1 ml of 800 mM NaCl, 50 mM NaPi, pH=7.02. The solution was heated to 90 °C for 5 min. Then, the solution was cooled over 4 hrs to 5 °C. The solution was then diluted to the working volume (2-3 ml) with cold buffer (same as above). The procedure was identical for **13/15**; also **16/14** and **17/15**.

#### *Thermal Denaturation Studies of 12/14 and 13/15*

Hybridized samples of **12/14** and **13/15** were placed in 3 ml of 800 mM NaCl, 50 mM NaPi, pH=7.02 in a quartz cell. These solutions were placed in a HP 8452A spectrometer with a Peltier heating accessory. The samples were heated to 70 °C and cooled to 22 °C 4 times in succession. Spectra were acquired at 260 nm at a rate of 0.5 °C min<sup>-1</sup>. Control strands **16/14** and **17/15** were analyzed in the same fashion. T<sub>m</sub> **12/14** 47.8 ± 0.4 °C, **16/14** 47.7 ± 0.7 °C, **13/15** 51.3 ± 0.5 °C, **17/15** 49.7 ± 0.5 °C

#### *Circular Dichroism Spectra of 12/14, 16/14, 13/15, and 17/15*

Duplex DNA was prepared as described above. After degassing and sealing in atmosphere-controlled cuvettes (see Chapter 2) under argon, CD spectra were acquired from 320 nm to 220 nm. Using the method of Fairall [35], tertiary structure was assigned.

#### *Enzyme Digestion of 12 and 13*

2.4  $\mu$ l Phosphodiesterase (PDI) at an activity of 39 unit/ml and 4.0  $\mu$ l alkaline phosphatase (AP) at an activity of 0.1 unit/ $\mu$ l were combined with 0.8  $\mu$ l of 1 M  $\text{MgCl}_2$ , 5.0  $\mu$ l tris buffer (pH=7.5), 44  $\mu$ l  $\text{H}_2\text{O}$  and 4 nanomoles of **6** and **7** separately. These solutions were incubated at 37 °C for 16 hrs. The solutions were then filtered over 2 micron filters to remove the protein. The resulting supernatant was then analyzed by HPLC using a 100 mM TEA Ac, 2%  $\text{CH}_3\text{CN}$ , pH=7.0 mobile phase in  $\text{CH}_3\text{CN}$ .

#### *EPR experiments*

1 ml of saturated cobalt (III) pentamine chloride solution was prepared. 200  $\mu$ l aliquots of this solution were used to dissolve **4**, bis-(2,2'-bipyridine) bis-cyano ruthenium (II), bis-(2,2'-bipyridine) bis-imidazole ruthenium (II), and bis-(2,2'-bipyridine) (cyano) (imidazole) ruthenium (II) at concentrations of 1-2 mM. Immediately after mixing the solutions they were subjected to the following procedure: 150  $\mu$ l the solutions were transferred to an EPR tube. The tube was then subjected to an unfiltered xenon arc lamp while simultaneously being frozen in a clear dewar with liquid nitrogen. In several cases immediate color changes were visible. The tubes were then transferred to a second dewar

also filled with liquid nitrogen. This dewar was secured in the cavity of the spectrometer and spectra acquired at 77 K.

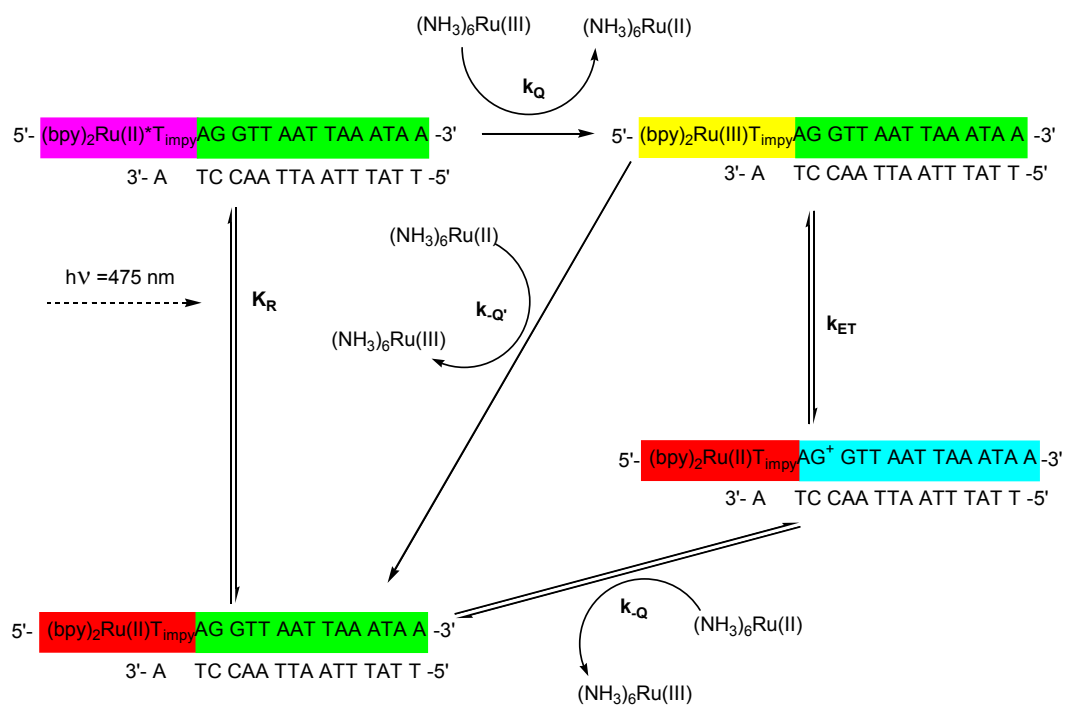
## *Chapter 10*

### **GENERATION OF A GUANINE RADICAL IN SINGLE-STRANDED DNA**

#### **10.1. *Photophysics of 4***

Once the duplex **13/15** was fully characterized, its charge transport possibilities could be investigated. As discussed in Chapter 2, since we are most interested in ground state charge transfer events, the “flash/quench” experiment [40] is the preferred method for investigating ET in DNA. A schematic representation of the precise experiment can be found in Figure 10.1-1.

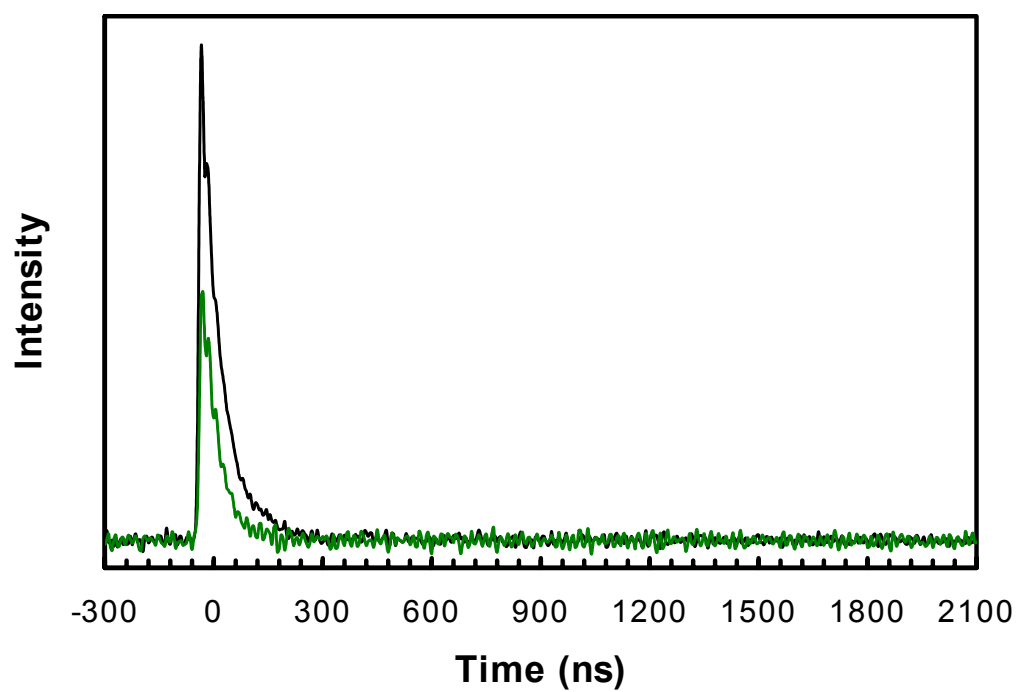
Working in the flash-quench framework, the first order of business was to fully understand the excited state dynamics of the model complex, **4**. To that end, **4** has been examined by a fluorimeter to give the range of excited state emission (640 nm to 880 nm) and quantum yield data ( $\Phi = 3.5 \times 10^{-3}$ ) [25]. Combining these results with absorption data (Table 9.1-1), an experiment was designed. It was decided that the best place to excite the complex was at 475 nm. Although somewhat on the red edge of the MLCT, it was thought that this choice would produce the excited state while avoiding photo-induced decomposition. **4** was photo-excited by the use of a pulsed Nd:YAG laser that drives a



**Figure 10.1-1:** Schematic representation of the flash/quench methodology as applied to metallated DNA.

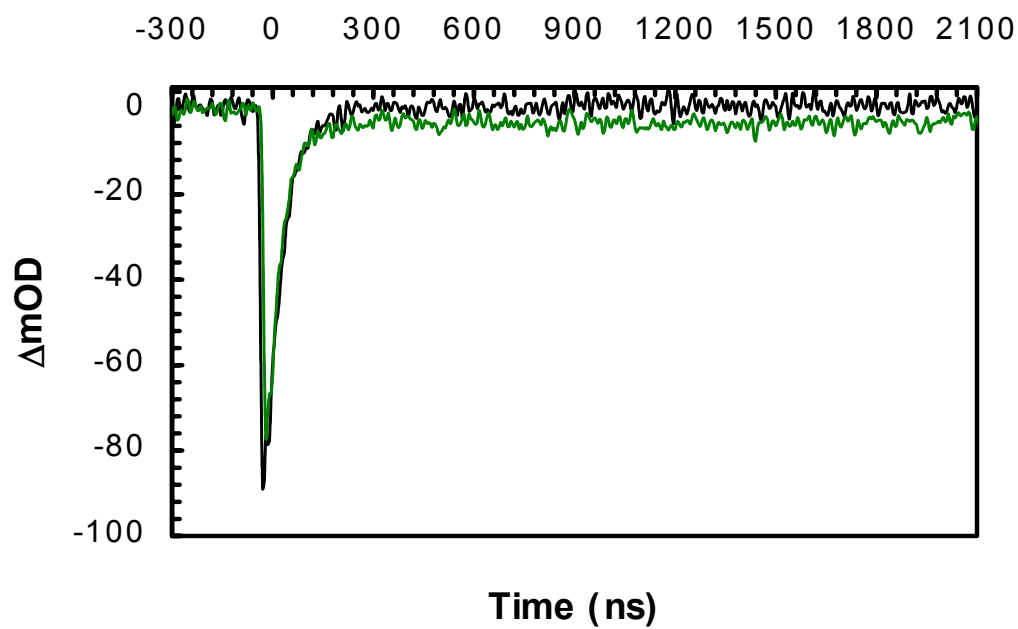
MOPO and both emission and transient absorption spectra were recorded using the previously described NS1 (see Chapter 2).

By observing the emission at 720 nm the lifetime of the excited state was determined;  $\tau = 60$  ns ( $k = 1.61 \times 10^7$  s<sup>-1</sup>). Not only could the excited state be generated, but by using copious amounts (15 mM) of ruthenium (III) hexamine as a quencher, the excited state (emission at 720 nm) could be quenched from  $\tau = 60$  ns to  $\tau = 43$  ns ( $k = 2.3 \times 10^7$  s<sup>-1</sup> Figure 10.1-2). Another method used to verify the photo-excitation of **4** was to observe the absorption change at 450 nm after the laser pulse. Since 450 nm is squarely in the MLCT of the complex, a bleach with a recovery rate identical to the emission decay rate is expected: when the excited state is generated, the population of **4** that is excited no longer has the same electronic structure. Therefore, the excited molecules do not display the same absorption properties leading to what is commonly referred to as a “bleach”. This is exactly what was observed (Figure 10.1-3). In addition, copious amounts of the exogenous electron acceptor, Ru(III)(NH<sub>3</sub>)<sub>6</sub> altered the observed decay of the excited state; the quencher greatly increased the time that it took for the transient absorption at 450 nm to return to 0 (the ground state). This can be interpreted to mean that some of the excited state was being oxidized by the exogenous Ru(III) species resulting in the oxidized version of **4**. The eventual return to the ground state can be rationalized in terms of recombination of oxidized **4** with Ru(II)(NH<sub>3</sub>)<sub>6</sub> (Figure 10.1-3). A Stern-Volmer plot of varying concentrations of quencher has shown that for **4** quenching is collisional, not static [25]. The amount of ruthenium (III) generated in the flash quench experiment is small; but



**Figure 10.1-2:** NS1 emission spectra, 30  $\mu\text{M}$  **4** in 800 mM NaCl 50 mM NaPi pH 7.0 at 720 nm. (—) without  $\text{Ru(III)(NH}_3)_6$  ; (—) with 15 mM  $\text{Ru(III)(NH}_3)_6$ .

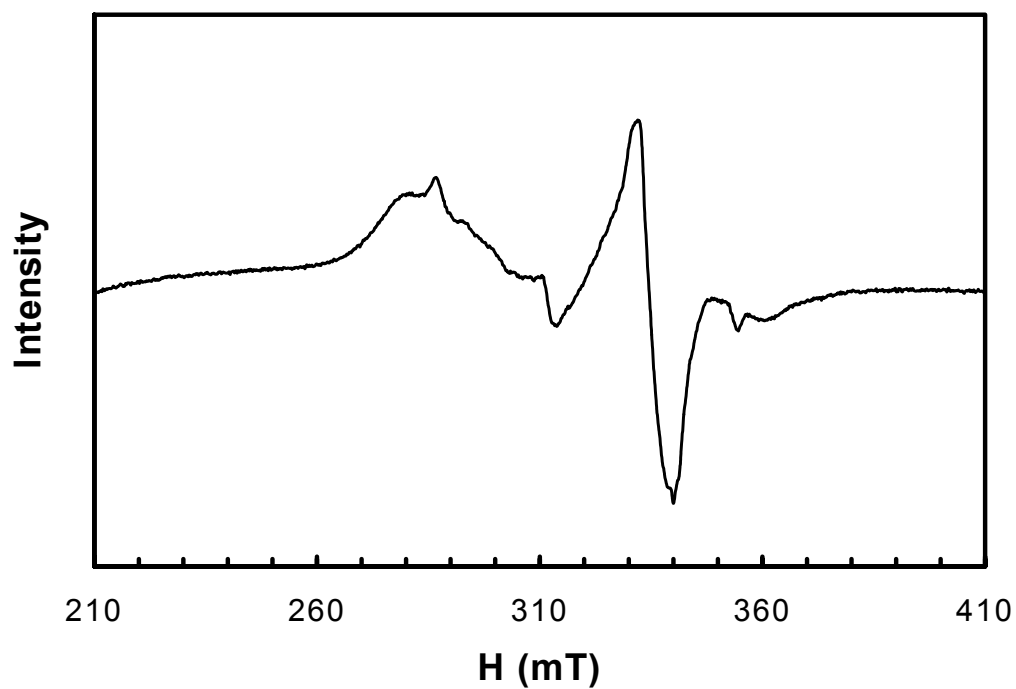




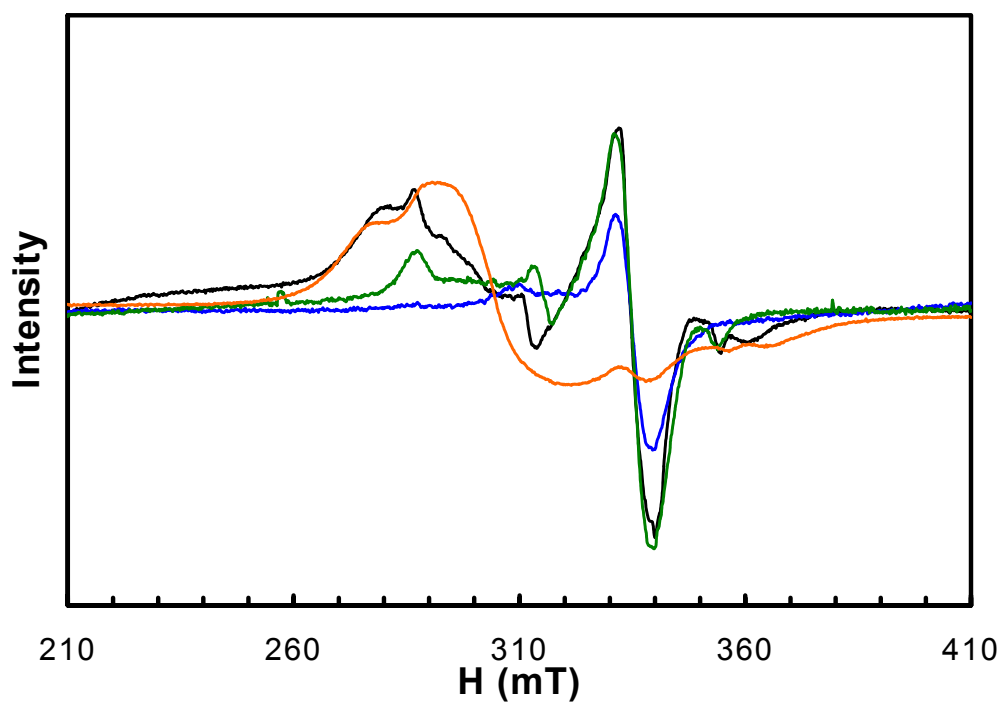
**Figure 10.1-3:** NS1 transient absorption, 30  $\mu M$  **4** in 800 mM NaCl 50 mM NaPi pH 7.0 at 450 nm. (—) without  $Ru(III)(NH_3)_6$  ; (—) with 15 mM  $Ru(III)(NH_3)_6$ .

existent. It was hoped that there would be enough oxidation to effect the ground state electron transfer between the metal complex and Gu.

More proof that one could photogenerate the Ru(III) version of **4** by bimolecular oxidation of the excited state was obtained by X-band EPR. Using the flash/quench/freeze technique, the excited state of **4** was oxidized by  $\text{Co(III)(NH}_3)_5\text{Cl}$ . The frozen solution was then examined by EPR, exhibiting the spectrum shown below (Figure 10.1-4). This EPR spectrum was determined to be most likely a Ru(III) spectrum by comparison with several other  $(\text{bpy})_2\text{Ru(III)LL'}$  spectra generated in the same way (Figure 10.1-5).



**Figure 10.1-4:** Flash/quench/freeze X-band EPR of 1 mM **4** in an 800 mM NaCl 50 mM NaPi pH 7.0 buffer saturated with  $(\text{NH}_3)_5\text{Co(III)Cl}$  at 77 K. Settings:  $\nu = 9.461918$  GHz; modulation frequency = 30 kHz; modulation amplitude = 3.0 G; microwave power = 63.77 mW; time constant = 5.12 ms; conversion time = 20.48 ms; 40 scans.



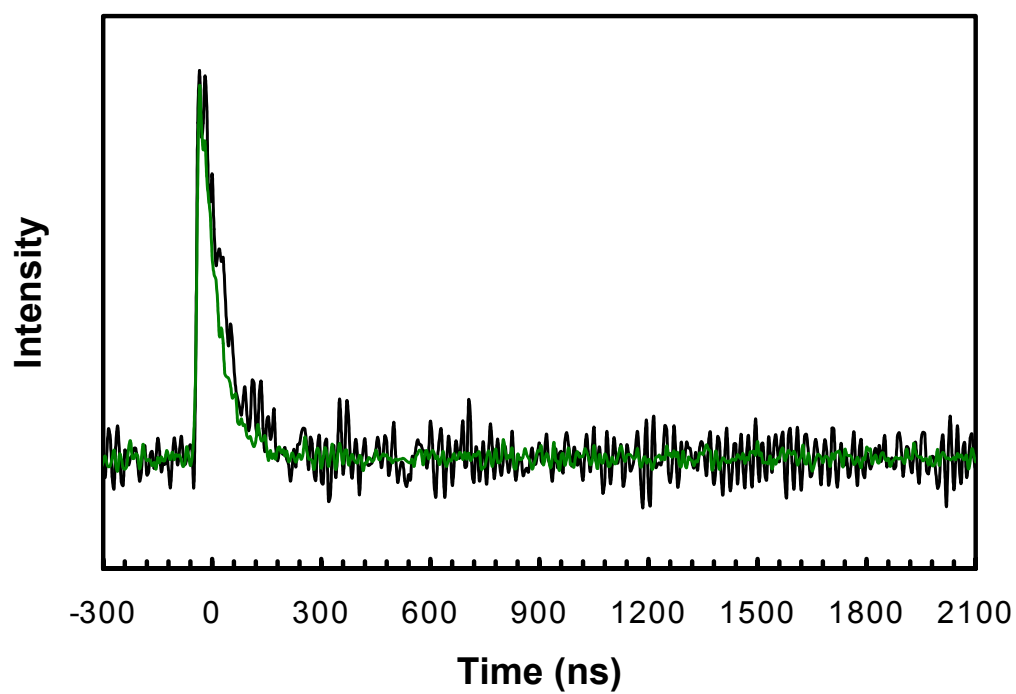
**Figure 10.1-5:** Comparison of flash/quench/freeze X-band EPR spectra for several complexes. Settings: modulation frequency = 30 kHz; modulation amplitude = 3.0 G; microwave power = 63.77 mW; time constant = 5.12 ms; conversion time = 20.48 ms; 40 scans. (—) **4** ( $\nu = 9.461918$  GHz); (—)  $(\text{bpy})_2\text{Ru(III)(CN)(im)}$  ( $\nu = 9.461528$  GHz), (—)  $(\text{bpy})_2\text{Ru(III)(CN)}_2$  ( $\nu = 9.462034$  GHz), (—)  $(\text{bpy})_2\text{Ru(III)(im)}_2$  ( $\nu = 9.463098$  GHz).

## 10.2. *Photophysics of Metallated DNA*

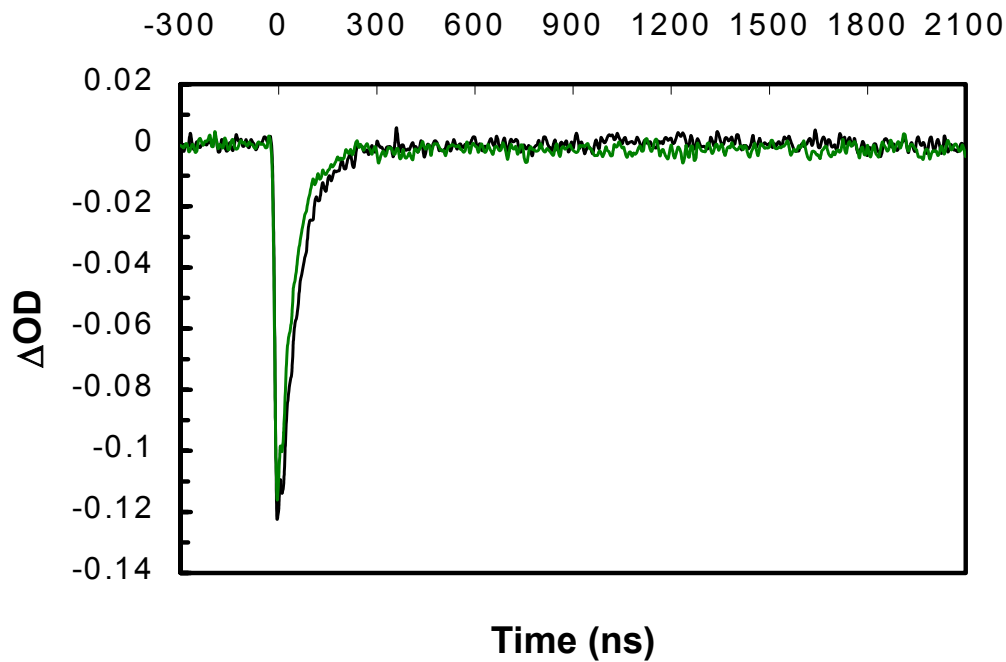
For the first experiment, **13** was subjected to the same laser experiment as those depicted in Figures 10.1-2 and 10.1-3 above. The emission changed slightly without quencher, resulting in an excited state lifetime of  $\tau = 72$  ns ( $k = 1.4 \times 10^7$  s<sup>-1</sup>, as compared to the 60 ns lifetime of **4**, see Table 9.1-1). Upon addition of quencher, the lifetime was substantially reduced to  $\tau = 50$  ns (Figure 10.2-1). However, no generation of ruthenium (III) was observed (Figure 10.2-2). Further, the bleach at 450 nm could not be fit by a multi-exponential function; as it should be if there were two processes causing the decay of the excited state (e.g.,  $k_R$  and  $k_Q$ ). Another troubling result of this experiment was the lack of any spectroscopic evidence for Gu radical at the expected wavelengths [30].

Subjecting metallated double-stranded DNA (**13/15**) to the same experiment gave similar results. Once again, the lifetime of the excited state was extended to  $\tau = 66$  ns ( $k = 1.5 \times 10^7$  s<sup>-1</sup>); and quenched to  $\tau = 55$  ns ( $k = 1.8 \times 10^7$  s<sup>-1</sup>, Figure 10.2-3). The same lack of ruthenium (III) generation was observed at 450 nm (Figure 10.2-4). Again, probing for a Gu radical proved fruitless.

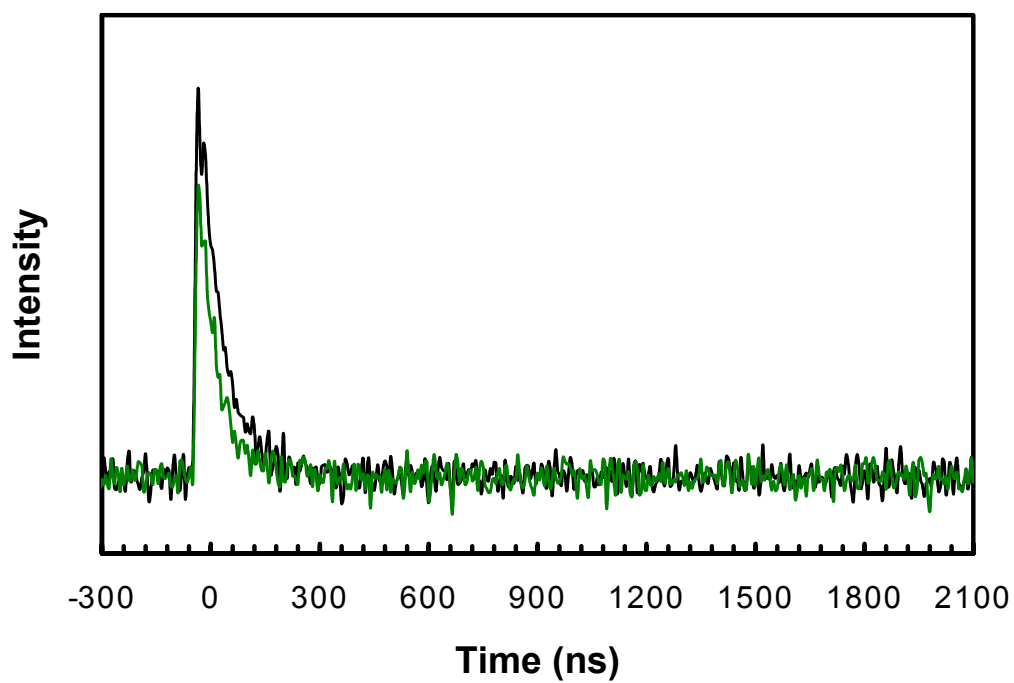
These results could be explained two ways. It could be that the quenching is no longer collisional- that is, it could be that the excited state is quenched and then the oxidized metal complex attached to the DNA recombines essentially instantaneously with the reduced quencher ( $k_{-Q}$  is very fast, Figure 10.1-1). On the other hand it could be that the forward rate of electron transfer is very fast; that is, as soon as the metal complex is



**Figure 10.2-1:** NS1 emission spectra, 15  $\mu\text{M}$  **13** in 800 mM NaCl 50 mM NaPi pH 7.0 at 720 nm. (—) without  $\text{Ru(III)(NH}_3)_6$  ; (—) with 20 mM  $\text{Ru(III)(NH}_3)_6$ .

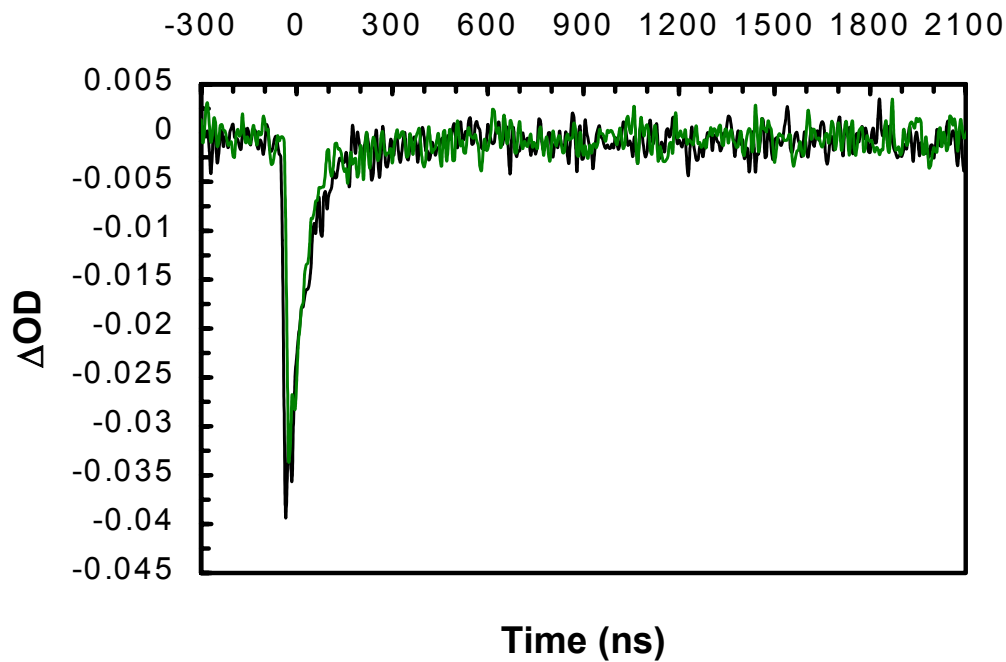


**Figure 10.2-2:** NS1 transient absorption, 15  $\mu M$  **13** in 800 mM NaCl 50 mM NaPi pH 7.0 at 450 nm. (—) without  $Ru(III)(NH_3)_6$  ; (—) with  $Ru(III)(NH_3)_6$ .



**Figure 10.2-3** NS1 emission spectra, 20  $\mu\text{M}$  **13/15** in 800 mM NaCl 50 mM NaPi pH 7.0 at 720 nm. (—) without  $\text{Ru(III)(NH}_3)_6$  ; (—) with 20 mM  $\text{Ru(III)(NH}_3)_6$ .

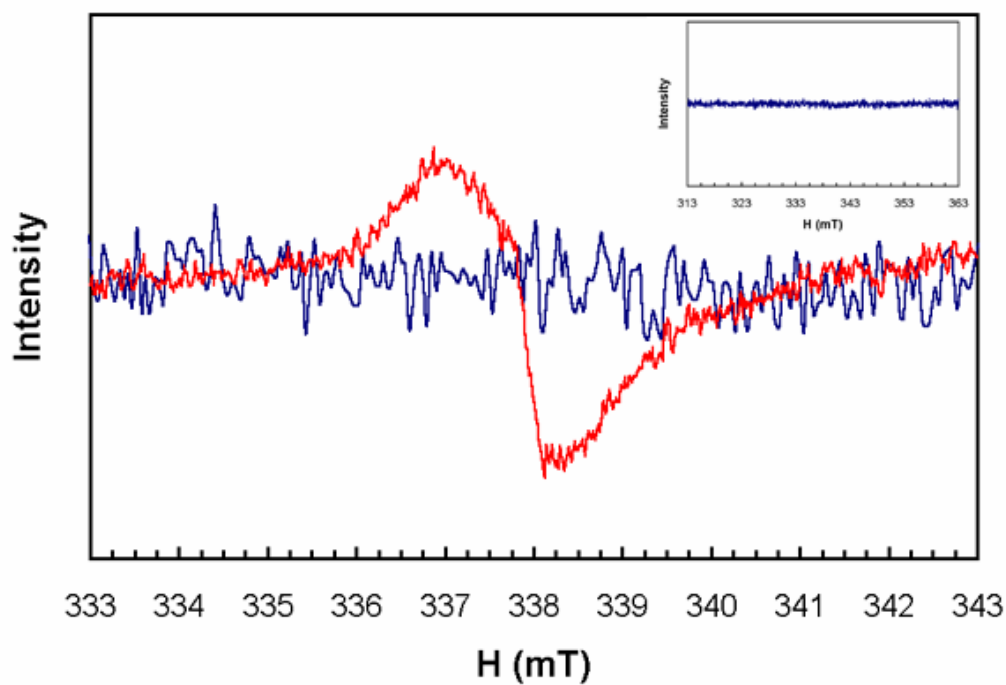




**Figure 10.2-4:** NS1 transient absorption, 20  $\mu\text{M}$  **13/15** in 800 mM NaCl 50 mM NaPi pH 7.0 at 450 nm. (—) without  $\text{Ru(III)(NH}_3)_6$  ; (—) with 20 mM  $\text{Ru(III)(NH}_3)_6$ .

oxidized, it oxidizes a Gu. Coupled with a fast rate of return to the initial conditions, this could account for the data ( $k_{ET} \gg k_Q$ ,  $k_Q$  fast, Figure 10.1-1).

Given the relevant potentials involved, the second hypothesis seemed attractive. In order to establish this mechanism, it needed to be shown that the photogenerated Ru(III) species was capable of oxidizing guanine in the DNA strand. To that end, freeze quench EPR of solutions containing **12** and **13** in 50 mM KPi pH 7.0 saturated with  $(\text{NH}_3)_5\text{Co(III)Cl}$  were obtained (the ionic strength was lowered to permit more Co(III) to be dissolved). In the case of **13** a X-band EPR signal was acquired which closely matched the reported spectrum for a guanine radical [41]. In the case of **12** no signal was apparent (Figure 10.2-5). Initially, this was taken to suggest that the actual potential of the guanine nucleobase under these conditions was somewhat higher than predicted; this was inferred from the fact that when two guanines were side by side, the potential is predicted to drop, perhaps enough to be in our oxidation range. Unfortunately, the fact that no signal is seen in **12** is somewhat problematic for this view. If our hypothesis was right, we would have to see a Ru(III) spectra, similar to the one shown in Figure 10.1-4. Ultimately, though, the results of the experiment with **13** suggest that the lack of optical evidence for Ru(III) noted above is in fact due to rapid oxidation of the nearby guanine base. Thus, strands similar to **13** would make an excellent scaffold for studying multi-step ET through DNA if they were equipped with suitable donor moieties.



**Figure 10.2-5:** Comparison of X-band flash/quench/freeze EPR spectra for **12** and **13** in 50 mM KPi pH 7.0 buffer saturated with  $(\text{NH}_3)_5\text{Co(III)Cl}$  at 77 K. Settings:  $\nu = 9.500970$  GHz; modulation frequency = 10 kHz; modulation amplitude = 1.0 G; microwave power = 63.92  $\mu\text{W}$ ; time constant = 1.28 ms; conversion time = 10.24 ms; 30 scans. (—) **12**; (—) **13**. Inset: wide sweep spectrum of **12** showing no evidence for Ru(III) version of the metal label.

## *Chapter 11*

### CONCLUSIONS

A synthetic strategy for the incorporation of metal coordination complexes into DNA at the 5' position has been thoroughly established. As a corollary, synthetic schemes also exist for incorporation of similar diimine ligands at other positions [42]. DNA strands containing ruthenium (II) complexes have been successfully synthesized and characterized: in the case of **13/15**, there is little perturbation relative to the un-metalated analog; **12/14** shows some perturbation relative to the un-metalated standard. Flash-quench laser experiments on single- and double-stranded DNA have failed to produce conclusive evidence for the formation of a Gu radical. There is some evidence from EPR spectroscopy that guanine is oxidized by Ru(III), at least in the case where there are two Gu's side by side.

An avenue of inquiry that may prove rewarding for the investigation of the dynamics of Gu oxidation is to substitute a more oxidizing species for the ruthenium complex. To this end, high-potential complexes **9** and **10** have been synthesized. Incorporation of these complexes into analogs of **12** and **13** would provide an excellent opportunity to study the oxidation of Gu in DNA. One concern is that the high potential of the rhenium complexes makes them too strongly oxidizing; that is, in the flash/quench experiment, electron transfer to the photogenerated Re(II) complex may be strongly

inverted. However, given the poor track record for the estimation of the potentials of bases in DNA, it may be that the relevant potentials would yield a  $-\Delta G^0$  that was near  $\lambda$ .

In any case, these studies show that it is in principle possible to oxidize interior Gu bases in DNA through a site-specifically incorporated photo-active metal. This means that DNA could be manipulated into exhibiting multi-step ET as a result of Gu oxidation given the appropriate donors. Such an approach would allow for the dynamics of this process to be examined. This work is part of the more general body of study of ET in DNA which is resurrecting the idea that DNA might mediate charge transfer over significant distances. This is an enticing solution to many questions regarding the biological activity of DNA. For instance, long-range ET might explain how repair enzymes locate mismatches or lesions in DNA helix, as these features certainly would impede multi-step ET. Once again, as in the azurin case, nature appears to be poised to avoid the slew of problems introduced by short electron tunneling distances through resorting to a multi-step, radical mediated method of moving charge.

## REFERENCES

- [1] Murphy, C. J.; Arkin, M. R.; Ghatlia, N. D.; Bossmann, S.; Turro, N. J.; Barton, J. K. Fast Photoinduced Electron-Transfer Through DNA Intercalation *Proc. Natl. Acad. Sci. U.S.A.* **1994**, *91*, 5315-5319.
- [2] Harriman, A. Electron Tunneling in DNA *Angew. Chem. Int. Edit.* **1999**, *38*, 945-949.
- [3] Singh, B. B. Migration of Radiation Damage in DNA *Adv. Biol. Med. Phys.* **1968**, *12*, 245-250.
- [4] Fromherz, P.; Rieger, B. Photoinduced Electron-Transfer in DNA Matrix from Intercalated Ethidium to Condensed Methylviologen *J. Am. Chem. Soc.* **1986**, *108*, 5361-5362.
- [5] Nakatani, K.; Dohno, C.; Ogawa, A.; Saito, I. Suppression of DNA-Mediated Charge Transport by BamHI Binding *Chem. Biol.* **2002**, *9*, 361-366.
- [6] Armitage, B. Photocleavage of Nucleic Acids *Chem. Rev.* **1998**, *98*, 1171-1200.
- [7] Lewis, F. D.; Wu, T. F.; Liu, X. Y.; Letsinger, R. L.; Greenfield, S. R.; Miller, S. E.; Wasielewski, M. R. Dynamics of Photoinduced Charge Separation and Charge Recombination in Synthetic DNA Hairpins with Stilbenedicarboxamide Linkers *J. Am. Chem. Soc.* **2000**, *122*, 2889-2902.
- [8] Lewis, F. D.; Kalgutkar, R. S.; Wu, Y. S.; Liu, X. Y.; Liu, J. Q.; Hayes, R. T.; Miller, S. E.; Wasielewski, M. R. Driving Force Dependence of Electron Transfer Dynamics in Synthetic DNA Hairpins *J. Am. Chem. Soc.* **2000**, *122*, 12346-12351.
- [9] Sani, L.; Schuster, G. B. Long-Distance Charge Transport in DNA: Sequence-Dependent Radical Cation Injection Efficiency *J. Am. Chem. Soc.* **2000**, *122*, 11545-11546.
- [10] Wan, C. Z.; Fiebig, T.; Schiemann, O.; Barton, J. K.; Zewail, A. H. Femtosecond Direct Observation of Charge Transfer Between Bases in DNA *Proc. Natl. Acad. Sci. U.S.A.* **2000**, *97*, 14052-14055.
- [11] Meade, T. J.; Kayyem, J. F. Electron-Transfer through DNA – Site-Specific Modification of Duplex DNA with Ruthenium Donors and Acceptors *Angew. Chem. Int. Edit. Engl.* **1995**, *34*, 352-354.

- [12] Meggers, E.; Dussy, A.; Schafer, T.; Giese, B. Electron Transfer in DNA from Guanine and 8-oxoguanine to a Radical Cation of the Carbohydrate Backbone *Chem. Eur. J.* **2000**, *6*, 485-492.
- [13] Giese, B. Long-Distance Charge Transport in DNA: The Hopping Mechanism *Acc. Chem. Res.* **2000**, *33*, 631-636.
- [14] Berlin, Y. A.; Burin, A. L.; Ratner, M. A. Charge Hopping in DNA *J. Am. Chem. Soc.* **2001**, *123*, 260-268.
- [15] Bixon, M.; Jortner, J. Charge Transport in DNA via Thermally Induced Hopping *J. Am. Chem. Soc.* **2001**, *123*, 12556-12567.
- [16] Li, X.-Q.; Zhang, H.; Yan, Y. A Superexchange-Mediated Sequential Hopping Theory for Charge Transfer in DNA *J. Phys. Chem. A* **2001**, *105*, 9563-9567.
- [17] Giese, B.; Spichy, M.; Wessely, S. Long-Distance Charge Transport through DNA: an Extended Hopping Model *Pur. Appl. Chem.* **2001**, *73*, 449-453.
- [18] Armitage, B. Photocleavage of Nucleic Acids *Chem. Rev.* **1998**, *98*, 1171-1200.
- [19] Taylor, J.-S. Unraveling the Molecular Pathway from Sunlight to Skin Cancer *Acc. Chem. Res.* **1994**, *27*, 76-82.
- [20] Taylor, J. S.; Nadji, S. Unraveling the Origin of the Major Mutation Induced by Ultraviolet-Light, the C-T Transition at DtpDc Sites – a DNA- Synthesis Building Block for the Cis-Syn Cyclobutane Dimer of DtpDu *Tetrahedron* **1991**, *47*, 2579-2590.
- [21] Cichon, M. K.; Arnold, S.; Carell, T. A <6-4> Photolyase Model: Repair of DNA <6-4> Lesions Requires a Reduced and Deprotonated Flavin *Angew. Chem. Int. Edit.* **2002**, *41*, 767-770.
- [22] Letsinger, R. L.; Wu, T. F. Use of a Stilbenedicarboxamide Bridge in Stabilizing, Monitoring, and Photochemically Altering Folded Conformations of Oligonucleotides *J. Am. Chem. Soc.* **1995**, *117*, 7323-7328.
- [23] Salunkhe, M.; Wu, T. F.; Letsinger, R. L. Control of Folding and Binding of Oligonucleotides by Use of a Nonnucleotide Linker *J. Am. Chem. Soc.* **1992**, *114*, 8768-8772.
- [24] Lewis, F. D.; Wu, T. F.; Zhang, Y. F.; Letsinger, R. L.; Greenfield, S. R.; Wasielewski, M. R. Distance-Dependent Electron Transfer in DNA ?Hairpins *Science* **1997**, *277*, 673-676.

- [25] Frank, N. L.; Meade, T. J. 5' Modification of Duplex DNA with a Ruthenium Electron Donor-Acceptor Pair Using Solid-Phase DNA Synthesis *Inorg. Chem.* **2003**, 42, 1039-1044.
- [26] Hurley, D. J.; Tor, Y. Metal-Containing Oligonucleotides: Solid-Phase Synthesis and Luminescence Properties *J. Am. Chem. Soc.* **1998**, 120, 2194-2195.
- [27] Stemp, E. D. A.; Arkin, M. R.; Barton, J. K. Oxidation of Guanine in DNA by Ru(phen)<sub>2</sub>(dppz)<sup>3+</sup> Using the Flash-Quench Technique *J. Am. Chem. Soc.* **1997**, 119, 2921-2925.
- [28] Olson, E. J. C.; Hu, D. H.; Hormann, A.; Barbara, P. F. Quantitative Modeling of DNA-Mediated Electron Transfer between Metallointercalators *J. Phys. Chem. B* **1997**, 101, 299-303.
- [29] Steenken, S.; Jovanovic, S. V. How Easily Oxidizable Is DNA? One-electron Reduction Potentials of Adenosine and Guanosine Radicals in Aqueous Solution *J. Am. Chem. Soc.* **1997**, 119, 617-618.
- [30] Burrows, C. J.; Muller, J. G. Oxidative Nucleobase Modifications Leading to Strand Scission *Chem. Rev.* **1998**, 98, 1109-1151.
- [31] Candeias, L. P.; Steenken, S. Electron-Transfer in Di(Deoxy)Nucleoside Phosphates in Aqueous- Solution - Rapid Migration of Oxidative Damage (Via Adenine) to Guanine *J. Am. Chem. Soc.* **1993**, 115, 2437-2440.
- [32] Wilson, E. DNA Charge Migration: No Longer an Issue *Chem. Eng. News* **2001**, 79, 29-29.
- [33] Voet, D.; Voet, J. G. *Biochemistry*; 2nd ed.; John Wiley & Sons Inc.: New York, 1995 1361.
- [34] Lodish, H.; Baltimore, D.; Berk, A.; Zipursky, S. L.; Matsudaria, P.; Darnell, J. *Molecular Cell Biology*; 3 ed.; W.H. Freeman Company: New York, 1996
- [35] Fairall, L.; Martin, S.; Rhodes, D. The DNA-Binding Site of the Xenopus Transcription Factor-IIIa Has a Non-B-Form Structure *Embo J.* **1989**, 8, 1809-1817.
- [36] Warren, M. A.; Murray, J. B.; Connolly, B. A. Synthesis and Characterisation of Oligodeoxynucleotides Containing Thio Analogues of <6-4> Pyrimidine-Pyrimidinone Photo-Dimers *J. Mol. Biol.* **1998**, 279, 89-100.



- [37] Fuertes, M. A.; Perez, J. M.; Gonzalez, V. M.; Alonso, C. Empirical Validation of a Two-state Kinetic Model for the B-Z Transition of Double-Stranded Poly[d(G-m(5)C)] *J. Biol. Inorg. Chem.* **1999**, *4*, 759-765.
- [38] Kypr, J.; Stepan, J.; Chladkova, J.; Vorlickova, M. Circular Dichroism Spectroscopy Analysis of Conformational Transitions of a 54 Base Pair DNA Duplex Composed of Alternating CGCGCG and TATATA Blocks *Biospectroscopy* **1999**, *5*, 253-262.
- [39] Shready, R. D. *Spectroscopy* **1991**, *6*, 14-17.
- [40] Chang, I. J.; Gray, H. B.; Winkler, J. R. High-Driving-Force Electron-Transfer in Metalloproteins – Intramolecular Oxidation of Ferrocyclochrome-C by Ru(2,2'-Bpy)<sub>2</sub>(Im)(His-33)<sup>3+</sup> *J. Am. Chem. Soc.* **1991**, *113*, 7056-7057.
- [41] Schiemann, O.; Turro, N. J.; Barton, J. K. EPR Detection of Guanine Radicals in a DNA Duplex Under Biological Conditions: Selective Base Oxidation by Ru(phen)<sub>2</sub>dppz<sup>3+</sup> Using the Flash-Quench Technique *J. Phys. Chem. B* **2000**, *104*, 7214-7220.
- [42] Krider, E. S.; Miller, J. E.; Meade, T. J. 2'-Modified Nucleosides for Site-Specific Labeling of Oligonucleotides *Bioconj. Chem.* **2002**, *13*, 155-162.